

Hydrological and erosion responses to man-made and natural disturbances – Insights from forested catchments in South-central Chile

Dissertation submitted to the Faculty of Mathematics and Natural Sciences at the
University of Potsdam, Germany
for the degree of Doctor of Natural Sciences (Dr. rer. nat.) in Geoecology

Christian Heinrich Mohr



Potsdam, September 2013

This work is licensed under a Creative Commons License:
Attribution - Noncommercial - Share Alike 3.0 Germany
To view a copy of this license visit
<http://creativecommons.org/licenses/by-nc-sa/3.0/de/>

Published online at the
Institutional Repository of the University of Potsdam:
URL <http://opus.kobv.de/ubp/volltexte/2014/7014/>
URN <urn:nbn:de:kobv:517-opus-70146>
<http://nbn-resolving.de/urn:nbn:de:kobv:517-opus-70146>



View from Nahuelbuta National park across the central inner valley towards the Sierra Velluda, close to the study area, Biobío region, Chile.

Quien no conoce el bosque chileno, no conoce este planeta...

Pablo Neruda

*The climate is moderate and delightful and if the country were to be cleared of forest, the
warmth of ground would dissipate the moisture...*

The Scot Lord Thomas Cochrane commanding the Chilean navy in a letter to the Chilean
independence leader Bernardo O'Higgins about the south of Chile, 1890,
cited in [*Bathurst*, 2013]

Preface

When I started my PhD studies, my main intention was to contribute new knowledge about the impact of forest management practices on runoff and erosion processes. To this end, together with our Chilean colleagues, we established a network of forested catchments on the eastern slopes of the Chilean Coastal Range with water and sediment monitoring devices to quantify water and sediment fluxes associated with different forest management practices. The data thus obtained allowed us to calculate water balances and sediment budgets of exotic plantation forests prior to any forestry intervention. Then on February 27th 2010 the magnitude 8.8 Maule Earthquake struck the study area and affected the hydrological processes fundamentally. The seismic waves stimulated the hydrological process system resulting in observed changes in streamflow discharge. Owing to the fact that seismo-hydrological processes and interactions are limited in space and time, the observed hydrological phenomena offered the unique opportunity to better understand the coupled interaction between near-surface tectonics and the hydrological cycle in general and the mechanisms of certain hydrological processes in particular. Therefore, I took the chance and extended my PhD research which resulted in the thesis presented here.

One part of my thesis investigates changes in hydrology and soil erosion associated with forestry activities while the other part explores hydrological responses to earthquakes. At first glance, these two fields of research seem to be unrelated and acting on distinct spatiotemporal scales. Nevertheless, they are both results of changing environmental conditions whether induced by human activity or due to rather rare seismic processes. Natural and man-made disturbances can push a hydrologic system beyond the range of previously experienced behavior, which opens a window to understanding the regional hydrological cycle and its processes as a whole. The understanding of process responses to disturbances are not restricted to academic interest but has implications for water supplies and the development of best management practices to mitigate the impact of forest interventions on stream water quality and quantity.

I finally merged both research fields into a common framework that I have named *Hydrological and erosion responses to man-made and natural disturbances – Insights from forested catchments in south-central Chile*.

Table of contents

Content	i
List of Figures	v
List of Tables	x
Abstract	xii
Zusammenfassung.....	xiv
1. General introduction and background	1
1.1. Hydrological and erosion responses to man-made disturbances	3
1.1.1. Plantation forestry	4
1.1.2. Plantation forestry in Chile	4
1.1.3. Hydrological and hydro-geomorphic consequences of intensive plantation forestry	5
1.2. Hydrological and erosion responses to natural disturbances	11
1.2.1. Earthquake hydrology	11
1.2.2. The origin of post-seismic changes in streamflow	13
1.3. Chile – country of earthquakes	15
1.4. The Nacimiento hydrological and erosional study sites	16
1.5. Aims, objectives and approaches	19
1.6. Author’s contributions and publications	22
2. Effect of Pinus radiata and Eucalyptus globulus plantations on water resources in the Coastal Range of the Biobío region, Chile	23
2.1. Introduction	24
2.2. Methods and study sites	25
2.3. Results	33
2.4. Discussion	36
2.5. Conclusion	40
2.6. Acknowledgments	40
2.7. Supplementary Information: Original paper published in Spanish	40

3. Runoff and soil erosion processes after clear cutting	41
3.1. Introduction	42
3.2. Study area	44
3.3. Methods	46
3.3.1. Experimental strategy and sampling design	47
3.3.2. Soil conditions	49
3.3.3. Data Analysis	50
3.3.4. Random Forest Model setup	51
3.4. Results	53
3.4.1. Soil and surface properties	53
3.4.2. Results of drip-type rainfall experiments	54
3.4.2.1. Infiltration and runoff production	54
3.4.2.1. Sediment transport and erosion rates	57
3.4.3. The hydrological and erosional response as a function of environmental variables	59
3.4.3.1. Infiltration and runoff response	59
3.4.3.2. Erosion and sediment yield	61
3.5. Discussion	63
3.6. Conclusions	70
3.7. Acknowledgements	71
3.8. Supplementary Information	72
 4. Seasonal logging, process response, and geomorphic work	 74
4.1. Introduction	75
4.2. Study sites	76
4.3. Methods	78
4.3.1. Field sampling	78
4.3.2. Sediment rating curve (SRC)	79
4.3.3. Quantile Regression Forests (QRF)	79
4.3.4. QRF model	80
4.4. Results	81
4.5. Discussion	85
4.6. Conclusions	89
4.7. Acknowledgements	89

4.8. Physics-based modelling efforts of water and sediment fluxes	
following clear cutting using WASA-SED	90
4.8.1. Hydrology	90
4.8.2. Sediment fluxes	92
4.8.3. Synopsis of the modelling studies and implications	93
4.9. Supplementary Information	93
5. Streamflow response in small upland catchments in the Chilean Coastal	
 Range to the MW 8.8 Maule earthquake on February 17th 2010	98
5.1. Introduction	100
5.2. Maule earthquake and Araucania aftershock	101
5.3. Study area and weather conditions	101
5.4. Methods and Data	106
5.5. Approach	108
5.6 Observations and results	109
5.7 Discussion	116
5.7.1. Where does the excess water come from?	117
5.7.2. Increase in streamflow discharge by enhanced permeability?	118
5.7.3. Increase in streamflow discharge by dynamic strain?	120
5.7.3.1. Intensified magnitude of diurnal oscillations of	
streamflow discharge	125
5.7.4. Increase in streamflow by tilting of the landscape?	126
5.8. Conclusions and synopsis	127
5.9. Acknowledgement	128
6. Response of vadose zone water to earthquake	129
6.1. Conceptual model of vadose zone water response to earthquakes	137
6.2. Supplementary Information	139
6.2.1. Methods	139
6.2.1.1. Observation of streamflow, rainfall and soil moisture	139
6.2.1.2. Rescaling of evapotranspiration rates and	
normalization of discharge	139
6.2.1.3. Modelling	140
6.2.1.3.1. Modelling of Groundwater flow	140

6.2.1.3.2. Modelling of co-seismic water mobilization from the vadose zone	140
6.2.1.3.3. Inverse modelling of evapotranspiration	141
6.2.2. Supplementary Figures	145
6.2.3. Supplementary Table	147
7. Summary and Conclusions	148
7.1. Summary and conclusions	149
7.1.1. Main results, implications and limitations	149
7.1.2. Synthesis	156
7.1.3. Future work	158
7.1.3.1. Groundwater	158
7.1.3.2. Hydrological and hydro-geomorphic processes	159
7.1.3.3. Ecohydrology	160
7.1.3.4. Earthquake hydrology	160
7.1.4. Final remarks	162
8. Bibliography	163
9. Acknowledgements	189
Curriculum Vitae	191

Table of Figures

Figure 1.1: Generalized hydrological cycle and processes in forests.	7
Figure 1.2: Well in China responding to the December 26, 2004, M9.2 Sumatra earthquake 3200 km away.	12
Figure 1.3: Hydrographs of San Lorenzo River, CA responding to the M 7.3 Loma Prieta earthquake and Mattole River, CA responding to the M 6.0 Honeydew earthquake.	13
Figure 1.4: Interactions between earthquakes and hydrological processes.	14
Figure 1.5: Seismo-tectonic setting of the South-Central Chile megathrust.	15
Figure 1.6: Overview showing the installed network of experimental catchments.	17
Figure 1.7: Specific objectives of the thesis and organization of chapters.	21
Figure 2.1: Location of the forested experimental catchments in Nacimiento, Chile.	26
Figure 2.2: Spatio-temporal variation of soil water content (% Vol) of catchments forested with <i>Pinus radiata</i> and <i>Eucalyptus globulus</i> .	34
Figure 3.1: Location of the study area and sites of the rainfall simulation experiments.	43
Figure 3.2: Mean monthly temperature and rainfall for Meñir meteorological station during the period from 01/2000 to 12/2008.	46
Figure 3.3: Sketch of rainfall simulator.	47

Figure 3.4: Topsoil texture according to USDA soil classification.	53
Figure 3.5: Example hydrographs showing runoff and erosion response to applied rainfall of different rainfall intensities and forest management practice.	55
Figure 3.6: Steady state infiltration rates (mm/h) as a function of applied rainfall intensity and forest management practice.	56
Figure 3.7: Mean runoff yields as a function of forest management practice and applied rainfall intensity and ratios between the runoff yields of the young and old clear cuttings after 120 minutes of runoff as a function of applied rainfall intensity.	57
Figure 3.8: Mean sediment yields as a function of forest management practice and applied rainfall intensity and ratios between the sediment yields of the young and old clear cuttings after 120 minutes of runoff as a function of applied rainfall intensity.	58
Figure 3.9: Ratios between the erosion rates of the young and old clear cuttings as a function of applied rainfall intensity.	59
Figure 3.10: Performance and predictor importance of Random Forest infiltration and runoff yield models.	60
Figure 3.11: Random Forest infiltration rate models performance and predictor importance according to each forest management practice.	62
Figure 3.12: Random Forest sediment yield model performance and predictor importance according to each forest management practice.	64
Figure 3.13: Hydrographs showing specific daily discharge during the years 2008 and 2009 for the control and treatment catchment. Specific discharge quotients between control and treatment catchments are shown during the years 2008 and 2009.	65
Figure 3.14: Observed preferential flow patterns in topsoil along recent and former root systems and desiccation cracks of recent clear cutting of San Antonio.	65

Figure 3.15: Hysteresis loop show temporal suspended sediment concentration-discharge relationship for untreated control catchment and logged catchment during the same rainfall-runoff event.	69
Figure 4.1: Sediment rating curves for the catchments and location of study catchments.	77
Figure 4.2: Pictures showing the experimental catchments, the logging procedure and the suspended sediment monitoring devices.	77
Figure 4.3: Water discharge and SSC dynamics under unlogged and logged conditions during two rainfall events.	82
Figure 4.4: Monthly double mass-curve between the sediment yields of catchments logged during rainy and dry season, and the unlogged control catchment.	83
Figure 4.5: Fraction of instantaneous sediment transport rates normalized to catchment maximum as a function of monitoring time during which these rates were not exceeded. Fraction of total sediment load normalized per catchment as a function of the fraction of total monitoring period for unlogged conditions, rainy-, and dry-season logging.	84
Figure 4.6: Variable importance of the Quantile Regression models for each catchment scaled to 100%.	85
Figure 4.7: QRF model results of SSC dynamics during extreme peak flow for undisturbed and logged conditions during two rainfall events.	86
Figure 4.8: Simulated discharge and sediment yields using WASA-SED.	91
Figure 5.1: Location of the study area in relation to the epicenters of Maule earthquake and the Araucanía Aftershock.	102
Figure 5.2: Soil moisture (vol. %) measured along transects of access tubes.	103

Figure 5.3: Hydrographs of the catchments showing the hydrological response of the 9 smaller catchments to the earthquake.	109
Figure 5.4: Hydrograph of Pichón grande showing the post-seismic increase in streamflow and the difference between daily maximum and minimum baseflow discharge.	110
Figure 5.5: Pre-seismic vs. post-seismic recession constants.	111
Figure 5.6: Water temperature at streamflow gauges of catchments 1, 3, 4, 6, 8, 9 and 10 and air temperature for the period from 25 Feb 2010 to 1 Mar 2010.	113
Figure 5.7: Hydrographs showing no hydrological response to the Araucanía aftershock in the streamflow.	114
Figure 5.8: Normalized daily mean water and air temperatures for the period from 16 Feb 2010 to 10 March 2010.	117
Figure 5.9: Distance from epicenter vs. earthquake magnitude for locations with seismically induced streamflow increase.	122
Figure 5.10: on previous page: Schematic sketch of a hillslope in the study area prior to, during and after the earthquake.	124
Figure 6.1: Location map showing the study catchment and the epicenter of the Maule earthquake of 27 Feb 2010. Studied catchment showing the vegetation cover, the stream network and the streamflow gauging station.	130
Figure 6.2: Observed and modelled streamflow for periods prior to and after the earthquake.	131
Figure 6.3: Observed co-seismic drop in streamflow in a subset of adjacent catchments.	132

Figure 6.4: Water retention curve for the deep soil and measured soil moisture.	135
Supplementary Figure 6.1: Rescaled evapotranspiration rate-diurnal streamflow amplitude relationships for pre- and immediate post-seismic periods during baseflow conditions.	145
Supplementary Figure 6.2: Daily mean streamflow discharge and amplitudes of diurnal streamflow cycling for the period from April 17 th 2008 to October 25 th 2011	146
Figure 7.1: Simplified illustration of infiltration excess and saturation excess overland flow mechanisms on timber harvest areas.	151
Figure 7.2: Seismo-hydrological process mechanisms in saturated and vadose zone.	155
Figure 7.3: Hydrograph of Pichón grande covering the complete study period.	158

List of Tables

Table 1.1 on next page. Effects of forestry management practices on water yields, hydrological processes and sediment transport under different environmental conditions and at different spatial scales.	10
Table 1.2. Water and sediment flux monitoring program performed.	19
Table 2.1. Hydro-geomorphologic characteristics of the <i>Pinus radiata</i> and <i>Eucalyptus globulus</i> catchments.	26
Table 2.2. Characteristics of the <i>Pinus radiata</i> and <i>Eucalyptus globulus</i> plantations.	28
Table 2.3. Values of total precipitation, interception loss, streamflow, quick flow, base flow, evapotranspiration, soil water content and total sediment export for <i>Pinus radiata</i> and <i>Eucalyptus globulus</i> .	35
Table 3.1. Main features of the studied catchments.	45
Table 3.2. Random Forest predictor and response variables.	51
Table 3.3. Average surface cover in of total plot cover.	54
Table 3.4: Hydrological and erosional responses according to simulated rainfall intensity and forest management practice.	72
Table 3.5. Estimated lag times for control and treatment catchment.	77
Table 4.1. Number of total samples for each catchment.	79
Supplementary Table 4.1: Predictor variables used for QRF-modelling.	93
Supplementary Table 4.2: Performance of QRF models and sediment rating curves.	94

Supplementary Table 4.3: Bulk data and modelled annual suspended sediment yields in 2009 and 2010 of control catchment, rainy-season clear cutting and dry-season clear cutting.	94
Supplementary Table 4.4: Monthly suspended-sediment yields based on bulk data during the study period 2009-2010.	95
Supplementary Table 4.5: Monthly SSY estimates by QRF during study period 2009-2010 at the catchment outlets.	96
Supplementary Table 4.6: Average predicted SSC-values based on the QRF and SRC approach.	97
Table 5.1. Main characteristics of the experimental catchments.	105
Table 5.2. Summary of hydrological response to the Maule earthquake.	112
Table 5.3. Median correlation coefficients.	116
Supplementary Table 6.1. Estimated whole-catchment daily evapotranspiration.	147

Abstract

Logging and large earthquakes are disturbances that may significantly affect hydrological and erosional processes and process rates, although in decisively different ways. Despite numerous studies that have documented the impacts of both deforestation and earthquakes on water and sediment fluxes, a number of details regarding the timing and type of de- and reforestation; seismic impacts on subsurface water fluxes; or the overall geomorphic work involved have remained unresolved. The main objective of this thesis is to address these shortcomings and to better understand and compare the hydrological and erosional process responses to such natural and man-made disturbances. To this end, south-central Chile provides an excellent natural laboratory owing to its high seismicity and the ongoing conversion of land into highly productive plantation forests.

In this dissertation I combine paired catchment experiments, data analysis techniques, and physics-based modelling to investigate: 1) the effect of plantation forests on water resources, 2) the source and sink behavior of timber harvest areas in terms of overland flow generation and sediment fluxes, 3) geomorphic work and its efficiency as a function of seasonal logging, 4) possible hydrologic responses of the saturated zone to the 2010 Maule earthquake and 5) responses of the vadose zone to this earthquake.

Re 1) In order to quantify the hydrologic impact of plantation forests, it is fundamental to first establish their water balances. I show that tree species is not significant in this regard, i.e. *Pinus radiata* and *Eucalyptus globulus* do not trigger any decisive different hydrologic response. Instead, water consumption is more sensitive to soil-water supply for the local hydro-climatic conditions.

Re 2) Contradictory opinions exist about whether timber harvest areas (THA) generate or capture overland flow and sediment. Although THAs contribute significantly to hydrology and sediment transport because of their spatial extent, little is known about the hydrological and erosional processes occurring on them. I show that THAs may act as both sources and sinks for overland flow, which in turn intensifies surface erosion. Above a rainfall intensity of ~20 mm/h, which corresponds to <10% of all rainfall, THAs may generate runoff whereas below that threshold they remain sinks. The overall contribution of *Hortonian* runoff is thus secondary considering the local rainfall regime. The bulk of both runoff and sediment is generated by *Dunne*, saturation excess, overland flow. I also show that logging may increase infiltrability on THAs which may cause an initial decrease in streamflow followed by an increase after the groundwater storage has been refilled.

Re 3) I present changes in frequency-magnitude distributions following seasonal logging by applying Quantile Regression Forests at hitherto unprecedented detail. It is clearly the season that controls the hydro-geomorphic work efficiency of clear cutting. Logging, particularly dry seasonal logging, caused a shift of work efficiency towards less flashy and mere but more frequent moderate rainfall-runoff events. The sediment transport is dominated by *Dunne* overland flow which is consistent with physics-based modelling using WASA-SED.

Re 4) It is well accepted that earthquakes may affect hydrological processes in the saturated zone. Assuming such flow conditions, consolidation of saturated saprolitic material is one possible response. Consolidation raises the hydraulic gradients which may explain the observed increase in discharge following earthquakes. By doing so, squeezed water saturates the soil which in turn increases the water accessible for plant transpiration. Post-seismic enhanced transpiration is reflected in the intensification of diurnal cycling.

Re 5) Assuming unsaturated conditions, I present the first evidence that the vadose zone may also respond to seismic waves by releasing pore water which in turn feeds groundwater reservoirs. By doing so, water tables along the valley bottoms are elevated thus providing additional water resources to the riparian vegetation. By inverse modelling, the transient increase in transpiration is found to be 30-60%. Based on the data available, both hypotheses, are not testable.

Finally, when comparing the hydrological and erosional effects of the Maule earthquake with the impact of planting exotic plantation forests, the overall observed earthquake effects are comparably small, and limited to short time scales.

Zusammenfassung

Landmanagement und tektonische Prozesse haben einen erheblichen Einfluss auf das Abflussverhalten und den Wasser-, sowie den Sedimenthaushalt von Gebirgsregionen. Sowohl forstwirtschaftliche Bewirtschaftung, als auch starke Erdbeben sind Impulse, die hydrologische und Erosionsprozesse, sowie deren Prozessraten beeinflussen. Obwohl zahlreiche Arbeiten bereits den Einfluss von forstlicher Bewirtschaftung (Abholzungen, Aufforstungen) als auch von Erdbeben auf Wasser und Sedimentflüsse dokumentiert haben, bleiben wichtige Fragen offen. Wie entscheidend ist der Zeitpunkt der Abholzung und des nachfolgenden Wiederaufforstens? Wie wirken seismische Störungen auf unterirdische Wasserflüsse? Wie ändert sich die Leistung geomorphologischer Arbeit nach Kahlschlägen? Zur Erforschung dieser Fragen bietet sich das südliche Zentralchile aufgrund seiner hohen lokalen seismischen Aktivität und der kontinuierlichen Umwidmung von Flächen in hochproduktive Plantagenwälder hervorragend an. Letztere verursachen sich häufig verändernde Umweltbedingungen durch kurze forstwirtschaftliche Rotationszyklen.

Diese Dissertation betrachtet Einzugsgebiete mit vergleichbarer naturräumlicher Ausstattung. Dabei werden experimentelle Datenerhebung, ein Monitoring-Programm und Datenanalysetechniken mit prozessbasierter Modellierung kombiniert. Ziel der vorliegenden Arbeit ist:

1) *die Untersuchung des Einflusses von Plantagenwäldern auf den lokalen Wasserhaushalt.* Hier zeigt sich, dass die Baumart (*Pinus radiata* vs. *Eucalyptus globulus*) eine eher sekundäre Wirkung auf den lokalen Wasserhaushalt besitzt. Vielmehr ist der Bodenwasserspeicher unter dem gegebenen lokalen Hydroklima der entscheidende Faktor für den Wasserverbrauch der Aufforstungen.

2) *die Untersuchung des Verhaltens von Kahlschlagflächen im Hinblick auf Quellen oder Senkenwirkung für Oberflächenabfluss und Sedimenttransport.* Hier zeigt sich, dass diese Flächen sowohl als Quelle als auch als Senke für Oberflächenabfluss und Sedimenttransport wirken können – abhängig von der Regenintensität. Übersteigt diese ~20 mm/h, was <10 % der lokalen Niederschlagsereignisse entspricht, generieren Kahlschlagflächen *Horton*-Oberflächenabfluss (Infiltrationsüberschuss) und Sedimenttransport. Unterhalb dieses Schwellenwerts wirken sie als Senke. In Anbetracht der lokalen Niederschlagsintensitäten ist der Gesamtbeitrag des *Horton*-Oberflächenabflusses daher sekundär. Der Großteil des Abflusses entsteht durch *Dunne*-Oberflächenabfluss (Sättigungsüberschuss). Zudem zeigt die vorliegende Arbeit, dass Abholzen die Infiltrabilität

erhöhen kann. Dies führte dazu, dass zunächst der Gebietsabfluss abfällt bevor er erst nach Auffüllen des Grundwasserspeichers signifikant ansteigt.

3) *Die Untersuchung des Einflusses von Kahlschlägen auf die hydrogeomorphologische Arbeit und ihre Effizienz.* Durch das Anwenden von Quantile Regression Forests (QRF) wird auf kurzer Prozessskala gezeigt, dass Abholzung zu unterschiedlicher Jahreszeit zu signifikanten Veränderungen im Sedimenttransport führt. Vor allem Kahlschläge die während der Trockenzeit durchgeführt werden, verursachten einen Bedeutungsverlust von seltenen, stärkeren Abflussereignissen zu Gunsten der häufigeren, jedoch weniger starken Ereignissen. Hierbei dominierte der *Dunne*-Oberflächenabfluss. Dies stimmt mit den Ergebnissen eines prozessbasierten hydrologischen Modells (WASA-SED) überein. Es ist somit eindeutig die Jahreszeit, die die Leistung der hydro-geomorphologischer Arbeit nach Kahlschlägen prägte.

4) *die Untersuchung von Grundwasserreaktionen auf das M8.8 Maule Erdbeben.* Unter Grundwasserbedingungen kann der gesättigte Saprolith mit Verdichtung auf die Erdbebenschütterungen reagieren. Dieser Prozess erhöht den hydraulischen Gradienten, der eine plausible Erklärung für den beobachteten Anstieg am Gebietsausfluss nach dem Erdbeben liefert. Die Verdichtung mobilisiert Grundwasser, das zudem von der ungesättigten Bodenmatrix aufgenommen werden kann. Hierdurch erhöht sich das Wasservolumen im Wurzelraum und begünstigt die Pflanzaktivität. Eine solche Aktivitätserhöhung spiegelt sich in verstärkten Tagesgangamplituden wider.

5) *die Untersuchung von hydrologischen Reaktionen auf das Erdbeben in der ungesättigten Zone.* Hier zeigt sich, dass auch Bodenwasser aus der ungesättigten Bodenzone durch Erdbebenschütterungen freigesetzt werden kann und den darunter liegenden Grundwasserspeicher zufließt. Hierdurch steigt der Grundwasserspiegel in den Talböden und erhöht dort die Pflanzenwasserverfügbarkeit. Durch inverse Modellierung wurde ein erdbebenbedingter Anstieg der Pflanzenaktivität von 30-60% quantifiziert. Beide Hypothesen sind jedoch auf Basis der verfügbaren Daten nicht eindeutig verifizierbar.

Vergleicht man den Effekt des Erdbebens auf den Wasserhaushalt mit dem Effekt der exotischen Plantagenwälder zeigt sich, dass die Gesamtwirkung des Erdbebens auf den Wasserhaushalt vergleichsweise klein war und sich zudem auf kurze Zeiträume beschränkte.

1. General introduction and background

Hydrological and hydro-geomorphic processes in forested ecosystems are not static but change over time and space. Spatiotemporal changes can result from land cover modification due to vegetation decline, biogeographic shifts as a response to climate change, man-made stream flow distortion or deforestation. Thus, the geo-hydrological environment continuously evolves potentially at greater rates in the future because of increasing human impact [Wagner *et al.*, 2010]. Following Bronstert *et al.*, [2009], man-made hydrological change can be distinguished as three major groups according to their external causes: Responses to (1) climate change; (2) land cover change such as conversion of land for agriculture, forestry, industrialization and urbanisation; and (3) the increasing demand for water resources in particular for agriculture, industrial activities, and navigation. Such stressors control the quality and quantity of water available [Wagner *et al.*, 2010]. Increased demand and projections into the foreseeable future point to changes in frequency and magnitude of hydro-geomorphic hazards. Hazards include floods, droughts or sediment pulses triggered by extreme rainfall events owing to increased hydrologic variability [e.g., Davidson *et al.*, 2012]). Episodic natural hazards such as volcanic eruptions or earthquakes also contribute to hydrologic variability [e.g., Major and Mark, 2006; Montgomery and Manga, 2003]. Thus, the world is expected to face a decline in security for water and other natural resources [Thompson *et al.*, 2011]. High demand for a dwindling resource causes strong competition for a resource that is already scarce in many regions. This competition is expected to be most severe in the least resilient of nations [Wagner *et al.*, 2010].

Man permanently changes the environment. Thus, properties, as well as boundary and initial conditions, do not remain stationary but respond to external drivers in different ways. The key to understanding today's hydro-geomorphic process regimes lies therefore in understanding the temporal co-evolution of topography, tectonics, vegetation, soil, and river networks, etc. in interaction with man [Wagner *et al.*, 2010]. This view challenges the traditional approach of assuming stationarity using historical data for model building and prediction when focussing beyond the "interpolable" future. Following Kirchner [2006] we can argue that past observations can hardly give the "right answers for the right reasons". Consequently, historical data may form a reliable benchmark to test hydrological and hydro-geomorphological process hypotheses but only if system changes are not too severe and the critical assumption of stationarity is justified. Historical data, however, cannot provide any sound basis for extrapolating under radically changing environmental conditions.

Earth systems affected by human footprint or (rare) natural disturbances may result in complex and previously unobserved phenomena or (non-stationary) feedbacks when extrapolating. The complexity arises from nonlinear, non-additive, heterogeneous and dynamic processes involving interaction and feedbacks of hydrologic, geomorphic, biogeochemical, ecologic and human systems [Bronstert *et al.*, 2009; Kirchner, 2006; Wagener *et al.*, 2010]. Among the most prominent examples of feedbacks between man and regional hydrology is the Aral Sea where water withdrawal for agricultural demand caused a massive drying-out. The desiccation triggered the extinction of the aquatic ecosystem, a reduction in regional rainfall to one third of its original value and the lake in flow to one sixth [Gaybullaev *et al.*, 2012]. On-site effects comprise the severe die-back for vegetation due to the precipitation of toxic sodium chloride and sodium sulfate delivered by aeolian transport of salt and dust from the exposed former sea bottom [Micklin, 1988]. Spectacular changes can also occur by natural disturbances. Earthquake-water feedbacks provide such examples which may even challenge basic physics concepts such as conservation of mass in a presumably closed watershed [Wang and Manga, 2010a]. Such –sometimes surprising – behaviour cannot easily be derived from understanding the system components in isolation [Kirchner, 2006].

These two examples underpin the need to account for feedbacks between land cover changes, rare natural disturbances, and the (regional) hydrological (and hydro-geomorphic) process responses. Such an integrative approach is crucial to understand the response to and resilience of ecosystems to disturbances in a more comprehensive way. This process knowledge involves more than just academic curiosity. It is fundamental to build hydrological response predictions. Indeed, significant advance in understanding interactions and feedbacks of earth surface processes has been achieved, e.g. connectivity of hillslopes to streams on different spatial scales, stream-vegetation interaction or modelling hydrological factors affecting mass wasting initiation, among others [e.g., Sidle and Onda, 2004; Wagener *et al.*, 2010]. However, we are far from understanding such changing systems. Following Jones *et al.* [2009] we can highlight that the principles of forest hydrologic responses are indeed well established, but prediction under changing conditions remains a challenge.

This short outline demonstrates that much more research is needed at high complexity levels (of both space and time) in order to understand hydrologic responses to disturbances. Against this background, I designed this thesis to explore how hydrological and hydro-geomorphic systems respond to, and evolve under, natural and man-made disturbances. The examples presented here comprise high impact logging and responses to a high magnitude earthquake in experimental headwater catchments of the Chilean Coastal Range.

1.1. Hydrological and erosion responses to man-made disturbances

Forests are distinct and complex vegetation communities. Their canopy structures, organic floor, and root systems form an intricate environment that significantly affects water and energy transfers between ground and the atmosphere [Bonan, 2008; Chang, 2006]. The establishment and management of exotic plantation forests are associated with substantial changes to these controls and thus disturb both water quality and quantity as well as related hydrological and earth surface processes [e.g. Brown *et al.*, 2005; Sidle *et al.*, 2006]. Under these conditions, we can thus regard man-made forests as an example of artificially disturbed natural systems.

1.1.1. Plantation forestry

By 2005, land-use activities, mainly due to agricultural expansion and timber extraction, had caused a global net loss of some 7-11 million km² of forest over the last 300 years [Foley *et al.*, 2005]. The results of global supply and demand analysis point to an increasing demand for wood products, owing to continuous increases in population and income [FAO, 2010]. During the last four decades, natural forest resources have declined considerably in numerous countries due to forest clearing, degradation or withdrawal from production [Sutton, 1999]. This trend is expected to intensify in the foreseeable future despite the growing concern over using natural forest for timber and pulp production. Instead, environmental, preservationist and political groups are claiming to conserve the remaining natural forests in their original state. This conflict requires that growing demand will have to be supplied from a declining, more restricted forest resource base. In other words: The pressure of the remaining forests to produce more wood is likely to increase in the foreseeable future. To solve this dilemma the only viable answer is to shift the wood production from natural forests to intensively managed man-made plantation forests [Iroumé, 2005].

Forest plantations account for only a small fraction of the global forest area. Following FAO [2006] forest plantations are defined as “forests of introduced species and in some cases native species, [that are] established through planting or seeding, with few species, even spacing, and/or even-aged stands.” They provide wood, fibre and non-wood forest products but may also provide recreational, amenity, protective and soil and water conservational functions. By 2005 only 4% of the estimated 4 billion hectares of forest areas comprise plantation forests [FAO, 2010]. Shifting the wood production to man-made forest has an undeniable benefit: It leaves the remaining natural forests for nonwood-producing objectives,

i.e. wilderness protection, biodiversity conservation (e.g., species or age diversification), recreational demands [e.g., *Foley et al.*, 2005; *Sutton*, 1999]. Although plantation forests do not meet such high ecological standards, they deliver both multiple-habitat forests and provide productive tree crops and have also become a significant sink of atmospheric carbon (e.g., [*Foley et al.*, 2005]). Thus forestry has developed into an important factor in the global water market as it is competing with other economic sectors, the environment and with society for water resources [*Foley et al.*, 2005]. In consequence, a responsible management of plantation forests with respect to the environment is certainly obligatory [*Iroumé*, 2005]. A responsible management involves scientifically sound predictions of freshwater occurrence, circulation, distribution and quality, and associated processes in order to establish a firm basis for an acceptable and robust trade-off between economic gain and environmental protection [*Foley et al.*, 2005]. However, since different parties with different interests are involved, there is no general agreement how best management practices should look like.

1.1.2. Plantation forestry

Chile has developed an important forestry sector based on some 2.6 million hectares of man-made forest which contributes 12.5% of total exports equal to 3.6% of Gross Domestic Product (GDP) [*Iroumé and Palacios*, in rev.]. According to the Global Forest Census of 2005, Chile accounted for 2% of the global area of productive plantation forests [*FAO*, 2006]. Near 95% of the Chilean forest economy comes from man-made forests that cover some 3% of the national territory or 13% of the forest lands [*Iroumé*, 2005]. The plantations are established with exotic species, among them *Pinus radiata* (Monterey pine) and *Eucalyptus globulus* representing 64 and 29 %, respectively [*Iroumé and Palacios*, in rev.]. Although radiata pine has been planted since the beginning of the 20th century to control erosive processes [*Toro and Gessel*, 1999], the 1974 Law Decree 701 set the starting point for increases in planted area from some 375 thousand ha by the end of 1973 to 2.6 million hectares in 2011 [*Iroumé and Palacios*, in rev.]. When this decree expired in 1994, the new Law 19,561 redirected the policy focus to subsidize plantations meant to protect fragile soils, rehabilitate eroded lands and incentivize forest establishment by small landowners [*Niklitschek*, 2007]. Today, the plantation forests are found mainly between 34 and 41° south.

The domestic economic role of forestry is likely to gain weight because it has a realistic chance for expansion: First, it benefits from the economic revenue of plantation forests and, second, it profits by the existence of some 2 million hectares of plantable but yet uncovered lands. Despite the economic importance and the fact that forestry provides a major

income source for many people, particularly in rural and poor areas, afforestation with fast growing exotic species has ended up being less socially and politically accepted. In public forums and the media plantation forests have been blamed for impacts on the environment, soil and water resources causing both annual and summer water deficits in the particularly vulnerable areas.

1.1.3. Hydrological and hydro-geomorphic consequences of intensive plantation forestry

Deforestation and afforestation substantially alter the hydrological and hydro-geomorphic systems of forested landscapes [e.g., *Bathurst et al.*, 2010] (Figure 1.1). The analysis of hydrological consequences of intensive forestry operations on water yield, water quality and erosion have received much attention worldwide [e.g., *Bosch and Hewlett*, 1982; *Brown et al.*, 2005; *Carr and Loague*, 2011; *Farley et al.*, 2005; *Gomi et al.*, 2005; *Lane et al.*, 2004] including Chile [*Bathurst et al.*, 2011a; *Bathurst et al.*, 2011b; *Birkinshaw et al.*, 2011; *Huber and Iroumé*, 2001; *Huber et al.*, 2008; *Iroumé and Huber*, 2002; *Iroumé et al.*, 2005; *Iroumé et al.*, 2006; *Iroumé et al.*, 2010; *Lara et al.*, 2009; *Oyarzún et al.*, 1998; *Schuller et al.*, 2006; *Schuller et al.*, 2013; *Uyttendaele and Iroumé*, 2002]. At a global scale afforestation and deforestation are among the most prominent land use changes in terms of ecological [*Foley et al.*, 2005] and hydrological effects [*Calder*, 1992]. Although the establishment of plantation forests on land previously in pasture, under cultivation or bare has protected many areas from erosion, large scale forest operations severely disturb water, nutrient and sediment cycling within a catchment [e.g., *Carr and Loague*, 2011; *Cornish*, 1993; *Croke et al.*, 1999b; *Croke and Hairsine*, 2006; *Fahey*, 1994; *Foley et al.*, 2005; *Jones*, 2000; *Jones et al.*, 2009; *Montgomery et al.*, 2000; *Scott and Lesch*, 1997; *Sidle et al.*, 2006; *Uyttendaele and Iroumé*, 2002; *Wallbrink and Croke*, 2002].

Analyzing runoff, several studies point out that timber harvesting –and even intense thinning- may cause a significant increase in annual streamflow [e.g., *Cornish*, 1993; *van Dijk and Keenan*, 2007]. Timber harvest operations at the end of the rotation period remove the canopy and water yields generally return to (near) pre-establishment conditions benefitting from increased groundwater recharge [e.g., *Scott and Lesch*, 1997]. The magnitude and duration of post-harvesting effects on stream flows are a function of soil type, topography, aspect, geology, rainfall quantity, intensity and frequency, season, antecedent conditions, road networks, the extension and type of forest intervention and the characteristics of the vegetation that re-establishes after harvesting. Substantial effects in streamflow are noticeable only when at least 10-20% of the forest cover is reduced [*Brown et al.*, 2005] and up to the

end of the first years after logging: afterwards, because of vegetation regrowth, streamflow quickly returns to previous baseline levels [e.g., *Brown et al.*, 2005; *Fahey*, 1994]. Flow increase is more significant in wet temperate regions [e.g., *Keppler*, 1998] and proportional to harvested area in the catchment. [*Bosch and Hewlett*, 1982] estimated a 25-40 mm change in annual water yield per 10% change in forest cover depending on the tree species. The impact of forests and their removal is most evident for summer flows. Under forest cover, interception and transpiration capacity are at their highest levels during summer months when forests are in full vegetative growth and while foliage is densest. Higher transpiration losses are due to the deeper root systems of trees reducing soil water reserves which sustain base flows during dry periods [*Fahey*, 1994; *Iroumé et al.*, 2006; *van Dijk and Keenan*, 2007].

In most cases, increased peak flows after timber cutting are associated with wetter, hydrologically more responsive soils [e.g., [*Thomas and Megahan*, 1998]. Though numerous studies point out increasing peak flows after timber harvesting [e.g., *Bathurst et al.*, 2010; *Bathurst et al.*, 2011a; *Bathurst et al.*, 2011b; *Birkinshaw et al.*, 2011; *Fahey*, 1994; *Iroumé et al.*, 2006; *Jones and Grant*, 1996; *Pizarro et al.*, 2006; *Stednick*, 1996], the effect of storm type, i.e. magnitude and return periods remains controversial. Peak flows are stochastic and thus are required to be defined by magnitude *and* frequency [*Green and Alila*, 2012; *Kuras et al.*, 2012]. Restricting analysis to magnitude only may therefore lead to premature conclusions and incomplete management recommendations because the common approach of comparing treated and untreated catchments [e.g., *Jones and Grant*, 1996], requires physically identical watersheds subject to identical meteorological input and the same runoff processes [*Alila et al.*, 2010; *Alila et al.*, 2009; *Green and Alila*, 2012; *Kuras et al.*, 2012; *Lewis et al.*, 2010]. Such preconditions are inherently impossible.

Afforestation, in turn, tends to reduce groundwater recharge and net water availability because the trees intercept part of the precipitation and, owing to their deeper root system, transpire more water than grasses during the drier periods. By analyzing global data, *Farley et al.* [2005] showed that, compared to grassland, eucalypts reduce runoff by $75\pm 10\%$ whereas pines reduced runoff by $40\pm 3\%$. Similarly, *Scott and Prinsloo* [2008] showed that eucalypts reduce streamflow for $\sim 10\%$ for each 10% catchment afforested, slightly higher than for pine (7.7% for each 10% catchment area). In consequence, the establishment of plantation forests comes with long-term changes in rainfall partitioning patterns and chemistry [e.g., *Crockford and Richardson*, 2000; *Uyttendaele and Iroumé*, 2002], soil moisture patterns [e.g., *Huber et al.*, 2008], water yield [e.g., *Brown et al.*, 2005; *Scott and Lesch*, 1997], and water quality [e.g., *Uyttendaele and Iroumé*, 2002]. For example, *Calder et al.* [1997] showed groundwater

depletion due root-water uptake of 3400 mm/yr (!) in eucalypt plantation forests in India, far exceeding annual rainfall yield. However, the net effect of species vs. hydro-climatic conditions or groundwater supply remains controversially discussed [Brown *et al.*, 2005].

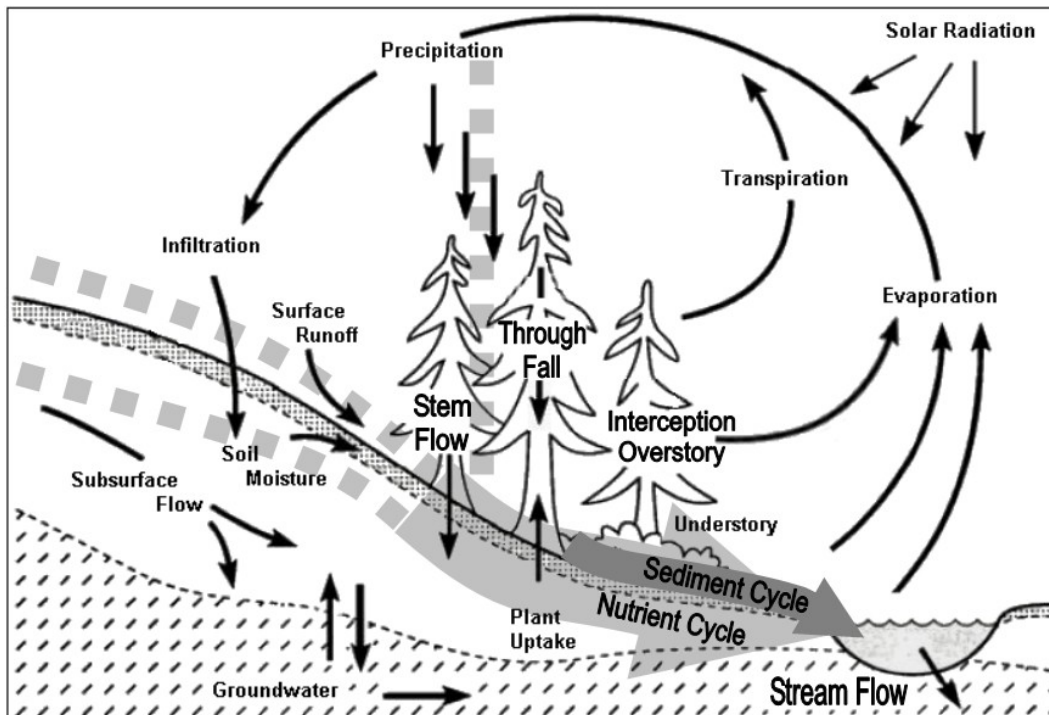


Figure 1.1: Generalized hydrological cycle and processes in forests [Iroum , 2005].

Forest type, ground cover and climate determine the amount of net precipitation, i.e. the sum of throughfall and stemflow that reaches the ground surface [e.g., Crockford and Richardson, 2000; Levia and Frost, 2003; Levia and Frost, 2006]. Throughfall and stemflow are the main sources of soil water for any forest, with stemflow being especially important for supporting growth of individual trees in areas of low rainfall [Huber and Oyarzún, 1983]. *Pinus radiata* (Monterey pine) and *Eucalyptus globulus*, the most common species in man-made forests of Chile [Iroumé and Palacios, in rev.], generate similar throughfall of 55-86% and 64-73% of gross precipitation, respectively. In contrast, pine generally exceeds eucalypt in terms of stemflow with 0-13 and 2-5% of gross precipitation, respectively [Crockford and Richardson, 1990; Crockford and Richardson, 2000; Huber and Iroumé, 2001; Levia and Frost, 2003]. Though the contribution of litter interception by forest floor cover may be substantial under certain conditions [e.g., Gerrits *et al.*, 2007], its overall fraction is minor [Chang, 2006]. Part, if not the whole, of interception losses represent an addition to total catchment evaporative losses (root-water uptake including interception storage). Consequently, soil moisture under deforested sites exceeds soil water contents under afforested sites.

Numerous studies show that one of the most important environmental issues associated with forestry arises from erosion and sedimentation processes [e.g., *Croke and Hairsine*, 2006; *Sheridan et al.*, 2008; *Sidle et al.*, 2006]. Harvesting and site preparation techniques that expose bare soil to erosive rainfall have the greatest potential to impact water quality. Upon established connectivity, logging may intensify overland runoff and deliver large volumes of sediment (and nutrients) into streams [e.g., *Iroumé*, 1990]. Overland flow mechanisms on harvest areas involve both infiltration excess and saturation excess overland flow due to soil compaction [*Malmer and Grip*, 1990] or higher soil moisture levels due to decreased root water uptake after logging [*Croke et al.*, 1999a]. *Lane et al.* [2004] even showed that logging does not automatically enhance overland flow but may increase subsurface storm flow along cracks and root channels following logging instead. In other words: All explanations may hold true for some specific local conditions and each study may provide evidence for distinct runoff mechanism dominance after logging, but the underlying process controls remain largely unclear or unexplored. Different spatiotemporal scales further complicate the comparability between the studies.

When logged, root strength rapidly decays facilitating shallow landslides that are additionally promoted by slow root-strength recovery over time and cumulative effects of previous harvests [*Sidle et al.*, 2006]. Reported rates of erosion in forested areas are mostly well below those in areas without forest cover [e.g., *Birkinshaw et al.*, 2011; *Pepin et al.*, 2010]. Although sedimentation impacts from forestry operations may remain irreversible under certain conditions, they are generally short-lived. Major impacts occur during and for a few years after harvesting [e.g., *Sidle et al.*, 2006], until the vegetation re-establishes and road surfaces and cut and fill slopes stabilize [e.g., *Walsh et al.*, 2011]. However, logging is neither necessarily associated with an increase in sediment transport nor is densely forested terrain essentially quiescent in erosion terms. Instead, *Gomi et al.* [2005] reported a decrease of 40% in sediment load after clear cuttings in Northern California while there is growing evidence of substantial erosion even under dense and undisturbed forest canopies [e.g., *Zimmermann et al.*, 2012]. Thus, the popular perception of forests as quiescent in hydro-geomorphic terms is misplaced.

The main sources of sediment in managed forests include roads, cut banks, slope failures and debris flows, stream bank erosion and channel scour [*Chappell et al.*, 2004; *Croke and Hairsine*, 2006; *Gomi et al.*, 2004; *Lane and Sheridan*, 2002; *Montgomery et al.*, 2000; *Motha et al.*, 2003; *Sidle et al.*, 2004; *Sidle et al.*, 2006; *Wemple et al.*, 2001]. In a recent study, *Schuller et al.* [2013] showed that timber roads may contribute up to 49% of

total load despite being a relatively small fraction of the catchment area (~4%; personal communication *P. Schuller*). Timber roads further improve hydrologic connectivity within catchments [*Sidle et al.*, 2004; *Wemple et al.*, 2001]. While there is broad agreement about the importance of forest roads, the role of harvest areas as *either* sources *or* sinks for overland flow and sediment remains ambiguous [e.g., *Brooks et al.*, 1994; *Croke et al.*, 1999a; *Croke et al.*, 1999b; *Wallbrink and Croke*, 2002]. Benefitting from their spatial extent, however, their cumulative hydro-geomorphic effect may often exceed even the effect of timber roads.

Reviews by *Bosch and Hewlett* [1982] and *Brown et al.* [2005] and most recently by *Dye* [2013] provide comprehensive compilations of hydrological and erosional effects of forest management. Table 1.1 on the next page highlights only some of the most prominent effects under different environmental conditions and at a wide range of spatial scales.

Table 1.1 on next page. Examples of distinct effects of forestry management practices on water yields, hydrological processes and sediment transport under different environmental conditions and at different spatial scales. The table is ordered by descending quantitative effect each management.

***a* depending on the spatial extent of thinning;**

***b* not returned to pre-harvest values 21-30 years before [Walsh et al., 2011];**

***c* decreasing up to drying-up [Scott and Lesch, 1997];**

***d* yearly reduction rates in water yields up to 250mm/yr following logging and immediate afforestation with eucalypts [Cornish, 1993];**

***e* depending on former land use, i.e. which land cover has been afforested such as grassland, pasture [Fahe , 1994].**

Here, change is given as relative change from pre-afforestation flows

Forestry operation	Hydrological/ Hydro-geomorphic responses	A Change (% of hydrological or hydro-geomorphological response)	Study area	Catchment size (ha)	Forest type	Climate zone	Prevailing soils		
Timber harvest	streamflow	+236 mm increase from dried creek	South Africa	26.2-36.9	<i>Eucalyptus grandis</i> , <i>Pinus patula</i> Plantation	Subtropical, 1167mm a ⁻¹ [Scott and Lesch, 1997]	Few centimetre deep soil		
		+105-204 [Carr and Loague, 2011]	CA, USA	10-473 [Henry, 1998]	Douglas Fir, Redwoods, grand fir	Mediterranean type 1190mm a ⁻¹ [Henry, 1998]	Clayey loam [Henry, 1998]		
		+128-187 [Cornish, 1993]	N.S.W., Australia	13-97	Old growth eucalyptus (100-500yrs)	Moist warm temperate climate, 1450-1750mm a ⁻¹ [Cornish, 1993]	Friable and structured Xanthothems, brown podsolises [Cornish, 1993]		
		110-180 (up to 464; different total rainfall) [Iroumé et al., 2005; Iroumé et al., 2006; Iroumé et al., 2010]	Southern Chile	10.8-89.9 [Iroumé et al., 2005]	<i>Pinus radiata</i> , <i>Eucalyptus nitens</i> plantation	Rainy temperate Mediterranean, 2000-2500 mm a ⁻¹	Loamy- red clays, volcanic ash [Iroumé et al., 2005]		
		+160 [Swank et al., 2001]	NC, USA	59.5	Mixed deciduous forest	Marine, humid temperate with cool summers and mild winters, 1890mm a ⁻¹	Hapludult and Dystrachrept		
		+66 [Fahey, 1994]	New Zealand	4.8-20.2 [Fahey, 1994; O'Loughlin et al., 1978]	<i>Pinus radiata</i> Plantation	1800-2500mm a ⁻¹ [O'Loughlin et al., 1978]	Shallow stony podzols [O'Loughlin et al., 1978]		
		110 [Iroumé et al., 2005]	Southern Chile	34.4	<i>Pinus radiata</i> , <i>Eucalyptus nitens</i> plantation	Rainy temperate Mediterranean 2000-2500mm a ⁻¹	Loamy- red clays, volcanic ash [Iroumé et al., 2005]		
		+48 [Swank et al., 2001]	NC, USA	59.5	Mixed deciduous forest	Marine, humid temperate with cool summers and mild winters, 1890mm a ⁻¹	Hapludult and Dystrachrept		
		131-216 [Jones, 2000]	OR, USA	10-101 [Jones, 2000; Jones and Grant, 1996]	Douglas fir, western hemlock, western red cedar, evergreen hardwoods	Pacific maritime climate with dry summers and wet winters, 2500mm a ⁻¹	Inceptisol, thick organic layers, deep sapsprolite [Jones and Grant, 1996]		
		+140 [Carr and Loague, 2011]	CA, USA	10-473 [Henry, 1998]	Douglas Fir, Redwoods, grand fir	Mediterranean type, 1190mm a ⁻¹ [Henry, 1998]	Clayey loam [Henry, 1998]		
Clear cutting	summer flows	+132 [Iroumé et al., 2006] - 206 [Iroumé et al., 2006]	Southern Chile	34.4	<i>Pinus radiata</i> Plantation	Rainy temperate Mediterranean type, 2000-2500mm a ⁻¹	Loamy- red clays, volcanic ash [Iroumé et al., 2005]		
		+114-115 [Swank et al., 2001]	NC, USA	59.5	Mixed deciduous forest	Marine, humid temperate with cool summers and mild winters, 1890mm a ⁻¹	Hapludult and Dystrachrept		
		+400 [Gomi et al., 2005] +1000 [Beschta, 1978]	OR, USA	75 [Beschta, 1978]; 101 [Gomi et al., 2005]	Douglas fir, alder	Pacific maritime climate with dry summers and wet winters, 2500mm a ⁻¹	Moderately stable, shallow, stony soil [Brown and Kryger, 1971]		
		123-269 [Gomi et al., 2005]	CA, USA	10-473 [Henry, 1998]	Douglas Fir, Redwoods, grand fir	Mediterranean type, 1190mm a ⁻¹ [Henry, 1998]	Clayey loam [Henry, 1998]		
		+230 [Birkinshaw et al., 2011]	Southern Chile	34.4	<i>Pinus radiata</i> Plantation	Rainy temperate Mediterranean type, 2000-2500mm a ⁻¹	Loamy- red clays, volcanic ash [Iroumé et al., 2005]		
		+128 [Dung et al., 2012]	Japan	0.35	<i>Japanese cypress</i> plantation	Moist temperate climate, rainy season June-July and typhoons Aug-Oct, ø 14°C; 2000mm a ⁻¹	Cambisol		
		+114 [Rupprecht et al., 1991]	W.A., Australia	80	Jarrah and marri forests	Hot and dry summers, winter rainfall, 1130mm a ⁻¹	Sandy loams		
		+160 [Dung et al., 2012]	Japan	0.35	<i>Japanese cypress</i> plantation	Moist temperate climate, rainy season June-July and typhoons Aug-Oct, ø 14°C; 2000mm a ⁻¹	Cambisol		
		+400-1800 [Douglas et al., 1992]	Malaysia	44	Native forest	Equatorial climate, ø 27°C, 2795±304 mm a ⁻¹ [Douglas et al., 1992; Walsh et al., 2011]	Loamy-silty loam [Walsh et al., 2011]		
		Selective thinning	Summer flow	125 [Webb et al., 2012]	N.S.W., Australia	302-770	Mixed eucalypt forest	Winter rainy season, 773 mm a ⁻¹	Yellow Earths, Brown Earths
-32-75 [Lane et al., 2005]	N.S.W., Vic, Australia			18-8700	Pasture → <i>Pinus radiata</i> , Eucalypt plantation	Winter rainfall climate, 775-1472mm a ⁻¹	No information		
-41-62 [Lane et al., 2005]	South Africa			31-190	Pasture → <i>Pinus radiata</i> , <i>Pinus patula</i> plantation	Summer rainfall climate, 1088-1436mm a ⁻¹	No information		
-45-53 [Fahey, 1994]	New Zealand			100-300	Pasture → <i>Pinus radiata</i> Plantation	Coastal climate, wet winters and dry summers, 1000-1400mm a ⁻¹	Well-drained silt loams		
-4-31 [Cornish, 1993]	N.S.W., Vic, Australia			13-97	Logging → <i>Eucalyptus laeovipinea</i>	Moist warm temperate, 1450-1750mm a ⁻¹	Friable, strongly structured, <1m depth, colluvium		
-32-43 [Little et al., 2009]	South-central Chile			25250-70770	Native forest → <i>Pinus radiata</i> plantation	Mediterranean-type, 718-835mm a ⁻¹	Intermediate-fine sands		
-30 [Brown et al., 2005]	South Africa			27	Grassland → <i>Pinus radiata</i> plantation	summer rainfall climate, 1298mm a ⁻¹	Few centimetre deep soil		
-20-30 [Fahey, 1994]	New Zealand			100-300	Pasture → <i>Pinus radiata</i> plantation	Coastal climate, wet winters and dry summers, 1000-1400mm a ⁻¹	Well-drained silt loams		
Afforestation/ conversion	sediment flux			+160 [Dung et al., 2012]	Malaysia	44	Native forest	Equatorial climate, ø 27°C, 2795±304 mm a ⁻¹ [Douglas et al., 1992; Walsh et al., 2011]	Loamy-silty loam [Walsh et al., 2011]
				+400-1800 [Douglas et al., 1992]	Malaysia	44	Native forest	Equatorial climate, ø 27°C, 2795±304 mm a ⁻¹ [Douglas et al., 1992; Walsh et al., 2011]	Loamy-silty loam [Walsh et al., 2011]
		125 [Webb et al., 2012]	N.S.W., Australia	302-770	Mixed eucalypt forest	Winter rainy season, 773 mm a ⁻¹	Yellow Earths, Brown Earths		
		-32-75 [Lane et al., 2005]	N.S.W., Vic, Australia	18-8700	Pasture → <i>Pinus radiata</i> , Eucalypt plantation	Winter rainfall climate, 775-1472mm a ⁻¹	No information		
		-41-62 [Lane et al., 2005]	South Africa	31-190	Pasture → <i>Pinus radiata</i> , <i>Pinus patula</i> plantation	Summer rainfall climate, 1088-1436mm a ⁻¹	No information		
		-45-53 [Fahey, 1994]	New Zealand	100-300	Pasture → <i>Pinus radiata</i> Plantation	Coastal climate, wet winters and dry summers, 1000-1400mm a ⁻¹	Well-drained silt loams		
		-4-31 [Cornish, 1993]	N.S.W., Vic, Australia	13-97	Logging → <i>Eucalyptus laeovipinea</i>	Moist warm temperate, 1450-1750mm a ⁻¹	Friable, strongly structured, <1m depth, colluvium		
		-32-43 [Little et al., 2009]	South-central Chile	25250-70770	Native forest → <i>Pinus radiata</i> plantation	Mediterranean-type, 718-835mm a ⁻¹	Intermediate-fine sands		
		-30 [Brown et al., 2005]	South Africa	27	Grassland → <i>Pinus radiata</i> plantation	summer rainfall climate, 1298mm a ⁻¹	Few centimetre deep soil		
		-20-30 [Fahey, 1994]	New Zealand	100-300	Pasture → <i>Pinus radiata</i> plantation	Coastal climate, wet winters and dry summers, 1000-1400mm a ⁻¹	Well-drained silt loams		

1.2. Hydrological and erosion responses to natural disturbances

The most prominent natural disturbances include forest fires, pests, storms, volcanism and earthquakes [Attiwill, 1994]. Though they differ across time and space, they all disturb hydrological and sediment cycles. Volcanic eruptions and wildfires may dramatically boost surface runoff promoting surface erosion and sediment yields following the removal of protective tree cover, changes to soil-infiltration rates, and supply of highly erodible debris [e.g., Cannon *et al.*, 2001; Wondzell and King, 2003]. Hydrophobic hillslopes that are sealed following thick ash fall or wildfire and then exposed to runoff may increase the total sediment yield from mountainous catchments by 30-50% [Roering and Gerber, 2005]. Burnt areas are most vulnerable to erosion during the first few years following fire, or longer if re-vegetation is slow [Zelt and Wohl, 2004]. Subsequent rainstorm-triggered flooding, gully erosion, debris flows, and landslides mobilise the bulk of sediment. In thus disturbed forests sheet and rill erosion may attain rates of $>6 \text{ t ha}^{-1} \text{ yr}^{-1}$ [Grant and Wolff, 1991]. These cases document extremely high and short-lived transport of volcanoclastic debris in rivers, causing some of the highest sediment yields documented [Korup, 2012].

Compared to such catastrophic sediment pulses, earthquake-triggered hydrological and hydro-geomorphic, e.g. erosion, responses are generally smaller though long-term effects may be important [e.g., Dadson *et al.*, 2003; Hovius *et al.*, 2011; Parker *et al.*, 2011; Wang and Manga, 2010a; Xue *et al.*, 2013b]. In the case of the 2008 (M7.9) Wechuan earthquake, [Parker *et al.*, 2011] showed that seismicity-induced erosion may exceed orogenic growth on longer timescales. One of the most spectacular surface hydrologic phenomena associated with earthquakes is a large change in streamflow commonly observed following seismic shocks.

1.2.1. Earthquake hydrology

Hydrological changes have been documented after earthquakes, some of them immediately following the seismic shock, for thousands of years [Manga and Wang, 2007]. Examples include changes in water level in wells, liquefaction of soils, changes in the activity of mud volcanoes and geysers, the formation and disappearance of springs and changes in streamflow [Wang and Manga, 2010a]. Such hydrologic changes are not unexpected because earthquakes change stress, and physical properties of the subsurface, e.g. permeability of rocks, depend on stress which controls the rate of water flux [Manga and Wang, 2007]. What is more surprising is the large magnitude of some of the documented responses and the great

distance over which changes occur. For example, following the 2004 M9.2 Sumatra earthquake, groundwater erupted from a previously non-artesian well in China, 3200 km away from the epicentre, creating a fountain 60 m above the land surface (Figure 1.2).



Figure 1.2: Well in China responding to the December 26, 2004, M9.2 Sumatra earthquake 3200 km away. The picture is taken 2 days after the Sumatra earthquake. The fountain reached 50-60 m altitude when it was first sighted 1 day after the earthquake. Picture taken from Wang and Manga [2010a]

Such hydrologic phenomena are more than curiosities: Earthquakes stimulate the hydrological system which changes the boundary conditions immediately. Consequently, hydrological responses to earthquakes provide unique possibilities to analyze the *stimulated* hydrological cycle without the need to stimulate the system artificially. This step is required to gain a complete picture of the regional hydrological cycle and its processes. Hence, understanding the origin of hydrological responses to earthquakes is more than of academic interest. It can provide unique insight into near-surface hydrologic *and* seismic processes, interaction and feedbacks at spatial and temporal scales that are otherwise difficult to study. Further, understanding the origin of hydrological responses to earthquake may have applications to hydrocarbon migration and recovery [Beresnev and Johnson, 1994], geothermal systems [Manga *et al.*, 2012], and implications for water supplies [Chen and Wang, 2009] or underground waste repositories [Carrigan *et al.*, 1991].

Interestingly, there is also evidence for the opposite cause and effect. High-pressure water injected into a 5 km deep well to stimulate a reservoir of a geothermal project has triggered earthquakes of up to M3.4 earthquakes in Basel Switzerland [Deichmann and Giardini, 2009].

1.2.2. The origin of post-seismic changes in streamflow

Figure 1.3 shows two typical examples of enhanced streamflow following earthquakes. Because streamflow responds to precipitation across the watershed, earthquake-induced changes are best recorded and studied during dry season or dry periods. Increased streamflow occurs in the near- and intermediate field [Rojstaczer *et al.*, 1995; Wang *et al.*, 2004b]. Near-field is defined as the area within one fault length of the rupture, and intermediate-field as the area within several fault lengths [Manga, 2001]. The total excess discharge, i.e., the total volume of water released in excess of that expected in the absence of the earthquake, can be important. [Wang *et al.*, 2004b] estimated 0.7 km^3 for the magnitude M7.5 Chi-Chi earthquake.

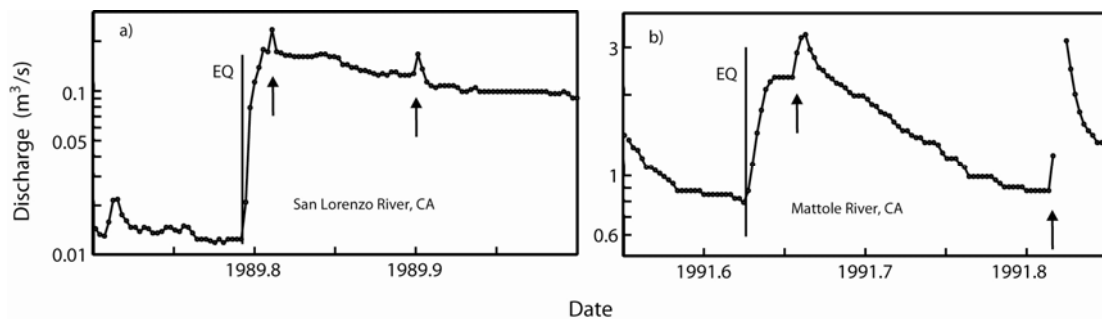


Figure 1.3.: Hydrographs of a) San Lorenzo River, CA responding to the M 7.3 Loma Prieta earthquake and b) Mattole River, CA responding to the M 6.0 Honeydew earthquake. Time of the earthquake is shown by the vertical line labelled EQ. Dates with precipitation are indicated with the small arrows. Vertical axis is a log scale. Figure taken from Manga and Wang [2007].

Earthquakes cause crustal stress and dynamic stress which initiate changes in hydrological processes (Figure 1.4). The current state of understanding changes in discharge can be divided into six categories [Manga and Wang, 2007]:

- (1) Expulsion of deep crustal fluids resulting from saturated cracks by coseismic elastic strain [e.g., Muirwood and King, 1993];
- (2) Changes in near-surface permeability [e.g., Briggs, 1991; Elkhoury *et al.*, 2006; Rojstaczer and Wolf, 1992; Rojstaczer *et al.*, 1995; Tokunaga, 1999];
- (3) Aquifer recharge by water release from elevated areas due to enhanced vertical permeability/connectivity [Wang *et al.*, 2004b]
- (4) Consolidation even up to liquefaction of near-surface deposits [e.g., Manga, 2001; Manga *et al.*, 2003; Montgomery and Manga, 2003];
- (5) Rupturing of subsurface reservoirs [e.g., Wang *et al.*, 2004a]; and
- (6) Release of water trapped in fault zones [e.g., Sibson and Rowland, 2003]

The latter two processes are sometimes merged together. However, they differ in the sign of the pressure changes [Manga *et al.*, 2012]. The differences between all these different explanations are not trivial because of their implications for the magnitude of crustal permeability, its evolution, and thus groundwater flow paths [Manga and Wang, 2007]. Ultimately, groundwater paths control most of the water supplies. All explanations may hold true for some specific local conditions. However, they often compete or even contradict each other in their implications for changes in water chemistry or crustal porosity [Rojstaczer *et al.*, 1995] which contradicts coseismic elastic strain opening and closing microcracks as proposed by [Muirwood and King, 1993]. Similar contradictions arise from proposed enhanced near-crust permeability supported by decreased water temperature [Wang *et al.*, 2012] or changed electrical conductivity [Charmoille *et al.*, 2005] but conflict with unchanged recession constants [Manga, 2001; Montgomery *et al.*, 2003]. Instead, Manga [2001] and Montgomery *et al.* [2003] proposed coseismic consolidation of saturated deposits. To summarize, under certain circumstances, earthquakes seem to trigger hydrological processes which cannot be entirely understood by our current state of knowledge. In fact, there is no need to restrict the observations to one single mechanism.

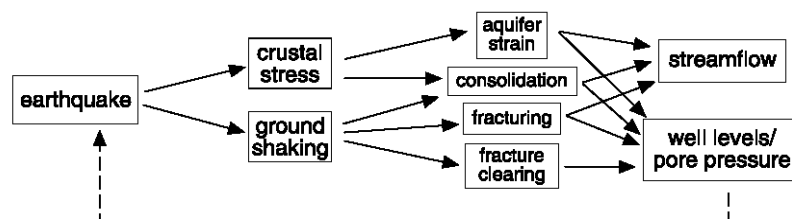


Figure 1.4. Interactions between earthquakes and hydrological processes [Montgomery and Manga, 2003].

Though these mechanisms often contradict each other, all previous studies share two common features: First, they all assume groundwater flow conditions exclusively (only one study suggesting response of shallowest water; Manga and Rowland [2009]), and second, the studied watersheds extend over large areas. The latter entails heterogeneous environmental conditions, such as geology and topography, which makes the unambiguous identification of the underlying hydro-seismological processes extremely difficult. A way out of this dilemma is to identify the source of the excess water by finding appropriate answers to questions such as

- Does the excess discharge originate from the shallow or deep subsurface?
- Do the responses of deep and shallow systems differ and if so how and why?
- Are there different responses of bedrock and unconsolidated materials?

Last but definitely not least, an assessment of the impact of earthquake induced changes in the regional water cycle remains entirely unexplored. Hence, a fundamental question needs to be addressed: How important are earthquake-induced changes for regional groundwater flow at all? And are any of these changes, e.g., permeability changes, permanent or do they recover?

1.3. Chile – country of earthquakes

Chile is a country of high seismicity (Figure 1.5) and has been the staging ground for two of the ten strongest registered earthquakes since 1900 (USGS NEIC Catalog, http://earthquake.usgs.gov/earthquakes/world/10_largest_world).

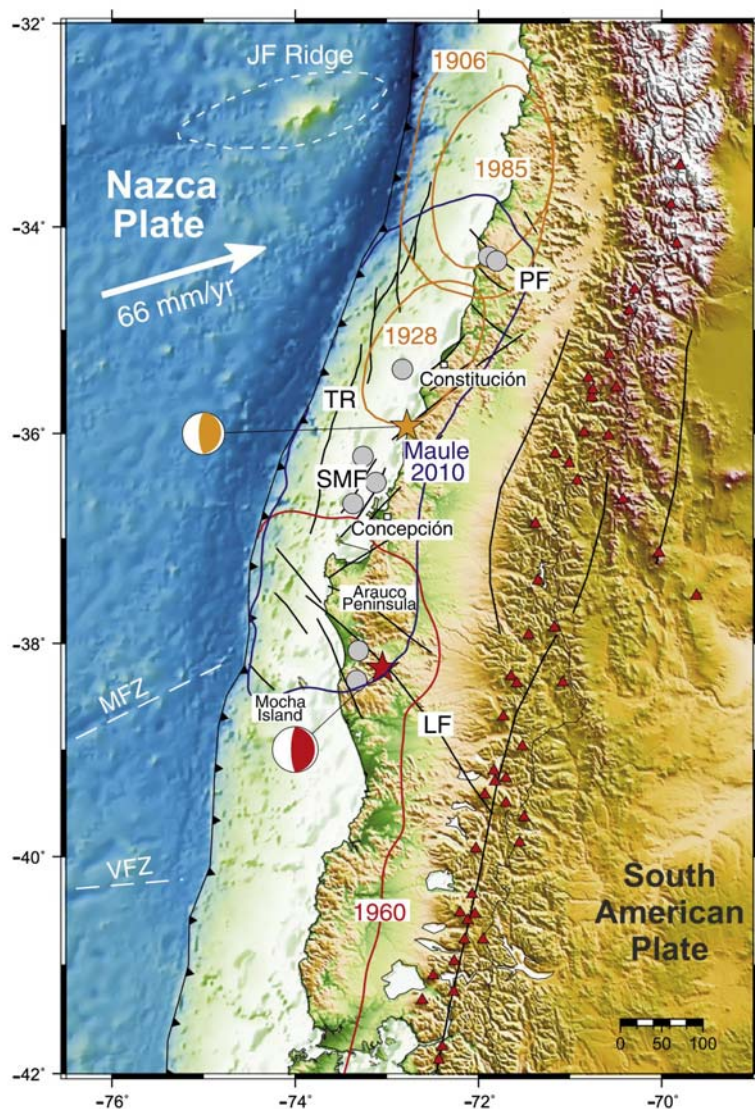


Figure 1.5.: Map showing the seismo-tectonic setting of the South-Central Chile megathrust. The blue and red lines depict the rupture zones (>1 m) and fault planes of the 2010 Maule and 1960 Valdivia earthquakes, respectively. The rupture zones of the 1906, 1928 and 1985 events are illustrated by orange lines. Gray circles are epicentral locations of largest Maule aftershocks ($M_w > 6.5$). Black lines show major plate faults: Thrust Ridge (TR), Santa María Fault (SMF), Lanahue Fault (LF) and Pichilemu Fault (PF). White dashed lines indicate the main oceanic features of the Nazca Plate: Juan Fernández Ridge (JF Ridge), and Mocha (MFZ) and Valdivia (VFZ) fracture zones. Active volcanoes are indicated by red triangles [Moreno *et al.*, 2012].

Major earthquakes exceeding $M 8.0$ have repeatedly ruptured the Nazca-South America plate interface along the Andean subduction zone where the Nazca Plate subducts the continental South American plate [Bookhagen *et al.*, 2006]. The Andean subduction zone

comprises three major seismic gaps along the Chilean coast. Recurrence intervals of >8.0M earthquakes are estimated to be around 83-123 years, depending on the segment of the subduction zone [Cisternas *et al.*, 2005b; Comte *et al.*, 1986]. The M8.8 Maule earthquake on February 27th 2010 closed the Darwin seismic gap [Lorito *et al.*, 2011; Moreno *et al.*, 2010] and caused intense ground shaking (up to 0.9g) for about 150 seconds (USGS NEIC Catalog, <http://earthquake.usgs.gov/earthquakes/eqarchives/epic>). Seismic gaps are zones likely to fail as inferred from plate tectonics and previous earthquake events. They are prone to failure because they form gaps in the spatiotemporal distribution of seismicity [Moreno *et al.*, 2010]. The strongest aftershock (Araucaria aftershock) occurred on January 2nd 2011 with a magnitude of 7.1 (USGS NEIC Catalog, <http://earthquake.usgs.gov/earthquakes/eqarchives/epic>). The Maule earthquake was preceded by three megathrust earthquakes in 1906 (M8.4) and 1985 (M7.8) hitting northern and north-central Chile and the 1960 (M9.5) Valdivia earthquake which ruptured the adjacent megathrust segment in the south (Figure 5). To this day, the latter remains the strongest registered earthquake (USGS NEIC Catalog, http://earthquake.usgs.gov/earthquakes/world/10_largest_world). The Valdivia event had been preceded the previous day by the M8.2 earthquake close to Concepción. In 1928, a megathrust earthquake (~M8) occurred in the northern part of the Darwin gap, likely having released only a relatively small fraction of the stresses accumulated since 1835. In 1835 the last great earthquake in the Darwin gap occurred with an estimated magnitude of ~M8.5 [Moreno *et al.*, 2010]. Four main tectonic features segment the plate along the Darwin gap: (1) north-south trending Thrust Ridge, (2) Santa María Fault (SMF), (3) Lanahue Fault (LF), and the previously unmapped Pichilemu Fault (PF) [Moreno *et al.*, 2012].

1.4. The Nacimiento hydrological and erosional study sites

The study sites are located close to the city of Nacimiento (37°29'S, 72°44'W) in the Biobío region about 500 km southward distance from the Chilean capital Santiago de Chile (Figure 1.6a). Nacimiento is within one of the national centers of timber and pulp production, where forestry is the most important economic sector of the whole area and which is recognized as the “wooden heart” of Chile [Patterson and Hoalst-Pullen, 2011].

The catchments are situated on the eastern slopes of the metamorphic coastal range facing the dry inner valley. All catchments are part of the Biobío river basin which is the most prominent river draining south-central Chile. The catchments cover between 7.8 and 412.9 ha and range in altitude between 250 and 450 m asl. All studied headwaters are restricted to the

uplands. Mean slopes vary from 14-22° though they may exceed 60° along creeks and road cuts.

The catchments are mainly used for intense plantation forestry. Most of the catchments (8 out of 11) were planted with *Pinus radiata* and *Eucalyptus globulus* before they were clear cut. These catchments were harvested during or after the study period. One catchment was already clear cut before the study was initiated and remained unplanted during the whole study period. One catchment covered with pine forest was selectively thinned. Two catchments retained secondary native forest and were excluded from any intervention.

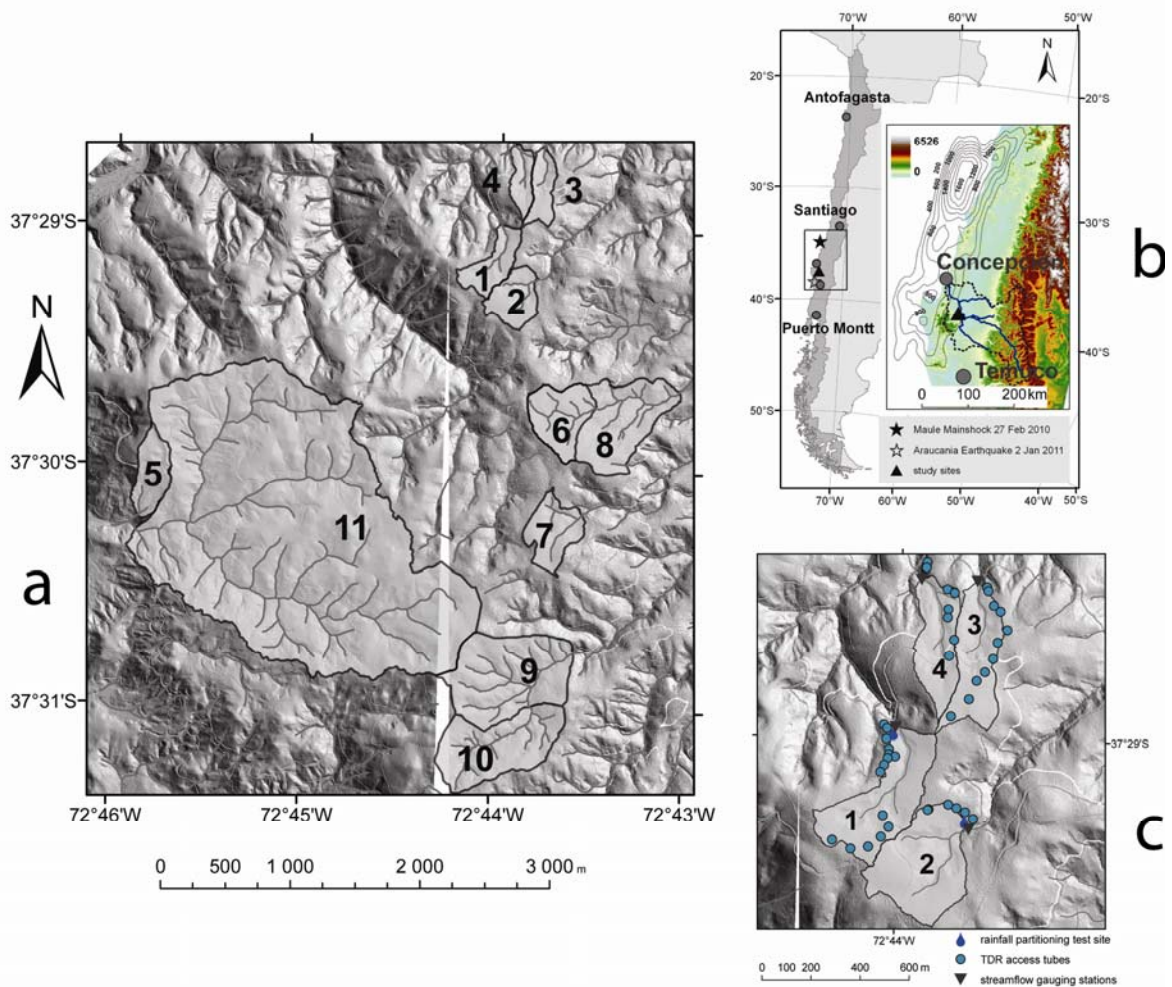


Figure 1.6.: (a) Overview showing the installed network of experimental catchments. Elevations are derived from airborne LiDAR. The number correspond to the numbering consistent with the following chapters of this thesis: 1: *P. radiata* control; 2: *P. radiata* selective thinning; 3 and 4: Former *P. radiata* plantation, clear-cutting in winter 2009 (3) and summer 2010 (4); 5: clear-cut in 2007 and laid fallow artificially; 6: *E. globulus* regeneration; 7: *E. globulus* plantation; 8: Mixed vegetation; 9: Native Forest; 10: Native Forest; 11: Juvenile *E. globulus* plantation. (b) Location of the study sites in Chile in relation to the epicenters of the Maule earthquake and the Araucaria aftershock, Biobío river basin is illustrated in the inset. Elevation data is derived from GTOPO30 data, the rupture contour lines are 2m [Tong *et al.*, 2010]; (c) Exemplary view of catchments #1-4 illustrating the location of TDR access tube transects, rainfall partitioning test sites and streamflow gauging stations.

The climate is subtropical Mediterranean style (rated as Csb according to the Koeppen-Geiger climate classification), meaning strong seasonality in both annual temperature and precipitation cycles: Annual average temperature is 13°C. Summer temperature can frequently exceed 40°C whereas winter temperatures can fall below 0°C at times. The hot summer temperatures promote high evapotranspiration rates. Long-term annual rainfall yields are ~ 1150 mm with the period from April-September contributing the bulk. Only 5% of the annual rainfall is spread across October to March. No creeks ever dried up during the study period despite very low summer flows.

Clayey-loamy Luvisol is the most common soil which is underlain by schistose bedrock that borders the granitic Nahuelbuta batholith to the south [*Melnick et al.*, 2009] making the local geology relatively homogeneous. A deeply weathered, loamy-sandy-textured saprolite layer of roughly 5-6 m depth acts as an interface below the soil layer and above the bedrock. The topsoil layer shows evidence of recent and former disturbances, e.g. truncated soil profiles, due to the action of timber harvesting.

The study sites lies close to the rupture zone at a distance of <130 km to the epicenter of the Maule Earthquake and the Araucania aftershock (Figure 1.6b).

A more detailed and study specific description of the studied catchments is given in chapters 2-6.

During the study period, the network thus consisted of catchments which were afforested with fast growing and water demanding plantation forests of different species while other catchments were clear cut using similar techniques but during different seasons and years. At the same time, the area was hit by a high magnitude earthquake and various (significant) aftershocks during dry stages of the study period. Together with the comparable geology, topography, soil type, their simple geometry and vicinity to each other, these experimental catchments provide exceptional preconditions to study the role of natural and man-made disturbances for hydrological and hydro-geomorphic processes.

Within the framework of this study, multiple field methods were applied to acquire data. Table 1.2 presents the data that has been obtained in each catchment (see also example in Figure 1.6c).

Table1.2. Water and sediment flux monitoring program performed. X indicates whether data is available or not for the respective catchment. *rainfall simulations have been conducted prior and after clear cutting in 2009.

Catchment #	Discharge	Suspended sediment	Bed load	Rainfall partitioning	Soil moisture	Water temperature	Rainfall simulations
1	X	X	X	X	X	X	-
2	X	X	X	X	X	-	-
3	X	X	X	-	X	X	X*
4	X	X	X	-	X	X	-
5	X	X	X	-	X	X	X
6	X	X	X	X	X	X	-
7	X	X	X	X	X	-	-
8	X	X	X	-	-	X	-
9	X	X	X	X	-	X	-
10	X	X	X	-	-	X	-
11	X	-	-	-	-	-	-

1.5. Aims, objectives and approaches

The main objectives of this research are:

- (1) To improve knowledge of the water balance effects of fast growing exotic species in plantation forests in Chile;
- (2) To further understanding of hydrological and erosion process responses associated with logging during different seasons; and
- (3) To enhance understanding of the coupled (real-time) interaction of near-surface tectonics and hydrogeological processes and properties by studying hydrological responses of the groundwater and the vadose zone to the Maule Earthquake.

To tackle the three objectives I have carried out the following work:

- Study the *Effects of Pinus radiata and Eucalyptus globulus plantations on water resource in the Coastal range of the Biobío region, Chile* (Chapter 2)
Chapter 2 investigates water balances and water quality of *Pinus radiata* and *Eucalyptus globulus* plantation forests by using a paired catchment approach. The field data thus obtained, e.g. soil moisture, runoff, interception loss, sediment transport are applied to the general water balance equation and statistically tested. Forest specific vs. (local) hydro-climatic effects on water consumption and sediment flux are discussed.
- Study the *Runoff generation and soil erosion processes after clear cutting* (Chapter 3)
Chapter 3 presents near-surface hydrological field data obtained by small scale rainfall simulation experiments on the forest floor and on harvest areas of different ages. The

field data is used to set up Random-Forest (RF) models to identify environmental controls and (dynamically altering) sources and sinks for runoff and sediment on harvest areas, respectively. The water and sediment fluxes observed at small scale, e.g. hysteresis effects, are linked to integrated observations at the catchment outlets.

- Study the *Seasonal Logging, Process Response, and Geomorphic Work* (Chapter 4)
Chapter 4 provides a catchment-scale estimate of sediment fluxes associated with clear cutting. To this end, Quantile-Regression-Forests-models (QRF) are set up comprising (1) time series variables evolving over time and (2) ‘switch variables’ that stratify data into pre- and post-earthquake periods in order to include changing environmental conditions. The modelled, high frequency sediment flux data are used to quantify sediment flux dynamics and changes in hydro-geomorphic work efficiency after logging during different seasons. Some complementary process-based modelling results of water and sediment fluxes after logging are briefly presented.
- Study the *Streamflow response in small upland catchments in the Chilean coastal range to the M_W 8.8 Maule earthquake on 27 February 2010* (Chapter 5)
Chapter 5 describes and evaluates possible near-surface seismo-hydrological processes under saturated flow conditions. The methods include recession analysis, water temperature signatures, simple diffusivity modeling, empirical magnitude-distance relations, and statistical analysis of catchment specific morphometric streamflow controls. Process hypotheses are discussed, based on Darcy’s equation, and concluding in a conceptual model of saturated zone response to earthquakes.
- Study the *Response of vadose zone water to earthquakes* (Chapter 6)
Chapter 6 proposes the response of the unsaturated zone to earthquakes supported by the development of a physics-based 1d-model. The numerical (hillslope-) model couples groundwater flow and evapotranspiration losses based on the ‘doing hydrology backwards’ approach with groundwater recharge from soil water. It is assumed that soil water is released when seismic shaking exceeds water retention. Process hypothesis are then tested quantifying streamflow response and enhanced vegetation activity following the earthquake. The results yielded a conceptual model of vadose-zone response to earthquakes.
- Chapter 7: *Summary and Conclusions*
Chapter 7 contains a critical discussion on if and how the three objectives may relate to each other, the overall summary, implications and conclusions and proposes future work.

The thesis structure is summarized in Figure 1.7. Chapters 2-6 are stand-alone manuscripts. These chapters are reproduced unmodified, except for cross-references which have been replaced by the respective chapter number. Chapter 2 has been published in a Spanish-speaking journal which required translation into English and thus slight modification (The unmodified paper can be found in the supplements). Chapter 4 contains a complementary section presenting the most important results and implications of physics-based water and sediment flux modelling. To be consistent with chapter 5, chapter 6 has been complemented by an illustration showing the conceptual model.

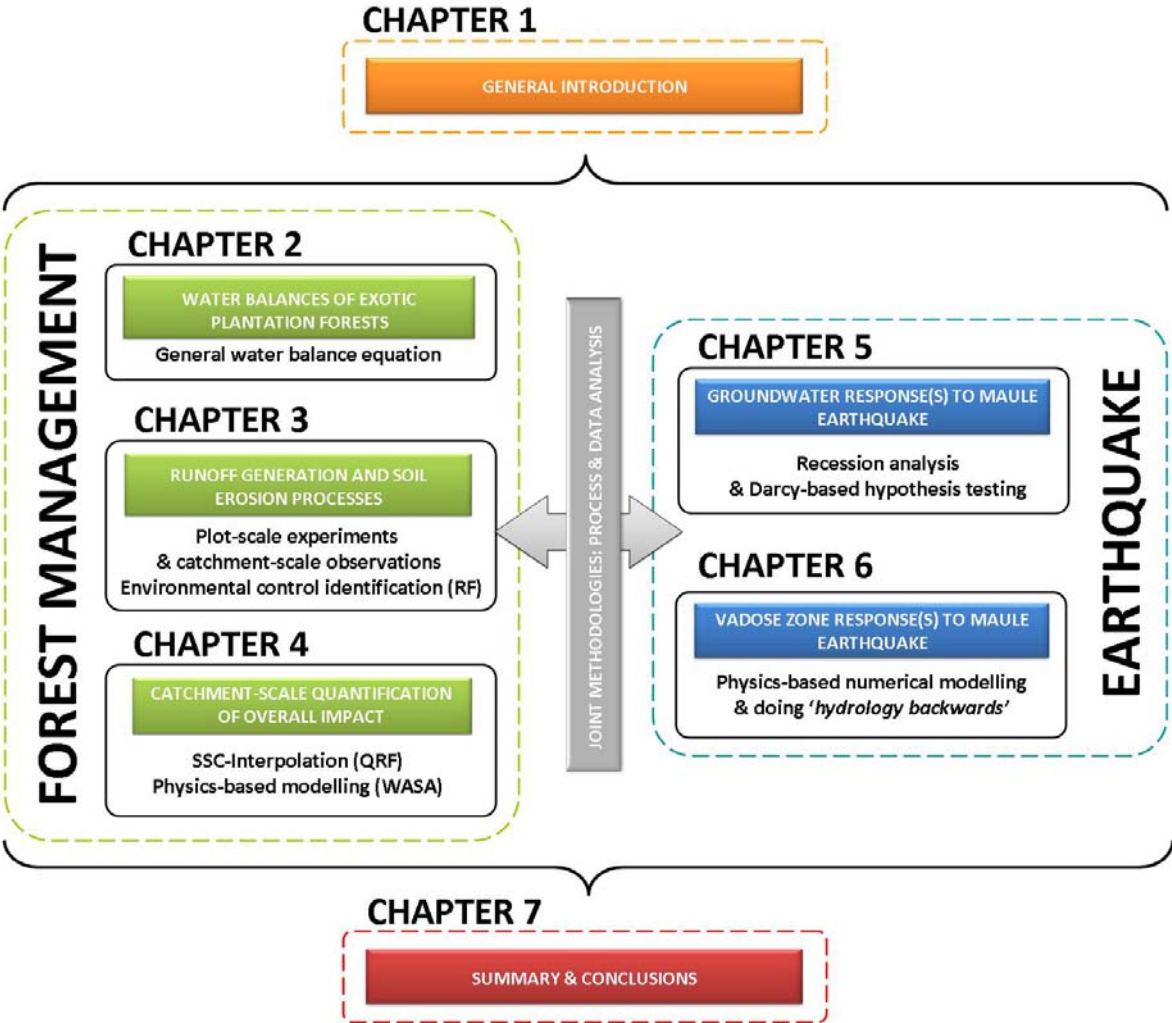


Figure 1.7.: Specific objectives of the thesis and organization of chapters. RF refers to Random Forest, QRF to Quantile Regression Forests and WASA is the acronym for the hydrological model Water Availability in Semi-Arid Environments [Guntner and Bronstert, 2004].

1.6. Author's contribution and publications

The bulk of the work described in chapters 1, 3-7 has been performed by the author. Significant contributions of data collection by Potsdam undergraduate students and invaluable discussion by the co-authors are acknowledged. The box presented in chapter 5 shows the main findings achieved by Potsdam undergraduate student Johannes Brenner and Braunschweig graduate student Christian Gläser. Both studies were co-supervised by the author. The author contributed significantly to chapter 2 by performing field data collection, statistical analysis and manuscript preparation (~30% of total work).

Chapters 2-6 are published or awaiting publication in international peer-reviewed journals as follows:

- Chapter 2 Huber, A., Iroumé, A., **Mohr, C.H.** and Frêne, C. (2010): The effect of *Pinus radiata* and *Eucalyptus globulus* plantations on water resource in the Coastal Range of Bió-Bío region, Chile, *Bosque* 31 (3):219-230.
- Chapter 3 **Mohr, C.H.**, R. Coppus, A. Iroumé, A., A. Huber and Bronstert, A. (2013): Runoff generation and soil erosion processes after clear cutting, *Journal of Geophysical Research – Earth Surface*, 118, 814 – 831, doi:10.1002/jgrf.20047, 2013.
- Chapter 4 **Mohr, C.H.**, A. Zimmermann, O. Korup, A. Iroumé, T. Francke, and Bronstert, A. (2013): Seasonal logging, process response, and geomorphic work. *Earth Surface Dynamics Discussions*, 1, 311-335 doi:10.5194/esurfd-1-311-2013.
- Chapter 5 **Mohr, C.H.**, D.R. Montgomery, A. Huber, A. Bronstert and Iroumé, A. (2012): Streamflow response in small upland catchments in the Chilean Coastal Range to the 8.8MW Maule Earthquake on February 27 2010, *Journal of Geophysical Research – Earth Surface*, 117, F02032, doi:10.1029/2011JF002138.
- Chapter 6 **Mohr, C.H.**, M. Manga, C.-Y. Wang, J.W. Kirchner and Bronstert, A.: Response of vadose zone water to earthquakes. (*Nature Geoscience*, under consideration)

Chapter II

Effect of *Pinus radiata* and *Eucalyptus globulus* plantations on water resources in the Coastal Range of the Biobío region, Chile

Abstract

Rainfall redistribution, temporal variation of streamflow discharge, soil water content, evapotranspiration, and sediment transport of two *Pinus radiata* and two *Eucalyptus globulus* catchments were determined. The catchments are located in the Coastal Range of southern central Chile. Due to their age, these plantations are to be harvested soon. The *P. radiata* plantations registered an interception loss of 17 and 16 %, values surpassing significantly the eucalyptus values of 10 and 11 %. The streamflows for the monitored period of 14 months at the two *Pinus radiata* catchments were 705 and 707 mm, and 439 and 500 mm for the two *Eucalyptus globulus* catchments. Despite the higher amount of rainfall reaching the soil in the eucalyptus-catchments, these catchments registered low streamflow compared to the pine-catchments. During the dry summer, all soils showed a severe reduction in their soil water content, exceeding the permanent wilt point in the soil's upper 30 cm. The *E. globulus*-catchments registered an evapotranspiration amount equal to 1582 and 1469 mm while it reached values of 1357 mm and 1298 mm in the *P. radiata*-catchments. These values correspond, for the *E. globulus*-catchments, to 74 and 68 % of total precipitation and 63 and 60 % for the *P. radiata*-catchments. These differences may be higher if water availability during summer drought does not limit the total evapotranspiration. The sediment export reached values of 237 and 615 kg/ha for the *P. radiata*-catchments and 152 and 125 kg/ha for the *E. globulus*-catchments during the monitored period.

Key words: streamflow, water balance, sediment transport, catchments, *Pinus radiata*, *Eucalyptus globulus*.

2.1. General introduction and background

There are diverse opinions on the real impact that forest plantations have on the water cycle and on the amount of erosion [Andreassian *et al.*, 2004; Boothroyd *et al.*, 2004; Brown *et al.*, 2005; Farley *et al.*, 2005; Gomi *et al.*, 2005; Hassan *et al.*, 2005; Hubbart *et al.*, 2007; Huber *et al.*, 2008; Iroumé *et al.*, 2006; Robinson *et al.*, 2003; Scott and Prinsloo, 2008]. In general, these authors agree that, years after the establishment of a plantation, streamflows begin to diminish due to the increase in the rate of evapotranspiration. After the final harvest, streamflow recovers to the initial levels, and the sediment transport rates increase.

Forests and particularly forestry plantations involve a major quantity of water in evapotranspiration, and register a higher water loss because of interception by the canopy, in comparison to other types of vegetative cover. The amount of these losses depend on the characteristics of the plantation (i.e. species, age and management), the quantity and intensity of the rainfall, and other meteorological conditions [Carlyle-Moses, 2004; Crockford and Richardson, 2000; Huber *et al.*, 2008; Iroumé and Huber, 2002; van Dijk and Bruijnzeel, 2001; Vega *et al.*, 2005].

The transport of suspended sediments has a fundamental role in the biogeochemical cycle of forested catchments [Karwan *et al.*, 2007]. These solids degrade the aquatic habitat and break the connections in the soil-water relationship, increase the transport of pollutants adsorbed on the particles, and increase the costs of treatment of water for public use [Gomi *et al.*, 2005; Rehg *et al.*, 2005]. The disturbances caused by forest management practices are responsible for intensifying the transport of suspended sediments [Hubbart *et al.*, 2007; Karwan *et al.*, 2007; May, 2007; Megahan *et al.*, 1995] which implicates important challenges for the trade-off between forest management and water quality [Karwan *et al.*, 2007].

The geomorphological units that are most degraded in the southern-central region of Chile are located on the eastern slope of the *Cordillera de la Costa*, or Coastal Range, in the so call *Secano Interior*, or the Interior Dryland, and mostly correspond to the Region of Biobio. In the past, this area was covered with native forests [Armesto *et al.*, 2010] that was extensively exploited, in many cases leaving the soil exposed to erosion. Currently, most of the surface area possesses herbaceous, bushy or forest plantation cover, or is used in agriculture and cattle raising. The degradation of these soils is most evident on hillsides with steeper slopes, and in soils that are heavily altered due to the preceding forestry interventions. The growing deterioration of these soils restricts its use to forestry activity, preferably to the afforestation with exotic fast growing species, and this has been a notable trend throughout

recent decades. In the Biobio Region, the area planted with *Pinus radiata* D. Don and *Eucalyptus spp.* is over 610.000 and 240.000 ha, respectively [INFOR, 2008].

Studies have been carried out in Chile on the consumption of water for both species [Huber *et al.*, 1998; Huber and Garcia, 1999; Huber and Iroumé, 2001; Huber *et al.*, 2008; Huber *et al.*, 1985; Huber and Trecaman, 2002; Huber and Trecaman, 2004; Iroumé *et al.*, 2006; Oyarzun *et al.*, 1985]. However, there is little evidence to indicate the magnitude of the erosive processes that are registered on these forested areas [Oyarzun, 1993; Oyarzun and Pena, 1995; Pizarro and Cuitino, 1999].

This study has the objective of contributing to the knowledge about the impact that forestry plantations have on the water resource in the central-south region of Chile. The hypotheses of this investigation are: a) the distinct characteristics displayed by the forest canopy affect the loss of water due to interception and thus the total quantity of water that reaches the ground in the catchment; b) that the uneven amount of water involved in evapotranspiration effects streamflows and c) that the dissimilarities between the different components of the hydrological cycle, and particularities of the catchments define the quantity of sediments transported. To test these hypotheses, water balances, hydrological dynamics and the sediment transport of micro-catchments forested with *Pinus radiata* D. Don and *Eucalyptus globulus* located on the eastern slope of the Cordillera de la Costa in the Region of Biobio, southern Chile, are compared.

2.2. Methods and study sites

Characteristics of the study area. For the study, four micro-catchments were chosen, located 3 km to the west of the city of Nacimiento, Biobio Region, Chile (latitude 37° 28" S, longitude 72° 42" W), belonging to the company Forestal Minico S. A. (Figure 2.1).

The catchments are located on the eastern slope of the Cordillera de la Costa, with less than 1.5 km between them. Two of these catchments are forested with *Pinus radiata* and the others with *Eucalyptus globulus*, and each one on the verge of reaching rotation age. The streambeds of the catchments were located in ravines that have been affected by hydric erosion over time. The mean slope is over 20 %, which induces substantial torrential action during the rainiest season of the year. The hydro-geomorphic characteristics of each catchment are presented in Table 2.1.

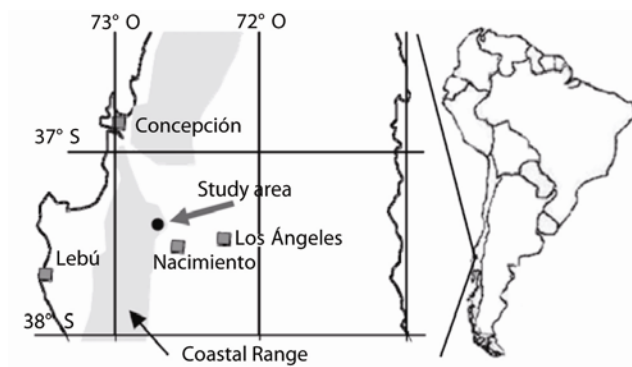


Figure 2.1. Location of the forested experimental catchments in Nacimiento, Chile.

The area has a Mediterranean climate with an annual rainfall of ~1150 mm which is concentrated between April and September [Fuenzalida, 1971; INIA, 1989]. There is a short dry season in the summer (less than four months) during which it does not rain more than 5% of the annual total.

Table.2.1. Hydro-geomorphologic characteristics of the *Pinus radiata* and *Eucalyptus globulus* catchments. Gravelius index describes the relation between the perimeter of the watershed and that of a circle having a surface equal to that of a watershed, the orographic coefficient is defined as (mean catchment altitude-altitude of the catchment outlet)/ catchment surface; drainage density as the sum of the lengths of all creeks of the catchment/ catchment surface; feed channel as the sum of the lengths of all tributaries in the catchment/ catchment surface; the mean distance length of the main channel/ square root of catchment surface and the storm ratio as the sum of first order channels/catchment surface.

	Catchment			
	Pine 1	Pine 2	Eucalypt 1	Eucalypt 2
Catchment area(ha)	12.55	13.98	16.72	21.1
Lenght of priniciple stream (km)	0.47	0.41	0.45	0.62
Catchment slope (%)	25.2	30.3	27.7	36.5
Slope of stream (%)	22	24	26	27
Perimeter (km)	1.7	1.57	2.0	2.1
Gravelius index	1.35	1.18	1.37	1.25
Mean altitude (m asl)	327	331	369	320
Orographic coefficient (m ² /ha)	85.01	78.44	81.48	48.51
Drainage density (km/km ²)	4.67	4.40	5.91	6.67
Feed channel (km/km ²)	0.21	0.23	0.17	0.15
Mean distance (km)	1.34	1.09	1.11	1.35
Storm ratio	37.16	31.48	35.33	31.63

Rainfall events in this zone have different durations and may last up to several days, and the intensities rarely surpass 20 mm/h. The precipitation of the zone is commonly of the cyclonic or frontal type. Considerable inter-annual differences are registered in its amount, and its local distribution is influenced by the topography of the mountain range. During rainfall events, and due to the high altitude of the catchments, the plantations are generally immersed in fog or clouds. The mean annual air temperature is 13 °C and oscillates between 7 °C in July and 19 °C in January. During summer, in days with high solar radiation, maximum temperatures can be registered above 40 °C. Due to the rapid ascent of the thermal state of the air, the relative humidity can descend to lower than 20%¹. These meteorological conditions promote high potential evapotranspiration.

Soils in the area derive from metamorphic rocks whose texture is influenced by its evolution and erosion. These soils range from sandy-loamy to clayey-loamy texture in the topsoils, and to sand and clay the deeper they are, with moderate internal drainage [*Schlatter et al.*, 2003]. The interface between the soil and bedrock comprises a deep and sandy saprolite. In the study sites, the soil had variable depths that fluctuated between 0.5 and 3 m.

The water infiltration velocity² of these soils in a saturated condition varies between 3 and 10 mm/h. The variability is principally due to the heterogeneous structure of the soils, which contain a considerable quantity of rocks and fragmented stones of different sizes. To this is added the spatial distribution of the roots of the herbaceous, bushy, previous and current forestry plantation vegetation, along with the disturbances that they were exposed to during previous forestry activities. Considering the intensity of the rainfall amounts in the study area, these characteristics are not an important obstacle to the wetting of the complete soil profile. The characteristics of the two pine plantations (*Pine 1* and *Pine 2*) are presented in Table 2.2. These plantations were established in 1987 with an initial density was 1250 trees/ha, and correspond to a second rotation. At the time of the study the trees were 23 years old, and were soon to be harvested. Two thinnings and one pruning at 6 meters above the ground had been carried out during the lifespan of the trees.

The soil under these plantations was covered by mulch, dominated by a layer of needles of not more than 2 to 3 cm thick in average, but reaching up to 8 cm thick in microdepressions. The herbaceous cover was scarce (< 25%), and principally comprised grasses that habitually die during the summer because of hydric stress. The bush cover was sparse, comprising mostly maqui (*Aristotelia chilensis* Mol.), blackberry, (*Rubus radicans* Cav.), as well as some arboreous species, still of low height, such as litre (*Lithraea caustica*

¹ Registers carried out during the study with thermal hydrographs

² Determined by double-ring infiltrometers [*Steubing and Fangmeier*, 2001]

Mol), boldo (*Peumus boldus* Mol.) peumo (*Cryptocarya alba* Mol), arrayán (*Luma apiculata* DC. Burret.), avellano (*Gevuina avellana* Mol.) and occasionally roble (*Nothofagus obliqua* (Mirb.) Oerst.).

Table 2.2, Characteristics of the *Pinus radiata* and *Eucalyptus globulus* plantations.

	Catchment			
	Pine 1	Pine 2	Eucalypt 1	Eucalypt 2
Age (years)	23	23	9	9
Mean height (m)	28.2	28.2	20.4	20.3
Tree density (ha ⁻¹)	320	315	1174	1326
DBH (cm)	36.0	35.4	15.9	15.2
Canopy cover (%)	65	65	50	55
Height of pruning (m)	5.9	5.7	-	-
Basal area (m ² /ha ⁻¹)	32.9	31.7	24.3	25.2
Riparian buffer (ha)	1.5	0.9	0.8	1.0

The stream of the *Pine 1* catchment contains along its entire course a riparian protection zone with a width of 13 m ± 4 m. In the *Pine 2* catchment, the protection zone had a width of 11 m ± 3 m. The bushy and arboreous layer of these zones presented a cover that fluctuated between 50 and 70 %, composed of quila (*Chusquea quila* Mol.), zarzamora, maqui, lingue, (*Persea lingue* Nees.), arrayán, avellano, boldo and oak. The herbaceous vegetational cover was low (< 25 %), and together, all the layers generated a cover of > 75 %.

The particularities of the two eucalyptus plantations are presented in Table 2.2. *Eucalyptus 1* was a second rotation plantation established in 1999. *Eucalyptus 2* was the same age, but comprised scrubland, or regeneration of stumps, with each stump having 2 or 3 trunks. The ground surface of each catchment was covered by homogeneous mulch that was no more than 2 cm thick in average. The shrub cover was sparse, composed principally of tetamillo (*Teline monspessulana* (L.) Koch) and some individuals of mosqueta (*Rubus ulmifolius* Schott f.). The herbaceous vegetation was also scarce, and comprised some grasses that die during the summer.

The streams of the catchment *Eucalyptus 1* comprised a riparian protection zone of a total section of 41 m ± 6 m along the entire course. In the lower part of the micro-catchment, close to the weir, a small flooded area was observed. The shrub and arboreous layer of this area gave a cover of close to 75%, composed of blackberry, quila, maqui and retamillo, with the occasional presence of some arboreous individuals of smaller size such as lingue, arrayán, peumo, roble and some pine trees. Also observed were several canelos (*Drimys winteri*

Forster) and nalcas (*Gunnera tinctoria* (Mol.) Mierbel.) in the flooded zone. The herbaceous cover was scarce (< 25 %), and principally composed of quilineja (*Luzuriaga radicans* Ruiz et Pavón.) and voqui (*Boquila trifoliolata* (DC) Decne), and also ferns (*Lophosoria quadripinnata* (Gmel.) Chr). The ground was covered by fractionated, eucalyptus leaf mulch, with an approximate average depth of 2 cm. Overall, total cover reached > 75%.

The stream of the *Eucalyptus* 2 catchment also comprises a riparian protection zone of 52 m ± 8 along its course. The bush and tree stratum of this area showed a cover of close to 60 %, made up of blackberry, quila, maqui and murta (*Ugni molinae* Turcz.), with the occasional presence of boldo, lingue, peumo, roble, piñol (*Lomatia dentata* (Ruiz et Pavón) Br.), naranjillo (*Citronella mucronata* (Ruiz et Pavón) and chupón (*Greigia sphacelata* (Ruiz et Pavón) Regel). The herbaceous cover was scarce (<25%) and the ground was covered by a mulch of eucalyptus leaves with an average thickness of 3 cm. Overall, total cover was close to 65 %.

Rainfall and Rainfall Partitioning. The quantity of gross precipitation that fell on the catchment was determined with a pluviograph (Hobo), located on an open field, close to the plantations. The total quantity of water that reached the ground (net precipitation) was divided into throughfall and stemflow:

$$P_N = P_{TH} + P_S \quad (2.1)$$

Where P_N = net precipitation (mm), P_{TH} = Throughfall (mm) and P_S = Stemflow (mm).

Due to the extraordinary temporal distribution of the precipitation during the study period, the measurement period was extended to September 2009. This was necessary so that the soils, at the end of this period, would reach water content similar to the initial values. This condition is an indispensable requirement in order to calculate the amount of water involved in evapotranspiration (see Equation (2.4) latter in the text).

The losses of water by interception were considered to be equivalent to the difference between the gross precipitation registered in an open field and the net precipitation:

$$I_C = P_G - P_N \quad (2.2)$$

Where I_C = water losses due to interception (mm) and P_G = gross precipitation (mm).

To quantify the rainfall partitioning, an area measuring 15x40 m was delimited in each catchment. The precipitations that reached the ground (throughfall) were collected by V shaped metallic gutter, 15 cm wide and 30 m long, installed at 30 cm above the ground. The fraction of the precipitations that reached the ground using the stems as a waterway (stemflow), was collected with rubber collars sealed around the stems of 15 trees in concordance with the method proposed by *Huber and Oyarzun* [1984]. The water collected in each case was channelled to its recipient equipped with a water stage logger.

To test for possible significant differences between the losses of water by interception between the different catchments, the values of the registered water for each one of the rainfall events were compared applying the Mann-Whitney test [*Crawley*, 2005].

Streamflow. Streamflow was measured at the outlets of each of the catchments by Thompson-style weirs made of concrete. Each construction was 3 m long, 1.5 m wide, and with a notch of 60°, whose vertex was located 50 cm above ground level. Due to the stony streambeds, the weirs were inserted at a depth of 50cm into the streambed in order to prevent subterranean leakage. Due to this necessity, a wall of 50 cm was implemented along the entire width of the spillway. This transformed the spillways into receptacles with a surface area of 4.5 m². They were used as traps for bedload and deposited suspended sediments, and at the same time, to act as basins for the suspended sediments that were moved downstream. In the frontal wall of the weir, at 29 cm along each lateral wall, and at the height of the base of its floor, doors were fixed at 30 cm wide and 20 cm tall. These closures were opened during the cleaning of the weir, in order to facilitate the evacuation of the water and of the material deposited at the bottom at the end of periodic controls. In order to determine the streamflow discharge, a hydrometric station was installed in each weir. This equipment, built at the Universidad Austral de Chile, functioned with the flotation principle at an accuracy of 2mm. Each weir was calibrated on site through periodic gauging to cover an ample range of streamflows to achieve the corresponding water stage rating curves (3rd degree polynomial equation, $R^2 = 0.999$, $P < 0.01$). The recording interval of was fixed at three minutes.

This information determined the temporal variation for discharge of each stream. Statistical comparisons were carried out on the hourly values of streamflow of the catchments using the Mann-Whitney U test. All the statistical analysis was developed using the statistical environment R [*R Core Development Team*, 2009]. In all the statistical analysis, the difference between treatments were considered significant when $P \leq 0.05$.

The coefficients were also determined for the streamflow of each catchment to obtain the simple relationship between the total streamflow of the study periods and the gross precipitation during the same time periods.

For each precipitation event that was manifested in the hydrograph, the fraction of quickflow was determined that participated in the total streamflow. For this partition the constant slope method was used. By doing so, the temporal variation of the contribution of quickflow to total streamflow was determined for all catchments. Here, quickflow refers to the portion of streamflow provided by overland flow and fast responding interflow while baseflow corresponds to the sum of deep subsurface flow and delayed shallow subsurface flow [Kendall and McDonnell, 1998].

Sediment Transport. To determine the quantity of suspended sediments that passed through each weir, a floating rectangular structure (50 x 30 cm) was built with 5 cm PVC tubes. To this frame, a 12 V electric pump was fixed, whose intake stayed submerged at 5cm depth. This location was maintained constant, given that the PVC structure was connected to two mobile arms 1.5 m long, fixed at the highest point of the lateral walls for the weir.

To obtain representative and homogeneous integrated samples, the pump sampled water volumes that were always directly scaled to water stage, with higher discharge contributing commensurately more than lower water stages. The water from four daily samples was stored for seven days in a receptacle. On this basis, weekly volume weighted bulk samples were calculated. The amount of sediment in this water was found using a filtration system with a vacuum pump. Fiberglass filters were used (Advantec GF75 477 mm) that were dried at 60°C for 48 hours. This value was multiplied by the discharge of the corresponding period to calculate the suspended sediment load.

Periodically, the sediments that had deposited in the bottom of the weir were quantified. In order to obtain these data, a device was constructed which consisted of an iron disc, 8 cm in diameter and 1 mm thick, that had a thin layer of rubber on its upper face. In the center of the upper face of the iron disk, there was a small iron rod, 5 mm diameter and 1.5 m long. Six of these structures were distributed systematically and equidistant in each of the weirs, positioned at 40 cm from each of the lateral walls.

To quantity of sediments deposited on each disc, a 4 cm diameter steel tube was placed such that one of its ends which had a sharp edge made contact with the rubber on the iron disc. At the other end, a handle was welded on that permitted it to be turned with force, pressing the tube against the rubber to secure a good seal. To maintain the equidistance to the

rod and also to ensure a concentric location on the disc, the tube had a floating guide in the interior. Once this positioning and contact was achieved, the 4 mm diameter tube was pressed to make a hermetic seal against the disc with a piece that was screwed onto the metal rod.

Subsequently, the device was taken out, and its contents placed in a receptacle. Again, the samples were dried at 60 °C for 48 h. The weight of the solid material was considered to correspond to the quantity of sediments that were deposited on the surface of each disc. The average value was obtained from the six discs and the area from the ground to the weir was extrapolated to calculate the total quantity of sediments deposited. Because only weekly and non-normally distributed data were available in this study, the statistical analysis was carried out by a more robust non-parametric Kruskal-Wallis test [Crawley, 2005].

Soil water and evapotranspiration. Approximately every 30 days, the spatio-temporal and distribution of the soil water content was determined up to a depth of 2.5 m. To this end, measurements were made with a TDR (TRIME-FM3 T3, Field Measurement Device Version P3, IMKO). These measurements were made along transects at 10 points, equally distributed across the lower, middle and upper slopes of the catchments. Depth increment was 10 cm. To determine the amount of water involved in the evapotranspiration of the catchments, the following equation was used following Chang (2006):

$$EvTr = P_G - Q - \Delta R - \Delta F \quad (2.3)$$

Where $EvTr$ = evapotranspiration, Q = streamflow discharge, ΔR = change in soil water storage and ΔF = change in the groundwater storage.

As it was not possible to determine the periodic groundwater variation, it was not possible to infer the temporal variation in evapotranspiration. In consequence, the quantity of water involved in evapotranspiration could only be established for the complete period, i.e. one hydrological year, assuming that the groundwater volume at the beginning of the study period was similar to that at the end ($\Delta F = 0$). Thus, the equation (2.3) could be simplified to the equation (2.4):

$$EvTr = P_G - Q - \Delta R \quad (2.4)$$

2.3. Results

Precipitation and Canopy Interception. The total precipitation during the study period (15 July 2008 - 30 September 2009) was 2149 mm (Table 2.3). The highest rainfall was registered between the months of May and September, while the dry months were exceptionally deficient in precipitations.

In the catchments with pine trees, the interception values that corresponded to each one of the rainfall events did not register statistical differences ($P = 0.846$), and a similar situation occurred among the eucalyptus catchments ($P = 0.370$). The plantation *Pine 1* had a higher interception value than *Eucalyptus 1* and 2 ($P < 0.05$ and $P < 0.01$), which was similar to the result that was registered between *Pine 2* and the two catchments of eucalyptus ($P < 0.01$ and $P < 0.001$).

Streamflow. The runoff coefficient for the two catchments planted with pine was 33 %, and for the *Eucalyptus 1* and 2 of 20 and 23 %, respectively (Table 4). The daily amount of water that passed through the weir of the forested catchments with pine during the entire period did not have significant statistical differences ($P = 0.680$). The situation between *Eucalyptus 1* and 2 was different ($P < 0.05$). There were also significant differences between *Pine 1* and *Eucalyptus 1* ($P < 0.01$) and between *Pine 2* and *Eucalyptus 1* ($P < 0.01$). The total streamflow in the *Pine 1* catchment showed a tendency to be higher than *Eucalyptus 2*, but the differences were not significant ($P = 0.588$). Similar results were obtained between the *Pine 2* and *Eucalyptus 2* catchments ($P < 0.356$).

The contribution of the subsurface component (base flow) to the total flow for the catchments with *Pine 1* and 2 were 73 and 74 %, respectively, and for the catchments *Eucalyptus 1* and 2 of 70 and 75%, respectively. There were no significant differences between the periodic values of the catchments with pine ($P = 0.230$), nor between those of eucalyptus ($P = 0.298$). Similar results were obtained between the catchments *Pine 1* and *Eucalyptus 1* and 2 ($P = 0.267$; $P = 0.305$) and between *Pine 2* and *Eucalyptus 1* and 2 ($P = 0.258$; $P = 0.317$).

Soil water and evapotranspiration. The spatio-temporal variation in the soil water content for the four catchments in the first 2.5 m of depth is presented in Figure 2.2 and Table 2.3.

The quantity of water involved in the total evapotranspiration for the entire period of *Pine 1* and 2 was equivalent to 1405 and 1388 mm, respectively (Table 2.3), which

corresponds to 65 and 64 % of the total precipitation, respectively. For *Eucalyptus 1* and 2, these values were 76 and 70 %, which is equivalent to 1630 and 1511 mm respectively (Table 2.3). When such relationships are calculated for net precipitation only, the values decreased for *Pine 1* and 2 to 58 and 56 % and for *Eucalyptus 1* and 2 73 and 66 %, respectively.

Sediment Transport. The temporal variation in the total quantity of sediments (bedload and suspended) for each the catchments is summarized in Table 2.3. The values between the pine catchments did not show statistical differences ($P = 0.311$). Neither did the catchments planted with eucalyptus ($P = 0.305$). Similar results were obtained between the catchments *Pine 1* and *Eucalyptus 1* and 2 ($P = 0.291$, $P = 0.301$) and *Pine 2* and *Eucalyptus 1* and 2 ($P = 0.316$ and $P = 0.301$).

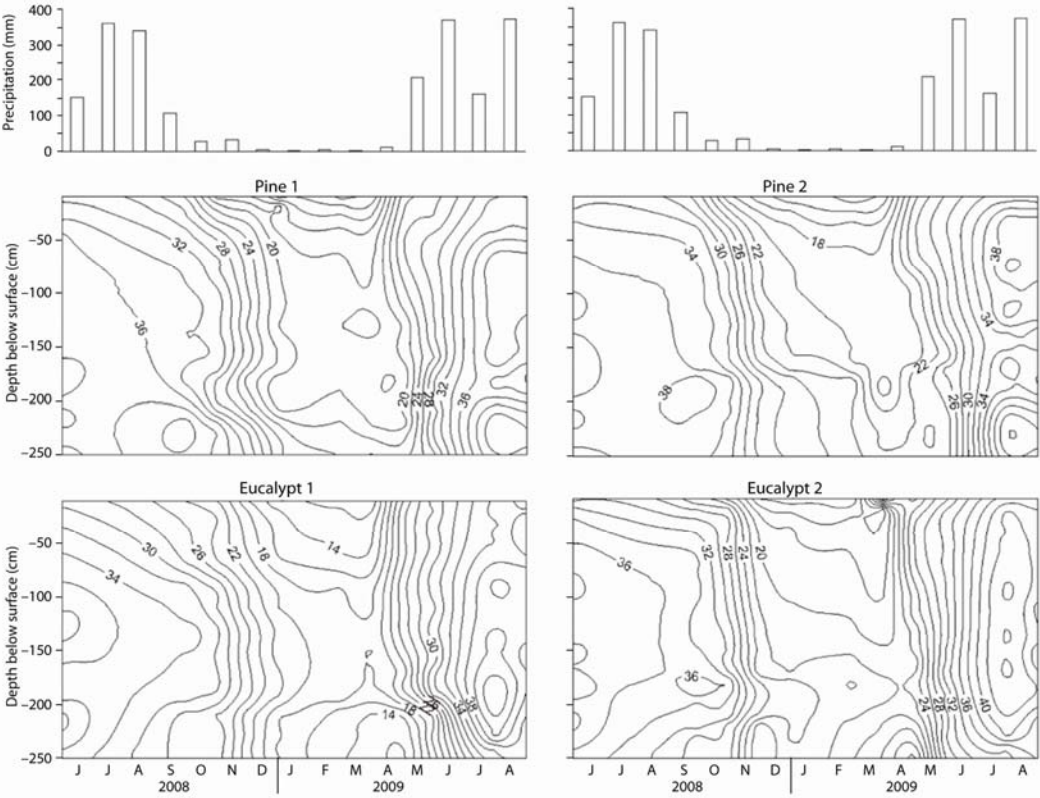


Figure 2.2. Spatio-temporal variation of soil water content (% Vol) of catchments forested with *Pinus radiata* and *Eucalyptus globulus*.

Table 2.3. Values of total precipitation (P), interception loss (I), streamflow (Q), quick flow (Qs), base flow (Qb), evapotranspiration (ET), soil water content (0-2.5 m) (soil) and total sediment export (St) for *Pinus radiata* (Pine 1 and 2) and *Eucalyptus globulus* (Eucalypt 1 and 2) catchments for the monitored periods. Data collection started June 15th, 2010; (-) indicates absence of data available.

month	2008						2009										
	6	7	8	9	11	12	1	2	3	4	5	6	7	8	9		
day	15	10	13	30	8	20	7	13	18	16	20	18	14	15	30		
#period	1 2 3 4 5						6 7 8 9 10 11 12 13 14 Σ										
Pine 1	P (mm)	209	231	412	38	32	1	6	4	16	156	237	308	266	234	2.149	
	I (mm)	38	39	43	12	19	3	4	2	7	37	37	43	38	35	357	
	Q (mm)	58	115	174	26	11	2	2	2	2	6	19	92	63	133	705	
	Qs (mm)	17	18	66	1	0	0	0	0	0	2	7	35	20	22	188	
	Qb (mm)	41	97	109	25	10	2	2	2	2	4	12	56	43	111	517	
	ET (mm)	-	-	-	-	-	-	-	-	-	-	-	-	-	-	1.405	
	soil (mm)	923	941	950	855	770	576	506	483	467	450	555	711	775	959	962	-
	St (kg/ha)	32	41	15	4	3	1	0	0	0	1	41	36	52	11	237	
Pine 2	I (mm)	41	33	40	11	16	3	4	3	5	32	39	38	35	37	337	
	Q (mm)	62	113	170	30	15	3	2	2	3	7	11	91	68	129	707	
	Qs (mm)	24	20	59	1	1	0	0	0	0	2	6	33	19	21	185	
	Qb (mm)	38	93	112	30	14	3	2	2	2	5	5	58	49	108	522	
	ET (mm)	-	-	-	-	-	-	-	-	-	-	-	-	-	-	1.388	
	soil (mm)	912	935	942	838	724	521	458	435	411	406	498	727	782	957	966	-
	St (kg/ha)	96	102	34	6	7	2	1	1	3	8	86	127	127	14	615	
	Eucalypt 1	I (mm)	21	35	32	15	16	2	2	3	1	6	22	12	28	20	215
Q (mm)		44	95	127	23	11	3	2	1	2	4	15	45	26	40	439	
Qs (mm)		17	16	40	1	0	0	0	0	0	2	8	23	10	12	130	
Qb (mm)		26	79	87	23	11	3	2	1	1	2	7	22	16	29	309	
ET (mm)		-	-	-	-	-	-	-	-	-	-	-	-	-	-	1.630	
soil (mm)		905	928	940	760	712	512	467	426	409	389	525	693	745	980	985	-
St (kg/ha)		68	22	11	6	2	0	1	2	1	3	17	10	7	2	152	
Eucalypt 2		I (mm)	31	36	30	18	9	1	2	4	2	13	20	20	31	18	235
	Q (mm)	56	99	151	28	14	3	3	2	2	6	16	42	28	50	500	
	Qs (mm)	17	12	43	0	1	0	0	0	0	2	8	21	10	11	124	
	Qb (mm)	39	86	108	28	14	3	3	2	2	4	8	21	18	39	376	
	ET (mm)	-	-	-	-	-	-	-	-	-	-	-	-	-	-	1.511	
	soil (mm)	924	941	951	816	747	542	522	502	494	484	579	778	823	1.055	1.062	-
	St (kg/ha)	51	15	9	6	2	0	1	1	3	4	14	8	7	2	125	

2.4. Discussion

Precipitations. The precipitation for the 14 month study period is similar to the long term average for 14 month-periods in the area (*INIA* 1989). In general, the temporal distribution is maintained, resulting in the pluviometric deficiency during the summer. During dry periods, almost all precipitation is intercepted by the forest cover. The differences between the characteristics of the plantations of pine and eucalyptus are the principal factors responsible for the unequal water loss due to interception. These dissimilarities are due principally to the fact that the conifers have a larger retention capacity than broadleaf species [*Crockford and Richardson*, 2000; *Fleischbein et al.*, 2005; *Huber and Iroumé*, 2001; *Link et al.*, 2004]. Also, the younger age of the eucalyptus plantations had an influence, generating a lower development of the canopy. These conditions generate a lower canopy cover, in spite of having a higher leaf density. As a result, the net precipitation in the catchments with eucalyptus is significantly higher than those with pine plantations.

The water losses by interception determined in the study are inferior to those registered by *Huber and Oyarzun* [1984], *Huber et al.* [1998], *Huber et al.* [2008], *Iroumé and Huber* [2000], *Iroumé and Huber* [2002], and *Huber and Iroumé* [2001] in other parts of Chile and by *Klaassen et al.* [1998], *Fleischbein et al.* [2005], *Deguchi et al.* [2006], and *Cao et al.* [2008] in other parts of the world. This is principally due to the high altitudinal location of the catchments, which allows the plants to be frequently immersed in fog or clouds during precipitation events. Under these meteorological conditions, the trees intercept a part of the humidity in the cloud cover as an addition to throughfall which in turn increases the net precipitation. This situation slightly undervalues the real value of the interception loss from these plantations in this zone. During light rain events with low intensity, the additional water input by fog interception means that the ground receives a quantity of rain that is higher than the precipitation on open fields. However, in every case, the water input by these sources, in comparison to the annual input by rain, is very low at this location. These tendencies are similar to those recorded by *Klaassen et al.* [1998], *Holder* [2004] and *Fleischbein et al.* [2005].

Soil water. The spatio-temporal variation in soil water was similar in the four catchments. At the beginning of Period 4, when the rains diminished and the meteorological conditions increased the intensity of evapotranspiration, a decrease was registered in soil water supply. This situation was manifested throughout the entire the profile, but with a higher intensity in the first 1.5 m of depth. In Periods 8 and 9, the soil water content in the

first 20 cm dropped to values lower than those of permanent wilting (14 % vol). This state was manifested especially in the herbaceous component of the vegetation that is killed by the lack of water.

At the beginning of the study, which coincided with the rainiest season of the year, the soil water content in the first 2.5 m of depth was similar for all of the catchments. This value is close to the soil water retention capacity. During the period with less precipitation and higher consumption of water by evapotranspiration, the water reserves diminished, reaching a minimum at the beginning of fall. As a consequence, the amount of water available for the development of trees dropped considerably. At the beginning of period 10, which coincided with the beginning of winter and a decrease in the intensity of evapotranspiration, there was a continuous recharge of soil water that reached a maximum in September in each catchment.

The maximum difference between the extremes of soil water content during all the periods in the pine catchments (512 and 560 mm) and eucalyptus (596 and 578 mm) was reduced. This is principally due to the fact that at the beginning of the study the soil profile in the different catchments was virtually saturated and at the end of the dry period, it had dropped to a minimum that was also similar in each catchment. This last situation was achieved because most of the soil water, especially in the first 1.5 m, was consumed by the plantations during the dry period. In consequence, this condition restricts the plantations from reaching their best growing potential during the summer [Andreassian *et al.*, 2004; Carroll *et al.*, 2000; Zhou *et al.*, 2002]. At the same time, this is a circumstance that reduces the differences that can exist between the extreme consumption of water from both species, especially during the periods which are deficient in rainfall [Putuhena and Cordery, 2000].

Streamflow. The temporal variation in the four outfalls from the catchments is principally regulated by the annual rainfall regime, the variation of soil water content and evapotranspiration [Blume *et al.*, 2007; Mayor *et al.*, 2009].

The extreme drainage of the soil water reserve during the dry period explains why the increase in precipitation from March to June does not lead to a similar increase of streamflow discharge. This water is required to saturate the soil profile first, and with that create the precondition to generate saturation excess overland flow capable of significantly increasing the total streamflow discharge.

The total streamflow from the two pine catchments for all periods was the same, which is reflected in the same runoff coefficients. This situation could be the consequence of the similarity that exists between both catchments and in the characteristics of the plantations.

The catchment *Eucalyptus 1* registered a lesser runoff coefficient in comparison to *Eucalyptus 2*. This difference could be the consequence of the lower slope of *Eucalyptus 1* [Blume et al., 2007; Carroll et al., 2000]. The runoff coefficients have a strong temporal variation because of being influenced by the climatic conditions, especially by the rainfall regime, soil saturation and evapotranspiration [Blume et al., 2007].

The streamflows from the catchments planted with pine registered a higher discharge for all periods than those with eucalyptus, although less water in these catchments actually reaches the ground, due to the higher interception loss.

Base flow is the principal component of total discharge in all the streams. Its participation varies according to the temporal distribution of the rainfall. During the winter, especially when soils are saturated, overland flow increases its relative participation in total streamflow at the expense of base flow. A contrary situation occurs during the dry season, where the lack of important rainfall causes base flow to be the exclusive component [Blume et al., 2007; Onda et al., 2001].

Evapotranspiration. The amount of evapotranspiration for both species agreed with results from other studies carried out in Chile that used different methodologies [Huber et al., 1998; Huber et al., 2008; Huber et al., 1985; Huber and Trecaman, 2002; Huber and Trecaman, 2004; Oyarzun et al., 1985].

The evapotranspiration, which included the loss of water by interception for all periods, was less in the catchments with pine than those with eucalyptus. As a consequence, in the present study, the eucalyptus plantations registered higher evapotranspiration. This result could be due to the characteristics that each species possesses, e.g. rooting depth, and because of the availability of a larger amount of groundwater as a consequence of smaller interception losses.

During the most rain-deficient season, evapotranspiration is sustained exclusively by the groundwater. In consequence, at the end of the dry period, the plants have consumed the majority of the water. This situation inhibits evapotranspiration during the summer, which reduces the potential difference between maximum water consumption between the two species. As a result, the effect of the different age, density and management of the plantations will not be manifested with full rigor in evapotranspiration. Subsequently, the maximum difference between the potential water requirements between pine and eucalyptus will be presented only when they have access to all the water required for the whole year, especially during the dry season.

In summary, the evapotranspiration of the different plantations is regulated more by the availability of groundwater during the precipitation-deficient periods than by the consumption potential of each plantation.

Sediment transport. The total amount of sediments transported in streams from the pine catchments is greater than those with eucalyptus. This difference can be explained by the wider protection zones of the streams in the eucalyptus catchments. The individual properties of the protection zones influence the sediment retention capacity [Boothroyd *et al.*, 2004; Gran and Montgomery, 2005; Hassan *et al.*, 2005].

Surprising is the larger quantity of evacuated sediments in the *Pine 2* catchment. This result can be explained by the stream passing through a small flood zone, which could have provided additional sediment supply.

The temporal variation in the export of sediments is principally influenced by the annual rainfall regime and, as a consequence, the intensity of the erosive overland flow [Beschta *et al.*, 2000; Gomi *et al.*, 2005; Karwan *et al.*, 2007]. The highest sediment transport is concentrated in the rainiest periods, and when the soil is saturated. This soil water condition is important in the generation of overland flow which in turn may promote surface erosion [Cammeraat, 2002; Mayor *et al.*, 2009; Turnbull *et al.*, 2010].

The uneven topographical characteristics of the catchments, the particularities of the ground cover, the intensity at which the soil is disturbed due to preceding forestry interventions, the characteristics of the riparian protection strips in the catchments and the dissimilar amounts of streamflow from the catchments with equal or different forestry plantations are responsible for the uneven transport of sediments [Gomi *et al.*, 2005; Karwan *et al.*, 2007; Moore and Wondzell, 2005].

According to CONAMA [1996], the total sediment yields evacuated per surface unit by the streams in the present study are considered light. These values are higher than those reported by Oyarzun and Peña [1995] in Chile, who used erosion plots for quantification. They are also greater than values reported by Gomi *et al.* [2005] for different conifer plantations located in the Pacific Northwest of the United States, which ranged between 1 and 100 kg/ha. These plantations are located on soils with metamorphic origin and have annual precipitation that varies between 700 and 2500 mm.

2.5. Conclusion

Due to the different characteristics of the canopy, the water losses due to interception are higher in the catchments covered with pine than in those with eucalyptus. The amount of water involved in evapotranspiration in the catchments with pine is less than those with eucalyptus. This influences in an inverse manner the amount of streamflow discharge which is mainly generated by base flow from the corresponding catchments. However, the differences between the species in terms of water consumption were surprisingly small because water consumption was more limited by the available soil moisture than by the species. The sediment load was greater in the pine catchments than in those with eucalyptus, a situation that can be explained by the distinct characteristics of the riparian areas along the streams. Overall, sediment transport was low in all catchments.

2.6. Acknowledgements

This study was financed with funding from the *Fondo Nacional de Investigaciones Científicas y Tecnológicas* (FONDECYT) Project number 1070218. Also important is the support received from the company Forestal Mininco S. A. Assistance by Mr. Rodrigo Bravo and Carlos Torres is appreciated.

2.7. Supplementary Information

Original paper published in Spanish

Huber, A. Iroumé, C.H. Mohr and C. Frêne (2010). Effect of *Pinus radiata* and *Eucalyptus globulus* plantations on water resource in the Coasta Range of Biobío region, Chile. *Bosque* **31** (3), 219-230, DOI: 10.4067/S0717-92002010000300006

Chapter III

Runoff generation and soil erosion processes after clear cutting

Abstract

Timber harvesting by clear cutting is known to impose environmental impacts, including severe disturbance of the soil-hydraulic properties which intensify the frequency and magnitude of surface runoff and soil erosion. However, it remains unanswered if harvest areas act as sources or sinks for runoff and soil erosion and whether such behavior operates in a steady state or evolves through time. For this purpose, 92 small scale rainfall simulations of different intensities were carried out under pine plantation conditions and on two clear-cut harvest areas of different age. Non-parametrical Random Forest statistical models were set up to quantify the impact of environmental variables on the hydrological and erosion response. Regardless of the applied rainfall intensity, runoff always initiated first and yielded most under plantation cover. Counter to expectations, infiltration rates increased after logging activities. Once a threshold rainfall intensity of 20 mm/h was exceeded, the younger harvest area started to act as a source for both runoff and erosion after connectivity was established whereas it remained a sink under lower applied rainfall intensities. The results suggest that the impact of microtopography on surface runoff connectivity and water repellent properties of the topsoil act as first order controls for the hydrological and erosion processes in such environments. Fast rainfall-runoff response, sediment-discharge-hystereses and enhanced post-logging groundwater recharge at catchment scale support our interpretation. At the end, we show the need to account for non-stationary hydrological and erosional behavior of harvest areas, a fact previously unappreciated in predictive models.

Key words: infiltration, runoff, erosion, connectivity, rainfall simulation, catchment

Published as C.H. Mohr., R. Coppus, A. Iroumé, A. Huber and A. Bronstert (2013). Runoff and soil erosion processes after clear cutting. *Journal of Geophysical Research* **118**, 814-831, DOI: 10.1002/jgrf.20047.

3.1. Introduction

The practice of clear cutting is known to cause severe environmental impacts [e.g., *Ziegler et al.*, 2006]. In most cases, clear-cut harvesting involves the use of heavy timber machinery which causes soil compaction and reduction of both macroporosity and infiltration capacity [e.g., *Malmer and Grip*, 1990]. As a consequence, peak flows may increase in both frequency and magnitude, promoting sediment transport [e.g., *Birkinshaw et al.*, 2011; *Carr and Loague*, 2012; *Croke et al.*, 2001; *Iroumé, et al.*, 2005; *Iroumé et al.* 2006; *Jones and Grant* 1996; *Malmer and Grip*, 1990]. Post-logging acceleration of landsliding rates may additionally intensify sediment transport after logging activities [*Montgomery et al.*, 2000], providing abundant sediment to be purged preferentially during low-frequency but high-magnitude rainfall-runoff events [e.g., *Coppus and Imeson*, 2002]. These landslides are often associated with the drainage of timber roads [*Montgomery et al.*, 2000] that are regarded as main sources for runoff and sediment in such environments [e.g., *Croke et al.*, 2001; *Lane and Sheridan*, 2002; *Motha et al.*, 2003]. In contrast, the role of the harvest area itself remains less clear, although its absolute contribution of runoff and sediment fluxes may often exceed that of forest roads as a consequence of its greater area. Owing to relatively low soil compaction compared with timber roads, skidder tracks or log landings, harvest areas are mainly considered as sinks for runoff and sediment transport due to restricted connectivity and limited sediment supply along the slopes [*Croke et al.*, 1999b; *Wallbrink and Croke*, 2002]. However, *Croke et al* [1999a] also demonstrated that runoff generation and sediment transport do occur on harvest areas, owing to uneven degrees of topsoil disturbance which allows the connectivity of erosive surface runoff along tracks of lower hydraulic conductivity. Similarly, *Brooks et al.* [1994] showed intensified runoff and sediment transport on compacted harvest areas of gentle slopes but increased infiltrability along the steeper slopes associated with enhanced surface retention capacity. Moreover, sediment supply on logged slopes is not necessarily limited. Logging activities are reported to increase soil erodibility by intermixing more dispersive subsoil into topsoil which augments the sediment storage along recently logged slopes with erodible sediment [e.g., *Burt et al.*, 1983; *Croke et al.*, 2001].

Hence the role of harvest areas is ambiguous. This comprehensive study explores the hydrological and erosional behavior of such harvest areas and focuses in particular on the following two key objectives:

(1) Under which environmental conditions do harvest areas act as sources and under which conditions do they act as a sinks for surface runoff and fine sediment transport?

(2) Is the hydrological and erosional response of such areas stable or do there exist tipping points where their hydrological and erosional performance dynamically switches along intrinsic threshold values?

To this end, the soil hydrological response to (simulated) rainfall was studied. For this purpose rainfall simulation experiments were carried out in a mature pine plantation and on two clear-cut harvest areas of different age with various rainfall intensities that conformed with the local rainfall regime. Non-parametric statistical Random Forest models were used to gain insight in the relation between environmental conditions and the soil hydrological and erosive responses. The plot-scale observations are then compared and discussed with observations made at the catchment outlets.

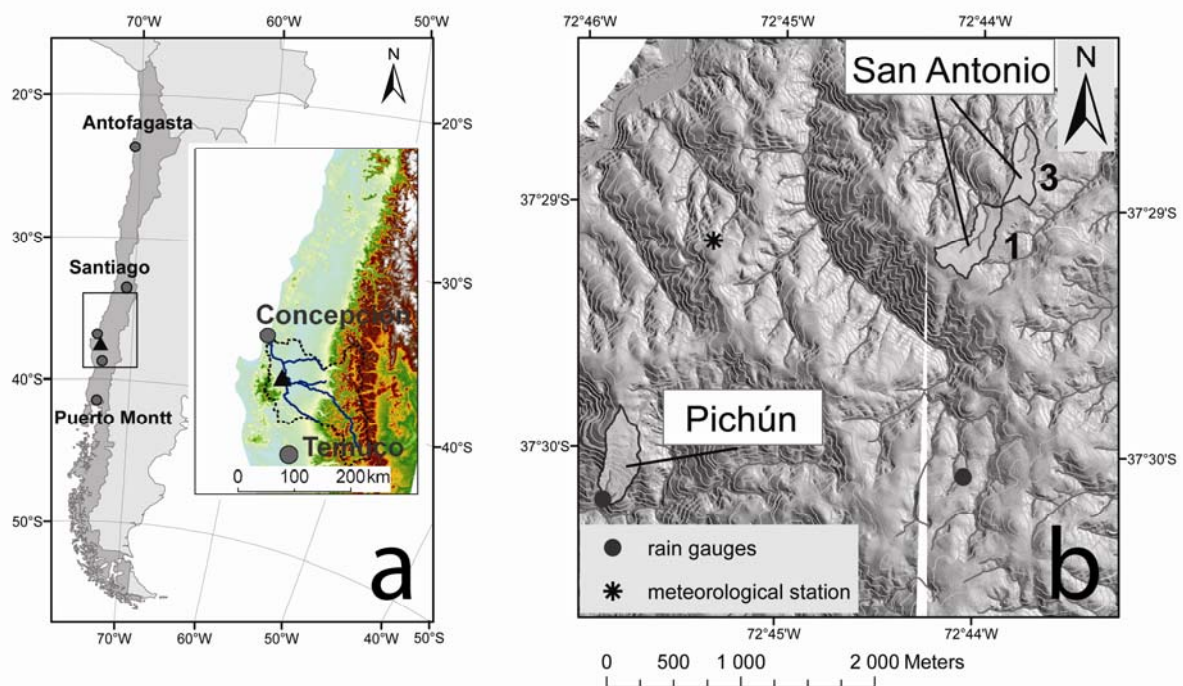


Figure 3.1. (a) Location of the study area is represented by the black triangle. The inset shows the B o-B o drainage system as a dotted line. The representation of the elevation (m asl) is derived from GTOPO30 data (<http://demex.cr.usgs.gov/DEMEX/>). (b) Sites of the rainfall simulation experiments within the experimental catchments are shown. The positions of the rain gauges and the closest meteorological station are represented. Contour lines correspond to 20 m, derived from a LiDAR DTM. The numbers correspond to (1) *Pinus radiata* control and (3) former *Pinus radiata* plantation, clear cutting during winter 2009 in San Antonio.

3.2. Study area




The study area is located on the eastern slopes of the metamorphic Coastal Range of South Central Chile, about 500 km south of Santiago in the Biobío Region, close to the city of Nacimiento (Figure 3.1a). All creeks within the study area are part of the Bío-Bío river basin which drains more than 24,000 ha of Southern-central Chile. The dominant land use within the Bío-Bío region is forestry which has promoted the development of this region into the national center of timber and pulp production [Patterson and Hoalst-Pullen, 2011]. Today the area shows one of the fastest growing rates in timber and pulp production worldwide [FAO, 2010]. The clear cutting technique remains the dominant practice and single clear cutting episodes may span areas of several hundreds of hectares. Here, a network of 11 experimental catchments (ranging between 250 and 480 m asl) was established in order to analyze hydrological and erosional processes of different forest management practices [Huber *et al.*, 2010]. The network involves clear-cut catchments which were harvested by the same techniques but differ in age and season of their latest clear cutting. At the same time, the small headwater catchments are homogeneous in terms of size, topography, geology, soil type and provide together with their simple geometry and vicinity exceptional settings for inter-catchment comparison (see Mohr *et al.*, [2012] for morphometric features and details). As a result, the network offers a promising opportunity to study the (apparent) contradictory role of harvest areas as previously outlined. To this end, this study is restricted to three catchments (Table 3.1) of which one persisted as a mature *Pinus radiata* D. Don. plantation during the study period (Figure 3.1b; San Antonio #1). This catchment was last logged and reforested in 1983 following a previous rotation also on *Pinus radiata*. Both the other catchments, hereafter named Pichún and San Antonio #3 after their administrative affiliation, were reforested in 1987 and 1983 respectively, following a previous rotation of *Pinus radiata*. All other catchments were excluded from this study because they were covered with secondary native forest, *Eucalyptus globulus* Labill plantations, or showed only little difference to the *Pinus rad.* stands of the control catchment. The Radiata pine plantations of Pichún and San Antonio #3 were clear cut and rubber-tired skidders were used to drag logs uphill to landings while cable logging was performed only in steep terrain.

Pichún was logged during the dry summer season in 2006 and then the area was artificially laid fallow though the application of herbicides. San Antonio #3 was logged during the rainy season between July 14th and August 10th 2009. Timber harvesting during the rainy season is economically beneficial because the immediate reforestation can be performed

under saturated soil conditions which in turn assures maximum soil water availability for the seedlings when the growing season starts.

Table 3.1. Main features of the studied catchments. * referring to pre- and post-logging experiments, respectively, conducted across the same catchment, ** Year of latest preceding clear-cutting corresponds to the year of plantation; * Planted with *Pinus radiata*, **** courtesy of Andreas Bauer.**

Catchment identification	San Antonio #1	San Antonio #3	Pichún
Rainfall simulation series	-	S.A. pre and S.A. post*	Pichún
Area (ha)	12.65	9.47	16.83
Forest management	control	winter clear cutting in 2009	summer clear cutting in 2006
Vegetation	<i>Pinus radiata</i>	-	-
Tree-density (tree/ha)	320	-	-
Year of plantation**	1983	1983***	1987***
Riparian buffer (ha)	0.83	1.15	1.24
Altitude (m asl)	328-377	255-320	131-373
Catchment slope (°)	14.7±8.5	18.2±10.2	22.4±11.0
Slope of stream (°)	10.0±7.3	15.1±10.7	18.0±9.1
Length of principle stream (m)	497	487	623
Max. flow length (m)	762	773	1068
Topographical wetness index	4.76 ±1.84	4.33±1.24	4.11±1.27
Perimeter (m)	1930	1738	2010
Gravelius Compaction Index	1.53	1.59	1.38

The area is characterized by a subtropical Mediterranean climate showing a pronounced seasonality. Annual average precipitation is 1150 mm, concentrated between April and September, which period contributes 95% of the total annual yield [Huber *et al.*, 2010]. Annual average temperature is 13°C and monthly mean temperatures range between 7°C in July and 19°C in January (Figure 3.2a). The summer temperature can exceed 40°C, enhancing high evapotranspiration rates and promoting very low topsoil water content during summer [Huber *et al.*, 2010]. Rainfall events are cyclonically or orographically driven and may last for several days. However, rainfall intensity is low and median rainfall intensity equals ~8.8 mm/h (mean 10 mm/h) for the Meñir station during the period from 01/2000 to 12/2008). 25% of the rainfall events fall below 4.8 mm/h while 75% do not exceed 13.8 mm/h and 95% are less than 23.2 mm/h. The highest intensity recorded reached 27.6 mm/h (Figure 3.2b). Though the Meñir meteorological station is farther away from the study area than the

Pichún station, it provides longer continuous rainfall records which were preferred to assess statistical rainfall properties owing to their similar local conditions in altitude and aspect.

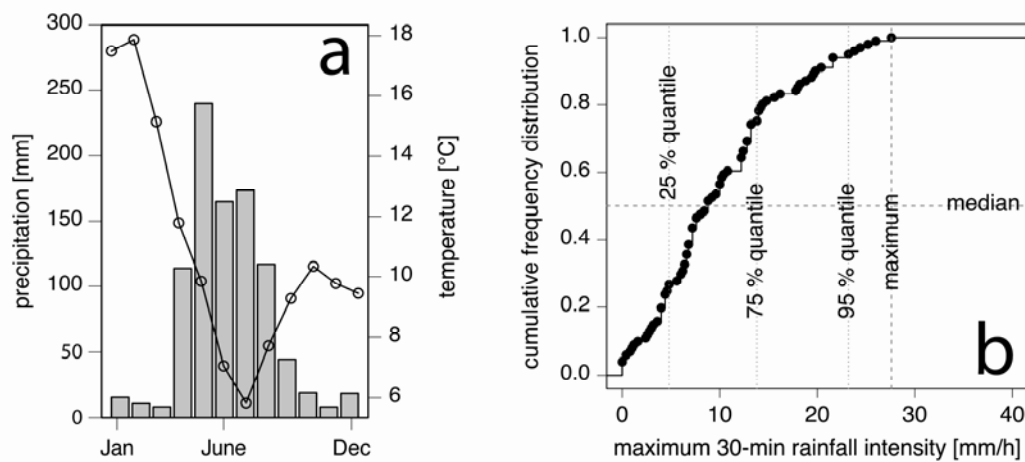


Figure 3.2. (a) Mean monthly temperature and rainfall for Meir meteorological station ($37^{\circ}58'$, $72^{\circ}77'$, 647 m asl) during the period from 01/2000 to 12/2008. Bars represent monthly rainfall (mm) and the line monthly average temperature ($^{\circ}\text{C}$). (b) Cumulative distribution function for maximum 30-min rainfall intensity at Meir station during the period from 01/2000 to 12/2008.

The dominant soil type is a clayey to loamy Luvisol and its structure is variable on a small scale due to embedded fragments of bedrock, a complex distribution of recent and former root systems, and direct disturbances by timber harvest. The soil is underlain by a deep saprolite layer [Mohr *et al.*, 2012]. Recent channel cuts and truncated soil profiles exposing low-conductive B-horizons show evidence of active soil erosion and landsliding processes triggered by forest clearing [Montgomery *et al.*, 2000].

3.3. Methods

Rainfall simulations have been successfully applied to define major water and sediment fluxes, their feedbacks, as well as their controlling factors triggering source or sink behavior [e.g., Cerdà, 1996; Cerdà, 1997; Cerdà and Doerr, 2005; Croke *et al.*, 1999a; Croke *et al.*, 1999b; Croke *et al.*, 2001; Croke *et al.*, 2006; Imeson *et al.*, 1992; Michaelides *et al.*, 2009; Wainwright *et al.*, 2000]. They permit the simultaneous observations of runoff initiation and erosion processes, complementing the quantitative data with qualitative observations and allowing the comparison of the hydrologic and erosional responses between different land use managements under controlled conditions [e.g., Cerdà, 1997; Michaelides *et al.*, 2009].

In order to meet the local topographic conditions and to provide low and long-lasting rainfall intensities, we modified the drip-plate type rainfall simulator based on *Bowyer-Bower and Burt* [1989]: Telescopic extensions (Figure 3.3a) allow adjustment to slopes up to 45° without inclining the drop-former box to ensure the homogeneous spatial distribution of the simulated rainfall. The rainfall intensity is controlled by interchangeable glass tubes (Figure 3.3b) of different diameters (here: 2 and 5 mm) based on the Bernoulli principle and confirmed by measuring the water volume leaving calibrated water supply containers (Figure 3.3c). An acrylic box (Figure 3.3d) features approximately 600 equally spaced drop-formers that distribute the water over the 0.5 m² plot. In order to generate more realistic drop size distribution, a 5mm-spacing-mesh randomly resizes the drops (Figure 3.3e).

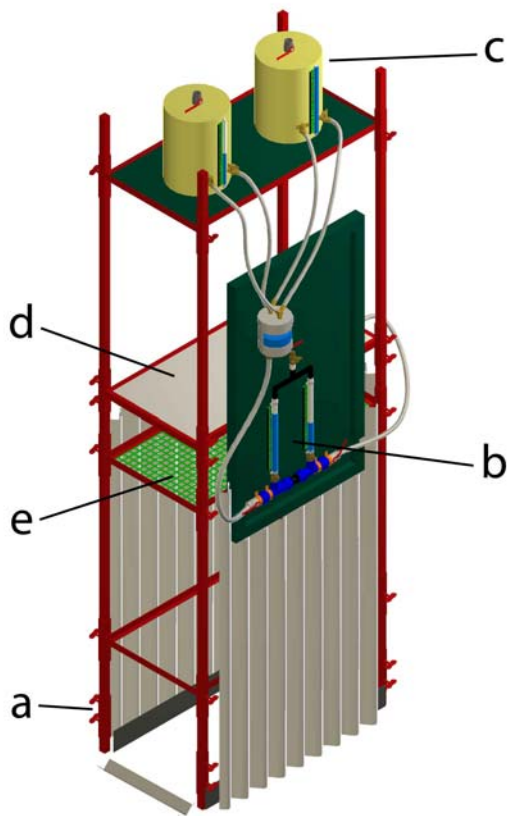


Figure 3.3. (a) Sketch of rainfall simulator, courtesy of Odette Morales (a: telescopic extensions; b: control panel including interchangeable glass tubes; c: water supply containers; d: drop-former box; e: drop size randomizer).

The streamflow discharge was monitored at a temporal resolution of 3 min by V notched Thompson-type weirs equipped with custom-built water stage loggers [*Huber et al.*, 2010; *Mohr et al.*, 2012]. The loggers provide an accuracy of 2 mm. Rainfall was registered at 0.2 mm accuracy by two Hobo tipping bucket rainfall gauges and a meteorological station (Davies Instruments, Advantage Pro Series) located at suitable and accessible sites (Figure 3.1b).

3.3.1. Experimental strategy and sampling design

During the dry summer season of 2009 (January-February) and 2010 (March 2010) a set of 92 rainfall simulations at 10, 20 and 40 mm/h intensity were performed under a mature 26 years old *Pinus radiata* stand (hereafter S.A. pre), an area which was logged by clear cutting in 2009 (hereafter S.A. post) and an area logged by clear cutting during the dry summer period in 2006 which had been laid fallow (hereafter Pichún). Hence, the time between the last preceding clear cutting and the time when the experiments were conducted,

was 26, 0.5 and 3 years for S.A pre, S.A. post and Pichún, respectively (Table 3.1). The S.A. pre and S.A. post experiments were all conducted within the San Antonio #3 catchment.

The applied 10 and 20 mm/h intensities represent the local natural rainfall intensities (Figure 3.2b). Additionally, a high intensity was applied to accentuate differences in hydrological and erosion responses [e.g., *Michaelides et al.*, 2009].

The simulations were conducted along upper, middle and lower slopes and the plots were selected by the representativeness of the surface cover and accessibility. The timber harvest of San Antonio disturbed the surface to such an extent that this approach was replaced in 2010 by a more suitable two-stage random sampling design [*de Gruijter et al.*, 2006]: In a first step, the study area was divided into equally sized sub-areas (“primary units”), three each for each slope segment. In a next step one primary unit was randomly selected out of each slope segment and ten sites were randomly selected, which were assigned in equal parts to the rainfall intensities randomly. This sampling design permits a high sample size, spread across the whole study area efficiently [*de Gruijter et al.*, 2006; *Hassler et al.*, 2011].

The infiltration rate was calculated by subtracting runoff rate from rainfall intensity after the runoff rate had been stabilized but had lasted for at least two hours. In order to account for the local slope, runoff volume was normalized to 1 m² of surface.

Runoff rates were determined by volume of runoff that was collected in sterile polyethylene bottles per time interval at a runoff gutter downslope. Time to runoff was estimated during the experiments and recalculated to rainfall (mm) necessary to initiate runoff. Runoff yields were determined by accumulating the runoff over the two hours from initiation of runoff. The collection of the first sample started at the moment of runoff initiation and ceased once sufficient sample was available for sediment analysis [*Michaelides et al.*, 2009]. The remaining samples were taken at intervals of 3 up to 30 minutes depending on the runoff rate and became longer during the latter part of the simulations when runoff rates became more stable. For the S.A. post-series, a tipping bucket rainfall gauge (0.2 ml accuracy) was used to determine runoff rates to improve temporal resolution. A receptacle beneath was used as a sediment collecting device. Sediment concentrations were determined gravimetrically with a accuracy of 0.5 mg after filtering the runoff samples through pre-weighed glass fibre filters (Advantec Glass Fiber Filter GF 75 47mm) and drying at 105°C for 48 h.

Sediment yields were calculated by summing the products of runoff volume and sediment concentration for each sampled time interval during 120 minutes of surface runoff (eq. 3.1).

$$SY = \sum_0^{120} R \cdot C \quad (3.1)$$

in which SY corresponds to the total sediment yield (g/m^2) after 120 minutes, R to runoff volume (l/m^2) measured during the sampling interval and C to the sediment concentration (g/l).

Brilliant blue dye tracer at a concentration of approximately 4 g/l was applied to a randomly selected subset of simulations to estimate infiltration patterns and depth prior to and after logging activities [e.g., *Blume et al.*, 2008; *Weiler and Naef*, 2003]. The depth of the wetting front was measured manually at 5 cm increments along profiles perpendicular to the plot. Standard deviation was used as a proxy for the uniformity of the wetting front.

3.3.2. Soil conditions

Prior to the experiments, each plot was characterized by slope, position and aspect according to *Jahn et al.* [2006]. The percentage of the vegetation, bare soil, stone and litter cover was estimated by a simple grid method as proposed by *Cammeraat* [1993]. Organic horizons were described after *Green et al.* [1993]. Initial topsoil moisture (0-5 cm depth) was assessed gravimetrically using soil cores which were extracted adjacent to the upper and lower boundary of the plot or by ThetaProbe soil moisture sensor (ML2x, Delta-T Devices) at a accuracy of $\pm 1\%$, which had been validated by core samples. Bulk density was determined from the same soil core samples [*Cammeraat*, 1993]. Soil texture was determined by *Rubilar* (unpublished soil data, 2008) in 14 pits spread across the study area. Hydraulic conductivity was estimated by double-ring infiltrometer measurements at approximately 30 cm depth following *Wu and Pan* [1997].

3.3.3. Data analysis

Due to non-normality of the data, non-parametric tests for statistical interference were applied. We assessed changes in infiltration rate, the depth of rain applied to initiate runoff, runoff yields, peak runoff, sediment yields, erosion rates, and differences in initial conditions due to forest management using a Wilcoxon rank sum test at a significance level of $\alpha=5\%$ [e.g., *Hassler et al.*, 2011].

We also used a statistical method called Random Forest model, which belongs to a family of methods using decision trees. Decision-tree-based methods are flow chart like structures and allow quantification of relevant predictor variables in high dimensional settings involving interaction [*Strobl et al.*, 2008]. Such decision trees are applied to differentiate data into various groups by separating them along finite predictor variables [e.g., *Vorpahl et al.*, 2012]. Random Forest models [*Breiman*, 2001], hereafter named RFs, consist of an ensemble of such decision trees. RFs were set up to quantify the impact of environmental variables on runoff generation and sediment transport. RFs are a robust non-parametric statistical method capable of handling large nonlinear, noisy, fragmented or intercorrelated data for regression [*Law and Wiener*, 2002; *Strobl et al.*, 2008]. They have been applied for a variety of hydro-geomorphological studies including runoff and sediment transport prediction [e.g., *Francke et al.*, 2008; *Zimmermann et al.*, 2012] or quantifying the impact of driving factors for landsliding [*Vorpahl, et al.* 2012].

RFs combine bootstrap aggregating ('bagging') with random variable selection [*Breiman*, 2001]. RFs use a randomly selected subset of data (called bootstrapped data) to grow decision trees. The predictions of the tree grown on that data are then tested against data not included in the bootstrapped data (called out-of-bag-data). As a result, the out-of-bag-data provide an unbiased model performance assessment. In practice, each tree is grown recursively by partitioning the data. At each split the data are divided into two groups according to a simple rule based on one of a random subset of predictor variables aiming in minimization of overall variance. Thus, the main parameters controlling RF models are the number of trees, the tree complexity in terms of maximum number of terminal nodes or maximum tree depth, the number of randomly selected predictor variables at each split and the size of the out of bag fraction for performance assessment. The overall RFs-prediction is then approximated by averaging all single trees' predictions [*Breiman*, 2001]. Though RFs consist of many noisy but approximately unbiased models and each classification tree itself is relatively inaccurate, they produce the right prediction when averaged [e.g., *Liaw and Wiener*, 2002; *Strobl et al.*, 2008]. Even though RFs can handle strongly intercorrelated data, the

quantification of the real impact of predictor variables is uncertain. In order to overcome this limitation, the variables were conditioned. Conditioning the variables is a way to avoid spurious correlations by revealing the true impact variables while excluding the covariate ones [Strobl *et al.*, 2008].

3.3.4. Random Forest Model setup

Response variables included steady state infiltration rate, mm to runoff, runoff and sediment yield after 120 minutes and maximum erosion rates. The set of predictor variables contained forest management practices, surface cover properties (bare soil, vegetation, stones, litter), days after last rainfall, slope, bulk density, depth of organic horizons and applied rainfall intensities (see chapter 4.1). In the case of sediment yield, constant infiltration rate, mean suspended sediment concentration (SSC) and maximum erosion rates were added. The maximum erosion rates model additionally contained mean and maximum sediment concentration, mm to runoff and peak runoff (see chapter 4.2). An overview of the variables used in this analysis is given in Table 3.2.

Table 3.2. Random Forest predictor and response variables. x indicates whether included or not in the corresponding RF model, * Predictor variable was used but left out in further analysis due to dominant predictor impact potentially hiding the influence of other predictor variables or after splitting into consistent forest management practices. ** refers to suspended sediment concentration (g/l).

Predictor variables	Response variables			
	Steady state infiltration rate	Mm to runoff	120 min sediment yield	Maximum erosion rates
Forest management	(X)*	(X)*	(X)*	X
Applied rainfall intensities	(X)*	X	X	X
Slope	X	X	X	X
Days after last rainfall	X	X	X	X
Soil moisture prior to the experiment	X	X	X	X
Bulk density	X	X	X	X
surface cover properties <ul style="list-style-type: none"> • Bare soil • Vegetation • Stone • Litter 	X	X	X	X
	X	X	X	X
	X	X	X	X
	X	X	X	X
Depth of organic horizons	X	X	X	X
Steady state infiltration rate			X	X
Mm to runoff				X
Peak runoff				X
Maximum erosion rates			X	
Maximum SSC**				X
Mean SSC**				X

Derived from iterative tuning, the RFs were grown for 500 individual trees and the number of randomly selected variables at each node m was set to 5. Maximal tree complexity was also set to 5 terminal nodes. This setup showed good agreement to recommended model setups [Law and Wiener, 2002]. For each predictor, the variable importance (VI) was

quantified as the loss of model performance when that predictor was omitted from the model.

Following *Strobl et al.* [2008] the importance of each predictor (VI) was calculated based on its conditional importance measure. The conditional VI of predictor P is calculated in different steps. First, the mean square error (MSE) of the “out-of-bag” (OOB) predictions for each tree is calculated, and then the values of the predictor variables are randomly permuted before their MSE is estimated again. Finally the difference d between mean square error (MSE) of the “out-of-bag” predictions for each tree and the MSE of the predictions with randomly permuted (eq. 3.2), conditioned values of predictor P^* reflect the unscaled permutation importance of the predictor variable averaged over all trees [*Strobl et al.*, 2008] (eq. 2)

$$d = MSE_{OOB}^{P^*} - MSE_{OOB}^P \quad (3.2)$$

with “out-of-bag” abbreviated as OOB and MSE referring to mean square error, which is determined by

$$MSE_{OOB} = \frac{\sum_{i=1}^n [RV_{obs} - RV_{mod}]^2}{n} \quad (3.3)$$

where RV refers to the observed and modelled value of each response variable and n is the number of records in out-of-bag-data.

In a next step, the sum over all individual differences d in MSE for each tree t with $t \in \{1, \dots, ntree\}$ was averaged over all trees and normalized by the standard error

$$VI_p = \frac{\frac{1}{ntree} \sum_{n=1}^{ntree} d}{\frac{\sigma(d)}{\sqrt{ntree}}} \quad (3.4)$$

By doing so, unimportant predictors yield low impact on model quality which in turn is reflected in low VI values. Finally, the predictor importance was normalized to 100% for comparison reasons.

Overall model performance was estimated by the squared Pearson coefficient R^2 between modelled and observed responses. All calculations were realized by the statistical environment R [*R Development Core Team*, 2009]. Random Forest model building was set up using the R-packages *randomForest* [*Law and Wiener*, 2002] and *party* [*Strobl et al.*, 2008].

3.4. Results

3.4.1. Soil and surface properties

The texture of the topsoil is relatively homogeneous across the whole study area (Figure 3.4) and can be described as loam and its minor variations [Schoeneberger *et al.*, 2002]. Carbon fragments are frequently embedded into the topsoil matrix across the whole area.

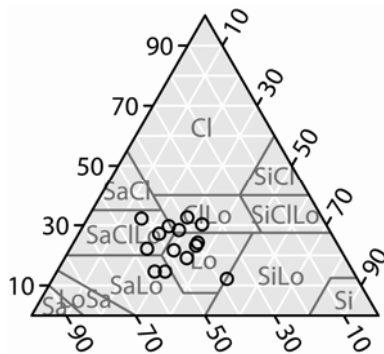


Figure 3.4. Topsoil texture (0-30 cm depth) according to USDA soil classification. Samples were taken across the whole study area from 14 pits, unpublished data.

All plots lie between 140 and 295 m asl along the upper, mid and lower slope sections. The mean plot slopes reached $20 \pm 8.1^\circ$ for S.A. pre, $15 \pm 6.6^\circ$ for S.A. post and $21 \pm 8.1^\circ$ for Pichún. Although statistical differences of local gradients of the plot between the distinct series do occur (p -value < 0.01), they are insubstantial considering their extensive range.

Apparent soil density prior to the clear cutting of San Antonio #3 and in Pichún showed no differences and averaged very similar values of $1.06 \pm 0.13 \text{ g/cm}^3$ and $1.07 \pm 0.20 \text{ g/cm}^3$, respectively ($p=0.36$). After clear cutting San Antonio #3, the topsoil was compacted to a density of $1.42 \pm 0.21 \text{ g/cm}^3$, a significant increase of more than 30% ($p < 0.05$).

Topsoil hydraulic conductivity (k_s) was significantly higher only at Pichún (18.6 mm/h) and double that at San Antonio #3, where it yielded similar values of 8.8 and 8.1 mm/h prior to and after the logging activities, respectively.

In general, topsoil moisture was very low and reached only $3.4 \pm 2.77 \text{ Vol}\%$ (S.A. pre), $3.7 \pm 1.64 \text{ Vol}\%$ (Pichún) and $5.2 \pm 2.96 \text{ Vol}\%$ (S.A. post). However, significant differences are indicated between all series ($p < 0.001$). The duration of the preceding dry period ranged over 19-32 days for Pichún, 35-56 days for S.A. post and 4-20 days for S.A. pre.

Surface cover is relatively homogeneous and dominated by pine needle litter ($95 \pm 7\%$) with a thickness of $2.7 \pm 1.2 \text{ cm}$ (Table 3.3) for S.A. pre. Native species like *Greigia landbeckii*, *Muehlenbeckia hastulata* or *Hypochaeris radicata* contributed to the remaining $5 \pm 7\%$ of the surface cover while both stones and bare soil were negligible. According to

Green *et al.* [1993] the organic horizons of the forest floor were classified as Mors which typically shows a tenacious consistency and a compact matted structure in the partly decomposed organic horizon. Although litter cover, which is mainly composed of recent harvest residues like branches and bark, remains high (39±43%) in S.A. post, bare soil cover is dominant (61±43%). The thickness of the organic horizons exhibited the highest variability under S.A. post conditions and yielded 1.7±2.3 cm as a result of denudation removing the litter from steeper slopes and depositing it in local depressions. Similar patchy patterns were observed in Pichún, where the variability in surface cover is highest: bare soil (53±21%) and litter (38±19%) cover most part of the surface but pioneer species, e.g. *Brassica rapa*, *Hypochaeris radicata*, *Cirsium vulgare* or *Rubus fruticosus* and stones were also present in some plots. The litter is similar in composition to post-logging San Antonio but had a lower average thickness (0.7±1.3 cm).

Table 3.3. Average surface cover in % of total plot cover. *Uncertainty corresponds to standard deviation.

	litter (%)	bare soil (%)	vegetation (%)	stones (%)
S.A. pre	95±7*	0±0*	5±7*	0±0*
S.A. post	39±43*	61±43*	0±0*	0±0*
Pichún	38±19*	53±21*	6±6*	3±3*

Topsoil disturbance due to former harvest action accentuated the microtopography which was most pronounced under the recent clear cutting conditions of S.A. post, with height differences of up to 10 cm within the plots.

3.4.2. Results of drip-type rainfall experiments

An overview of the hydrological response is presented in Table 3.4. [*This table has been removed to the supplementary information of this chapter for formatting reasons*].

3.4.2.1 Infiltration and runoff production

Runoff initiated fastest under plantation cover (S.A. pre) after 5.5±5.4 mm, 3.3±1.6 mm and 3.4±2.8 mm of applied rainfall under 10, 20 and 40 mm/h intensities, respectively (Table 3.4).

Surface runoff initiated faster on the recent clear cutting (S.A. post) than on the older one (Pichún) under all rainfall intensities though not indicated as substantial ($p>0.05$).

About two-thirds of all experiments followed a runoff pattern with a rapidly rising runoff limb towards a constant equilibrium runoff rate. The other experiments ($n=26$) showed an enhanced infiltration rate towards the end of the simulations (Figure 3.5), which was observed under 20 and 40 mm/h rainfall intensities, mostly under the plantation cover of S.A. pre ($n=14$).

Normalized to 1m^2 , peak runoff was highly variable among all forest management practices and rainfall intensities. Regardless of the applied intensities, S.A. pre generated the highest peak runoff rates (Table 3.4). Under 40 mm/h intensity, the recent clear cutting reached peak runoff rates of 198.7 ± 130.7 ml/min and this clearly exceeded the old clear cutting (140.0 ± 75.9 ml/min). This order changed under lower rainfall intensities, when Pichún nearly double those in S.A. post (95.9 ± 55.1 vs. 42.6 ± 40.7 ml/min and 32.6 ± 22.8 ml/min vs. 17.5 ± 24.4 ml/min, respectively). Despite differences among all forest management practices and rainfall intensities, they are significant only between the pre- and post-logging conditions of San Antonio under 10 mm/h intensity ($p=0.01$).

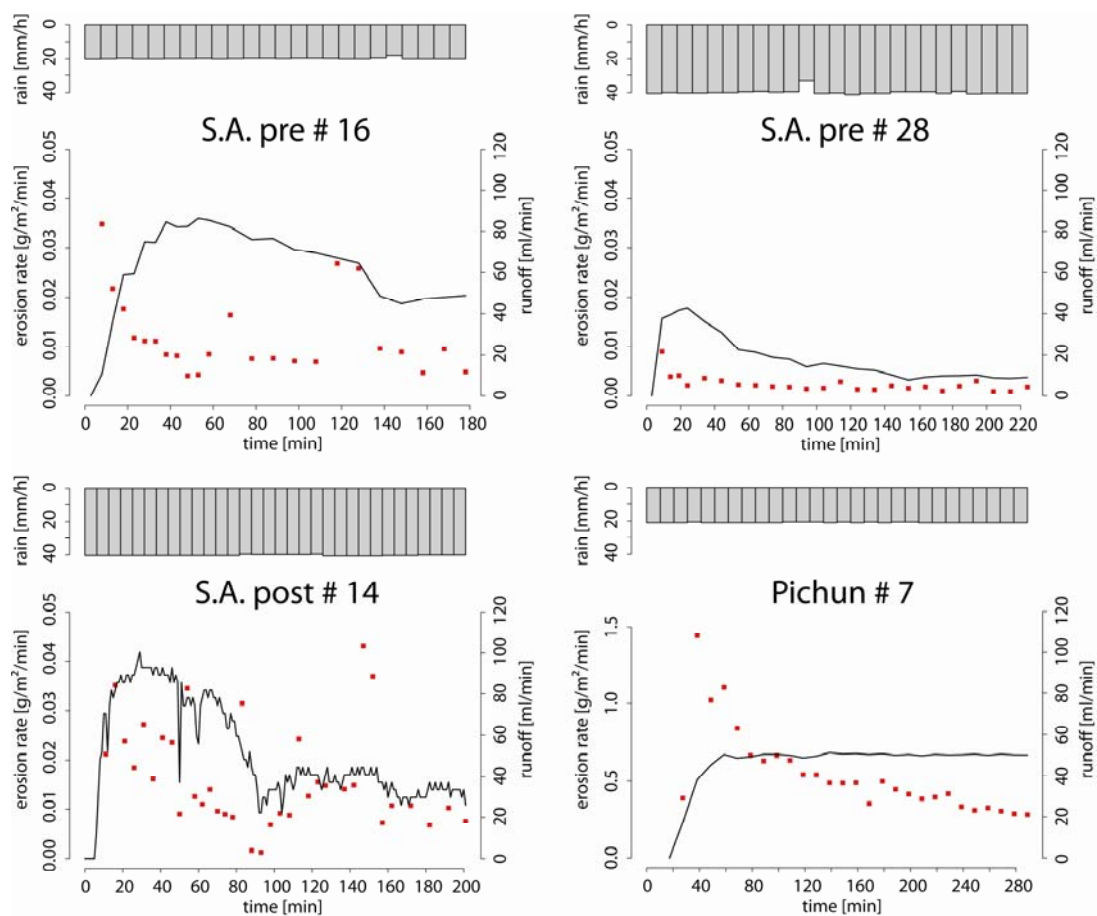


Figure 3.5. Example hydrographs showing runoff and erosion response to applied rainfall of different rainfall intensities and forest management practice. Pre-logging conditions are represented by the simulations #16 and #28 of S.A. pre, recent logging conditions by #14 of S.A. post and older logging by #7 of Pich n. Note different scales of

Pichún #7. Runoff rates ($\text{ml/m}^2/\text{min}$) correspond to black lines and red points refer to erosion rates ($\text{g/m}^2/\text{min}$). Grey bars on the top represent applied rainfall intensity in mm/h during intervals.

Infiltration rate is a function of rainfall intensity and infiltration capacity because infiltration rates increase as rainfall intensities become greater and finally converge at an intrinsic infiltration capacity [Dunne *et al.*, 1991]. Steady state infiltration rates did not show significant differences between the forest management practices among all applied rainfall intensities ($p > 0.05$). However, a slight change in infiltration rates of ~ 10 , 6 and 12% at 10, 20 and 40 mm/hr intensity, respectively, was observed under the recent clear cutting conditions of S.A. post and -4, 18 and 12% at 10, 20 and 40 mm/hr intensity, respectively, under the older clear cutting of Pichún (Figure 3.6a). Minor differences between the applied rainfall intensities fail to explain the observed changes (Table 3.4). The mean infiltration depths reached 12.2 ± 12.1 cm prior to and 8.9 ± 5.8 cm after the logging activities of San Antonio (Figure 3.6b) ($p = 0.51$).

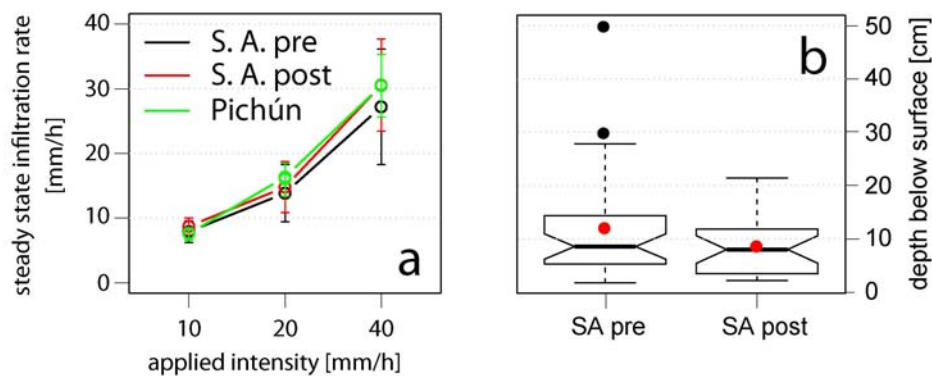


Figure 3.6. (a) Steady state infiltration rates (mm/h) as a function of applied rainfall intensity and forest management practice. Error bars show standard deviation. ($n = 12, 12$ and 12 for S.A. pre under 10, 20 and 40 mm/h ; $n = 10, 10$ and 10 for S.A. post under 10, 20 and 40 mm/h ; $n = 3, 9$ and 14 for Pichún under 10, 20 and 40 mm/h rainfall application). (b) Infiltration depth (cm) prior to ($n = 32$) and after clear cutting ($n = 30$) San Antonio. The red dots represent the mean values.

The unlogged plots of S.A. pre yielded most runoff under all intensities (2.8 ± 2.9 mm, 9.9 ± 7.5 mm and 22.5 ± 16.5 mm at 10, 20 and 40 mm/hr intensity, respectively) (Figure 3.7a). At 10 mm intensity Pichún clearly produced more runoff than S.A. post (2.74 ± 1.84 mm vs. 1.48 ± 2.35 mm) which flipped vice versa under 40 mm/h rainfall intensity when S.A. post yielded nearly double that for Pichún (18.2 ± 13.6 mm vs. 9.9 ± 6.9 mm). At 20 mm/h rainfall, both clear cuttings ended up similar ($p = 0.90$) yielding 8.04 ± 5.92 mm and 7.83 ± 3.83 mm,

respectively. Despite high variability, there is a strong positive linear relationship between runoff ratios between both clear cuttings (runoff yield S.A. post/ runoff yield Pichún) and increasing applied rainfall intensities. This relationship depicts a rainfall intensity threshold of ~19 mm/h above which the recent clear cutting starts exceeding the older one in terms of runoff yield (Figure 3.7b). Significant differences are only weakly indicated between Pichún and S.A. pre under 40 mm/h intensity ($p=0.05$).

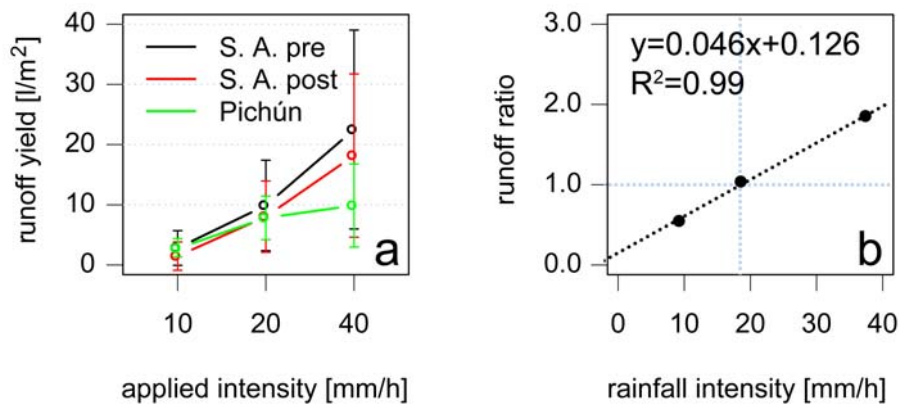


Figure 3.7. (a) Mean runoff yields as a function of forest management practice and applied rainfall intensity. Error bars represent standard deviation. (b) Ratios between the runoff yields of the young and old clear cuttings after 120 minutes of runoff as a function of applied rainfall intensity. The ratio is expressed as fraction (S.A. post/Pichún) of the mean values. The linear fit and the model performance (squared Pearson coefficient) are given. y corresponds to the mean runoff yield ratio and x to the applied rainfall intensity. The horizontal grey dashed line shows 1:1-ratio and the vertical grey dashed line illustrates the threshold rainfall intensity. ($n=12, 12$ and 11 for S.A. pre under $10, 20$ and 40 mm/h; $n=8, 9$ and 10 for S.A. post under $10, 20$ and 40 mm/h; $n=3, 5$ and 14 for Pichún under $10, 20$ and 40 mm/h rainfall application).

3.4.2.2. Sediment transport and erosion rates

Sediment yields were low and did not exceed 1g/m^2 after 120 min of rainfall application regardless of the intensity under the unlogged conditions of S.A. pre (Table 3.4). Under 10 mm/h rainfall intensity, S.A. post yielded only 0.85 ± 1.42 g/m^2 sediment, a value within the same order of magnitude of S.A. pre (Figure 3.8a) while Pichún yielded 5.65 ± 4.51 g/m^2 ($p<0.05$).

Under intermediate intensities, the both harvest areas had similar sediment yields ($p=0.26$) at 15.57 ± 19.45 and 23.57 ± 10.40 g/m^2 for the recent and old clear cutting, respectively. Overall maximum sediment yields were measured at 40 mm intensity for S.A.

post, being twice as high as for the Pichún sites ($45.74 \pm 70.40 \text{ g/m}^2$ vs. $22.14 \pm 15.47 \text{ g/m}^2$), which reached its maximum under 20 mm/h. However, differences do not appear to be significant ($p=0.71$). Like runoff yields, sediment ratios between both clear cuttings showed a similar threshold of 22.6 mm/h above which S.A. post starts to exceed Pichún (Figure 3.8b).

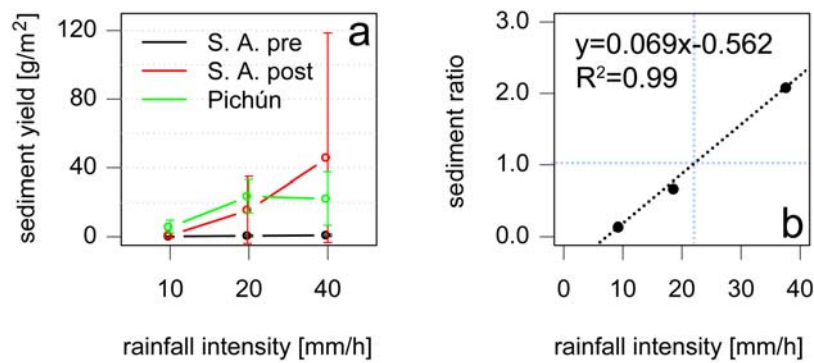


Figure 3.8. (a) Mean sediment yields as a function of forest management practice and applied rainfall intensity. Error bars represent standard deviation. **(b)** Ratios between the sediment yields of the young and old clear cuttings after 120 minutes of runoff as a function of applied rainfall intensity. The ratio is expressed as fraction (S.A. post/Pichún) of the mean values. The linear fit and the model performance (squared Pearson coefficient) are given. y corresponds to the mean sediment yield ratio and x to the applied rainfall intensity. The horizontal grey dashed line shows 1:1-ratio and the vertical grey dashed line illustrates the threshold rainfall intensity. ($n=11, 12$ and 11 for S.A. pre under 10, 20 and 40 mm/h ; $n=6, 6$ and 8 for S.A. post under 10, 20 and 40 mm/h ; $n=3, 4$ and 14 for Pichún under 10, 20 and 40 mm/h rainfall application).

Despite high variability, significant differences among erosion rates occurred between all forest management practices. Regardless of the rainfall intensities, erosion rates did not exceed $0.01 \text{ g/m}^2/\text{min}$ under unlogged conditions of S.A. pre. These values are clearly exceeded by rates observed under both clear cuttings even under low rainfall intensity (Table 3.4). While both clear cuttings showed similar erosion rates under intermediate intensity ($0.14 \pm 0.18 \text{ g/m}^2/\text{min}$ vs. $0.17 \pm 0.14 \text{ g/m}^2/\text{min}$), the younger harvest area doubled the rates of Pichún when 40 mm/h rainfall was applied. Under these conditions, S.A. post reached maximum rates of up to $3.8 \text{ g/m}^2/\text{min}$. Figure 3.9 depicts a similar positive linear relationship between the erosion ratios between both clear cuttings and increasing rainfall intensities points to similar threshold intensity.

The temporal evolution of the erosion rates showed two different patterns (Figure 3.5). Under pre-logging conditions of S.A. pre (17 out of 36) and the majority of the Pichún

experiments (17 out of 26), erosion rates showed an initial increase up to a peak erosion rate followed by a gradual decline over time. In contrast, under the recent clear cutting conditions of S.A. post, runoff rates are closely tracked by the erosion rates (Spearman's $\rho \sim 0.74$).

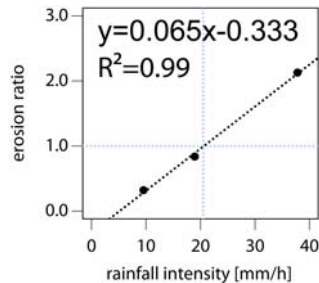


Figure 3.9. (a) Ratios between the erosion rates of the young and old clear cuttings as a function of applied rainfall intensity. The ratio is expressed as fraction (S.A. post/Pich n) of the mean values. The linear fit and the model performance (squared Pearson coefficient) are given. y corresponds to the mean erosion rate yield ratio and x to the applied rainfall intensity. The horizontal grey dashed line shows 1:1-ratio and the vertical grey dashed line illustrates the threshold rainfall intensity.

3.4.3. The hydrological and erosional response as a function of environmental variables

3.4.3.1. Infiltration and runoff response

Rainfall intensity was the most important predictor variable for infiltration rate since mean square error (MSE) increased by 42.2% when rainfall intensity is omitted (Figure 3.10c). An infiltration model including all forest management practices explained 71.8% of variance (Figure 3.10a). The same held true for the runoff yield model where rainfall intensity remained the most important variable (VI=31.5%), although the model explained only 15.8% of overall variance (Figure 3.10b and d).

Since a dominant predictor may hide other potentially important predictors [Law and Wiener, 2002], applied rainfall intensity was excluded for further analysis. However, none of the remaining predictors showed substantial impact on infiltration rate, and model performance decreased to only 12.5% of explained variance. In a next step, the distinct forest management practices were analyzed separately. Models based on such homogeneous classes did not perform satisfactorily and only the pre-logging-model (S.A. pre) performed slightly better (Figure 3.11a). This is surprising since variance is expected to be smaller within homogeneous classes. Here, the antecedent dry period showed some impact on infiltration rates (VI=15.6%; Figure 3.11d). However, overall model performances and predictor identification for either infiltration or runoff yield models were weak under all forest management practices (Figure 3.11a-f).

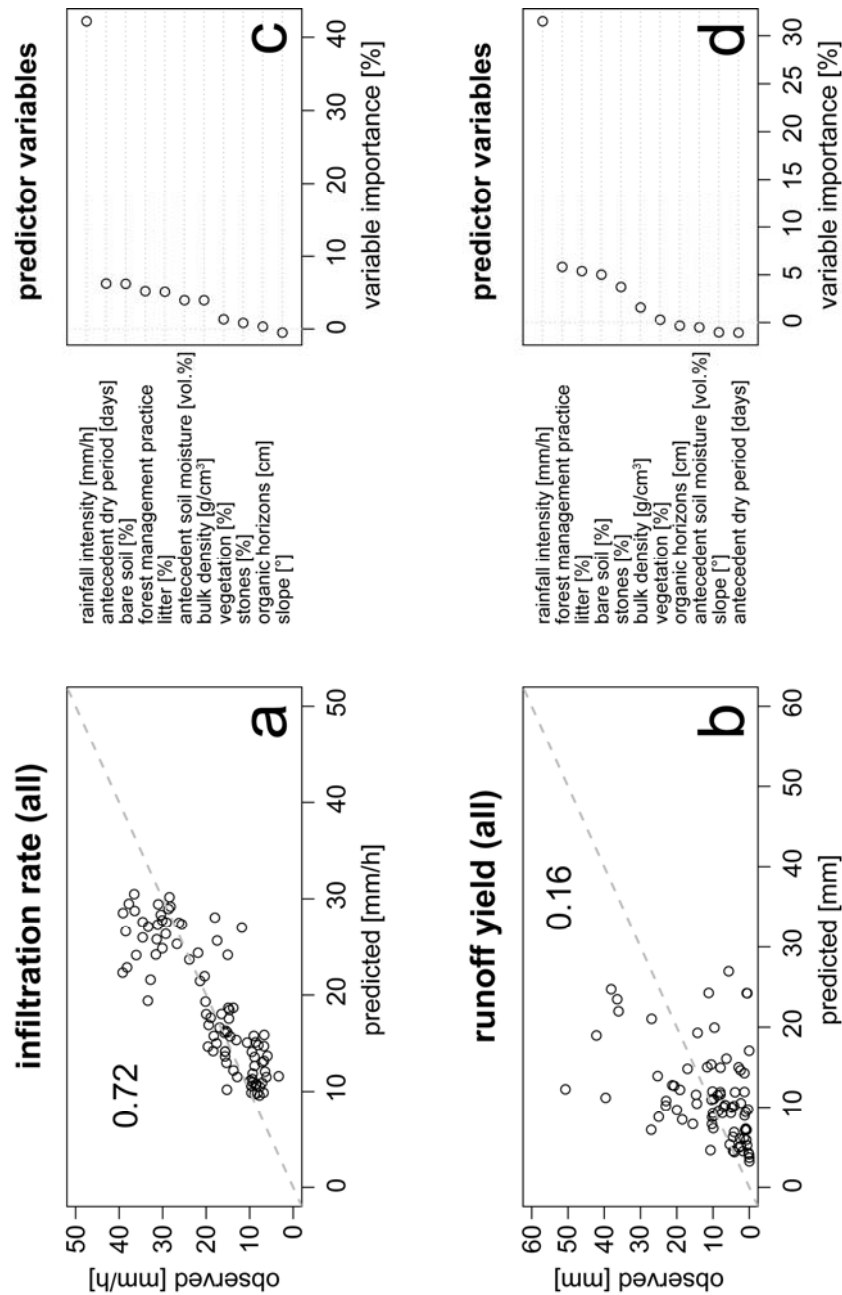


Figure 3.10. (a) Performance of (a) infiltration ($n=92$) and (b) runoff yield ($n=84$) models including all rainfall simulations. Numbers show model performance given as squared Pearson coefficients between modelled and observed values (c-d). Predictor importance is estimated for (c) infiltration model and (d) runoff yield model (predictors: rainfall intensity refers to the normalized applied rainfall intensity (mm/h) considering local slope, antecedent dry period refers to the dry period (days) prior to the experiments, bare soil, litter, vegetation and stones is expressed as percentage of total surface cover, forest management practice describes the classes of S.A. pre, S.A. post or Pich n, antecedent soil moisture (vol.%) was measured immediately prior the experiments, bulk density (g/cm^3) was measured adjacent to upper and lower boundary of the plot prior the experiments, organic horizons corresponds to the compound thickness of all lhf-layers (cm) and slope represents the local slope ($^\circ$)). Note: Even slight negative impact is given for distinct predictors.

The runoff initiation model performed poorly and explained only 18.8% of variance including all forest management practices. However, runoff initiation was more a function of depth of organic layers (VI=9.6%) and antecedent dry period (VI=10.5%) than related to forest management practice (VI=8.8%) or rainfall intensity (VI=2.8%). Analyzing the distinct forest management practices separately, the particular models performed even worse.

3.4.3.2. Erosion and sediment yield

Only when including antecedent sediment yields (after 30, 60 and 90 minutes of runoff) did the models perform well. These variables, however, were excluded due to strong intercorrelation effects. Such spurious correlation effects only mimic direct causal connection and may hide relevant but weaker predictor variables [*Strobl et al.*, 2008]. The sediment yield model for all forest management practices explained 51.8% of variance, slightly worse than under pre-logging conditions of S.A. pre (62.3%) and comparable to under recent clear cutting conditions of S.A. post (53.1%). For Pichún, the model performed very poorly (17.7%; Figure 3.12c). Maximum erosion rates were the most important predictors under all forest management practices (VI \leq 20.9%) while mean suspended sediment concentrations (SSC) showed some minor impact only under recently logged conditions (Figure 3.12d-f). Maximum erosion rates, in turn, are (weakly) related to maximum SSC (VI=10.9 %) and peak runoff (VI=10.9%) while the impact of the forest management practice itself is negligible. These models explained at most 51.0% of variance (S.A. post).

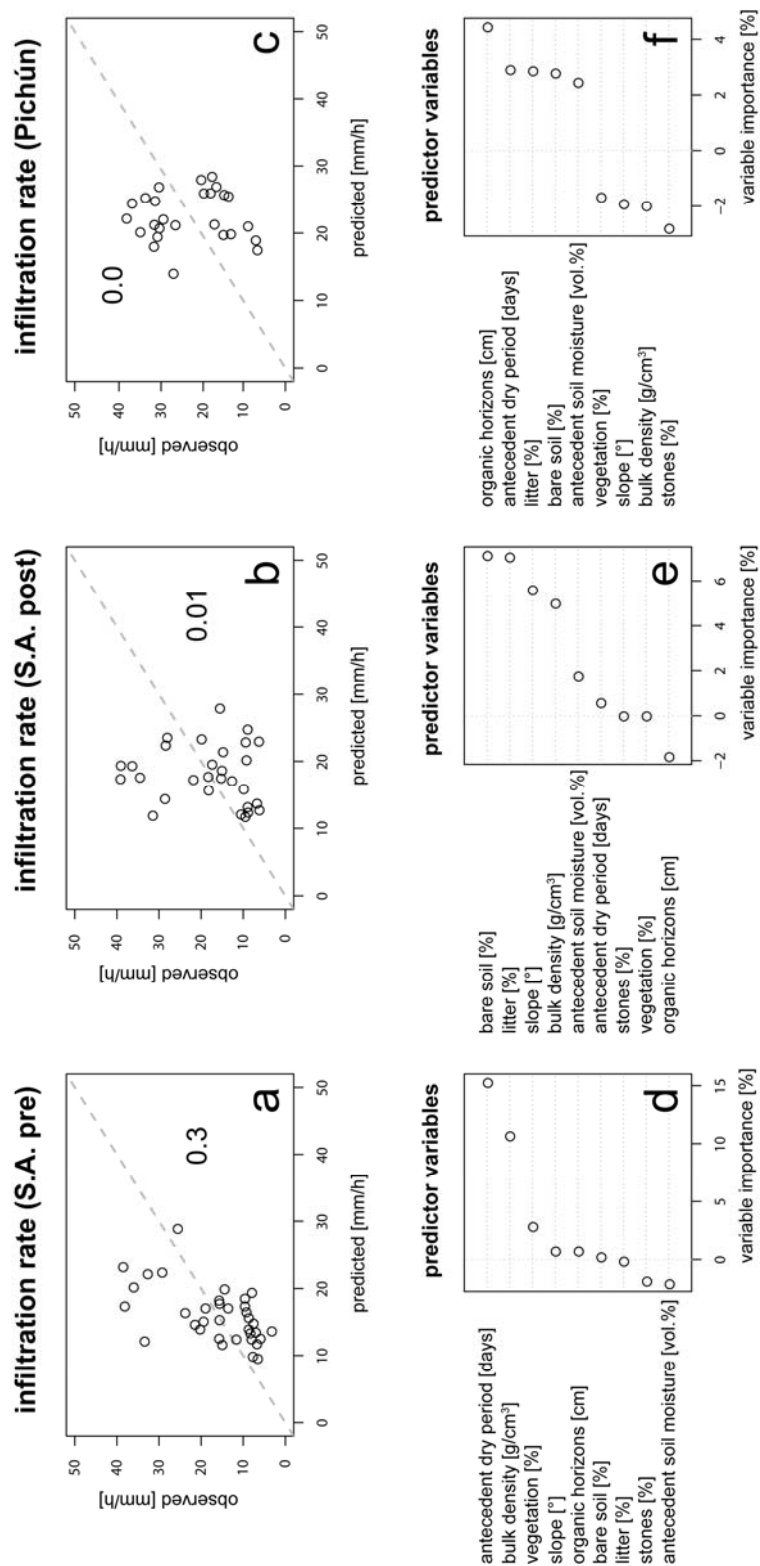


Figure 3.11. Infiltration rate model performance (a-c) and predictor importance (d-f) according to each forest management practice excluding applied rainfall intensity as predictor variable. ($n=36$ for S.A. pre, $n=30$ for S.A. post and $n=26$ for Pichún). Numbers show squared Pearson coefficient and indicate model performance (a-c). Note: even slight negative impact is given for distinct predictors.

3.5. Discussion

In contrast to an intensified surface runoff which is normally associated with post-logging topsoil compaction [e.g., *Bathurst et al.*, 2011a; *Bathurst et al.*, 2011b; *Birkinshaw et al.*, 2011; *Carr and Loague*, 2012], slightly higher post-logging infiltration and thus, lower runoff, was registered. These findings are counter intuitive because clear cutting is normally associated with decreased macroporosity after mechanical soil disturbance decreasing both infiltrability and hydraulic conductivity due to compaction [*Huang et al.*, 1996; *Malmer and Grip*, 1990]. Interestingly, a similar effect was also registered on a catchment scale. Figure 3.13 shows an increased probability of approximately 10% of lower streamflow discharge of a recently logged catchment (San Antonio #3) compared with an untreated control catchment (San Antonio #1). Hence, increased infiltration after logging activities is not restricted to plot scale. The apparent inconsistency of lower streamflow even prior to the timber harvest can be explained by the construction of timber road and site preparation which took place several weeks before the clear cutting started.

In consequence, the impact of logging activities lowering infiltration must have been compensated up to such an extent that post-logging enhancement of infiltration rates was established, or the time between two consecutive clear cuttings was too short to allow complete recovery of soil hydraulic properties to initial conditions [e.g., *Hofstede et al.*, 2002; *Ziegler et al.*, 2006]. Enhanced matrix flow promoting infiltration is not feasible as hydraulic conductivity remained unaffected. Moreover, soil compaction after the use of heavy timber machinery even exceeds the range of values reported for harvest areas under comparable environmental conditions [*Croke et al.*, 2001; *Gayoso and Iroumé*, 1991], which favours decreased porosity and thus lower matric flow conductivities [e.g., *Malmer and Grip*, 1990]. Thus, preferential flow processes are required to bypass water through the compacted and low conductive soil. The dye tracer experiments revealed preferential flow paths (Figure 3.14). Under dry and hydrophobic soil conditions, such processes may be initiated owing to low potential differences between macropores and soil matrix [*Weiler and Naef*, 2003].

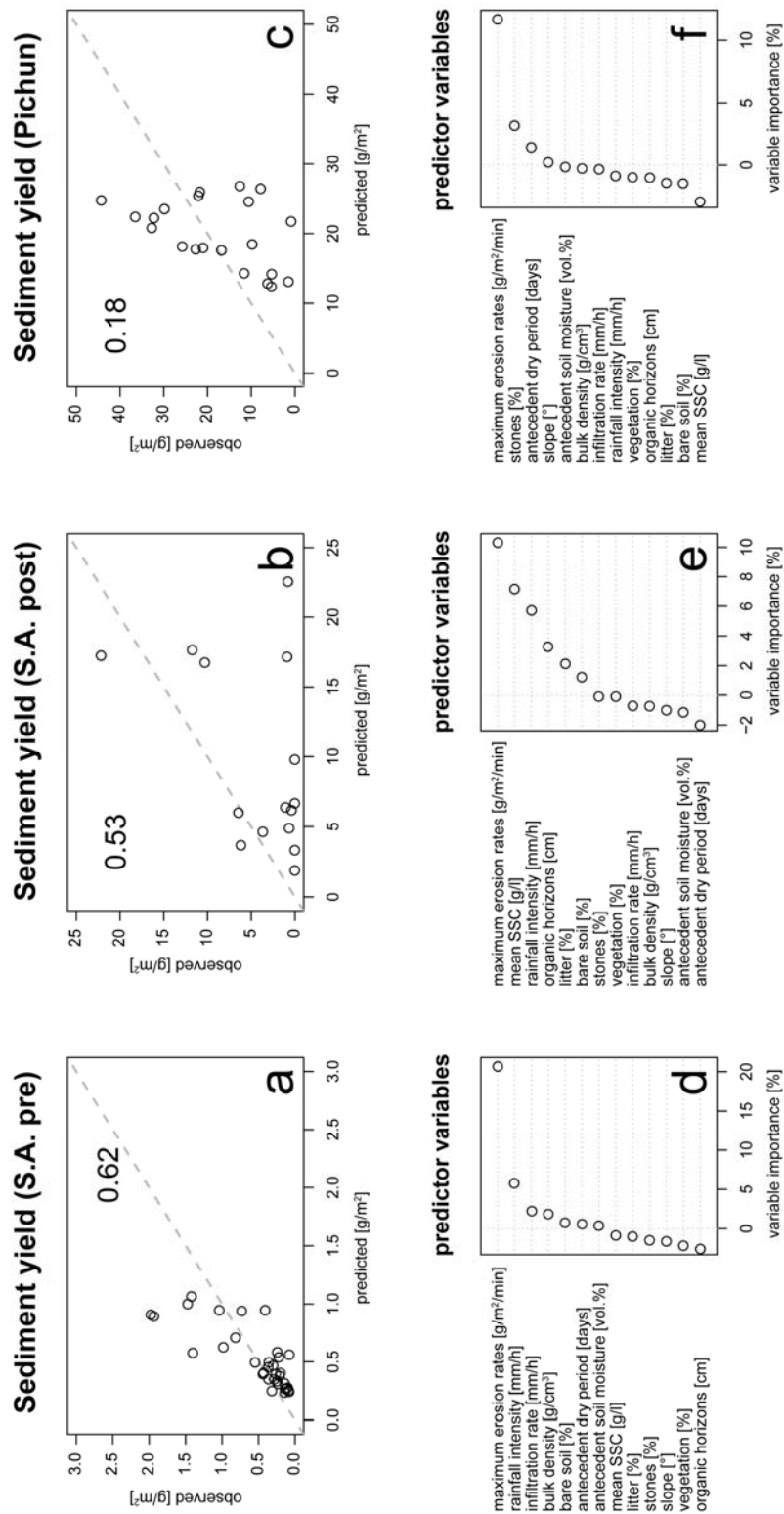


Figure 3.12. Sediment yield model performance (a-c) and predictor importance (d-f) according to each forest management practice. ($n=35$ S.A. pre, $n=21$ S.A. post, $n=22$ for Pichun). For variable explanation, see Figure 3.10. In addition, maximum erosion rates ($\text{g/m}^2/\text{min}$) registered during the simulations and mean SSC (suspended sediment concentration in g/l) were added as predictors. Numbers show squared Pearson coefficient and indicate model performance (a-c). Note: Even slight negative impact is given for distinct predictors.

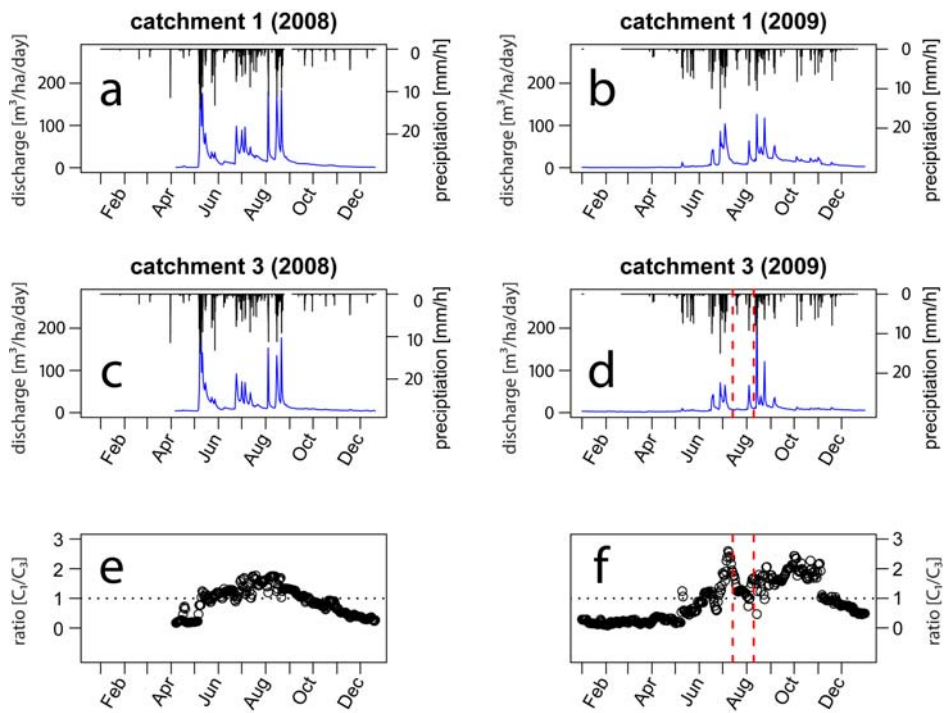


Figure 3.13. Blue hydrographs show specific daily discharge (m³) per hectare during the years 2008 (a and c) and 2009 (b and d) for the control and treatment catchment, respectively. Months are indicated at the bottom. Hourly rainfall intensities (mm/h) are given as black bars. Red dashed lines represent the period of logging activities. At the bottom, specific discharge quotients between control and treatment catchments are shown during the years 2008 (e) and 2009 (f). The black dotted line represents 1-1 ratio. Refer to Table 3.1 for catchment details.

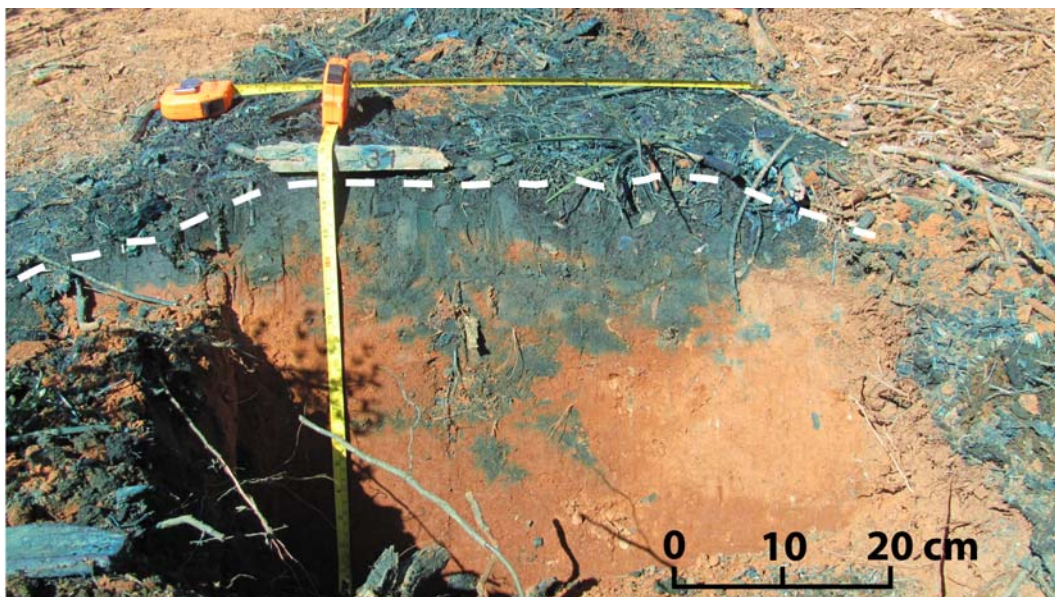


Figure 3.14. Observed preferential flow patterns in topsoil along recent and former root systems and desiccation cracks of recent clear cutting of San Antonio (simulation #31). White dashed line represents the surface edge.

Pre-logging observations suggest strong hydrophobic behavior of the organic layer. Firstly, antecedent dry periods show a (weak) impact on infiltration rates (Figure 3.11d) and runoff initiation (weakly) responded to the organic layers only under pine stands. Under comparable environmental conditions (undisturbed pine plantation, dry season and low soil moisture content), *Cerdà* [1998] showed reduced infiltration rates and fast runoff response owing to a water repellent surface. Pine and cypress litter consists of similar amounts of water repellent resins, waxes or aromatics [*Doerr et al.*, 2000]. *Miyata et al.* [2009] confirmed the importance of hydrophobic organic layers for fast runoff initiation and higher peak runoff under cypress plantation cover. Moreover, increasing infiltration rates towards the end of the experiments are primarily observed under plantation cover (39% for S.A. pre, compared to only 27% and 15% for S.A. post and Pichún, respectively) and imply declining water repellency of the organic horizons over time [e.g., *Imeson et al.*, 1992]. Finally, frequently observed charcoal fragments embedded in the topsoil provide independent evidence for former forest fires which are reported to promote water repellency [e.g., *Cerdà and Doerr*, 2005 *Doerr et al.*, 2000; *Imeson et al.*, 1992]. Considering the relatively high water volume applied under low rainfall intensities before runoff initiation (Table 3.4), the degree of declining water repellency by advancing topsoil wetting was high. Therefore it is not surprising that water repellency effects only emerged under higher rainfall intensity experiments [*Seifert*, 2011] (Figure 3.5).

As a result, infiltration increases when water repellent surfaces are broken up, as is the case during timber harvest. Heterogeneous microtopography shows variable degrees of surface disturbance/impact across the harvest area. Hence, infiltration is expected to enhance non-uniformly but in a patchy spatial distribution. However, variability in either infiltration rates or wetting front depth remained unaffected by the logging activities (Table 3.4, Figure 3.6b).

Preferential flow along macropores initiates when water supply exceeds all losses of matrix flow [*Beven and Germann*, 1982; *Bronstert and Plate*, 1997]. *Weiler and Naef* [2003] reported enhanced infiltration rates towards the end of their experiments when preferential flow had been triggered. The observations obtained here conform to their interpretation when the threshold hydraulic conductivities of 8-9mm/h for San Antonio and 18-19 mm/h for Pichún are considered. Owing to trapped air, macropore flux may be temporarily restricted [*Beven and Germann*, 1982], which may be reflected in the observed short peak in runoff preceding an intensified infiltration under 20 mm/h and 40 mm/h rainfall intensities (Figure 3.5).

Preferential flow processes do not only occur at the plot scale. Table 3.5 lists the lag times for the catchments San Antonio #1 and #2. Lag time refers to the time interval between the center of mass of a rainfall event and the observed peak flow at the catchment outlet [Dingman, 2002]. Two comparable rainfall events (June 2009 and August 2010) showed fast response (27-33 and 39-54 minutes, respectively). However, only when connectivity between fast draining vertical and underlying horizontal flow paths is provided, a rapid response to rainfall events may occur [Blume *et al.*, 2008; Montgomery *et al.*, 1997]. This requirement is met with the fast draining interface between the saprolite and bedrock as recently demonstrated by Mohr *et al.*, [2012].

Table 3.5. Estimated lag times for control and treatment catchment*. *no discharge data is available for Pich n; **June: 27.06.2009 23:00 - 28.06.2009 12:00 a.m.; soil moisture: 28.4 and 24.7 (vol.%) in catchment 1 and 3 measured on June 17th; *August 2009: 13.8.2009 23:00 - 14.8.2009 11:00; soil moisture: 38.4 and 36.9 (vol.%) for catchment 1 and 3 measured on August 13th; ****August 2010: 26.8.2010 8:00 – 26.8.2010 22:00; no soil moisture data available.**

	June 2009**			August 2009***			August 2010****		
Total precipitation [mm]	41.2			73.5			40.6		
Hourly peak intensities [mm/h]	6.9			12.9			10.2		
Event duration [h]	13			12			14		
	centroid	Q _{peak}	lag time (min)	centroid	Q _{peak}	lag time (min)	centroid	Q _{peak}	lag time (min)
San Antonio #1	4:24 a.m	4:57 a.m	33	5:10 a.m.	7:45 a.m.	155	12:36	13:15	39
San Antonio #3	4:24 a.m	4:51 a.m	27	5:10 a.m.	7:57 a.m.	167	12:36	13:30	54

Though water repellency and preferential flow paths provide a reasonable explanation for the observations, by themselves they are insufficient to explain the runoff and erosion threshold behavior of the harvest areas. Timber harvest enhanced hydraulic surface roughness by affirming the local relief [Clarke and Walsh, 2006; Malmer and Grip, 1990]. Under the surface conditions of the recent harvest area, runoff connectivity was established, particularly during the 40 mm/h rainfall intensity experiments after the retention capacity of surface storage was exceeded. Surface runoff initiated then as a function of saturated surface and rainfall intensity [Dunne *et al.*, 1991] along cascading runoff paths, e.g. skidder tracks or drag lines. These observations are in line with the threshold rainfall intensity of approximately 20 mm/h, above which the runoff on the younger harvest area started to overcome the retaining effect of local topography and started to outperform the less rugged terrain on the older one (Figure 3.7b). The runoff threshold is very similar to those observed for sediment yields and erosion rates (Figure 3.8b and Figure 3.9). As long as connectivity has not been established, prolonged ponding promotes infiltration and finally percolation recharging the groundwater.

The catchment scale response supports that interpretation (Figure 3.13). Thus, erosion may be surprisingly low even under the bare soil conditions of a young harvest area under low rainfall intensities. Once the threshold rainfall intensity has been exceeded, runoff and erosion severely intensifies.

Hence, our results suggest that timber harvest areas do not perform statically either as sinks or sources for runoff or erosion but instead switch their behavior along an intrinsic threshold. In consequence, one may ask if hydrological rainfall response models based on static rainfall-intensity-infiltrability-thresholds are sufficient under disturbed terrain conditions such as after logging activities [e.g., *Brenner, 2011; Carr and Loague, 2012; Ebel et al., 2008*]. Under the local meteorological conditions the young harvest area is expected to perform in 90% of the rainfall events as a sink for runoff and erosion (Figure 3.2b). Thus, severe erosive runoff will occur only during high intensity rainfall events (in approximately only 10% of cases) pointing to the importance of lower frequency but higher magnitude events following *Wolman and Miller [1960]*.

The erosion process itself differed considerably across the forest management practices. While the erosion rates are closely tracked by runoff rates under recent clear cutting conditions, the simulations conducted under the litter cover of S.A. pre reflect maximum transport during the early stages of the experiments (Figure 3.5 and Table 3.4). Hence, transport limitation provides a first order control of the erosion process under recent clear cutting conditions owing to abundant sediment supply or high erodibility [e.g., *Burt et al., 1983; Croke et al., 2001*]. Here, the soil erosion is intensified by abundant sediment availability after breaking-up formerly covered soil than by raising erodibility. Aggregate stability remained high after logging activities and reached 5.4 ± 0.7 at the surface ($n=468$) and 5.3 ± 0.7 in at 20-25 mm depth ($n=468$) on a relative scale from 0 to 6 [*Herrick et al., 2001*]. Though only sheet erosion processes may be simulated on plot scale, Figure 3.15 indicates similar processes on catchment scale. A clear figure-of-eight loop supports abundant sediment supply for the recently logged catchment while the clockwise loop, as observed under undisturbed forest plantation cover, suggests supply limitation [*Williams, 1989; Faul, 2011*].

A surprisingly good agreement between catchment scale response and low intensity rainfall experiments emerged. Normalizing the total transported sediment (273.3 kg/ha and 10.1 kg/ha for S.A. post and S.A. pre, respectively) on plot scale and experiment duration, erosion yields $0.59 \text{ g/m}^2/2\text{h}$ and $0.02 \text{ g/m}^2/2\text{h}$ under logged and untreated conditions, respectively (Table 3.4). Though soil erosion is high compared to undisturbed plantation

conditions [e.g., *Miyata et al.*, 2009] the results lie more in the lower range of reported soil erosion on different aged harvest areas [e.g., *Croke et al.*, 2001]. Nevertheless, the peak erosion rates registered on the young harvest area are comparatively high [*Michaelides et al.*, 2009].

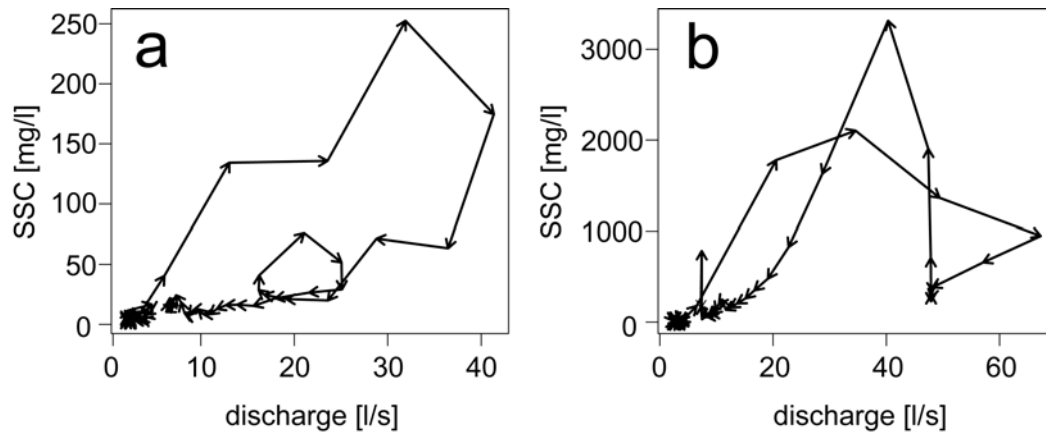


Figure 3.15. Hysteresis loop show temporal suspended sediment concentration (g/l)-discharge (l/s) relationship for (a) untreated control catchment (catchment #1 in Fig. 1b) and (b) logged catchment (catchment #3 in Fig. 1b) during the same rainfall-runoff event on August 11th -15th 2009. This event yielded 104.1 mm distributed over 92 hours with a maximum hourly intensity of 10.4 mm/h.

Nevertheless, differences in applied rainfall intensities and properties limit the comparison between studies on similar spatial scales [*Seeger*, 2007]. Transferability from plot to catchment scale is even more challenging owing to non-linear scaling relationships of runoff and erosion processes [e.g., *Benavides-Solorio and MacDonald*, 2001; *Parsons et al.*, 2006]. The overall *effects* are observable only on catchment scale and studies based on that scale will always incorporate greater level of complexities and interaction at the cost of better initial understanding. Initial but fundamental process understanding, the definition of the major water and matter fluxes and their feedbacks, in turn, are required for larger scale process understanding but only obtainable under the controlled conditions on plot-scale [e.g., *Wainwright*, 2000]. This point is basic, because results obtained on small scale may be crucial for elucidating some of the more complex interactions, which may be ‘averaged’ out on larger scales [*Wainwright et al.*, 2000]. In consequence, the scaling issues between both spatial scales are rather apparent when both scales are regarded as complete.

Finally, considering the patchy distribution of the hydrological and erosional response reversing with rainfall intensity, it is not surprising that the various hydrological and erosional responses did not exhibit a clear mutual relationship with other environmental predictor variables. For example, sites with high final infiltration rates sometimes needed only a few

mm of applied rainfall to initiate surface runoff while other sites showed low erosion rates despite high runoff rates. A similar difficulty in linking environmental variables with soil hydrological response was found by *Coppus* [2002], which finally limits the unequivocal determination of the underlying processes. In this context, the ‘memory’ of the landscape in terms of former land uses may play an important role, e.g. when assessing soil recovery times to its initial hydraulic properties and the duration of intra-rotational cycles [e.g., *Croke et al.*, 1999b; *Croke et al.*, 2001; *Hassler et al.*, 2011; *Ziegler et al.*, 2006]. In fact, a persistent impact of topsoil disturbances by previous logging is consistent with the unexpected higher post-logging infiltration rates and the missing clear relationships with environmental variables. Nevertheless, as data from unlogged and previously undisturbed sites are unavailable, this hypothesis cannot be tested.

In the end, this study largely represents a ‘snapshot’ of a specific set of environmental conditions at a distinct time [*Wainwright et al.*, 2000]. Repeating the experiments under different seasonal conditions, e.g. changes in soil moisture [e.g., e.g., *Cerdà*, 1997, *Cerdà*, 1998], and quantification of surface roughness, may overcome some of the limitations towards a more definite determination of the underlying processes.

3.6. Conclusions

We examined the hydrologic response of soils to clear cutting using rainfall simulations. Surprisingly, infiltration increased after clear cutting, a finding which apparently contradicts previous studies. This conflict, however, can be explained by a combination of two processes: (1) break-up of water repellent surface properties and (2) increased surface storage owing to interrupted surface runoff connectivity which in turn prolongs ponding. However, this is only the case under rainfall intensities of less than 20 mm/h. Under higher rainfall intensities, microtopography-connectivity establishes and intense surface runoff and subsequently soil erosion may be triggered. In consequence, harvest areas behave non-stationary and may switch from being a sink of runoff and erosion to being a source, a fact previously disregarded in predictive models.

Despite restrictions in spatial transferability, both spatial scales showed agreement in hydrological and erosional responses. In particular, very similar sediment yields observed on both scales highlight the reinforcing effect of clear cutting on soil erosion.

The results suggest that logging activities may have had such an impact that inter-harvest periods (here 26 years) may be too short for the soil to recover to its initial soil-

hydraulic properties. Considering the trend towards planting even faster growing species in Chile, e.g. *Eucalyptus globulus*, the problem is likely to be aggravated.

Finally, this study confirms the severe impact of clear cutting on water and soil resources and highlights the dominance of preferential flow processes in high-impact areas, such as intensive forestry. At the end, our findings emphasize the importance of pronounced surface roughness, e.g. by infiltration trenches, and the immediate reforestation in order to attenuate erosive surface runoff under such a low rainfall intensity regime.

3.7. Acknowledgements

The work presented herein is funded by the Chilean Government (Conicyt/BMBF 2009-092, Conicyt/BMBF 243-2010 and Fondecyt 1070218), the International Bureau of the German Ministry of Education and Research (CHL 08/03) and the Graduate School for Natural Disasters (GS NADI) of the University of Potsdam. We thank Forestry SA Mininco for access to our study catchments and financial support for the instrumentation of the catchments and Rafael Rubilar for providing soil data. The authors are particularly grateful to Rodrigo Bravo, Cristian Frêne, Odette Morales, Juan Pablo Navarro, Simon Plate, Franziska Faul, Johannes Brenner, Christian Gläser (University of Braunschweig) and Johanna Lein (University of Greifswald) for helping during the fieldworks. The authors would especially like to acknowledge Andreas Bauer who assisted also with graphics and Winnie Seifert for her help in the field and during data analysis. We thank Alexander Densmore, Simon Mudd, Artemi Cerdà and two anonymous reviewers for helpful critiques of a draft manuscript.

3.8. Supplementary information

Table 3.4: Hydrological and erosional responses according to simulated rainfall intensity and forest management practice.

20 mm/h:

^a simulation Nr 5 not considered in the sediment analysis due to very low runoff volume samples affecting the accuracy of sediment transport calculation; ^bsimulations Nr 9, 23 excluded in sediment analysis due to missing samples or too small sample volume; ^ccalculated max. SSC 34.63 (sim Nr 24) excluded due to very low runoff volume; ^dsimulations Nr 10 and 24 excluded in sediment analysis due to missing runoff samples or small sample volume; ^esimulations Nr 11, 16 and 23 excluded in sediment analysis due to missing runoff samples or small sample volume; ^fsimulations Nr 27 was excluded in sediment analysis due to small sample volume; ^gsimulations Nr 17, 30 and 31 were excluded in sediment analysis due to small sample volume; *** 0.001 significance level; ** 0.05 significance level

10 mm/h:

^a simulation Nr 5 not considered in the sediment analysis due to very low runoff volume samples affecting the accuracy of sediment transport calculation; ^bsimulations Nr 9, 23 excluded in sediment analysis due to missing samples or too small sample volume; ^ccalculated max. SSC 34.63 (sim Nr 24) excluded due to very low runoff volume; ^dsimulations Nr 10 and 24 excluded in sediment analysis due to missing runoff samples or small sample volume; ^esimulations Nr 11, 16 and 23 excluded in sediment analysis due to missing runoff samples or small sample volume; ^fsimulations Nr 27 was excluded in sediment analysis due to small sample volume; ^gsimulations Nr 17, 30 and 31 were excluded in sediment analysis due to small sample volume; *** 0.001 significance level; ** 0.05 significance level

40 mm/h intensity simulations

Applied intensity (mm h ⁻¹)		Generated Runoff (mm)		Runoff coefficient		Final infiltration rate (mm min ⁻¹)		Peak runoff (ml min ⁻¹)		30 minutes		60 minutes		90 minutes		120 minutes								
mean	s.d.	n	mean	s.d.	n	mean	s.d.	n	mean	s.d.	n	mean	s.d.	n	mean	s.d.	n							
S.A. pre	37.3	2.1	12	3.35 ^{***}	2.84	12	0.27	0.24	12	27.2	8.9	12	229.9	147.3	12	5.35	3.34	12	17.21	12.13	12	22.50	16.52	12
S.A. post	39.1	0.6	10	8.84	6.79	10	0.22	0.18	10	30.6	7.2	10	198.7	130.7	10	3.88	2.46	10	13.58	9.43	10	18.19	13.56	10
Pich n	37.3	2.5	14	12.99	7.85	14	0.18	0.11	14	30.5	4.9	14	140.0	75.9	14	1.46	1.08	14	6.93	5.01	14	9.88	6.89	14

Erosion response to 40 mm/h intensity simulations

SSC (g l ⁻¹)		Erosion rates (g min ⁻¹ m ⁻²)						Sediment yield (g m ⁻²) after																
mean	s.d.	n	mean	s.d.	n	min	max	mean	s.d.	n	mean	s.d.	n	mean	s.d.	n	mean	s.d.	n	mean	s.d.	n		
S.A. pre ^a	0.09	0.17	267	0.01	0.01	267	0.00	0.00	11	0.02	0.03	11	0.36	0.31	11	0.56	0.42	11	0.71	0.52	11	0.84	0.60	11
S.A. post ^b	1.84	2.34	238	0.44	0.74	234	0.13	0.23	8	0.98	1.41	8	11.71	16.48	8	26.28	39.06	8	37.92	58.6	8	45.74	70.40	8
Pich n ^c	1.87	2.37	329	0.20	0.16	329	0.08	0.07	14	0.40	0.28	14	6.34	4.77	14	12.11	8.96	14	17.62	12.21	14	22.14	15.47	14

20 mm/h intensity simulations

Applied intensity (mm h ⁻¹)		Generated Runoff (mm)		Runoff coefficient		Final infiltration rate (mm min ⁻¹)		Peak runoff (ml min ⁻¹)		30 minutes		60 minutes		90 minutes		120 minutes								
mean	s.d.	n	mean	s.d.	n	mean	s.d.	n	mean	s.d.	n	mean	s.d.	n	mean	s.d.	n							
S.A. pre	18.7	1.1	12	3.3	1.6	12	0.26	0.22	12	13.9	4.4	12	112.4	76.4	12	1.54	1.47	12	4.10	3.44	12	6.98	5.35	12
S.A. post	19.2	0.8	10	5.1	4.7	10	0.23	0.21	10	14.8	4.0	10	95.9	55.1	10	1.32	1.22	10	3.19	2.75	10	5.18	4.35	10
Pich n	19.0	1.1	9	13.3	14.5	9	0.14	0.13	9	16.3	2.5	9	42.6	40.7	9	0.78	0.74	9	2.27	1.94	8	4.90	2.99	6

Erosion response to 20 mm/h intensity simulations

SSC (g l ⁻¹)		Erosion rates (g min ⁻¹ m ⁻²)						Sediment yield (g m ⁻²) after																
mean	s.d.	n	mean	s.d.	n	min	max	mean	s.d.	n	mean	s.d.	n	mean	s.d.	n	mean	s.d.	n	mean	s.d.	n		
S.A. pre	0.09	0.03	293	0.01	0.01	293	0.00	0.00	12	0.02	0.03	12	0.18	0.21	12	0.36	0.48	12	0.45	0.52	12	0.54	0.56	12
S.A. post ^d	1.11	0.93	148	0.14	0.18	153	0.03	0.04	8	0.23	0.30	8	3.05	4.99	8	6.29	10.15	8	8.68	13.06	8	15.57	19.45	6
Pich n ^e	2.80	2.37	119	0.17	0.14	102	0.13	0.24	6	0.43	0.47	6	3.84	3.16	6	7.88	6.59	6	14.66	9.81	5	23.57	10.4	4

10 mm/h intensity simulations

Applied intensity (mm h ⁻¹)		Generated Runoff (mm)		Runoff coefficient		Final infiltration rate (mm min ⁻¹)		Peak runoff (ml min ⁻¹)		30 minutes		60 minutes		90 minutes		120 minutes								
mean	s.d.	n	mean	s.d.	n	mean	s.d.	n	mean	s.d.	n	mean	s.d.	n	mean	s.d.	n							
S.A. pre	9.6	0.6	12	5.5	5.4	11	0.18	0.16	12	7.9	1.7	12	56.2	47.7	12	0.39	0.47	12	1.04	1.09	12	1.99	2.00	11
S.A. post	9.6	0.3	10	11.5	9.0	7	0.09	0.14	10	8.7	1.3	10	17.5	24.4	10	0.22	0.42	10	0.58	1.02	9	0.94	1.60	9
Pich n	9.3	0.4	3	14.4	15.3	3	0.18	0.13	3	7.6	1.2	3	32.6	22.8	3	0.45	0.39	3	1.08	0.77	3	1.88	1.26	3

Erosion response to 10 mm/h intensity simulations

SSC (g l ⁻¹)		Erosion rates (g min ⁻¹ m ⁻²)						Sediment yield (g m ⁻²) after															
mean	s.d.	n	mean	s.d.	n	min	max	mean	s.d.	n	mean	s.d.	n	mean	s.d.	n	mean	s.d.	n	mean	s.d.	n	
S.A. pre ^f	0.13	0.16	138	<0.01	<0.01	138	<0.01	11	0.01	<0.01	11	0.06	0.05	11	0.11	0.09	11	0.16	0.13	11	0.21	0.15	11
S.A. post ^g	0.66	0.92	48	<0.01	<0.01	48	<0.01	7	0.01	0.02	7	0.25	0.28	7	0.49	0.65	7	0.69	1.00	7	0.85	1.42	6
Pich n ^h	1.24	2.36	50	<0.01	<0.01	50	<0.01	3	0.18	0.17	3	2.71	2.28	3	3.59	2.95	2	4.45	3.48	3	5.65	4.51	3

Chapter IV

Seasonal logging, process response, and geomorphic work

Abstract

Deforestation is a prominent anthropogenic cause of erosive overland flow and slope instability, boosting rates of soil erosion and concomitant sediment flux. Conventional methods of gauging or estimating post-logging sediment flux focus on annual timescales, but potentially overlook important geomorphic responses on shorter time scales immediately following timber harvest. Sediments fluxes are commonly estimated from linear regression of intermittent measurements of water and sediment discharge using sediment rating curves (SRCs). However, these often unsatisfactorily reproduce non-linear effects such as discharge-load hystereses. We resolve such important dynamics from non-parametric Quantile Regression Forests (QRF) of high-frequency (3-min) measurements of stream discharge and sediment concentrations in similar-sized ($\sim 0.1 \text{ km}^2$) forested Chilean catchments that were logged during either the rainy or the dry season. The method of QRF builds on the Random Forest (RF) algorithm, and combines quantile regression with repeated random sub-sampling of both cases and predictors. The algorithm belongs to the family of decision-tree classifiers, which allow quantifying relevant predictors in high-dimensional parameter space. We find that, where no logging occurred, $\sim 80\%$ of the total sediment load was transported during rare but high magnitude runoff events during only 5% of the monitoring period. The variability of sediment flux of these rare events spans four orders of magnitude. In particular dry-season logging dampened the role of these rare, extreme sediment-transport events by increasing load efficiency during more moderate events. We show that QRFs outperforms traditional SRCs in terms of accurately simulating short-term dynamics of sediment flux, and conclude that QRF may reliably support forest management recommendations by providing robust simulations of post-logging response of water and sediment discharge at high temporal resolution.

Key words: magnitude-frequency-distributions, Quantile Regression Forests, Sediment transport, seasonal logging, Chile

Published as C.H. Mohr., A. Zimmermann, O. Korup, A. Iroumé, T. Francke and A. Bronstert (2013). Seasonal Logging, process response and geomorphic work. *Earth Surface Dynamics Discussions* **1**, 311-335, DOI: 10.5194/esurfd-1-311-2013.

4.1. Introduction

Despite the on-going discussion of whether man-made forests are more prone to soil erosion than native forests or protect degraded soils from erosion instead, reported increases of soil erosion following timber harvest remain undisputed [Gomi *et al.*, 2005; Sidle *et al.*, 2006]. Such major impacts occur during, and a few years after, harvesting operations, before the vegetation re-establishes, and road surfaces and embankments stabilize. Clear cutting may intensify erosive overland flow [Malmer and Grip, 1990], trigger landslides along road cuts [Montgomery *et al.*, 2000], or cause debris flows, and river-bank erosion [Gomi *et al.*, 2004], eventually resulting in infrequent sediment pulses. Thus boosted erosion and re-deposition of soil promote the long-term decay of soil conservation functions not only on harvest patches, but also often in downstream areas [Sidle *et al.*, 2006].

Clear cutting is the most common technique of harvesting timber in the plantation forests of Chile. The nation is currently intensifying and extending its forestry sector, and recent projections point to increasing growth rates of timber and cellulose production [FAO, 2010], and an exacerbation of soil erosion in the future. Yet the forestry sector provides a major income source and thus requires a comprehensive assessment of the economic, social, and ecological benefits of forestry. Reliable knowledge of pre- and post-disturbance sediment fluxes is vital in this regard, and may be acquired by physics-based modelling or statistical treatment of field data. Chilean law mandates immediate replantation after clear cutting, thus limiting the time for sampling hydro-geomorphic impacts of clear cutting such that field data may not represent the full range of water and sediment fluxes. This drawback requires a data analysis technique capable of dealing with few samples of high variance under changing environmental conditions (Figure 4.1a).

Conventional sediment rating curves (SRC) rely on an empirical relationship between water discharge and suspended sediment concentration (SSC), but are prone to high uncertainty where SSC-discharge dynamics are subject to disturbances or nonlinear effects. Recent work revealed that antecedent rainfall, intra-event discharge dynamics [Francke *et al.*, 2008a; Zimmermann *et al.*, 2012], and disturbances due to clear cutting [Mohr *et al.*, 2013] strongly bias SSC prediction based on SRC. This calls for methods capable of reliably simulating antecedent and changing environmental conditions, and predicting SSC following clear cuts. Ideally, such methods should not only sufficiently capture the high rates of sediment transport immediately following timber harvest [e.g., Walsh *et al.*, 2011], but also the underlying process dynamics. Yet most work set out to quantify erosion response to logging has largely neglected high-frequency time series of water and sediment flux. Here we

use Quantile Regression Forests (QRF), a robust multivariate and non-parametric regression technique [Meinshausen, 2006] as a viable and more robust alternative to the traditional SRC approach. We are motivated by the successful application of QRF to successfully modelling multiple SSC peak events, and hysteresis loops between stream flow and suspended sediment discharge [Francke *et al.*, 2008a; Francke *et al.*, 2008b; Zimmermann *et al.*, 2012].

In this study we apply QRF to predict from a high-frequency (3-min) time series of stream discharge and discrete SSC samples the impacts of different seasonal logging on the frequency-magnitude distribution of catchment sediment flux. We show that this technique allows resolving changes to the distribution of geomorphic work at hitherto unprecedented detail, thus providing unique insights into hydro-geomorphic process dynamics following forestry operations.

4.2. Study sites

We focus on three small ($\sim 0.1 \text{ km}^2$) headwater catchments that are part of a network of eleven experimental catchments in the coastal mountains of south-central Chile, close to the city of Nacimiento in the Biobio River basin (Figure 4.1b). The catchments have largely similar size, geology, soils, hydrogeology, topography, and vegetation, but differing forestry practices. The dominant soil type is a clayey to loamy Luvisol that is locally disturbed by forestry operations, and underlain by a deeply weathered saprolite on top of schist bedrock (Mohr *et al.*, 2012). The climate is Mediterranean, and rainfall intensities are low and do not exceed 10 mm/h in average. Intense convective storms are extremely rare. Previous work shows that only 5% of the registered rainfall events exceed 23 mm h^{-1} [Mohr *et al.*, 2013].

Two catchments previously planted with *Pinus radiata* were logged by the same clear-cutting technique during different seasons: catchment #3 was clear cut during the winter rainy season (Jul-Aug 2009), and remained bare for ~ 1 year, whereas catchment #4 was harvested during the dry summer season (Feb 2010), and reforested shortly after (Figure 4.2a). The clear cut was done using heavy rubber-tired skidders to drag logs uphill to landings whereas cable logging was limited to steep slopes [Mohr *et al.*, 2013] (Figure 4.2b). Catchment #1 remained unlogged and covered with *P. radiata*, and served as a control catchment. On February 27, 2010, the study area was hit by the $M8.8$ Maule earthquake that caused ground shaking for 2.5 min at ground accelerations of $\sim 0.3 \text{ g}$. The regional hydrological response featured an abrupt drop in stream discharge followed by a rapid increase [Mohr *et al.*, 2012].

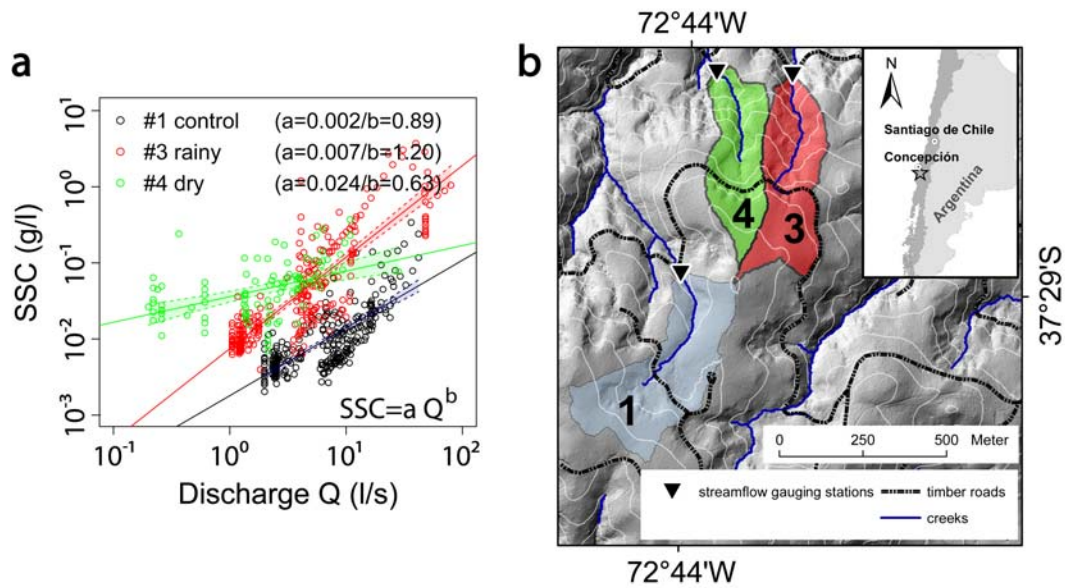


Figure 4.1. (a) Sediment rating curves for the catchments with fitted power-law intercepts a ($gs^b l^{(b+1)}$), slopes b , and 95%-confidence intervals about regression lines. (b) Location of study catchments (star in inset) including stream gauges; nearest rain gauge; and unpaved timber roads. Topography derived from LiDAR survey; contour spacing is 20 m. Numbers (consistent with previous work) refer to catchments. See *Huber et al.* [2010], *Mohr et al.* [2012] and *Mohr et al.* [2013] for detailed descriptions of these catchments.



Figure 4.2. Pictures showing the experimental catchments, the logging procedure and the suspended sediment monitoring devices. (a) Rainy season logged watershed (watershed #3) in the subsequent dry season (March 2010); (b) Skidder dragging logged stems uphill to the next landing in watershed #3; (c) Custom-built sediment sampling system: (1) Horizontal rotating table used to sample suspended sediment on event-base; (2) Recipient used to collect bulk sample of suspended sediment on weekly base.

4.3. Methods

4.3.1. Field sampling

We measured stream discharge with V-notch Thompson gauges equipped with custom-built water-stage recorders at a frequency of 3 min, and a water-level accuracy of 2 mm [Huber *et al.*, 2010, Mohr *et al.*, 2012, Mohr *et al.*, 2013]. To the best of our knowledge, such high temporal resolution is unique among similar monitoring studies. Rainfall was recorded by a Hobo tipping bucket with resolution of 0.2 mm. Hourly rainfall intensities were statistically tested using a Wilcoxon rank sum test at the 5%-significance level to test for differences between both studied years. Bulk monitoring data of sediment fluxes from June 2008 to September 2009 in these and adjacent catchments indicate that pine plantations were more prone to soil erosion than eucalyptus plantations [Huber *et al.*, 2010]. With bed load being negligible in the coastal mountains [Iroumé, 1992], i.e. <1% of the total load [Huber and Mohr, unpublished data], we acquired high-frequency data on instantaneous SSC from June 2009 to August 2010 in order to quantify sediment flux in response to logging activities. We sampled SSC on an event basis with an electric pump armed on a floating device submerging the pump aperture at a constant depth of 5 cm below the water surface in the weirs. We took instantaneous SSC samples on an event basis at 30- to 60-min intervals (Figure 4.2c). In the absence of significant rainfall events, we took at least one complementary daily sample during February/March, and August 2010 for characterizing low-flow conditions (Table 4.1). All SSC samples were then rounded to the next 3-minute interval to synchronize with discharge measurements. SSC were determined gravimetrically with an accuracy of 0.5 mg after filtering the runoff samples [Mohr *et al.*, 2013]. We obtained sediment yields by multiplying the SSC with the runoff volume summed over the respective time intervals

$$SSY = \int_{t_1}^{t_2} Q(t) SSC(t) \quad (4.1)$$

where SSY is suspended sediment yield (g s^{-1}), Q is instantaneous discharge (l s^{-1}), and SSC is instantaneous sediment concentration (g l^{-1}).

Table 4.1. Number of total samples for each catchment. Sample size of pre-logging period given in brackets.

Catchment	Sample number n	Start date	End date
#1	278	06/27/2009	08/15/2010
#3	276 ($n_{\text{pre}}=89$)	06/27/2009	08/29/2010
#4	100 ($n_{\text{pre}}=24$)	02/19/2010	08/28/2010

We complemented this event-based sampling by monitoring suspended sediment flux with weekly volume weighted bulk sampling [Huber *et al.*, 2010] (Figure 4.2c). Despite larger sampling intervals, this alternative monitoring scheme provided data without the need to interpolate SSC. We considered these data as first-order benchmarks for the modelled sediment fluxes. To obtain representative and homogeneous integrated samples, the pump sampled water volumes that are always directly scaled to water stage with higher discharge contributing commensurately more than lower water stages. Any integrated sample merged four samples each day over a period of one week [Huber *et al.*, 2010]. The sediment yields were then estimated following Eq. 4.1 as previously described.

4.3.2. Sediment rating curve (SRC)

For each catchment, we fitted sediment rating curves to a power-law function relating SSC values to the correlate discharge Q [e.g., Gomi *et al.*, 2005]

$$SSC = a Q^b \quad (4.2),$$

where a ($g s^b l^{(b+1)}$) and b are empirical fitting parameters of log-transformed data. Based on the SRC, we predicted SSC during the study period and performed the same 20-fold cross validation procedure as described for QRF (see 4.3.3).

4.3.3. Quantile Regression Forests (QRF)

Quantile Regression Forests (QRF) is a robust non-parametric regression technique [Meinshausen, 2006] that builds on Random Forest (RF) regression tree ensembles, a data mining method based on the repeated random selection of both training data and predictors [Breiman, 2001]. QRF is a generalization of the RF algorithm. For each node in each tree,

RFs calculate the mean of the observations that are split along this node. RF does not consider further information, whereas QRF considers the full distribution of all tree predictions [Meinshausen, 2006], thus quantifying inherent uncertainties of each model [Zimmermann *et al.*, 2012]. This step is needed for estimating prediction intervals, which encompass new observations with high likelihood. Both the RF and QRF algorithms also help to incorporate effects of variable interaction, and offer means of quantifying relative variable importance [Francke *et al.*, 2008a; Zimmermann *et al.*, 2012] by assessing the decline in model performance due to randomizing predictor variables during each iteration.

4.3.4. QRF model

We set up individual QRF models for each catchment to predict SSC from the (a) rainfall and discharge time series; (b) day of year to account for possible seasonality effects; and (c) change in discharge to capture dynamics between events [Francke *et al.*, 2008a]. We quantified antecedent hydro-meteorological conditions by computing predictor variables that integrated antecedent rainfall and discharge values over multiples of the sampling interval. Time interval and number of aggregation levels were set to 3 and 6, respectively. These settings describe the successive increase of aggregation windows into the past and their total number in the generation of the aggregated predictors. For example, P₂₈₋₈₁ refers to the rainfall accumulated between 28 and 81 min prior to a given SSC sample [Zimmermann *et al.*, 2012]. In order to prevent collinearity, overlaps between each window were avoided [Zimmermann *et al.*, 2012]. We added counter variables starting at the time of clear cutting to capture possible effects of timber harvest and vegetation recovery over time to involve changing environmental conditions. We further defined a switch variable that stratified the data into pre- and post-seismic periods for identify potential earthquake impacts (Supplementary Table 4.1).

We assessed the relative predictor importance based on permutation [Strobl *et al.*, 2008]. This measure accounts for multi-collinearity and associated overestimation of variable importance due to spurious correlation artefacts [Liaw and Wiener, 2002]. We validated model performance applying the root mean square error

$$RMSE = \sqrt{\frac{1}{N} \sum_{i=1}^N (x_i - \hat{x})^2} \quad (4.3)$$

for N measurements x_i , and predictions \hat{x}_i . In order to avoid arbitrary decisions during the validation procedure, e.g. size and location of the test data set, we applied a 20-fold cross validation leaving out continuous data blocks of 5% of the data to test the models, respectively [Zimmermann *et al.*, 2012]. We defined 10% of the SSC range (g l^{-1}) as a threshold range for acceptable model performance accounting for the distinct parameter range of measured SSC, and inherent erosion modeling limitations. Such limitations arise from unavoidable bias due to the random component of all measured data feeding any erosion model [Nearing, 1998]. Finally, we estimated suspended sediment yields for each 3-minute time step applying a Monte Carlo simulation [Francke *et al.*, 2008a]. To this end we randomly drew a SSC prediction from the distribution realized by the QRF model for each time step. Based on these samples, we estimated event dynamics and both monthly and annual sediment yields by summing up the products of Q and SSC at each time step over each target period. By repeating this procedure 250 times, we obtained a distribution of SSY estimates which was then checked for Gaussian shape. The latter allowed us to calculate their mean value and standard deviation to assess the spread of the predicted sediment yields [Zimmermann *et al.*, 2012].

4.4. Results

Compared to the traditional sediment-rating curve approach, QRF predicted SSC with high accuracy under both low- and high-flow regimes, as well as unlogged and logged conditions. Figure 3 illustrates the predictive accuracy for high SSC under disturbed conditions, and the additional advantage of QRF to compensate for poor, or impute missing, rainfall and discharge data (Figure 4.7a-c). The method also reproduced hysteresis loops, and the occurrence of multiple peak events (Figure 4.3). Treating errors $<10\%$ of the measured SSC range as acceptable, both QRF and SRC met this criterion across all catchments (Supplementary Table 4.2). Yet QRF generally outperformed SRC except for rainy-season logging where the large range of measured SSC values shrunk relative differences in model performance to $<1\%$.

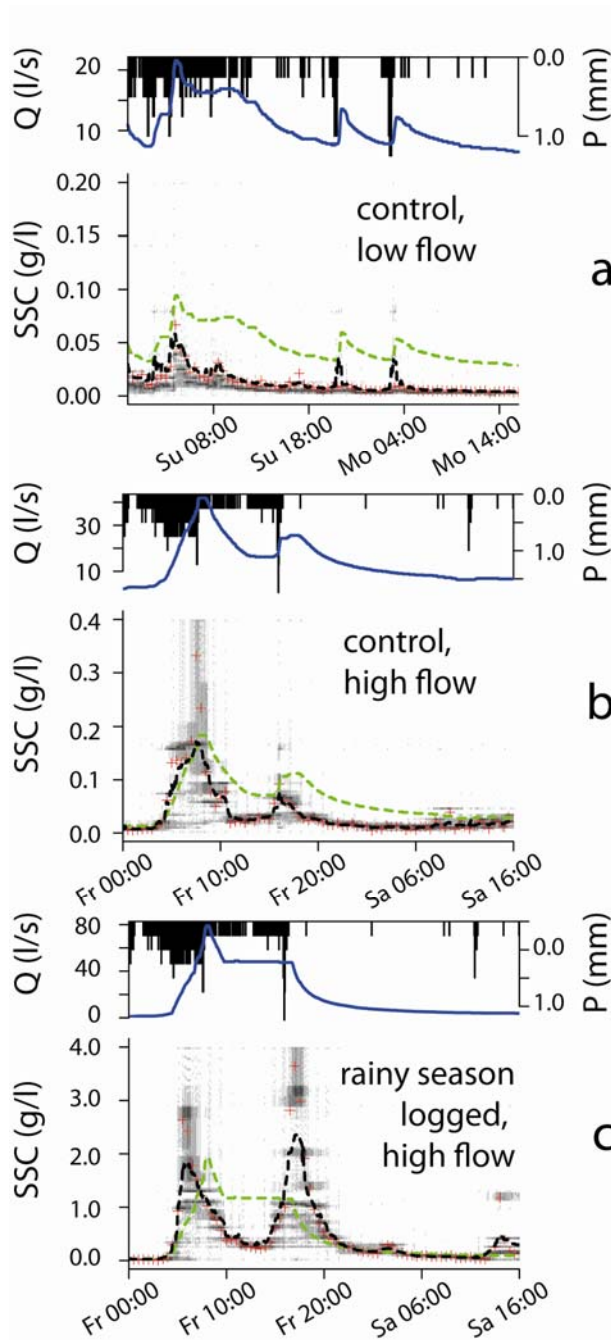


Figure 4.3. Water discharge and SSC dynamics under unlogged and logged conditions during two rainfall events. (a) Jun 27-29, 2009, catchment #1; (b-c) Aug 14-15, 2009, catchments #1 and #3. Density of SSC predictions of the QRF model for each time step encoded by SSC in coloured histograms; black dashed lines are means of these predictions; red crosses are measured SSC; green dashed lines are SSC predictions of the SRC. Data are from calibration period, i.e. periods are covered with SSC samples used for model building (see Figure 7 for limits to model predictions).

We compared monthly and annual specific suspended sediment yields (SSY) predicted from both QRF and SRC with the bulk data, using a Monte Carlo simulation [Francke *et al.*, 2008a] (Supplementary Tables 4.3-5). Specific sediment yield averaged for the first two years following rainy-season logging was $3.27 \pm 0.09 \text{ t ha}^{-1}$ or ~ 20 times the SSY predicted for unlogged conditions ($0.19 \pm 0.004 \text{ t ha}^{-1}$; $\pm 1 \sigma$). However, monthly SSY from the catchment planned to be harvested during rainy season exceeded that in the unlogged control catchment by a factor of ~ 5 even before logging commenced (Figure 4.4a). Similarly, the catchment that was subjected to dry-season logging yielded ~ 4 times the SSY of the control catchment before it was clear cut (Figure 4.4b). The decreasing slope of the double-mass curve after dry-season

logging indicates that soil erosion intensified over undisturbed conditions only after rainy-season logging.

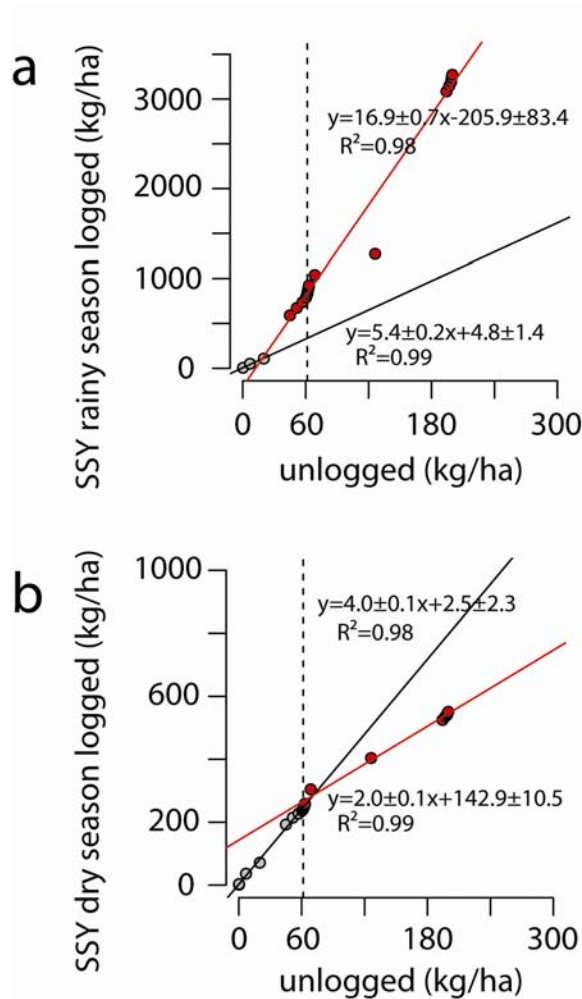


Figure 4.4. Monthly double mass-curve analysis between the sediment yields (SSY) of catchments logged during (a) rainy and (b) dry season, and the unlogged control catchment. Black vertical dashed line separates 2009 and 2010 study periods; grey and red circles are pre- and post-logging sediment yields, respectively; lines are best-fit linear regression models. Uncertainties are ± 1 standard deviations.

When normalized to the increase under unlogged control conditions, SSYs increased from 2009 to 2010 by $\sim 125\%$ following rainy-season logging, but decreased by $\sim 40\%$ after dry-season logging. This finding is in line with our bulk data measurements (Supplementary Table 4.3). Overall, QRF predicted substantially higher sediment yields than the SRC approach. Only for undisturbed conditions and dry-season logging were SRC predictions within the same order of magnitude. Based on bulk data, SRC underestimates annual SSY by a factor of 2-28 (Supplementary Table 4.3), despite overestimating sediment flux during individual peak runoff events (Figure 4.3; Supplementary Figure 4.1).

Our QRF-derived estimates show that, under unlogged conditions, $\sim 80\%$ of the total sediment load carried during the monitoring period was transported during only $\sim 5\%$ of the time. Most of the sediment was transported during rare, large runoff events. The instantaneous flux rate (g s^{-1}) variability of these rare events spanned four orders of magnitude, and thus more than the variability of all other rates occurring over 95% of the monitoring period

(Figure 4.5a). Our QRF data thus indicate that logging, regardless of its seasonal timing, coincided with a relatively increased contribution of moderate as opposed to extreme runoff events in terms of sediment transport. Thus, immediate post-logging effects on sediment transport involved the reduction of sediment transport during peak flow events while shifting the geomorphic work towards less flashy and more moderate events. We found this effect to be more pronounced for dry-season than for rainy-season logging (Figure 4.5b).

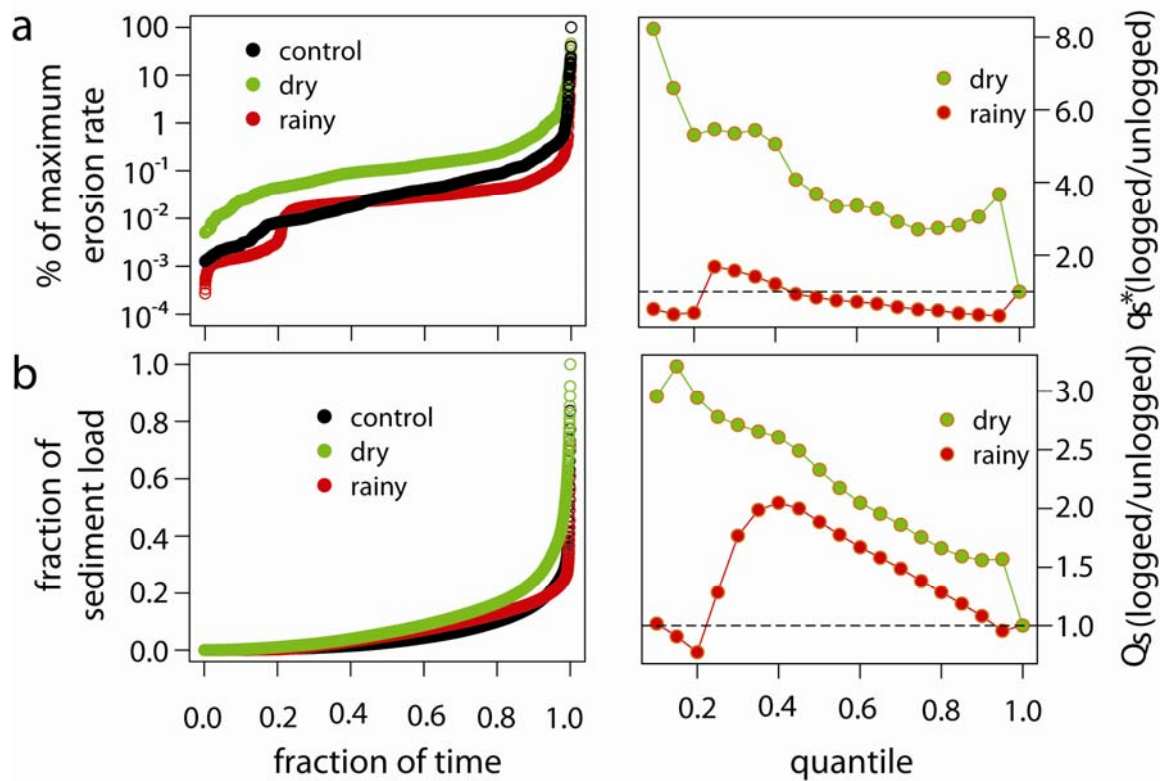


Figure 4.5. (a) Fraction of instantaneous sediment transport rates normalized to catchment maximum as a function of monitoring time during which these rates were not exceeded. (b) Fraction of total sediment load normalized per catchment as a function of the fraction of total monitoring period for unlogged conditions, rainy-, and dry-season logging. Right-hand panels show resulting ratios of instantaneous transport rates q_s^* , and total sediment loads Q_s , per quantile for logged versus unlogged conditions. Black vertical dashed lines are 1:1 ratio. Empirical cumulative distribution functions differ significantly ($p < 0.01$; Kolmogorov-Smirnov test).

To rank the contributions of different environmental controls as predictors of sediment flux we quantified their relative importance in terms of added total predictive accuracy (Figure 4.6). We found that antecedent rainfall accumulated 28 to 81 min prior to a given SSC sample was most influential for unlogged conditions, whereas the timing of logging was not. In contrast, logged catchments did not respond to such short-term rainfall memory. Instead, rainfall accumulated over 244-729 min, and 730-2181 min showed the highest importance for the catchments clear cut during the rainy, and dry seasons, respectively (Figure 4.6). Near-instantaneous discharges cumulated over 1-3 and 4-9 min prior to SSC sampling were

important for both unlogged and rainy-season logging catchments. Neither the day of year nor the timing of the 2010 earthquake showed any significant influence on the SSC predictions (Figure 4.6).

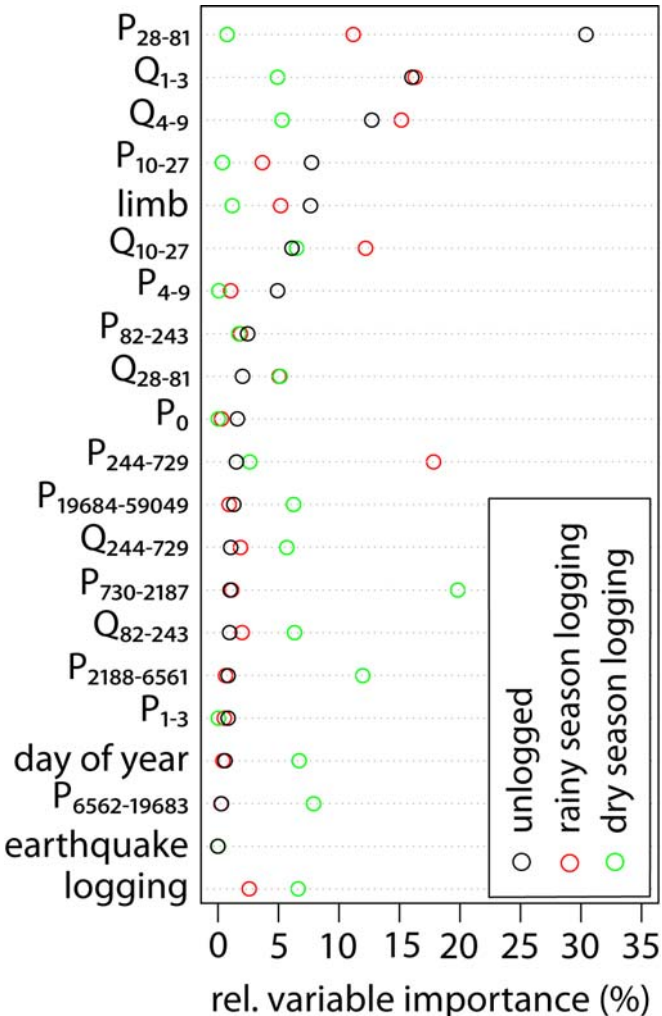


Figure 4.6. Variable importance of the Quantile Regression models for each catchment scaled to 100% in order to facilitate inter-catchment comparison. See Supplementary Table 4.1 for predictor variables.

4.5. Discussion

Our results show that high-frequency (3-min) time series of post-logging water and sediment fluxes are instructive with regard to understanding immediate hydro-geomorphic process response despite several unavoidable uncertainties. For one, our bulk sediment flux measurements are minimum estimates given their low temporal resolution compared to the fast hydrological response, so they do not fully capture potentially high SSC during intense rainfall events. Furthermore, we find that conventional sediment rating curves (SRCs) are sensitive to outliers, resulting in implausible high SSC (e.g. 10-15 g s⁻¹; Figure 4.7e), but remain below our QRF predictions on average (Supplementary Tables 4.3, 4.6).

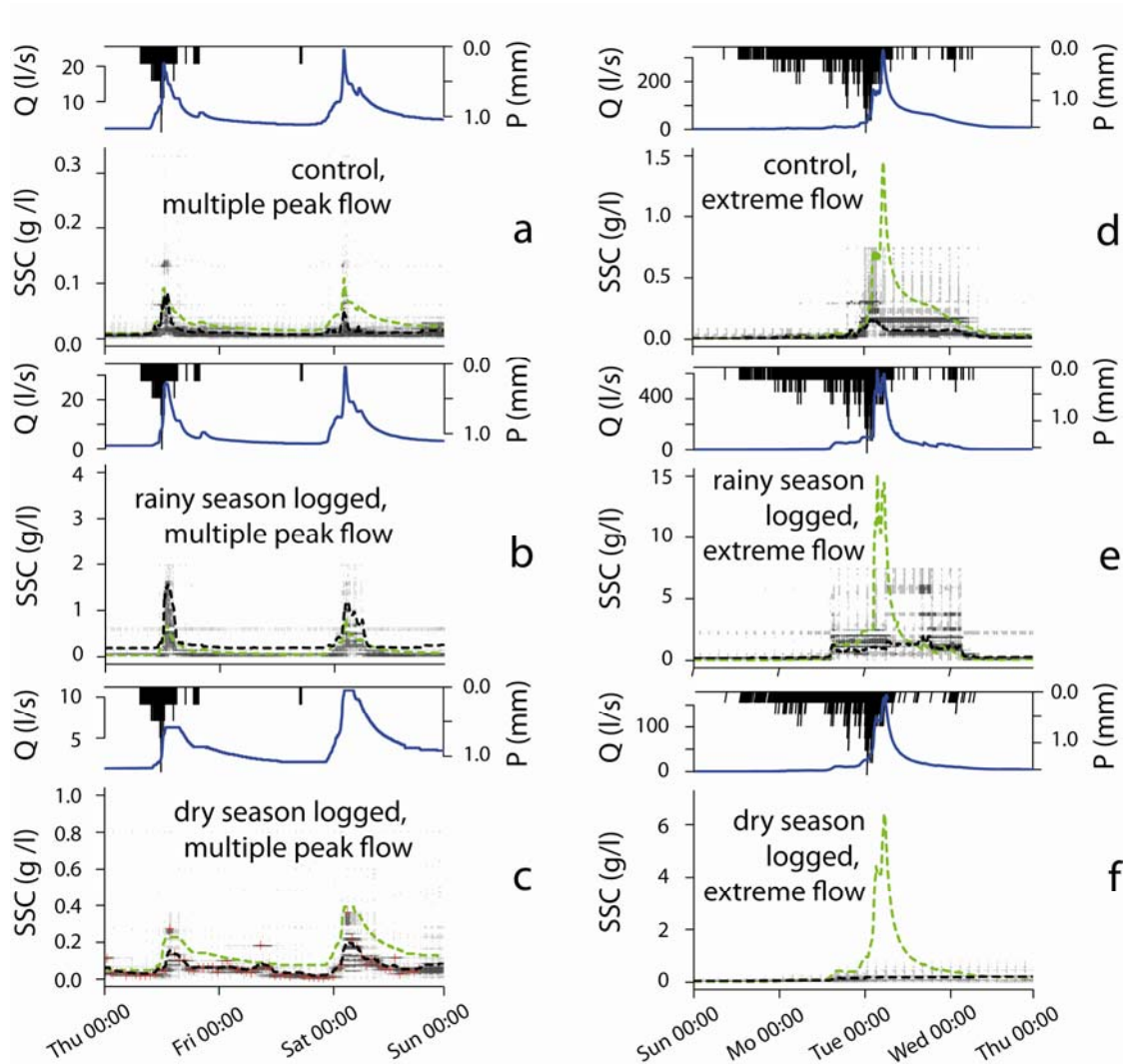


Figure 4.7. QRF model results of SSC dynamics during extreme peak flow for undisturbed and logged conditions during two rainfall events, i.e. Aug 15-18, 2010 (a-c) and Aug 26-28, 2010 (d-f). Density of SSC predictions of the QRF model for each time step encoded by grey histograms; black dashed lines are means of these predictions; red crosses are measured SSC; green dashed lines are SSC predictions based on SRCs.

Under the recorded low-flow regime [Huber *et al.*, 2010], SRCs underestimate the hydro-geomorphic work of more frequent though lower sediment fluxes, while they overestimate the less frequent higher-magnitude events. This finding supports earlier work arguing that SRCs significantly underestimate sediment fluxes [e.g., Asselman, 2000]. Overall, the QRF predictions cast a much more detailed and consistent light on high-frequency post-logging sediment flux, particularly with regard to systematic shifts in the frequency-magnitude distribution of high-frequency sediment transport rates and total loads (Figure 4.5). The choice of season for clear-cut logging is linked to distinct changes to the relative overall sediment transport efficiency with a general trend towards emphasizing

moderate flows, while dampening the efficiency of more rare and extreme events. Our results significantly expand down to the process time scale the notion that extreme sediment transport events may perform the bulk of geomorphic work [Korup, 2012]. Our findings also underscore the impact that logging may have on shifting the underlying frequency-magnitude distributions of water and sediment flux (Figure 4.5). We interpret these as statistically robust changes, given that QRF avoids over-fitting by randomly selecting both data and predictor subsets, while providing objective measures of their relative importance (Figure 4.6). Predictor importance also changes as a function of the logging season. The resulting predictions are not only in line with the base flow-dominated discharge, but also maintain low uncertainty because of the averaging out of low-precision predictions [Zimmermann *et al.*, 2012]. Nevertheless, QRF may have drawbacks for high magnitude rainfall-runoff events (Figure 4.7d-f) given the method's inability to extrapolate beyond the parameter space, and especially the monitoring period. Seasonal effects may not be fully represented in the time series (Figure 4.6) because our observation windows in time have significantly different rainfall patterns (Supplementary Table 4.4). Our study area is dominated by frontal rainfall events instead of high-intensity convective storms, and we caution against extrapolating our results for rainfall-runoff events of higher magnitude. In essence, QRF is a robust and versatile method for hindcasting high-frequency time series of water and sediment discharge, but not designed for predicting future events.

Compared with similar studies on logging effects [e.g., Gomi *et al.*, 2005], our QRF predictions indicate very low to even slightly decreasing post-logging sediment yields following dry-season logging when compared to unlogged conditions. Our observation of increased post-rainy-season logging sediment flux is consistent with previous work [e.g., Sidle *et al.*, 2006]. Yet the magnitude of this increase is small [e.g., Gomi *et al.*, 2004], and our SSY estimates are within the range reported for natural, undisturbed forests [Zimmermann *et al.*, 2012]. The observed decreases of SSY following dry logging (Figure 4.4b) may partly be due to prompt replanting of the logged slopes [Malmer and Grip, 1990]. Some maintenance works on a timber road in 2010 in the unlogged catchment are also likely to have contributed to elevating the local sediment supply given that unsealed timber roads may dominate sediment production per unit area in managed forests [e.g., Motha *et al.*, 2003]. Consequently, we expect that the thus elevated sediment flux in the unlogged catchment may have partly smothered the relative impact of logging in the other catchments.

We also exclude seasonal meteorological differences as drivers of the elevated SSYs in 2010, as rainfall was much higher in 2009 at comparable intensities (Supplementary Table

4.3). Moreover, the timing of the 2010 earthquake did not notably distort any of the SSC predictions (Figure 4.6) despite favourable conditions for post-seismic increases in sediment flux [Hovius *et al.*, 2011]. The limited earthquake response may be linked to a decisive lack of post-seismic rainfall in 2010, which may have otherwise triggered mass wasting. Plantations of *P. radiata* are prone to mass wasting because of their low root-strength compared with other species [Watson *et al.*, 1999]. When logged, they rapidly decay in root-strength [Sidle, 1991]. Shallow landslides are also promoted by slow root-strength recovery rates and cumulative effects of preceding rotations [Sidle *et al.*, 2006]. Given that root decay and regrowth have opposite trends over time, we expect maximum mass wasting rates 2-3 years after logging [Watson *et al.*, 1999]. Hence, our immediate post-logging predictions of SSC (Figure 4.6) are consistent with mechanistic slope-stability models [Sidle *et al.*, 2006]. During the monitoring period of this study, however, we regard the contribution of mass wasting processes as minor, and hitherto insufficient, for explaining the hydro-geomorphic post-logging regimes.

The QRF-derived variable importance plot supports the notion of a predominant overland flow mechanism of recent harvest areas (Figure 4.6). Infiltration capacity may increase on recently logged areas, thus impeding infiltration-excess overland flow generation under the low rainfall intensities observed [Mohr *et al.*, 2013]. Alternatively, high-duration rainfall is required to elevate groundwater levels, which in turn initiate erosive saturation-excess overland flow [Dunne and Black, 1970], and connect sediment sources to the drainage network. The relevance of several antecedent rainfall characteristics for predicting post-logging sediment fluxes reflects the local rainfall regime, where low-intensity and long-duration rainfall events successively saturate the soil layers over time, thus permitting erosive overland flow [Huber *et al.*, 2010]. Compared with rainy-season logging, the measured SSC following dry-season logging also responded to significantly longer time lags. The lower cohesion of wet soil elevates sediment supply for erosive overland flow during timber machinery action in the rainy season. Hence, the susceptibility to soil erosion is higher compared to logging in dry soil conditions. The distinct micro-topography left by heavy machinery persisted following dry-season logging until the subsequent rainy season, thus impeding overland-flow connectivity, and requiring larger volumes of water to re-establish connectivity [Mohr *et al.*, 2013]. In contrast, SSC under unlogged conditions appears to be modified by more short-term antecedent rainfall characteristics (Figure 4.6). Such flashiness may indicate effects of hydrophobic plantation forest cover [e.g., Miyata *et al.*, 2009].

4.6. Conclusions

Our study provides novel insights into the immediate hydro-geomorphic process response to different seasonal timber harvest operations. We find that Quantile Regression Forests (QRF) outperform sediment rating curves (SRC) in terms of accurately predicting post-logging sediment yields at the process scale. Using empirical sediment rating curves may lead to grave underestimates of sediment fluxes from managed forests. Our unprecedented high-frequency data on post-logging water and sediment fluxes from three Chilean headwater basins corroborates the widely held view that most sediment transport is accomplished within a few rare high-discharge events, particularly at the timescale of immediate hydro-geomorphic process response. Moreover, QRF-based hindcasting underlines that it is the seasonal timing of clear cutting that dictates the amount of shift in the frequency-magnitude relationship of sediment transport, eventually redistributing geomorphic work from rare, extreme events to more moderate ones. Dry-season logging led to a much higher dampening of extreme events, whereas rainy-season logging accentuated the contrasts in instantaneous transport rates. Post-logging increases in sediment flux, most likely driven by saturation-excess overland flow, were an order of magnitude higher following rainy-season clear cutting.

Our work motivates further testing of whether QRF are suitable tools for longer-term time series, thus allowing direct comparison with studies that recorded the annual to decadal net effects of logging and hydro-geomorphic recovery. Still, given that data scarcity and variability are common for post-logging disturbances, we find that Quantile Regression Forests turns out to be a robust and promising tool for quantifying in detail high-frequency time series of water and sediment fluxes following clear-cut operations.

4.7. Acknowledgements

We thank Andreas Bauer, Johannes Brenner, Franziska Faul, Rodrigo Bravo and Cristian Frêne Conget for helping in field and during data analysis. We are grateful to Forestal Mininco for providing access to our experimental catchments, and acknowledge Anton Huber for support and advice. This study is co-funded by the International Bureau of the German Federal Ministry of Education and Research and the Chilean Government (CONICYT/BMBF 2009-092 and 2010-243).

4.8. Physics-based modelling efforts of water and sediment fluxes following cleat cutting using WASA-SED

In this study, physics-based modelling has been performed in two catchments which were logged in 2007 and 2009 (San Antonio #3 and Pich n, see chapter II and III) [Brenner, 2011; Gläser, 2009]. To this end, The WASA-SED model has been applied for the periods 01-12/2008 (Pich n) and 01-12/2010 (San Antonio).

WASA-SED model is a semi-distributed hydrological process model [Guntner and Bronstert, 2004], which is coupled with erosion and sediment transport routines (SED) [Mueller et al., 2010]. Hence, using WASA-SED provides a tool for simulating and quantitatively estimating water and sediment fluxes. Though this model has been developed for semi-arid climates and has been applied only on larger scales, the model was applied to the study area because of its accentuated seasonal rainfall regime and high summer air temperatures. The main motivation of these modelling efforts was to explore whether WASA-SED would provide meaningful results (1) under such disturbed environmental conditions, and (2) on a rather small study area. Moreover, such process modelling is the only way to provide insights into the potential transferability of the physical laws used to simulate water and sediment discharge.

In the following I am going to briefly present the most important outcomes of the WASA-Sed simulations and their implications for the study. The modelling was conducted by undergraduate student Johannes Brenner (University of Potsdam) (San Antonio) and graduate student Christian Gläser (Technical University of Braunschweig) (Pich n).

4.8.1. Hydrology

Though the overall water balances can be plausibly simulated in Pich n and San Antonio, e.g. with averaged annual runoff coefficients of ~ 0.4 [Brenner, 2011], the faithful simulation of hydrological processes dynamics in both catchments is rather poor. This was particularly the case during the changing seasons, i.e. from dry to rainy season, and from rainy to dry season. Moreover, both modelling studies yielded contrasting results. For San Antonio, Brenner [2011] clearly showed the dominance of interflow, which made up 63% of the total flow. In Pich n, however, Gläser [2009] estimated $\sim 66\%$ of groundwater flow, whereas interflow only contributed $\sim 24\%$ of the total flow. In both modelling studies, the fraction of overland flow was $\sim 12\%$ of the total flow. Furthermore, Gläser [2009] identified infiltration excess overland flow as the predominant overland flow mechanism in contrast to saturation excess overland flow in San Antonio [Brenner, 2011]. Hence, in this case WASA-

SED may give suitable results in terms of the local water balances as the sum of all fluxes, but likely for the wrong reasons [Kirchner, 2006]. This is because the individual water fluxes, e.g. the runoff components groundwater flow, interflow, and overland flow, are not adequately simulated as single fluxes, while the overall water yields, i.e. the sums of all involved water fluxes remain plausible. Brenner [2011] argued that such outcomes may result from the single permeability approach, which conflicts with frequent preferential flow paths bypassing the low conductive soil matrix. Preferential flow patterns are associated with near-surface soil disturbances and thus small-scale heterogeneity of soil-hydraulic properties following loggings (see Chapter 3.5). Moreover, the flow routing approach of WASA-SED could not be applied to the studied catchments because of spatial scale constraints, i.e. the studied catchments are too small to establish a flow routing using tributaries. This resulted into a transfer of water and sediment to the outlet that is too fast compared to the observations, as the simulated, extremely flashy, rising and falling limbs show. Hence, the runoff mechanisms and their timings could not be captured in a satisfactory way by WASA-SED. This is an important finding, since hillslope sediment fluxes are driven by erosive overland flow, which in turn complicates robust prediction of sediment fluxes.

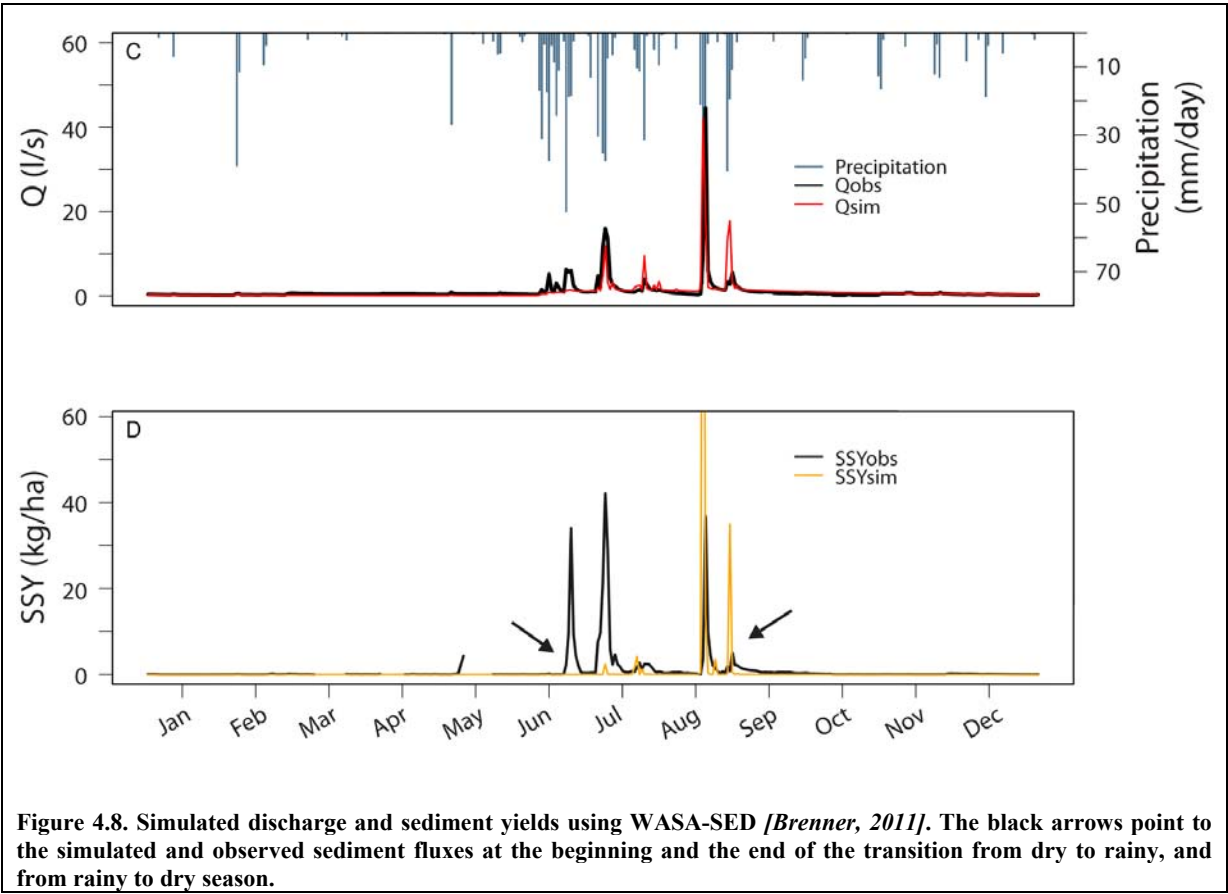


Figure 4.8. Simulated discharge and sediment yields using WASA-SED [Brenner, 2011]. The black arrows point to the simulated and observed sediment fluxes at the beginning and the end of the transition from dry to rainy, and from rainy to dry season.

4.8.2. Sediment fluxes

In the WASA-SED model, sediment flux is restricted exclusively to rainy seasons. This implies that sediment flux is driven only by saturation excess overland flow because rainfall intensities did not show any temporal pattern, and remained at similar levels throughout the rainy season instead.

Under these conditions, simulated annual sediment yields reached < 75% of the observed sediment flux [Brenner, 2011], indicating consistent, though conservative model results. However, when compared with the observations, simulated sediment flux is overestimated towards the end of the rainy season (under saturated soil conditions, see Figure 2.2. in Chapter 2.3). In contrast, the model results underestimated or even failed to reproduce any sediment flux at the beginning of the rainy season when soils are still saturated (Figure 4.8). At the same time, the rainfall intensities do not substantially change over the seasons. This could explain infiltration excess driven sediment flux.

The over- and underestimation of sediment flux at the end and beginning of the rainy season, respectively, conflicts with the observations. Such systematic temporal pattern in sediment transport thus suggests that saturation excess overland flow may indeed control the bulk of the sediment load. However, this mechanism cannot explain the sediment flux at the beginning of the rainy season. Thus, other overland processes than saturation excess overland flow are required to explain the sediment load that is transported (mainly) at the beginning of the rainy season.

4.8.3. Synopsis of the modelling studies and implications

At the end of the dry season when the first rainfalls occur, the soils are far from being saturated. Under these conditions, the WASA-Sed modelling results are consistent with the identified threshold above which infiltration excess overland flow may be triggered which in turn additionally contributes to the sediment fluxes on timber harvest areas. However, the contribution of infiltration excess overland flow to total sediment flux is underestimated. At the end of the rainy season when soils are saturated, the model overestimates saturation excess driven sediment fluxes.

4.9. Supplementary Information

Supplementary Table 4.1: Predictor variables used for QRF-modelling.

Predictors	Description
Q ₁₋₃	Discharge accumulated over 1-3 minutes prior the SSC measurement
Q ₄₋₉	Discharge accumulated over 4-9 minutes prior the SSC measurement
Q ₁₀₋₂₇	Discharge accumulated over 10-27 minutes prior the SSC measurement
Q ₂₈₋₈₁	Discharge accumulated over 28-81 minutes prior the SSC measurement
Q ₈₂₋₂₄₃	Discharge accumulated over 82-243 minutes prior the SSC measurement
Q ₂₄₄₋₇₂₉	Discharge accumulated over 244-729 minutes prior the SSC measurement
P ₀	Rainfall registered at the same time of the SSC measurement
P ₁₋₃	Rainfall accumulated over 1-3 minutes prior the SSC measurement
P ₄₋₉	Rainfall accumulated over 4-9 minutes prior the SSC measurement
P ₁₀₋₂₇	Rainfall accumulated over 10-27 minutes prior the SSC measurement
P ₂₈₋₈₁	Rainfall accumulated over 28-81 minutes prior the SSC measurement
P ₈₂₋₂₄₃	Rainfall accumulated over 82-243 minutes prior the SSC measurement
P ₂₄₄₋₇₂₉	Rainfall accumulated over 244-729 minutes prior the SSC measurement
P ₇₃₀₋₂₁₈₇	Rainfall accumulated over 730-2187 minutes prior the SSC measurement
P ₂₁₈₈₋₆₅₆₁	Rainfall accumulated over 2188-6561 minutes prior the SSC measurement
P ₆₅₆₂₋₁₉₆₈₃	Rainfall accumulated over 6562-19683 minutes prior the SSC measurement
P ₁₉₆₈₄₋₅₉₀₄₉	Rainfall accumulated over 19684-59049 minutes prior the SSC measurement
limb	Raising of falling discharge limb during SSC measurement
day of year	Day of year
earthquake	Switch variable separating pre- from post-earthquake sample periods
logging	Continuous counter variable starting at the time of the clear cutting

Supplementary Table 4.2: Performance of Quantile Regression Forest models (QRF) and sediment rating curves (SRC) with 20-fold cross-validation of SSC predictions using root mean squared error (RMSE). *20 parameters; ** 21 parameters; * 2 parameters.**

Catchment	SSC range (g l ⁻¹)	RMSE (g l ⁻¹)	
		QRF	SRC*** (SSC = aQ^b)
#1	0.002-0.332	0.01*	0.03
#3	0.004-3.646	0.06**	0.07
#4	0.007-0.363	0.05**	0.10

Supplementary Table 4.3: Bulk data and modelled annual suspended sediment yields in 2009 and 2010 at the catchment outlets of control catchment (#1), rainy-season clear cutting (#3) and dry-season clear cutting (#4). Annual rainfall yields from local rain gauges [Mohr *et al.*, 2012]; errors are ± 1 standard deviation.

	Year	Catchment #1 (t ha ⁻¹ yr)	Catchment #3 (t ha ⁻¹ yr)	Catchment #4 (t ha ⁻¹ yr)	Rainfall (mm yr ⁻¹)
Measured bulk data	2009	0.15	0.28	0.22	1463.9
	2010	0.56	0.88	0.55	1120.8
QRF	2009	0.06 \pm 0.00	0.83 \pm 0.01	0.39 \pm 0.00	
	2010	0.14 \pm 00	2.43 \pm 0.08	0.48 \pm 0.01	
SRC	2009	0.02	0.08	0.12	
	2010	0.02	0.12	0.14	

Supplementary Table 4.4: Monthly suspended-sediment yields [kg/ha] based on bulk data during the study period 2009-2010 at the catchment outlets; errors are ± 1 standard deviation. Grey shaded cells are post-logging periods. Monthly rainfall from rain gauges #1, #2 and #3 (Figure 1b).

Study period	Monthly SSY Catchment #1 (kg ha ⁻¹)	Monthly SSY Catchment #3 [(kg ha ⁻¹)	Monthly SSY Catchment #4 (kg ha ⁻¹)	Monthly rainfall (mm)
01/2009	0.4	2.0	1.1	3.44
02/2009	0.3	1.8	0.8	6.45
03/2009	0.4	6.3	0.9	2.37
04/2009	0.3	0.2	1.5	14.94
05/2009	1.2	4.6	4.1	207.60
06/2009	34.2	62.9	28.5	371.48
07/2009	42.8	73.2	24.6	160.61
08/2009	50.3	103.3	132.2	372.26
09/2009	12.8	10.5	15.9	88.40
10/2009	2.3	6.9	3.1	146.41
11/2009	2.7	3.0	6.1	83.17
12/2009	1.7	3.2	2.2	6.72
01/2010	2.0	3.0	1.6	10.96
02/2010	2.7	4.8	3.1	81.42
03/2010	1.4	6.1	3.9	6.97
04/2010	1.4	8.6	4.4	1.49
05/2010	3.3	23.8	17.0	62.50
06/2010	21.4	84.5	119.6	316.77
07/2010	342.2	117.6	230.1	214.35
08/2010	177.3	448.7	131.7	258.97
09/2010	7.1	25.2	24.9	23.51
10/2010	3.5	39.9	4.6	38.84
11/2010	1.6	114.2	5.5	48.80
12/2010	0.6	3.3	5.6	55.78

Supplementary Table 4.5: Monthly SSY [kg/ha] estimates by QRF during study period 2009-2010 at the catchment outlets. Errors are ± 1 standard deviation. Grey shaded cells indicate post-logging periods.

Study period	Monthly SSY Catchment #1 (kg ha ⁻¹)	Monthly SSY Catchment #3 (kg ha ⁻¹)	Monthly SSY Catchment #4 (kg ha ⁻¹)
01/2009	0.15±0.00	2.72±0.04	1.81±0.02
02/2009	0.11±0.00	2.27±0.04	1.04±0.01
03/2009	0.10±0.00	1.84±0.03	0.55±0.00
04/2009	0.00±0.00	0.00±0.00	0.00±0.00
05/2009	0.09±0.00	0.70±0.05	0.21±0.01
06/2009	6.48±0.11	40.50±1.20	33.37±0.36
07/2009	13.02±0.39	62.09±2.95	35.04±0.48
08/2009	24.95±0.44	481.91±10.57	120.63±1.65
09/2009	6.62±0.07	84.26±1.16	22.51±0.21
10/2009	5.65±0.07	60.45±0.73	12.51±0.10
11/2009	3.20±0.03	55.55±0.74	8.54±0.08
12/2009	1.17±0.01	38.75±0.50	6.24±0.04
01/2010	0.48±0.00	30.08±0.41	4.55±0.04
02/2010	0.78±0.04	28.78±0.41	4.03±0.04
03/2010	0.45±0.00	29.14±0.41	5.78±0.04
04/2010	0.00±0.00	0.01±0.00	0.00±0.00
05/2010	0.07±0.00	3.90±0.15	0.97±0.02
06/2010	5.32±0.17	117.28±2.09	46.54±0.56
07/2010	57.58±1.41	232.17±5.86	99.39±1.15
08/2010	67.89±2.45	1814.79±76.20	121.28±2.84
09/2010	2.79±0.03	58.56±0.75	11.02±0.10
10/2010	1.52±0.02	46.56±0.58	4.57±0.05
11/2010	0.99±0.01	44.61±0.60	6.34±0.06
12/2010	0.45±0.00	34.12±0.43	3.35±0.03

Supplementary Table 4.6: Average predicted SSC-values based on the QRF and SRC approach. *In order to account for disturbed conditions of catchments #3 and #4, both years (2009 and 2010) were averaged separately.

Catchment	Predicted SSC (QRF) (g l ⁻¹)		Predicted SSC (SRC) (g l ⁻¹)	
	mean	median	mean	median
#1	0.01	0.01	0.09	0.03
#3*	0.16	0.18	0.04	0.02
#4*	0.05	0.05	0.04	0.02

Chapter V

Streamflow response in small upland catchments in the Chilean Coastal Range to the MW 8.8 Maule earthquake on February 27th 2010

Abstract

Hydrological response to earthquakes has long been observed, yet the mechanisms responsible still remain unclear and likely vary in space and time. This study explores the baseflow response in small upland catchments of the Coastal Range of south-central Chile after the M_w 8.8 Maule earthquake of February 27th 2010. An initial decline in streamflow followed by an increase of up to 400% of the discharge measured immediately before the earthquake occurred, and diurnal streamflow oscillations intensified after the earthquake. Neither response time, nor time to maximum streamflow discharge showed any relationship with catchment topography or size, suggesting non-uniform release of water across the catchments. The fast response, unaffected stream water temperatures and a simple diffusion model point to the sandy saprolite as the source of the excess water. Baseflow recession analysis reveals no evidence for substantial enhancement of lateral hydraulic conductivity in the saprolite after the earthquake. Seismic energy density reached $\sim 170 \text{ J/m}^3$ for the mainshock and $\sim 0.9 \text{ J/m}^3$ for the aftershock, exceeding the threshold for liquefaction by undrained consolidation only during the mainshock. Although increased hydraulic gradient due to ground acceleration-triggered, undrained consolidation is consistent with empirical magnitude-distance relationships for liquefaction, the lack of independent evidence for liquefaction means that enhanced vertical permeability (probably in combination with co-seismic near-surface dilatancy) cannot be excluded as a potential mechanism. Undrained consolidation may have released additional water from the saturated saprolite into the overlying soil, temporarily reducing water transfer to the creeks but enlarging the cross-section of the saturated zone, which in turn enhanced streamflow after establishment of a

new hydraulic equilibrium. The enlarged saturated zone facilitated water uptake by roots and intensified evapotranspiration.

Key words: Chile, Maule, earthquake, evapotranspiration, liquefaction, streamflow.

Published as C. H. Mohr, D. R. Montgomery, A. Huber, A. Bronstert and A. Iroumé, (2013). Streamflow response in small upland catchments in the Chilean coastal range to the MW 8.8 Maule earthquake on 27 February 2010, *Journal of Geophysical Research*, **117**, F02032, doi:10.1029/2011JF002138.

5.1. Introduction

Hydrological responses to earthquakes include increased streamflow discharge, loss or appearance of springs, changes in subsurface groundwater levels and modifications of hydrochemical properties, like water temperature and water turbidity [Montgomery and Manga, 2003; Roeloffs, 1996; Wang and Manga, 2010a; Wang and Manga, 2010b]. Co-seismic increases in streamflow discharge can be attributed to the expulsion of water from storage by elastic strain, enhanced hydraulic permeability, changes in the hydraulic head or a combination of these processes. Hence, increased streamflow can be induced by the deformation of aquifers [e.g., Muirwood and King, 1993; Roeloffs et al., 2003; Wang et al., 2004b] or fractures in the rock strata due to ground acceleration and shaking, resulting in more efficient drainage of the aquifer through enhancement of fracture systems and thereby enhancing groundwater exfiltration rates [e.g., Briggs, 1991; Brodsky et al., 2003; Charmoille et al., 2005; Elkhoury et al., 2006; Rojstaczer et al., 1995; Rojstaczer and Wolf, 1992; Tokunaga, 1999]. Wang et al. [2004a] introduced the concept of anisotropic permeability change through which co-seismically enhanced vertical permeability allows a rapid downward draining of groundwater and recharging of the underlying aquifers while the horizontal permeability remains unaffected.

Seismic shaking causes a readjustment of the relative position of clasts and compaction of unconsolidated materials [Wang et al., 2001]. Under undrained conditions, pore-water pressure increases and may trigger liquefaction [Manga, 2001; Manga et al., 2003; Montgomery et al., 2003; Wang et al., 2001], a process by which the rigidity of saturated deposits is reduced to zero and the sediments become fluid-like, and expels water that, in turn, increases streamflow discharge. Each of these processes has been thought to explain observed co-seismic hydrological response in particular circumstances.

Previous studies reported hydrological responses for meso-scale catchments ($>10^2$ km²) that produce baseflow discharges greater than ~ 8.5 l/s [e.g., Montgomery et al., 2003]. Catchments of larger spatial extent, however, are mainly composed by heterogeneous geology and topography [e.g., Wang et al. 2004a] which in turn complicate the clear identification of the underlying hydro-seismological processes. In this study, we examine near-surface hydrological response to a high-magnitude earthquake in upland catchments of small spatial extent ($< 10^1$ km²) and homogeneous geological and topographical settings in the Chilean Coastal Range. The small catchment size and relative homogeneity allow exploration of the mechanics controlling earthquake-triggered hydrologic response. We infer from the observed response of small and physiographically comparable headwater

catchments that the observed changes in streamflow are likely due to undrained compaction or increased vertical permeability of near-surface material and vertical enlargement of the saturated zone. As the water table rises, the greater cross section of the saturated zone contributes to increased post-seismic subsurface flow towards the creeks.

5.2. Maule earthquake and Araucania aftershock

The Maule earthquake occurred on February 27th 2010 at 3:34 a.m. local time with a moment magnitude (M_w) of 8.8, the 6th strongest earthquake ever recorded. The hypocenter was located offshore at a depth of 35 km, approximately 105 km north of the City of Concepción (Lat.: 36.4°S, Long.: 73.4°W) [Vigny *et al.*, 2011]. The Maule earthquake was a shallow, thrust-faulting event along the convergent margin where the oceanic Nazca plate subducts beneath continental South America. This event ruptured the Nazca margin over a length of approximately 600 km and closed the Concepción-Constitución or Darwin seismic gap of the Andean subduction zone [Lorito *et al.*, 2011, Madariaga *et al.*, 2010; Moreno *et al.*, 2010; Sparkes *et al.*, 2010]. With a duration of ~150 seconds it was an extraordinarily long rupture event and the felt intensity reached VIII on the modified Mercalli scale. More than 300 aftershocks of moment magnitude $> M_w$ 5.0 occurred before May 2010, 21 of which exceeded M_w 6.0. The Araucania earthquake, the most intense aftershock, occurred on January 2nd 2011 with a moment magnitude (M_w) of 7.1 (USGS NEIC Catalog, <http://earthquake.usgs.gov/earthquakes/eqarchives/epic>). The hypocenter was located at a depth of 21 km at the southern end of the aftershock region, about 70 km northwest of the City of Temuco (Lat.: 38.4°S, Long.: 73.3°W). The earthquake lasted for ~20 seconds and the felt intensity reached VII on the modified Mercalli scale.

5.3. Study area and weather conditions

Streamflow response to the earthquake was recorded by a network of 10 experimental catchments established in the Chilean coastal range to analyze hydrological and erosional processes of different forest management practices [Huber *et al.*, 2010]. The catchments are located about 500 km south of Santiago, on the eastern slope of the Coastal Range facing the dry central valley between the cities of Concepción and Los Angeles in the Bio-Bio Region, close to the city of Nacimiento (Fig. 5.1). The epicenters of the main earthquake and the aftershock were located ~130 km and ~110 km, respectively, from the study area, which

experienced an estimated maximum ground velocity of ~ 30 cm/s and ~ 4.0 cm/s, respectively. Maximum ground acceleration at the study sites reached 0.25-0.30 g for the main shock and 0.05-0.10 g for the Araucania aftershock (USGS NEIC Catalog, <http://earthquake.usgs.gov/earthquakes/eqarchives/epic>). Geodetic GPS-measurements at approximately 24 km distance revealed westward motion of ~ 230 cm and vertical settling of ~ 50 cm at the study sites [Vigny *et al.*, 2011].

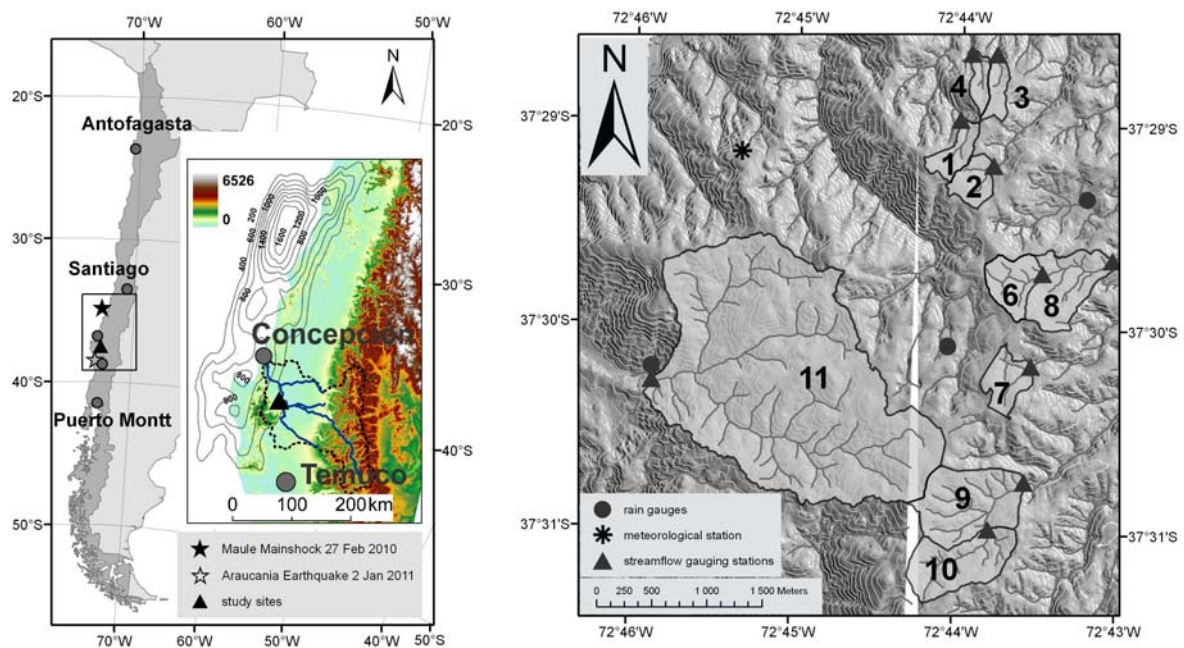


Figure 5.1. Location of the study area in relation to the epicenters of Maule earthquake (27 Feb 2010) and the Araucania Aftershock (2 Jan 2011) on the left. The inset shows the B o-B o drainage basin as a dotted line. The contours show the slip in the main shock; the contour interval is 200 cm [Tong *et al.*, 2010]. The representation of the elevation (m asl) is derived from GTOPO30 data (<http://demex.cr.usgs.gov/DEMEX/>). On the right, the location of the monitored catchments showing the positions of the rain gauges, the meteorological station and the streamflow gauging stations. Elevations are derived from a LiDAR DEM and the contour interval is 20m. The numbers correspond to the following catchments: 1: *Pinus rad.* Control; 2: *Pinus rad.* selective thinning; 3 and 4: Former *Pinus rad.* Plantation, clear-cutting in winter 2009 (3) and summer 2010 (4); 6: *Eucal ptus glob.* regeneration; 7: *Eucal ptus glob.* plantation; 8: Mixed vegetation; 9: Native Forest; 10: Native Forest; 11: Juvenile *Eucal ptus glob.* plantation.

The study area is characterized by a subtropical Mediterranean climate. Annual average precipitation is 1150 mm, concentrated between April and September and contributing 95% of the total annual yield. Annual average temperature is 13°C and summer temperature can exceed 40°C, producing high evapotranspiration rates. Although soil water content is low during summer [Huber *et al.*, 2010], soil moisture in the deepest soil layers was high prior the earthquake (Fig. 5.2). According to Huber *et al.* [2010], the deeper soil

layers/saprolite becomes saturated when soil moisture comes up to 0.35-0.41 cm³/cm³. These values are comparable to typical porosities of sandy clay loam, which can reach ~ 0.39 cm³/cm³ [Rawls *et al.*, 1993]. Moreover, due to the high stone content of lower soil layers (up to 90 %) at least a partial saturation of the saprolite layer is expected. According to Scheffer and Schachtschabel [2010] only minor capillary rise of some tens of centimeters may be expected in sandy soil texture. Thus, a shallow, and likely perched, groundwater table was likely at about 200 cm depth prior to the earthquake (Fig. 5.2).

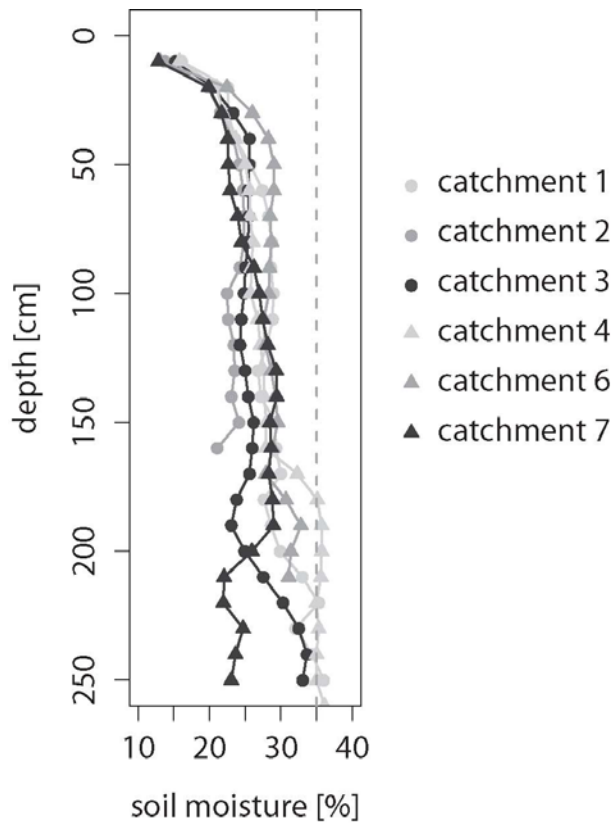


Figure 5.2. Soil moisture (vol. %) measured along transects of access tubes (n=6-15) by TRIME-TDR on 19 Feb 2010. Dashed line represents minimum water content (35%) needed to saturate the saprolite [Huber *et al.*, 2010].

The catchments vary from 7.8 to 412.9 ha in size and altitudes range between ~250 and 450 m asl. All catchments are in the uplands and extend up to the ridges of the coastal mountain range. Mean slopes vary from 14-22° but exceed 60° along the creeks or road cuts, promoting active gully formation along the road cuts and steep former timber drag lines perpendicular to the creeks. The small size and similar shape and slope among the catchments facilitate inter-catchment comparison [e.g., Bosch and Hewlett, 1982], but limit the potential to investigate contrasting catchment properties. The mean stream gradients vary between 10 and 15°. Despite local gradient variations, the stream profiles are mainly straight in shape with minor deviations: stream profiles of catchments 2, 6, and 9 are slightly concave, whereas the stream profiles of catchments 7 and 10 are slightly sigmoidal. The

study catchments are drained by a single creek except for catchments 6, 7, 8 and 11 which consist of at least two major tributaries. The length of the principal streams (the longest tributary) varies from 400 m in catchment 2 to 2700 m in catchment 11. Schist bedrock is exposed in the channel beds and alluvial deposits are present only locally. The catchments preferentially face to the north and east and drain towards the Bío-Bío River (Fig. 5.1).

All streams are surrounded by a 7.5 - 15 m wide planted riparian buffer strips on each side. The buffer strips are composed of dense native brush and deep-rooting trees, including Arrayán (*Luma apiculata* DC. Burret), Boldo (*Peumus boldus* Mol.), Roble (*Nothofagus obliqua* Mirb.) and Lingue (*Persea lingue* Nees). In most cases the buffer strips are restricted to the steep slopes close to the creeks but may also extend into small wetlands, as in the case of catchment 2. The buffers account for 5.6 to 22.6% of total catchment area and are intended to protect the streams from sediment input due to timber harvest of plantations of fast growing and highly water consuming exotic *Pinus radiata* D. Don and *Eucalyptus* spp. Two catchments (No. 9 and 10) are excluded from silvicultural exploitation and retain native forest. The main characteristics of the catchments are summarized in Table 5.1.

The dominant soil type is a clayey to loamy Luvisol with variable structure on a small scale due to fragments of bedrock within the topsoil, a complex distribution of recent and former root systems, and disturbance by timber harvest. The soil patchiness enhances the variability of hydraulic conductivity and intensifies preferential flow patterns [e.g., Ziegler *et al.*, 2006]. Truncated soil profiles exposing low-conductive B-horizons and evidence of recent incision indicate active soil erosion and landsliding, likely triggered by forest clearing [e.g., Montgomery *et al.*, 2000]. During the first rainy season after the earthquake numerous landslides were observed, mostly concentrated at road cuts. Soil depth typically ranges between 160 and 170 cm but some road cut exposures of soil exceed 250 cm. At its base, the loamy-sandy saprolite can reach depths of 560 ± 215 cm and overlays homogeneous schist, which forms the geological basement and parental material [Melnick *et al.*, 2009]. Field surveys confirm the saprolite to be a highly permeable layer because subsurface flow has been observed exfiltrating from this layer in road cuts during dry summer months. The near-surface part of the schist is heavily fractured and together with the saprolite forms an unconfined near-surface aquifer. The total depth of the unconsolidated and fractured material locally exceeds 700 cm.

Table 5.1. Main characteristics of the experimental catchments.

catchment	1	2	3	4	6	7	8	9	10	11
area (ha)	12.65	13.47	9.47	7.76	20.47	17.43	36.51	54.15	41.30	412.90
landuse	control	selective thinning	clear-cutting winter 09	clear-cutting summer 10	regeneration	plantation	mixed forestry	control	control	plantation
vegetation	<i>Pinus radiata</i>	<i>Pinus radiata</i>	-	-	<i>Eucalyptus globulus</i>	<i>Eucalyptus globulus</i>	<i>Eucalyptus glob.</i> & <i>Pinus rad.</i>	Native species	Native species	<i>Eucalyptus globulus</i>
tree-density (tree/ha)	320	315	-	-	1326	893	-	-	-	-
plantation age (yr)	24	24	-	-	10	10	24/10*	-	-	3
riparian buffer (ha)	0.83	0.90	1.15	1.0**	4.62	0.97	7.42	20.49***	19.16***	45.30
altitude (m asl)	328-377	333-367	255-320	246-318	322-366	369-407	259-367	376-476	389-467	320-476
catchment slope (°)	14.7±8.5	14.2±8.6	18.2±10.2	20.4±10.8	18.4±9.9	15.4±8.8	18.9±9.2	21.6±9.4	19.9±9.1	19.4±10.3
slope of stream (°)	10.0±7.3	13.0±8.9	15.1±10.7	18.1±10.7	13.2±9.2	9.8±6.9	11.8±9.6	15.2±9.4	13.3±8.8	11.6±9.2
length of principle stream (m)	497	399	487	466	532	454	1323	1625	921	2694
max. flow length (m)	762	692	773	711	1284****	890****	1420****	2044	1330	3682
wetness index	4.76 ±1.84	4.48±1.08	4.33±1.24	4.00±1.15	4.41±1.17	4.65±1.19	4.34±1.23	4.21±1.17	4.22±1.13	4.15±1.25

Weather conditions around the time of the Maule earthquake were dry despite an extraordinarily wet February 2010 when 82 mm of rainfall greatly exceeded the long-term monthly average of 7 mm. Two major rainfall events contributed to the greatest part of the February rainfall. The first event occurred February 6th-7th and contributed ~60 mm, the second event occurred February 17th-18th and contributed ~20 mm. Between February 19th and May 5th 2010 no significant precipitation was recorded. Hence, during this period, the total discharge was contributed by baseflow exclusively. Strong transpiration of the vegetation layer during the dry summer months [Huber *et al.*, 2010] governed pre-seismic baseflow recession. The last intense rainfall event before the aftershock delivered a total of 23 mm between December 10th and 11th 2010 6 mm of rainfall on December 17th did not generate significant runoff. Total precipitation in December 2010 was 42 mm, well within the long-term monthly average.

5.4. Methods and Data

The streamflow in all catchments was monitored by V-notched Thompson-type weirs except for the catchment with the largest spatial extent (No. 11; Pichún grande). Here, discharge was measured by a flume. Water stage was recorded by a custom-built float at a sampling interval of 3 minutes with an accuracy of 2 mm. For a subset of catchments, the water temperature was measured inside the weirs by Hobo-Pendant water temperature loggers (Hobo Pendant temp., Ref. UA-001-64) with the same temporal resolution (3 min) and an accuracy of ± 0.54 °C. Precipitation was recorded by three Hobo tipping bucket rainfall gauges distributed over the study area at suitable and accessible sites (Fig. 5.1).

To determine the effect of the earthquake, discharge records were compared for clear differences in streamflow prior to and after the seismic events. In order to minimize the effect of precipitation on total discharge, only baseflow as the component of streamflow provided by groundwater was considered [Manga, 2001]. Since low pre-seismic baseflow discharge has been measured across all catchments, the Pichún grande catchment is analyzed in the most detail. This catchment is by far the largest in spatial extent and shows the highest discharge which, in turn, imparts greater accuracy to the discharge measurements. The baseflow was determined by the constant slope method, which graphically determines the baseflow component of total discharge by connecting the point of initial hydrograph rise with the end of the hydrograph recession of equal discharge prior to the rise by a straight line [e.g., Blume *et al.*, 2007; Dingman, 2002]. The response time was estimated for all catchments as

the time lag between the earthquake and the first rise in streamflow exceeding the pre-seismic discharge. In order to quantify the effect of the seismic event on streamflow discharge, the maximum percentage change in post-seismic baseflow was calculated and the excess water for a subset of catchments was estimated from the difference between the observed discharge and an estimate of what the discharge would have been in the absence of an earthquake [Manga, 2001].

Hydraulic conductivity, which can be estimated by the hydrograph recession constant, is a parameter closely related to the geometrical and physical properties of the aquifer. Thus, the recession constant can be used to describe aquifer-scale transient groundwater flow from an unconfined aquifer seeping into a stream [e.g., Manga, 2001; Manga *et al.*, 2003; Montgomery *et al.*, 2003]. Although recession analysis only considers isotropic hydraulic permeability [Wang *et al.*, 2004a] and neglects capillary effects, it is a suitable tool to detect catchment-scale, earthquake-caused changes in hydraulic properties [e.g., Manga *et al.*, 2003]. We compared pre- and post-seismic recession constants calculated by the constant k method [Blume *et al.*, 2007]:

$$\delta Q/\delta t = -k \cdot Q(t) \quad (5.1)$$

which can be rearranged to yield

$$k = -\delta Q/\delta t \cdot 1/Q(t) \quad (5.2)$$

where k is the recession constant (1/day) and $Q(t)$ is discharge at time t (m^3/day). Due to low baseflow discharge was summed up to daily volume, which in turn negatively affects the accuracy of the water stage-discharge relation. Summing up to daily volume makes the recessions smoother since short timescale variations are averaged making the determination of k more reliable.

In order to quantitatively characterize topological properties of the catchments, high-resolution digital terrain models (DTM) based on airborne LiDAR data were analyzed. LiDAR is able to penetrate dense vegetation cover which makes it an accurate tool for surface analysis under forest canopy [Reutebach *et al.*, 2003]. The surface analysis was achieved with ArcGIS or SAGA-GIS. All hydrological calculations were done with the statistical software R.

5.5. Approach

After the earthquake, a strong increase of streamflow discharge –the most striking hydrological response to the earthquake – was preceded by an immediate but transient drop of streamflow. Infiltration excess overland flow and saturation overland flow are not possible sources of the increased post-seismic flow because there was no rainfall for several days prior to the earthquake. The observed streamflow in the experimental catchments during the study period originated from groundwater sources as exfiltrating groundwater flow or return flow. Groundwater flux is governed by the hydraulic gradient $\delta h/\delta l$ of the groundwater (δh corresponds to the difference in hydraulic head over the length of the flow path δl) and the hydraulic conductivity k_f of the aquifer releasing water into the creek, which can be described by the Darcy-equation:

$$Q = vD \cdot A = k_f \cdot \delta h / \delta l \cdot A \quad (5.3)$$

where Q is discharge, vD is the Darcy-velocity (filter velocity) and A is the cross section of the aquifer perpendicular to the flow direction. Substituting the product of the aquifer height H and the specific aquifer width (or unit width) w for A yields:

$$Q = k_f \cdot \delta h / \delta l \cdot H \cdot w \quad (5.4)$$

According to eq. (5.4), a rise in groundwater exfiltration would take place if at least one of the variables or terms of that equation increases. Neither the unit aquifer width w nor the aquifer height H can directly change as a result of the earthquake because the catchments are restricted to the upland headwaters. Considering the topographical position of the catchments, no higher elevated regions are present in the vicinity. Thus, there is no possibility of additional groundwater being released from an elevated hinterland, e.g. the Andes Mountains, recharging the local groundwater of the catchments by an elevated hydraulic head from outside the topographically defined drainage basin. Hence, the observed hydrological response to the earthquake was a result of autochthonous changes in either hydraulic conductivity k_f and/or the hydraulic gradient $\delta h/\delta l$ within the catchments.

5.6 Observations and results

The hydrographs of all study catchments showed streamflow response immediately after the earthquake (Fig. 5.3 and 5.4). The hydrological responses showed similar but not uniform patterns among the catchments. Most of the catchments (6 out of 10) experienced an immediate drop in discharge within the first 3 minutes of sampling after the earthquake, followed by a large increase in streamflow. A summary of the streamflow responses of each catchment is shown in Table 5.2.

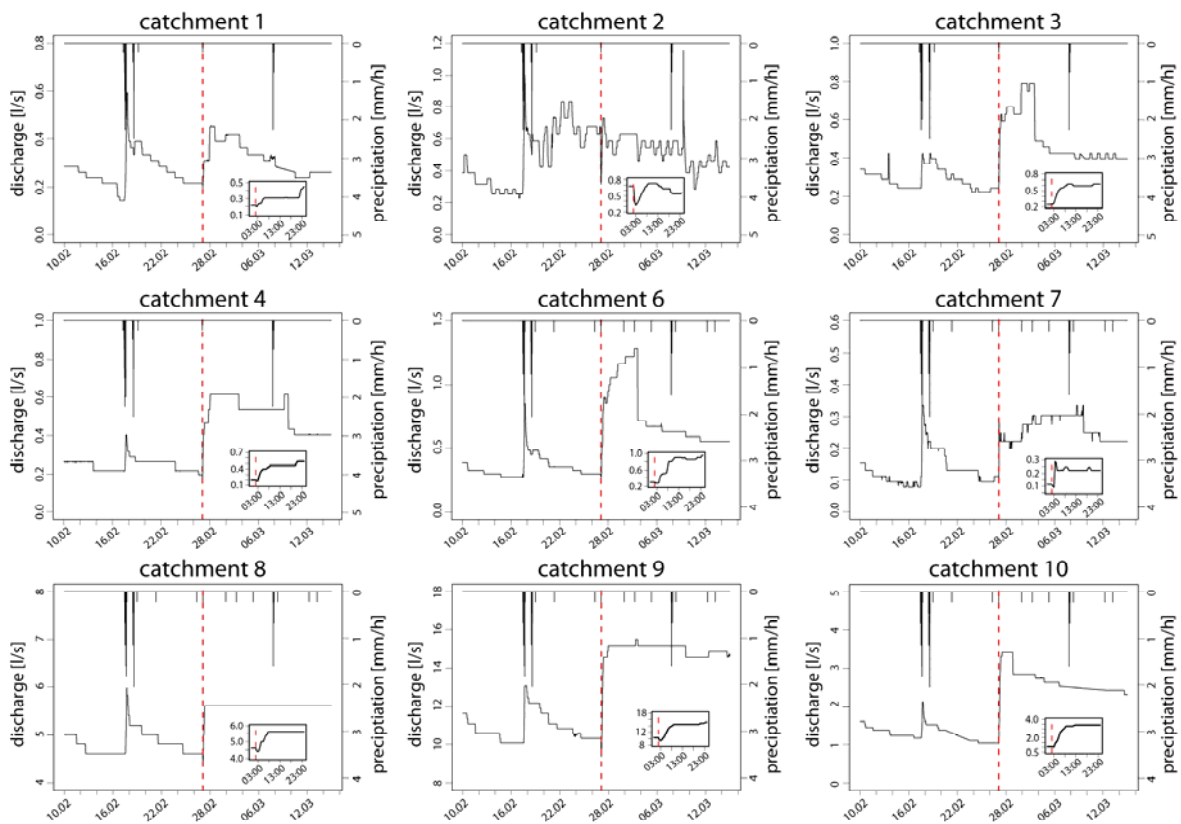


Figure 5.3. Hydrographs of the catchments showing the hydrological response of the 9 smaller catchments to the earthquake. The small inset figures show in greater detail the immediate co-seismic decline of streamflow discharge on 27 Feb 2010. The dotted red lines represent the earthquake.

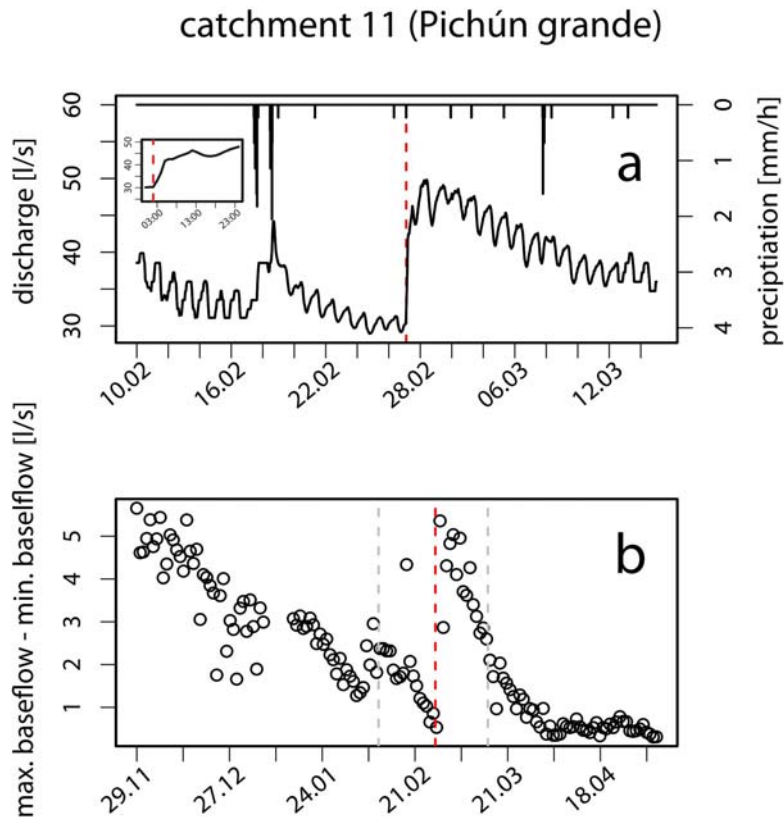


Figure 5.4. Hydrograph of Pichún grande (catchment No. 11) showing the post-seismic increase in streamflow on the top (a). The small inset figure shows in greater detail the immediate co-seismic response of streamflow discharge on 27 Feb 2010. At the bottom, difference between daily maximum and minimum baseflow discharge (l/s) for Pichún grande (catchment No. 11) during the period from 29 Nov 2009 to 25 Apr 2010 is shown (b). The dotted grey lines indicate the time period shown in (a). The dotted red lines represent the earthquake.

In quantitative terms, the increase in the mean baseflow after the earthquake is the most striking hydrological signal. In contrast to the widely reported increase in streamflow [e.g., *Manga et al.*, 2003; *Montgomery and Manga*, 2003; *Muirwood and King*, 1993; *Rojstaczer et al.*, 1995] an initial decline in streamflow is reported rarely [*Rojstaczer and Wolf*, 1992; *Tertulliani and Cucci*, 2009]. In all of the study catchments, the magnitude of post-seismic streamflow increase greatly exceeded the co-seismic drop. With a reaction time of 15 minutes to up to 3 hours, the observed increases ranged between 110 - 400 percent of the baseflow registered immediately prior to the earthquake. The time to post-seismic peak

discharge varied between 5-6 hours (catchments No. 2 and 8) to more than 4 days (catchments No. 6, 7 and 9, see Table 5.2).

After reaching the post-seismic maximum discharge, the discharge receded gradually in most catchments. In some catchments (e.g., catchments No. 3 and 6), the slope of the post-seismic decrease in streamflow was comparable to the steep increase. Despite substantial scatter, pre- and post-seismic recession constants do not exhibit a consistent change, as shown by the overlap of error bars with the 1:1-line (Fig. 5.5). Statistical tests only showed a significant decrease in catchment No. 11 while some recession constants in catchments No. 2, 3, 4, 8, and 11 slightly decreased and others increased (catchments No. 1, 7). A linear model fit with 1000 bootstrapped samples yielded the following model:

$$k_{post} = 1.02 \cdot k_{pre} + 0.03 \quad (5.5)$$

where k_{post} is the recession constant k after the earthquake and k_{pre} prior to the earthquake. Although the standard deviations for both the slope and intercept are considerable (0.51 and 0.09, respectively), pre and post seismic k do not show significant differences.

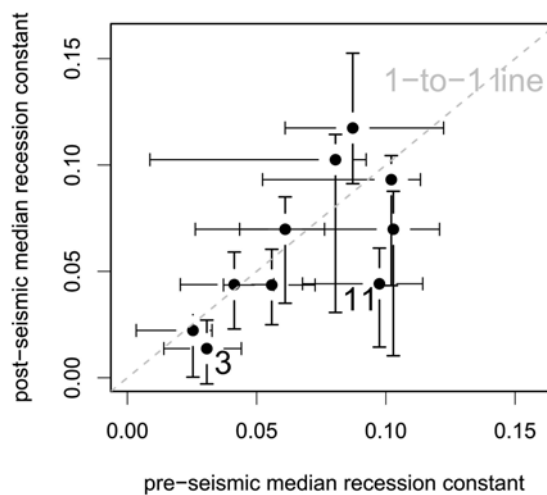


Figure 5.5. Pre-seismic vs. post-seismic recession constants, calculated as daily values (m^3/day) for all catchments. The pre-earthquake period continued from 17 Apr 2008 to 26 Feb 2010. For post-earthquake recession constants, the period from 27 Feb 2010 to 12 Jul 2010 was considered. Error bars show range of values for individual rainfall events. Recession constants were calculated with the R-package Tiger [Reusser, 2010, <http://cran.r-project.org/web/packages/tiger>].

Table 5.2.. Summary of hydrological response to the Maule earthquake in the experimental catchments. $Q_{co-seismic}$ is defined as the streamflow discharge registered immediately before the earthquake (2:33 a.m. local time.), min. $Q_{post-seismic}$ refers to the minimal streamflow discharge measured during the initial decline after the earthquake and max. $Q_{post-seismic}$ to the maximum streamflow discharge registered after the earthquake (ignoring runoff response to rainfall events). Daily mean water temperatures (in °C) are given for 10 days pre- and post-seismic periods. Pre-seismic period continued from 17 Feb 2010 to 26 Feb 2010 and post-earthquake period from 27 Feb 2010 to 8 Mar 2010. Change of temperatures after the earthquake was tested by using the Kruskal-Wallis test and differences were taken to be significant with $p < 0.05$. Significant differences are indicated by the asterisk.

catchment	1	2	3	4	6	7	8	9	10	11
$Q_{co-seismic}$ (l/s)	0.22	0.68	0.24	0.20	0.30	0.11	4.62	10.32	1.04	30.32
min. $Q_{post-seismic}$ (l/s)	0.19	0.32	-	0.18	0.28	0.10	4.46	9.4	1.03	-
max. $Q_{post-seismic}$ (l/s)	0.46	0.73	0.79	0.62	1.28	0.33	5.61	15.51	3.42	49.83
Increase (%)	210	110	330	310	430	300	120	150	330	160
response time (min)	47	179	20	60	113	56	101	101	50	15
time of max. $Q_{post-seismic}$ (date + time)	2010-02-28 03:30	2010-02-27 09:00	2010-03-01 22:00	2010-02-28 02:00	2010-03-03 06:00	2010-03-03 09:30	2010-02-27 08:00	2010-03-03 09:00	2010-02-27 12:30	2010-02-28 01:00
pre-seismic stream temperature (°C)	13.9 ± 0.1	-	13.7 ± 0.2	14.1 ± 0.2	12.7 ± 0.1	-	13.2 ± 0.2	12.5 ± 0.1	12.9 ± 0.2	-
post-seismic stream temperature (°C)	14.3 ± 0.2*	-	14.4 ± 0.4*	14.7 ± 0.4*	13.2 ± 0.2*	-	13.7 ± 0.3*	13.0 ± 0.3*	13.3 ± 0.3*	-
stream temperature (°C) Feb. 27 th	14.1	-	14.3	14.8	13.0	-	13.6	12.9	13.3	-
stream temperature February 28 th	14.6	-	15.2	15.5	13.4	-	14.1	13.6	16.7	-

Diurnal oscillations in streamflow like those observed in catchment 11 are commonly reported and are directly related to evapotranspiration and the replenishment of depleted groundwater storage [Gribovszki *et al.*, 2010]. An increase in the magnitude of the diurnal oscillations is observed in Pichún (No. 11) immediately after the earthquake (Fig. 5.4). Here, the magnitude of diurnal oscillation is defined as the difference between daily maximum and minimum discharge ($Q_{max} - Q_{min}$). The oscillation in Pichún increased from < 1.0 l/s prior to the earthquake to 4-5 l/s for the first days after post-seismic peak streamflow on February 28th. Daily maximum discharge occurred in the early mornings and minimum discharge in late afternoons. The observed intensification contrasts with the general trend of declining magnitude of diurnal oscillations starting in December 2009. Diurnal discharge oscillations returned to pre-seismic conditions (<1 l/s) at the end of March 2010.

Catchment No. 2 is a special case since its stream crosses a small wetland directly upslope of the weir. In this catchment, the co-seismic decline of streamflow is highest, decreasing to less than half the pre-seismic discharge and continuing for about 5 hours. The magnitude of the diurnal oscillations of between 0.1 and 0.2 l/s remained unaffected by the earthquake. Only on February 27th was the magnitude significantly higher (0.4 l/s) as a result of the strong initial co-seismic decline.

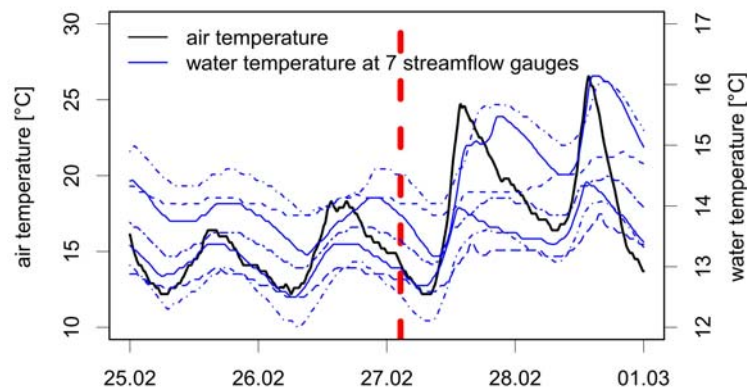


Figure 5.6. Water temperature at streamflow gauges of catchments 1, 3, 4, 6, 8, 9 and 10 and air temperature recorded at the meteorological station for the period from 25 Feb 2010 to 1 Mar 2010. Water temperature is represented by blue lines and air temperature by the black line, both smoothed by a 60-min running mean filter. The time of the earthquake is marked by the red dashed line.

Alterations of streamflow temperature may provide deeper insights into the mechanisms of hydrological response [e.g., Manga and Rowland, 2009]. In this study, however, air temperature did not remain stable but varied around the time of the earthquake. That this affected the stream water temperature is evident in the close link between air and

water temperatures and the pronounced diurnal temperature cycles during the period from February 25th to March 1st (Fig. 5.6).

Heat flow provides information on tectonic processes while groundwater flow may affect subsurface temperature [Wang *et al.*, 2012]. Hence, changes in groundwater or stream water may be useful to decipher hydro-tectonic processes.

The average increase of all stream temperatures was 0.5 ± 0.1 °C during a period of 10 days prior and 10 days after the earthquake, while air temperature increased by 1.6 °C from 14.6 ± 1.3 °C to 16.2 ± 1.8 °C. Maximum mean air temperatures reached 17.8 and 18.8 °C on February 27th and 28th 2010, exceeding pre-seismic average temperatures by 3.2 and 4.2 °C and post-seismic temperatures by 1.6 and 2.6 °C. On February 27th stream water temperatures of all catchments exceeded average pre-seismic temperatures. The water temperatures registered in all catchments on February 28th exceeded both the average pre- and post-seismic average temperatures (see Table 5.2). Hence, it is not surprising that the significant post-seismic increase of streamflow temperature observed in all catchments tracked air temperature.

The Araucania aftershock on January 2nd 2011 caused neither an increase or initial decline in streamflow discharge nor a change in streamflow temperature in any of the study catchments (Fig. 5.7).

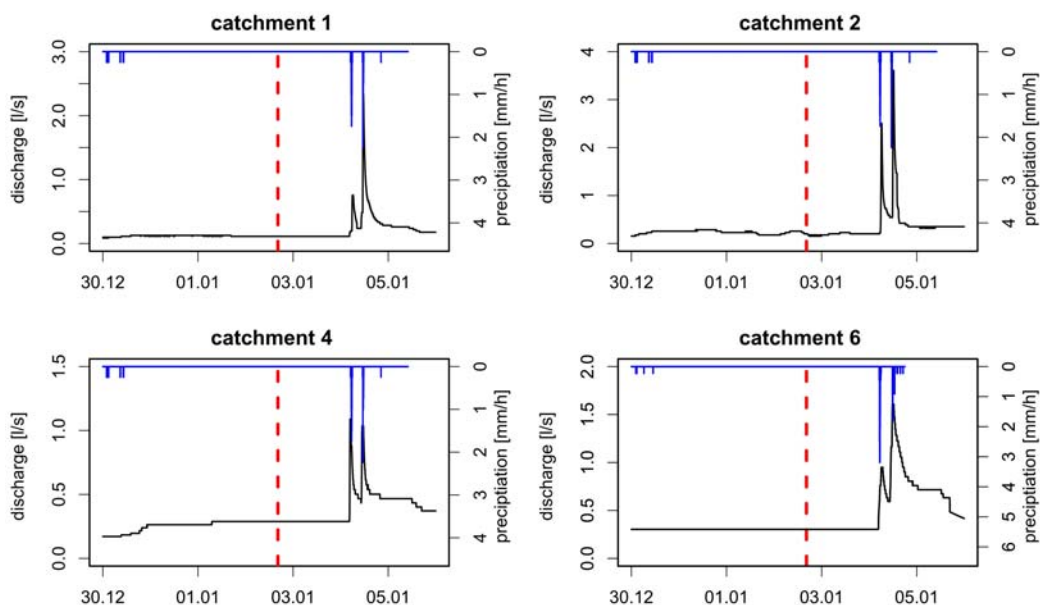


Figure 5.7. Hydrographs showing no hydrological response to the Araucania aftershock in the streamflow. Here, only catchments No. 1, 2, 4 and 6 are presented for the period of 31 Dec 2010 to 6 Jan 2011 as representative examples; none of the monitored catchments showed any hydrological response to the aftershock.

The observed response of the study catchments can be summarized as an immediate co-seismic decline in streamflow continuing for a period of up to 2 hrs, followed by a significant increase in baseflow (~110-400 %) within a response time of 15 min to 3 hours, accompanied by an increase in the diurnal oscillation by up to one order of magnitude for a period of 30 days. No discernible change in either streamflow temperature or recession constants was associated with the earthquake.

Although similarities in the hydrological response indicate similarity of the underlying processes, variable duration and magnitude of excess flow or differences in response time also reflect differences in hydro-geomorphic properties among the catchments. First- and second-order topographical indices (mean catchment slope, Gravelius compactness index), average wetness index and stream properties (length, average gradient and shape) were all correlated to the magnitude of increase in streamflow discharge, reaction time of the hydrological response and time to post-seismic peak streamflow discharge [Table 5.3, see *Wilson and Gallant, 2000*]. The Gravelius compactness index describes the ratio between the perimeter of a catchment and the perimeter of a circle with the same area. This index is only suitable for inter-basin comparison of the same spatial scales [*Bardossy and Schmidt, 2002*], as is the case here. Stream lengths were calculated by threshold contributing area of 2 ha, which corresponds to channel head locations determined from field observations and GPS.

Hydrological variables like co-seismic discharge or minimum and maximum post-seismic discharge were also considered in the correlation analysis. Due to small sample size ($n=10$) and non-normal distribution, bootstrapping was performed to assess accuracy in statistical analyses. Bootstrapping is a simple resampling technique and involves choosing and analyzing random samples with replacement from the same dataset. This means that each sample is selected separately and randomly from the original dataset and a particular sample from this dataset could appear multiple times in the bootstrap sample. Increasing the number of samples may reduce the effects of random sampling errors but cannot augment the information content of the original data. Bootstrapping may be used for estimating the statistics in the case of small sample size or unknown distribution because it measures these statistics when sampling from an approximating distribution. Based on such sampling repeated 1000 times, the strongest correlation has been found between post-seismic streamflow increase and co-seismic discharge, post-seismic maximum and minimum streamflow discharge. All of these variables, in turn, exhibit correlation to the scaling variables of catchment size, stream length, longest flow path and catchment perimeter. These results are similar to the observations of *Montgomery et al. [2003]*. Topographical indices

and stream properties (mean stream slope, mean catchment slope and mean topographical wetness index (TWI) as a function of slope are uncorrelated with streamflow increase, response time or time to post-seismic peak streamflow discharge. Both response time and time to post-seismic streamflow increase are not correlated to any topographical index, with a correlation coefficient only reaching -0.41 for the catchment size and Gravelius compactness index (Table 5.3).

Table 5.3. Median correlation coefficients based on 1000 bootstrapped samples. Co-seismic streamflow discharge, minimum and maximum post-seismic discharge and post-seismic increase in streamflow discharge are considered in l/s, response time and time to post-seismic peak streamflow discharge in minutes after the earthquake, stream and catchment slopes in degree (°), catchment area in hectares and stream length, perimeter and longest flow path in meters. Gravelius Index and TWI (Topographical Wetness Index) are dimensionless.

	post-seismic increase of streamflow discharge	response time	time to post-seismic peak streamflow discharge
post-seismic increase of streamflow discharge	1.00	-0.40	-0.02
response time	-0.40	1.00	-0.08
Time to post-seismic peak streamflow discharge	-0.02	-0.08	1.00
co-seismic streamflow discharge	0.99	-0.31	-0.03
minimum post-seismic streamflow discharge	0.99	-0.34	-0.07
maximum post-seismic streamflow discharge	0.99	-0.34	-0.05
mean slope of stream	-0.08	0.08	0.05
mean catchment slope	0.44	-0.29	0.14
TWI	-0.46	0.15	0.15
Gravelius Index	-0.30	-0.41	-0.31
Stream length	0.94	-0.29	-0.05
catchment area	0.99	-0.41	-0.11
perimeter	0.97	-0.36	-0.15
longest flowpath	0.97	-0.27	0.05

5.7. Discussion

The observed pattern of hydrological response constrains possible mechanisms for the source of the excess water.

5.7.1. Where does the excess water come from?

Due to the high evapotranspiration rates of the exotic plantations and juvenile native forest, streamflow decreased continuously during the dry season. The small volume of streamflow makes the water temperature more susceptible to variations in air temperature due to facilitated heat exchange with the land and/or atmosphere [*Manga and Rowland, 2009*]. The close relationship between water and air temperature can be seen in their similar dynamics (Fig. 5.6) and their relationship remained unaffected by the earthquake. Expanding

the analysis to a longer period of time (Feb 16th-March 10th), no substantial temperature changes before and after the earthquake have been observed which cannot be explained by air temperature variations (Fig. 5.8). *Manga and Rowland [2009]* attribute unaffected temperatures of pre- and post-seismic waters to a common near-surface source.

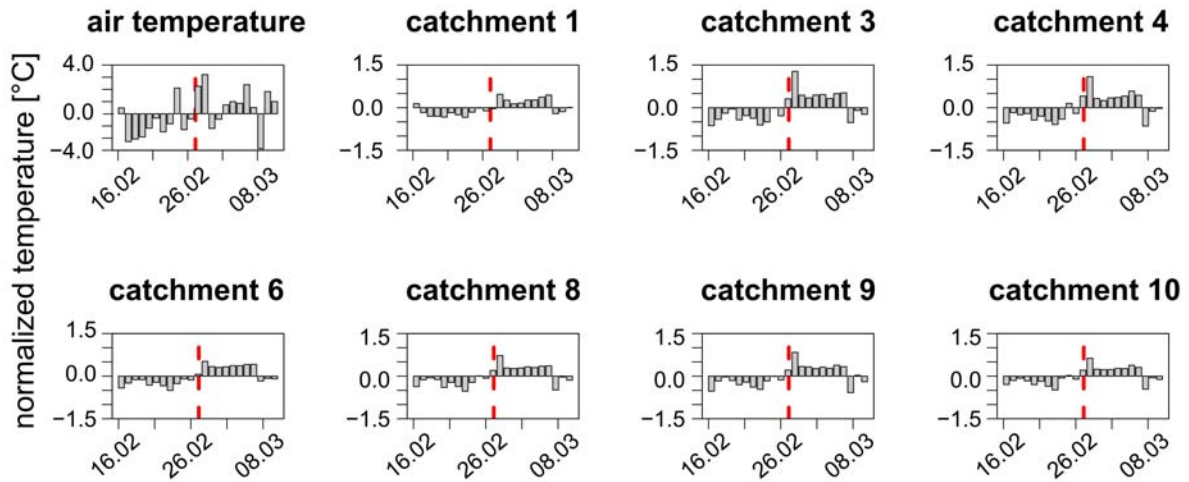


Figure 5.8. Daily mean water and air temperatures (°C) for the period from 16 Feb 2010 to 10 March 2010 normalized to the corresponding mean temperature over that period. Although some differences between pre- and post-seismic water temperatures are apparent, they remain coupled to air temperature throughout the measurement period. The time of the earthquake is highlighted by the red dashed lines.

Mid-crustal fault displacement processes that expel fluids generally result in increased water temperature [*Nakamura and Wakita, 1984; Rojstaczer et al., 1995; Sato et al., 1992; Wang and Manga, 2010a*], whereas a decrease in water temperature may be related to increased groundwater recharge induced by earthquake-enhanced vertical permeability [*Wang et al., 2012*]. Although the accuracy of streamflow temperature measurement is limited, and may not capture millidegree scale response, our water temperature measurements support a shallow source for the observed earthquake-induced streamflow variations.

A shallow source is also indicated by incorporating observed hydrologic response times into the relationship derived by *Roeloffs [1996]* to estimate the source depth:

$$z = \sqrt{\frac{T \cdot D}{11}} \quad (5.6)$$

where z is depth below the water table in metres, D the hydraulic diffusivity (m^2/s) and T the time scale of pore-pressure dissipation to the water table in seconds. For a typical diffusivity

of fine sand (such as the coarsest grain size fraction of the loamy soil covering the saprolite) [$\sim 10^{-1}$ m²/s, *Roeloffs*, 1996] the response times of 15 min to 3 hrs indicate a maximum depth of $\sim 6 \pm 2.1$ m averaged over all catchments. This depth is consistent with the saprolite-bedrock-interface.

Assuming a source of the water equally distributed across the catchment, the response time and time to peak discharge are expected to be related to drainage area, its related features (e.g., longest flowpath), and its shape (e.g., compactness) among catchments with comparable conditions in soil, geology, topography and land use [*Dingman*, 2002]. Hence, under these conditions, time to peak runoff or response time are expected to show a relationship with catchment size [e.g., *Montgomery and Dietrich*, 2002]. However, this is not the case (see Tab. 5.3) and thus an equally distributed source of the excess water is unlikely. Consequently, we infer that the excess water has been released from patchy sources across the catchments.

The fast streamflow response indicates sources located close-by the creeks since proximity of the source area to the creeks facilitates a fast response at the catchment outlet (see Tables 2 and 3, *Dingman*, 2002). A strong correlation between the magnitude of the post-seismic increase and the stream length supports this assumption. Catchment size is also strongly correlated to the magnitude of the post-seismic increase and confirms the importance of catchment scale on the magnitude of the post-seismic increase, similar to the findings of *Montgomery et al.* [2003] for streamflow response to the Nisqually earthquake.

5.7.2. Increase in streamflow discharge by enhanced permeability?

Discharge is directly related to hydraulic conductivity (eq. 5.3) and reflects an integrated response over the whole catchment [e.g., *Ebel et al.*, 2008; *Montgomery and Dietrich*, 2002]. The similar pre- and post-earthquake recession constants show that the lateral hydraulic conductivity has not experienced any consistent enhancement among the catchments (Fig. 5.5), comparable to findings of *Manga* [2001], *Manga et al.* [2003] and *Montgomery et al.* [2003]. Consequently, any seismically induced increase in lateral hydraulic conductivity was minor and/or spatially limited, and failed to enhance substantially the lateral hydraulic conductivity on a catchment scale. Hence, neither seismically induced fracturing as proposed by *Briggs* [1991], *Rojstaczer et al.* [1995] and *Rojstaczer and Wolf* [1992] nor dislodging of obstacles from fractures due to dynamic strain [*Elkhoury et al.*, 2006; *Mogi et al.*, 1989; *Roeloffs*, 1998] are a suitable explanation for the observed post-seismic streamflow increase. Dynamic ground shaking might have additionally fractured the

topmost schist and thereby enhanced permeability locally. However, streamflow generation by subsurface stormflow is controlled by the most permeable layer (here, the saprolite) where no consistent increase of hydraulic conductivity occurred averaged across the catchment. Hence, possible effects of a slight increase in the permeability of the topmost schist layer are likely masked by the high permeability of the overlying saprolite as streamflow recession analysis would only reveal the hydraulic conductivity of the saprolite. Nevertheless, some additional water might have been expelled from the fissures into the saprolite.

Enhanced lateral permeability may increase streamflow discharge (see eq. 5.3) but is inconsistent with the observation of an initial streamflow decrease. However, changes of vertical permeability cannot be detected by recession analysis. *Wang et al.* [2004a] reported that topographical position influenced the decrease or increase of streamflow discharge for the Chi-Chi earthquake in Taiwan. Under the force of gravity, unconfined groundwater flows from elevated areas to lower areas. Consequently, upland areas – such as the headwaters in the mountainous region reported here – are typically assumed to be recharge areas while lowlands or downriver valleys are considered as discharge areas [e.g., *Dingman*, 2002] Under these assumptions, an enhancement of vertical permeability causes a drop of the groundwater table in the mountainous terrain and an increase in streamflow in the lower-elevation discharge area where the released groundwater exfiltrates. The Chi-Chi study covered catchments of 10^3 km² spatial extent with extensive networks of tributaries in mountainous regions up to 4000 m asl in the Central Range, which is made of metamorphic rocks of various grades whereas the foothills are composed of folded and faulted sandstone and shale. Under pre-earthquake conditions, the vertical permeability has been impeded due to impervious layers promoting lateral flow. During the earthquake, the vertical permeability increased through the formation of sub-vertical cracks in the sedimentary foothills which in turn enhanced the recharge of the underlying aquifers. As a result enhanced streamflow discharge in the lower area has been recorded [*Wang et al.* 2004a]. Similar observations were also reported by *Tokunaga* [1999] and *Rojstazcer* [1995] after the Kobe and Loma Prieta Earthquakes. In contrast to the highly differentiated geological setting and topographical gradient of the Chi-Chi study, the small headwater catchments reported here are restricted to mountainous terrain and do not extend to the larger-scale regional discharge areas of the foothills or lowlands. Nevertheless, local discharge is evidenced by perennial streamflow even during long-lasting dry summer periods which in turn are fed by groundwater recharge such as along the catchment crests.

Dilatancy describes the expansion of a material in response to shear and through which its volume increases by loosening up its structure due to the propagation of cracks. Although dilutant microcracks, preferentially oriented parallel to the direction of main stress, increase the porosity [Scholz, 2010], pore water redistribution and groundwater transmission could temporarily lower hydraulic head and cause an initial but transient drop in streamflow discharge, as touched on by Wang *et al.* [2001] for the Chi-Chi alluvial fan. This conflicts with the transient increase of hydraulic head caused by undrained consolidation. The dilutant (subvertical?) microcracks, in turn, may have provoked greater vertical permeability resulting in a post-seismic streamflow discharge. Although recession analysis [Blume *et al.*, 2007] allows us to reject substantial changes in lateral groundwater movement, we cannot dismiss vertical permeability enhancement.

5.7.3. Increase in streamflow discharge by dynamic strain?

Assuming unchanged aquifer geometry, eq. 4 shows that the hydraulic gradient $\delta h/\delta l$ has to change if hydraulic conductivity remains unchanged. Ground shaking increases dynamic strain and may cause compaction of undrained saturated near-surface sediments or soils, causing liquefaction that transiently releases water to streams due to closer packing of the sediments [Manga, 2001; Manga *et al.*, 2003; Montgomery *et al.*, 2003; Wang *et al.*, 2001]. The maximum distance from epicenters where liquefaction has been observed may be expressed as an empirical function of earthquake magnitude [Papadopoulos and Lefkopoulos, 1993]:

$$M = -44 + 3 \cdot 10^{-8} Re + 0.98 \log Re \quad (5.7)$$

where M is earthquake moment Magnitude (M_w) and Re the maximum epicentral distance in km. All the study catchments lie within this range for the Maule and Araucanía event (Fig. 5.9). Although the observed hydrologic response is consistent with this global dataset for liquefaction-induced streamflow increases, this does not necessarily mean that liquefaction is indeed the mechanism for the observed response. M and Re are useful parameters for comparing and relating hydrological responses. However, a single physically based and quantifiable parameter such as the seismic energy density is more suitable. Wang and Manga [2010b] define seismic energy density (the summation of ground motion over all relevant modes) as the “maximum seismic energy available in a unit volume to do work on sediment or rock”.

They empirically define a seismic energy density threshold for triggering liquefaction based data from southern California:

$$\log r = 0.48 M - 0.33 \log e - 1.4 \quad (5.8)$$

where r is the actual epicentral distance in km and e refers to the seismic energy density (J/m^3) [Wang and Manga, 2010b]. In addition, laboratory experiments support the field-based evidence for the occurrence of a liquefaction threshold driven by undrained consolidation [Wang and Manga, 2010a].

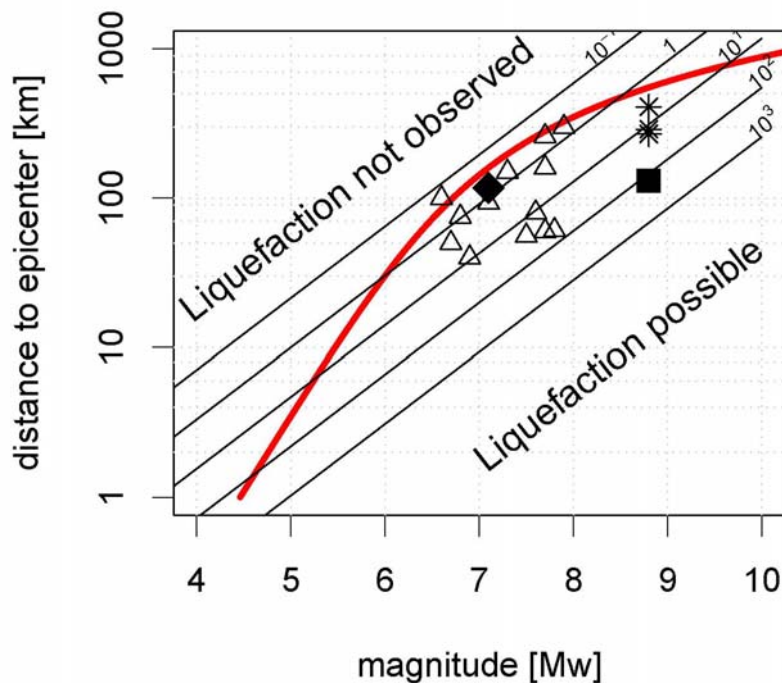


Figure 5.9. Distance from epicenter vs. earthquake magnitude for locations with seismically induced streamflow increase. Circles and triangles represent data compiled by Wang and Manga [2010a]. Red line represents the empirical relationship to describe observed liquefaction as a function of earthquake magnitude and distance to epicenter [Papadopoulos and Lefkopoulos, 1993]. Inclined lines represent seismic energy density from 10^{-1} to $10^3 \text{ J}/\text{m}^3$ [Wang and Manga, 2010b]. Black square represents Maule earthquake and the black diamond the Araucania aftershock in the studied catchments. Asterisks represent observed streamflow increase during the Maule earthquake in three other catchments in southern Chile.

According to Wang and Manga [2010b], a minimum seismic energy density of $10^{-3} \text{ J}/\text{m}^3$ is required to initiate groundwater level changes but a minimum of $0.1 \text{ J}/\text{m}^3$ is necessary to initiate liquefaction. Liquefaction by undrained consolidation is reported to be limited by a required seismic energy density of $30 \text{ J}/\text{m}^3$ which in turn closely corresponds to the near-field

boundary within one rupture length of the epicenter [*Wang, 2007; Wang and Manga, 2010a*]. Thus, undrained consolidation may cause liquefaction-induced streamflow increase only in the near-field. As Figure 5.1 shows, all catchments lie within the rupture zone. Hence, under suitable geologic and hydrologic conditions, liquefaction by undrained consolidation may be expected for the catchments. Across all catchments, the mean estimated seismic energy density reached $168.2 \pm 5.6 \text{ J/m}^3$ for the mainshock, more than 5 times greater than the initiation threshold for liquefaction by undrained consolidation. Even though the epicentral distance is smaller for the Araucania aftershock (~110 km), the maximum seismic energy density of $0.9 \pm 0.4 \text{ J/m}^3$ during the aftershock was less than a tenth of that required to initiate liquefaction by this mechanism (see *Wang [2007]* for discussion of liquefaction mechanisms beyond the near-field).

Liquefaction susceptibility is closely related to water content and the sensitivity for sediments to consolidate [e.g., *Wang, 2007; Chia and Wang, 2009; Wang and Manga, 2010a*]. Nevertheless, the similar post-seismic recession constants do not indicate significant consolidation (eq. 5.5). Although a liquefaction-triggered streamflow increase by undrained consolidation is possible, field evidence for liquefaction, e.g. conic sand craters, boils or cracks [e.g., *Papadopoulos and Lefkopoulos, 1993; Wang and Manga, 2010a*], is lacking. Liquefaction is a consequence of pore-pressure increase when sediments consolidate in ‘undrained’ conditions during earthquakes [*Wang and Manga, 2012*]. Although undrained consolidation generally requires a confined saturated layer, which is not the case for the saturated saprolite, *Wang and Manga [2010a]* argued that transient pore pressures can increase under unconfined conditions if the duration of seismic shaking is relatively short compared to the time required to dissipate pore pressure in the unconsolidated sediment. Yet, the Maule event continued extraordinarily long. Nevertheless, complete liquefaction of the unconsolidated saprolite into a fluid-like substance is not required to explain the streamflow increase since a near-subsurface fluid pressure rise is sufficient.

As reported by *Carrigan et al. [1991]*, volumetric strain enhances horizontal groundwater flow, but also elevates the water table into the unsaturated zone. The rise, however, is limited by the volume of the water which had been mobilized by undrained compaction which, in turn, decreased the porosity [*Manga, 2001; Wang et al., 2001*]. Thus, undrained consolidation of the sandy saprolite would force water in a patchy pattern to rise upward towards the water table [*Lee et al., 2004; Wang et al., 2001*] while under pre-seismic conditions the groundwater table remained deeper providing low baseflow discharge and restricting plant transpiration to riparian vegetation due to groundwater access by deep

rooting species (see Fig. 5.10 a and b). As the topsoil was dry during the earthquake (see Fig 5.2), the ascended water is likely to be absorbed by the soil matrix (*Scheffer and Schachtschabel, 2010*). Wetting of the formerly unsaturated zone is indicated by the intensification of the diurnal streamflow oscillations (see 5.7.3.1). Despite the instantaneously increased hydraulic head, the flow is temporarily reduced as the expelled water saturates a portion of the formerly unsaturated zone. The temporarily reduced flow is expressed as a delayed streamflow increase at the catchments' outlets. Hence, an abrupt but transient initial decline of streamflow is expected (see insets in Fig. 5.3), and the initial drop of streamflow discharge would continue until a new hydraulic equilibrium has been established between the saturated and unsaturated zones. Under this newly established equilibrium the rise of the water table ceases and the enlarged cross section of the lateral subsurface flow now enhances streamflow discharge following eq. 5.4 (see Fig. 5.10c). However, these observations are not restricted to liquefaction or undrained consolidation processes. An elevated groundwater table along the headwater valley bottoms may also be triggered by enhanced vertical permeability.

The short duration of such an initial decline will not be observable at larger scales [e.g., *Manga, 2001; Manga et al., 2003; Montgomery et al., 2003*] because any short signals from small tributaries will be averaged over longer periods when they merge together and the discharges are superimposed. Thus, it is not surprising that the longest excess flow was sustained in Pichún grande. In the case of Pichún grande, excess flow equaled 8-9 mm until May 4th when the first significant rainfall event of the rainy season occurred, masking the streamflow response to the Maule earthquake. This value is comparable to the response of Ship Creek to the Alaska earthquake on March 27th 1960 under winter low flow conditions and limited water availability for streamflow generation [*Manga, 2001*]. Thus, the extended stream-network may explain the missing initial decline in catchments of a larger scale (see catchment No. 10 in Fig 5.3 and Fig. 5.4) but fails to explain the missing decline in catchment No. 3 and near-surface undrained consolidation may explain the hydrological response to the Maule earthquake and the lack of response to the aftershock.

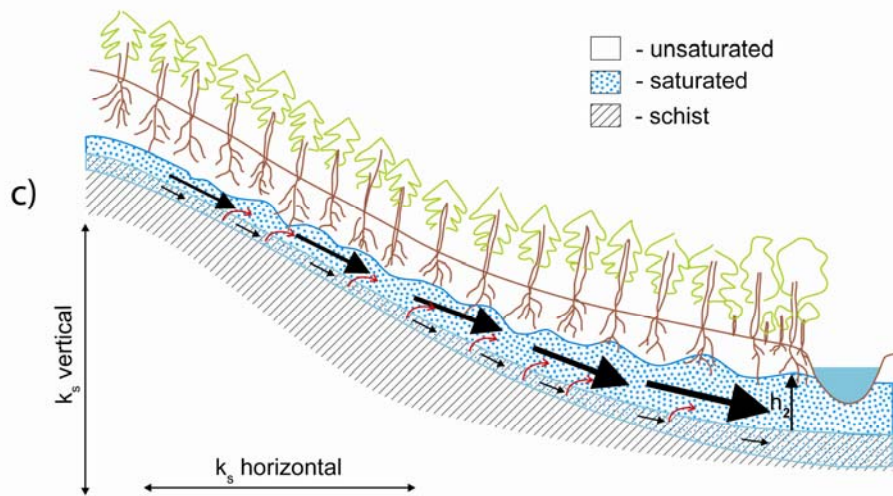
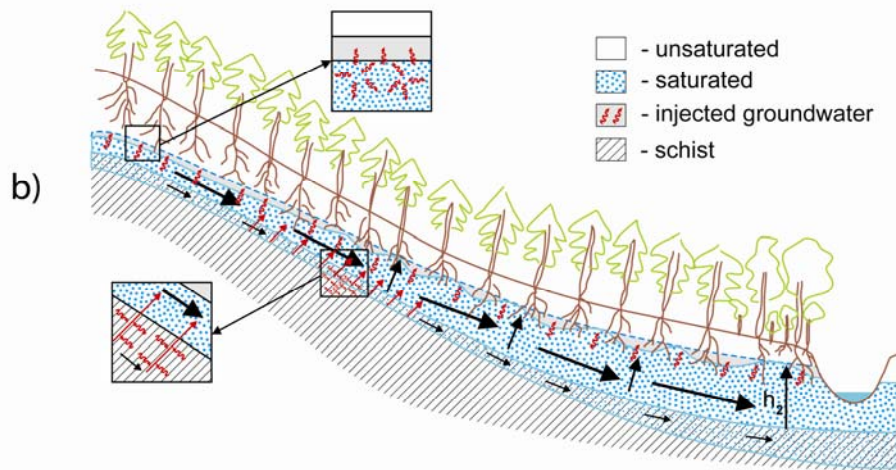
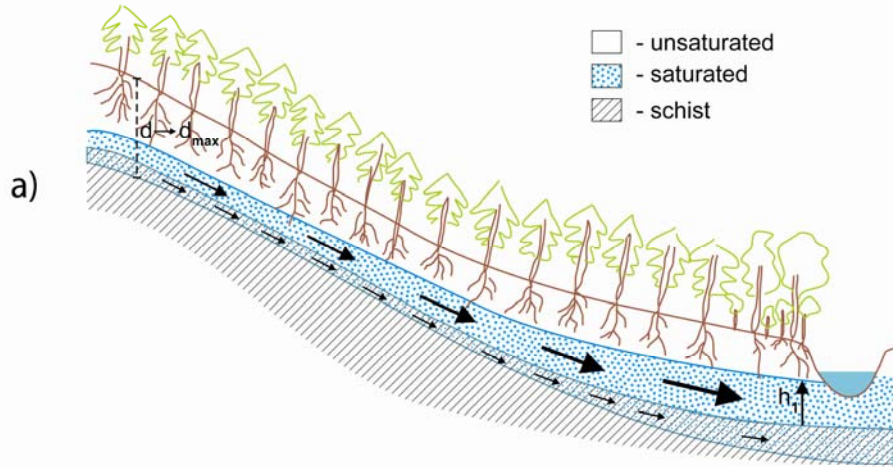


Figure 5.10 on previous page: (a) schematic sketch of a hillslope in the study area prior to the earthquake. h_1 corresponds to the height of the cross-section of saturated zone flow and d to the maximum depth of the water table. Thickness of black arrows indicates relative volume of subsurface flow and thickness of dots relative content of water in each geological unit.

(b) schematic sketch during the earthquake. h_2 corresponds to the vertically enlarged cross-section of the saturated zone flow. Red arrows indicate expulsion of water from fissures/cracks of the topmost schist into the saprolite layer. Rolling red arrows represent dynamic strain caused by seismic ground shaking.

(c) schematic sketch of the hillslope after the earthquake under unchanged lateral and vertical hydraulic conductivity conditions. Rolling red arrows represent additional water squeezed out from the topmost schist contributing to streamflow discharge.

5.7.3.1. Intensified magnitude of diurnal oscillations of streamflow discharge

Earthquakes are reported to affect whole ecosystems [Attiwill, 1994]. However, in this study, an enhancement in plant activity is observed, which is expressed by an intensification of diurnal oscillations of streamflow. Diurnal streamflow oscillations are governed by diurnal variability in hydraulic gradients in the unsaturated zone, as driven by the diurnal cycle of water uptake by vegetation cover which is highest during the afternoons, forcing the flux of soil water towards the roots and surface, and ceases during the night. Under these conditions, plant activity influences the amount of water available for streamflow generation and results in diurnal oscillations which are directly related to evapotranspiration and the replenishment of the depleted groundwater storage. Hence, maximum discharge occurs during the early mornings and minimum discharge during afternoons [Dyck and Peschke, 1995; Gribovszki *et al.*, 2010]. Thus, diurnal oscillations intensify when vegetation cover has access to additional water. Such intensified plant transpiration is documented in the increased magnitude of post-seismic diurnal oscillation in Pichún (Fig. 5.4). Water expelled by undrained consolidation would augment the vertical extent of the capillary fringe and the saturated zone, which would facilitate root access and thus higher plant water consumption. However, a local water table rise along the headwater valley bottoms due to enhanced vertical permeability (see 5.7.2) could produce a similar effect.

Because groundwater is ~150-200 cm below ground surface along hillslope transects, during the dry season due to sparse rainfall and high water consumption [Huber *et al.*, 2010] groundwater access is restricted to deep-rooting species along the riparian buffer strips (Fig. 5.10c). Assuming unrestricted plant access to groundwater, streamflow discharge of all catchments (except the clear cuts) should show at least some diurnal oscillation in

streamflow. It is therefore not surprising to find diurnal streamflow oscillations in Pichún, which has the largest spatial extent of the riparian buffer zone (catchment No. 11, see Table 5.1). Here, the magnitude of diurnal oscillations decreased over time due to the depletion of groundwater by evapotranspiration, lack of rainfall and weather conditions which decreases potential evapotranspiration.

Catchment No. 2 shows a diurnal streamflow oscillation that remained unaffected by the earthquake. As it includes a small wetland it is likely that this catchment has, in general, a groundwater table closer to the surface and thus more water available for transpiration.

5.7.4. Increase in streamflow by tilting of the landscape?

An increased $\delta h/\delta l$ due to tilting of the landscape is unlikely because it would lead either to an increased or decreased slope and some catchments should experience an increase and some a decrease in streamflow, depending on their geographical orientation. Catchments No. 9 and 11 experienced similar streamflow increases (160 and 150 % respectively) but differ in their orientation whereas catchments with the same mean orientation (e.g., catchments No. 7 and 8) show high variability in relative increase (Fig. 5.1 and Table 5.2). Steeper inclined slopes would also increase the surface flow velocity and thus the discharge in the streamflow, as the slope of the channel is directly related to the velocity [Dingman, 2002]. By analogy, enhanced vS would result in a higher discharge only for a period of the duration of the flow time in the creek. Considering a length of several 100s of metres and a flow velocity of approx. 0.2-0.4 m/s, this time is less than 1 hour. The study area is close to a hinge of vertical displacement separating the uplift area in the west from the subsidence area to the east [Farias *et al.*, 2010]. Hence, the vertical displacement is only minor compared to the lateral displacement. Vigny *et al.* [2011] showed co-seismic horizontal displacement of approx. 210 cm and vertical subsidence of ~40 cm within the study area, values similar to the land-level changes of approximately -50 cm reported by Farias *et al.* [2010] for flooded river banks of the Bío-Bío River at ~45 km distance. However, assuming a non-uniform subsidence of approx. 0.4-0.5 m across the study area and the given altitude difference of the streams of 57 m (catchment 2) to 245 m (catchment 11) along at stream length of 400 to 2700 m (see Tab. 1), the possible effects on stream slope are negligible. Moreover, that subsidence is rather likely to cause retardation of streamflow discharge and high streambed roughness within the area [Ansejo, 2011] additionally suggests attenuation of any effect of a slight modification of streambed slopes.

Co-seismic streamflow discharge is highly correlated to catchment size (correlation coefficient 0.97, see section 6 for methodological details) and shows the importance of catchment scale on the pre-earthquake streamflow. Post-seismic streamflow increase is correlated to catchment size, too, which makes it very unlikely that the earthquake reshaped the extent of the drainage system. Consequently, an increased hydraulic gradient due to tilting of the landscape cannot explain the observed phenomena.

5.8. Conclusions and synopsis

The streamflow discharge records presented here show for the first time near-surface hydrological response to a high-magnitude earthquake in small homogeneous upland catchments. The baseflow response to the mainshock showed a similar but non-uniform pattern in their initial decline preceding a strong post-seismic increase and intensified diurnal streamflow oscillations. All catchments remained unaffected by the aftershock. Although minimal enhancement of lateral hydraulic conductivity was spatially limited, vertical permeability increase is probable. Substantially unchanged water temperatures show that the common source of pre- and post-seismic streamflow remained unaffected by the earthquake. Our findings indicate that the excess water originated from the saprolite-bedrock interface. Our analysis further showed that the water was released in an unequal pattern across the catchments and elevated the groundwater table which enhanced plant transpiration. Our results are consistent with the empirical magnitude-distance-relationship and the thresholds of seismic energy density needed to initiate liquefaction by undrained compaction. Although our findings allow the interpretation that undrained consolidation (perhaps even up to liquefaction) caused an initial decline followed by a subsequent post-seismic increase in streamflow discharge and intensified root water uptake, field evidence for liquefaction is lacking and enhanced vertical permeability (perhaps combined with coseismic dilatancy) provides a potential alternative explanation for the observed hydrologic response. Our results imply that further differentiation of the undrained consolidation mechanisms is crucial for understanding co-seismic streamflow increases.

5.9. Acknowledgements

The work presented herein is funded by the Chilean Government (Conicyt/BMBF 2009-092 and Fondecyt 1070218), the International Bureau of the German Ministry of Education and Research (CHL 08/03) and the Graduate School for Natural Disasters (GS NADI) of the University of Potsdam. We thank Forestry SA Mininco for access to our study catchments and financial support for the instrumentation of the catchments, Rafael Rubilar for providing soil data and Andreas Bauer for assistance with graphics (figure 5.10). We thank Chi Wang, Michael Manga and Frank Krüger for constructive and helpful discussion and Alex Densmore, Simon Mudd and three anonymous reviewers for comments that significantly improved the manuscript.

Chapter VI

Response of vadose zone water to earthquakes

Abstract

Hydrological responses to earthquakes are induced by coseismic strain and/or changes in permeability caused by the passing seismic waves [Wang and Manga, 2010a]. Previous interpretations and models [Elkhoury *et al.*, 2006; Manga and Rowland, 2009; Wang *et al.*, 2004b] assume that such responses occur exclusively in the saturated zone. Here we show that earthquakes may also release soil water from the vadose zone, which in turn may elevate groundwater levels and increase streamflow. After the 2010 magnitude 8.8 Maule earthquake several small Chilean catchments showed brief co-seismic drops in stream discharge, followed by rapid increases in streamflow and amplified diurnal cycles lasting 5-10 days, consistent with higher evapotranspiration rates and thus greater availability of water to vegetation. Our results imply that large earthquakes may increase the connectivity between the vadose zone and deeper groundwater, release soil water from the vadose zone to the groundwater table, and expand the capillary fringe; these may in turn enhance transpiration. A simple hydrological model also demonstrates that when seismic energy exceeds the threshold of soil water retention in the vadose zone, unsaturated soil water can be released into aquifers, thus increasing streamflow. Thus the unsaturated zone may play a previously unappreciated, and potentially significant, role in hydrological responses to earthquakes.

Key words: Chile, earthquake, evapotranspiration, modelling, streamflow, vadose zone.

Under consideration of *Nature Geoscience* as C. H. Mohr, M. Manga, C.-Y. Wang, J.W. Kirchner and A., Bronstert. Response of vadose zone water to earthquakes.

While hydrological responses to earthquake are sometimes viewed as mere curiosities [Wang and Manga, 2010a], they provide insight into the coupled interaction between tectonics and hydrogeological processes and properties. Mechanisms invoked to explain the observed hydrological responses include expulsion or leakage of water from deformed or ruptured aquifers [Muirwood and King, 1993; Wang et al., 2004a], fracturing of aquifers [Brodsky et al., 2003; Elkhoury et al., 2006; Manga et al., 2012; Rojstaczer and Wolf, 1992; Wang et al., 2004b], and consolidation of saturated sediments [Manga, 2001]. While these mechanisms differ substantially from each other, they all assume exclusively saturated groundwater flow conditions, with only one study suggesting that there may also be a response in the unsaturated zone based on isotopic characteristics of water discharged after an earthquake [Manga and Rowland, 2009]. The direct effect of earthquakes on catchment-scale hydrological processes in the vadose zone remains entirely undocumented and unexplored.

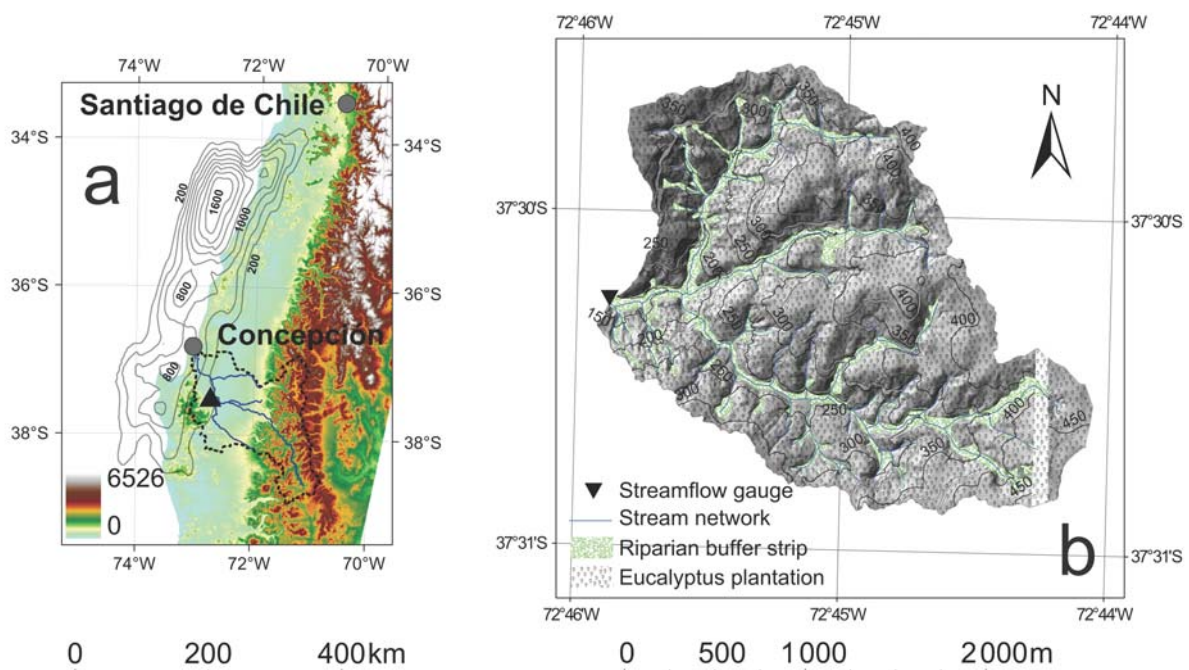


Figure 6.1. (a): Location map showing the study catchment (indicated by the black triangle) and the epicenter of the Maule earthquake of 27 Feb 2010. The dotted line represents the Biobio River basin. The contours show the slip in cm during the main shock [Tong et al., 2010]; the contour interval is 200 cm. Elevation (m asl) is derived from GTOPO30 data (<http://demex.cr.usgs.gov/DEMEX/>). **(b):** Studied catchment showing the vegetation cover, the stream network and the streamflow gauging station. Elevations (m asl) are derived from a LiDAR DEM. Contour interval is 50 m. The bright vertical stripe is due to missing LiDAR elevation data.

Here we use data from small headwater catchments and their response to the 2010 Maule (Chile) earthquake to infer the response of the unsaturated zone to earthquakes. To this

end, we develop a model that couples groundwater flow [Manga, 2001] and recharge [Wang et al., 2004b] with evapotranspiration fluxes [Kirchner, 2009] to quantify streamflow and evapotranspiration responses to the earthquake by simulating diurnal streamflow oscillations.

The studied catchment is homogeneous and simple in terms of geology and geometry compared with previous studies of hydrological responses to large-magnitude earthquakes [Wang and Manga, 2010a]. It extends over an area of 413 ha in the Chilean coastal range (Fig. 6.1a). At the time of the earthquake, most of the catchment was covered by a two-year old *Eucalyptus spp.* plantation with shallow roots not exceeding 100 cm in depth. Deeper-rooting native species (>200 cm in average), e.g. Arrayán (*Luma apiculata DC. Burret*), Boldo (*Peumus boldus Mol.*), and Roble (*Nothofagus obliqua Mirb.*), are found in a 45 ha riparian buffer strip along the stream in the valley bottom and its steep tributaries [Mohr et al., 2012] (Fig. 6.1b). The magnitude 8.8 Maule earthquake on February 27th 2010 caused intense ground shaking for about 150 seconds. The strongest aftershock (Araucaria aftershock) occurred on January 2nd 2011 with a magnitude of 7.1. No rainfall was recorded before or after each earthquake, leading to low baseflow conditions and enabling us to identify the streamflow response to the earthquake.

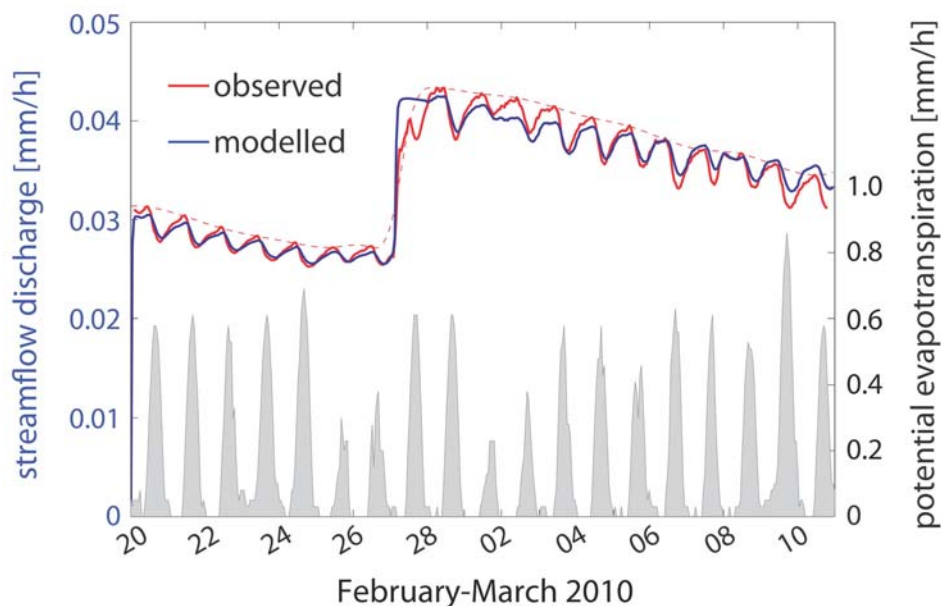


Figure 6.2. Observed and modelled streamflow (mm/h) for periods prior to and after the earthquake. The grey bars represent potential evapotranspiration rates (mm/h). The dashed red line indicates the maximum streamflow rates assuming negligible nightly evapotranspiration calculated by spline interpolation. The dashed black line shows the time of the earthquake.

We can identify three distinct responses after the main shock. First, streamflow increased substantially (Fig. 6.2). Second, diurnal streamflow oscillations were amplified (Fig. 6.2). Third, in smaller, adjacent catchments, the increase in discharge was preceded by a short initial drop in streamflow (Fig. 6.3). The temperature of the stream water did not change [Mohr *et al.*, 2012]. We next evaluate two classes of mechanisms that can explain these responses.

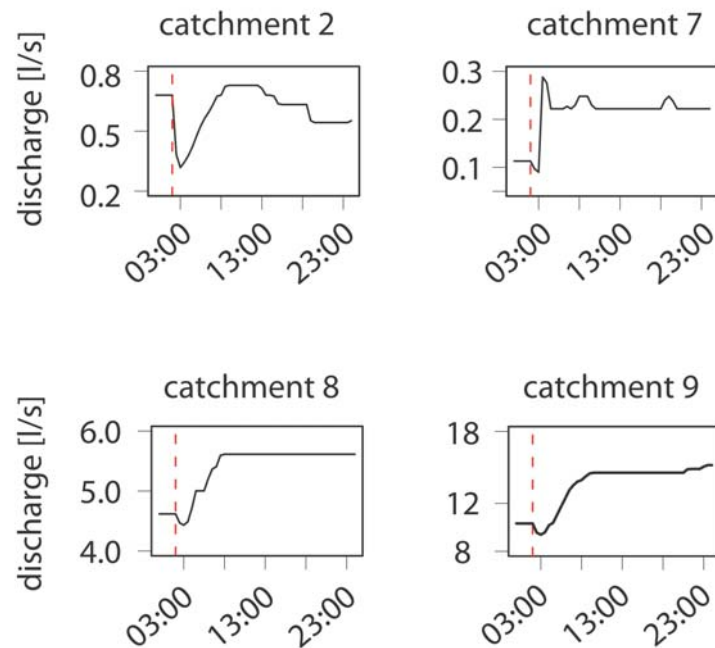


Figure 6.3. Observed co-seismic drop in streamflow in a subset of adjacent catchments. The dashed red lines indicate the time of the earthquake. The catchment numbering is consistent with a previous study [Mohr *et al.*, 2012] in order to allow transferability.

Under dry weather conditions, such as before and after the earthquake, diurnal streamflow cycling reflects alternating changes in groundwater storage in the riparian zone owing to day-time evapotranspiration losses by root water uptake. Evapotranspiration is limited by soil water availability [Jhorar *et al.*, 2004] and the night-time replenishment of depleted groundwater from upslope [Kirchner, 2009]. Changes in the atmospheric conditions after the earthquake may be excluded as a cause for the post-seismic increase because potential evapotranspiration – a measure of the atmospheric demand driven by temperature, wind and insolation – did not change substantially after the earthquake (Fig. 6.2). When restricted to dry-season conditions, the slope of the relationship between potential evapotranspiration and discharge oscillations slightly increased. However, we consider the difference as minor because the post-seismic data clearly lie within the scatter of the pre-

seismic points (supplementary Figure 6.1). On the other hand, the increase in the amplitude of diurnal streamflow oscillations after the earthquake ($p < 0.05$) is consistent with an increase in the rate of evapotranspiration (ET) by enhanced post-seismic root water uptake.

From the diurnal discharge cycles, we estimate ET before and after the earthquake using three different methods (supplementary material). All three methods result in an evapotranspiration increase of 30-60% for 5-10 days following the earthquake. The amplitude of the diurnal streamflow cycles after the earthquake is similar to the amplitude of the cycles during periods of similar average streamflow several months before the earthquake (supplementary Figure 6.2), when groundwater and/or soil moisture levels were higher. This implies that the earthquake suddenly increased the availability of near-stream groundwater and soil water to both streamflow and evapotranspiration, comparable to its availability several months before the earthquake. The increased streamflow and diurnal cycling, and the inferred increase in evapotranspiration, are consistent with the hypothesis of a sudden rise in near-stream groundwater levels, possibly including an upward extension of the capillary fringe in the riparian zone that would make soil water more available to vegetation. How could the earthquake have caused this increase in water availability near the stream, and where did the water come from?

Increases in permeability are commonly invoked to explain increases in discharge [Elkhoury *et al.*, 2006; Rojstaczer and Wolf, 1992; Manga *et al.*, 2012] after earthquakes. Previous analysis of the gradual decrease in discharge after the Maule earthquake inferred essentially unchanged catchment-scale permeability following the earthquake [Mohr *et al.*, 2012]. If we assume that permeability increases everywhere by an amount proportional to its previous value and restrict the problem to entirely subsurface flow conditions, discharge would increase by an amount proportional to the permeability change, and water levels in the subsurface would decrease. In these catchments, however, the increases in the amplitude of diurnal fluctuations suggest higher water levels in the subsurface.

The intensity of seismic shaking may have been great enough to dilate the shallowest sediments and form cracks [Wang *et al.*, 2004b]. Dilatancy describes the increase of porosity due to the propagation of cracks which preferentially form perpendicular to the direction of maximum tension [Scholz, 2010]. Based on data from Taiwan, an estimated seismic energy density of 530 J/m³ is sufficient to initiate such crack formation [Wang *et al.*, 2004b] (though this value has considerable uncertainty [Wang and Manga, 2010a]). In the absence of relevant data from Chile, we estimated the seismic energy density based on data from southern California. The Maule earthquake generated energy densities of the same order of magnitude

in our catchment ($\sim 170 \text{ J/m}^3$), and indeed, surface cracks were observed after the earthquake on ridges or road fills where a missing overburden allows near-surface cracking by surface expansion due to seismic stress [Anderson and Anderson, 2010]. Water is then expected to migrate from saturated pores into the new cracks. As a result, the hydraulic head is lowered and streamflow is disrupted temporarily. Such decreases are in fact seen in several small headwater catchments immediately after the Maule earthquake (Fig. 6.3). However, these initial drops are only expected to be seen in the smallest catchments, because in larger catchments, short-lived signals will be obscured by averaging of discharge from multiple tributaries and by dispersion in longer channels [Mohr *et al.*, 2012].

The release of water into cracks or drainage from the unsaturated zone liberates water that ultimately raises hydraulic heads in the aquifers feeding the streams. We now consider the possibility that seismic shaking could have released water held in the unsaturated zone. In particular, we propose that, just as a sponge releases water when shaken, water can be mobilized from an unsaturated soil whenever the energy imparted by seismic waves exceeds its matric potential.

Superimposing the seismic energy on the matric potential during the earthquake (see supplementary information) would elevate the water retention threshold by 10^3 Pa , thus mobilizing water from regions with soil moisture contents between 33 and 36% considering the sandy texture of the subsoil (Fig. 6.4a). Soil moisture measurements before the earthquake along transects show near-saturated conditions in the deeper soil ($>180 \text{ cm}$) and there is enough available soil water to account for the post-seismic excess streamflow discharge. The water released from 180-250 cm depth during shaking would equal up to 20 mm of excess flow and be available to recharge the underlying aquifer (Fig. 6.4b).

Though the duration of shaking is relatively short, we suggest it lasts long enough to release vadose zone water to recharge groundwater for several reasons. First, fast vertical drainage along preferential flow paths, e.g. along root channels or soil cracks, is common in this study area [Mohr *et al.*, 2013]. Second, transient stresses from seismic waves can clear clogged (macro-) pores which would enhance downward drainage [Manga *et al.*, 2012]. Finally, co-seismic near-surface cracking creates additional fast vertical flow paths [Wang *et al.*, 2004b]. As the released vadose zone water recharges the groundwater, the groundwater table rises and extends the ‘active zone’ of high evapotranspiration. We define the ‘active zone’ as the region where the distance between the groundwater table and the root zone is small enough that the root water uptake is linked to the groundwater at least by a capillary fringe which in turn allows maximum evapotranspiration rates. Under these assumptions, all

groundwater needs to be connected to the drainage network in order to reflect losses by evapotranspiration in the streamflow records.

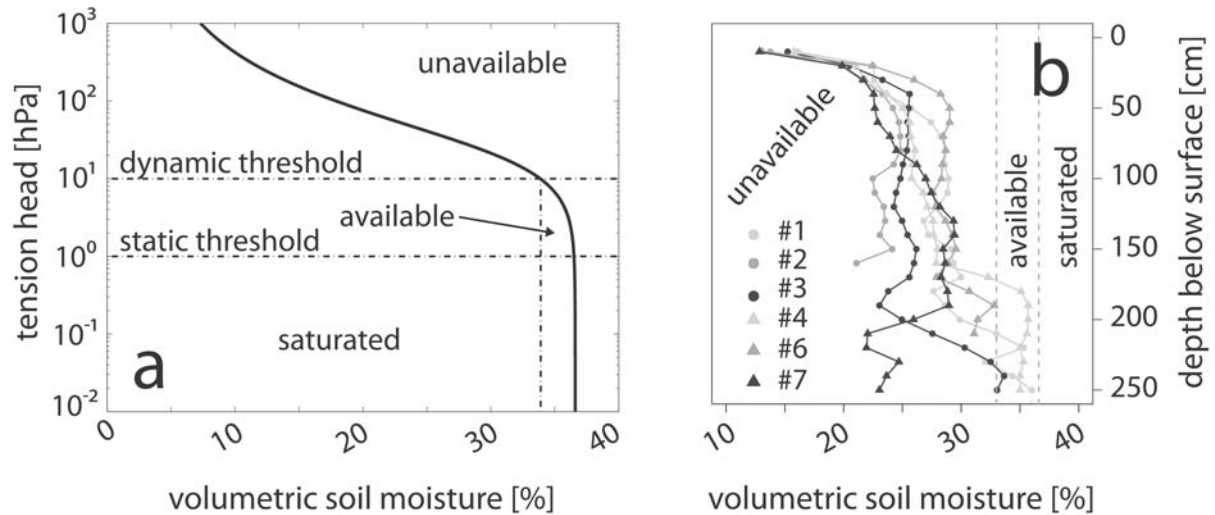


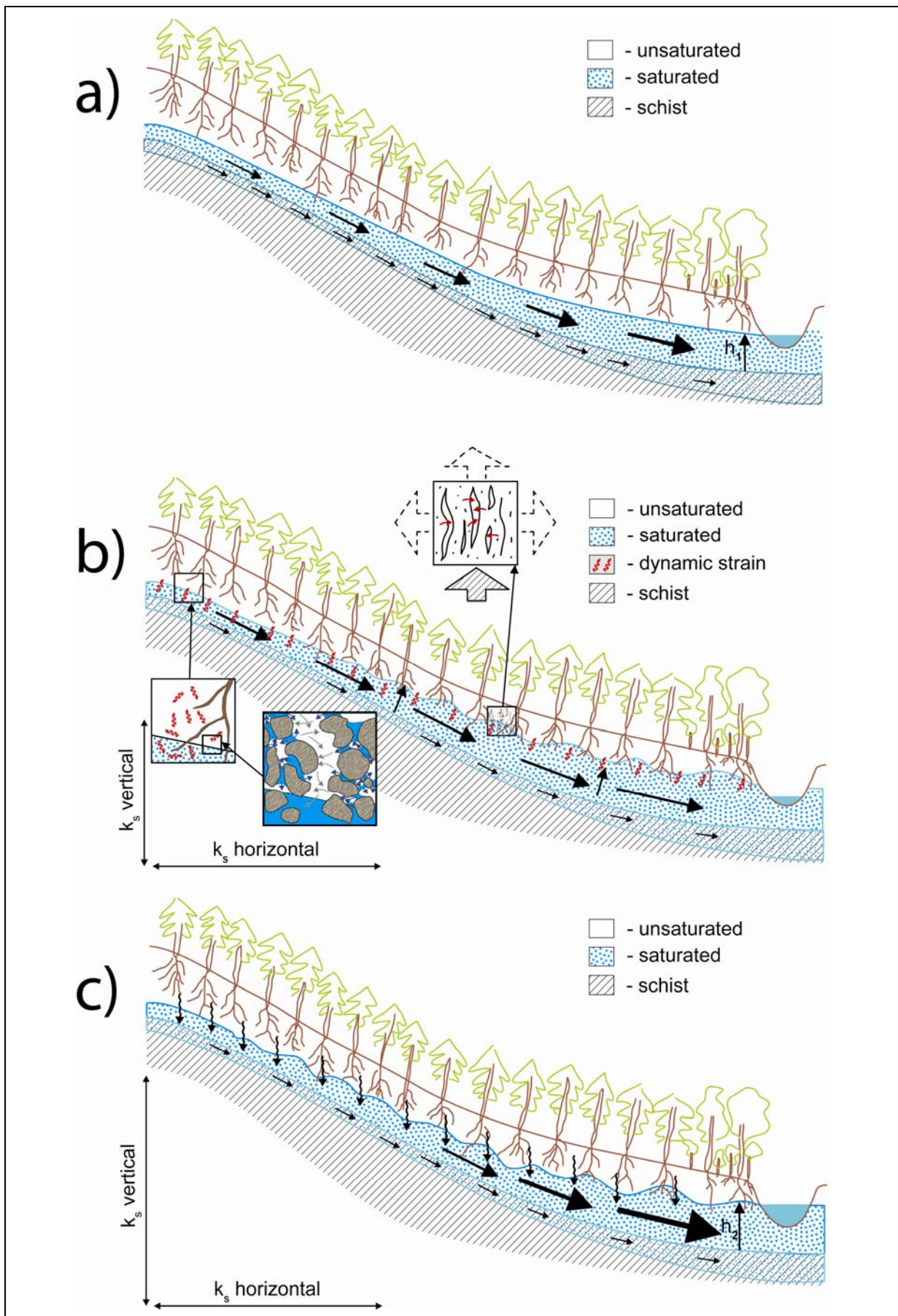
Figure 6.4. (a): Black curve shows the water retention curve for the deep soil (>160-170 cm below surface [Mohr *et al.*, 2012]) which was parameterized for sandy soils with the following van Genuchten parameters [Wosten *et al.*, 1999]: residual water content $\theta_{res}=0.025$, saturated water content $\theta_{sat}=0.366$; $\alpha=0.0430$ and $n=1.5206$. (European soil database; http://eussoils.jrc.ec.europa.eu/esdb_archive/ESDBv2/popup/hy_param.htm). The upper horizontal dashed line shows the matric potential equivalent to seismic potential and the lower dashed line indicates saturation. The vertical dashed line shows the threshold for the sandy soil prone to saturation. The arrow indicates the available soil moisture. **(b):** Soil moisture (vol. %) measured by TRIME-TDR on 19 Feb 2010 in access tubes along transects (supplementary information). Dashed vertical lines span the range of water contents of the saprolite which may be prone to saturation during ground shaking when seismic potential equals or exceeds matric potential. Relatively high soil moisture contents at shallow depths probably represent the wetting front of the 20mm-rainfall event on Feb 17th-18th, immediately before the soil moisture measurements but 9 days before the earthquake.

To model this mechanism, we treat the water released from the vadose zone as a source of water in the groundwater flow equation. A sink term representing evapotranspiration loss is added to the model (supplementary information). We find a good fit to the observed discharge record without changing lateral hydraulic conductivity (Fig. 6.2) but instead by elevating hydraulic head by (1) the release of additional water from the vadose zone and (2) enhanced vertical permeability owing to dilatancy to increase streamflow discharge. Our model yields ~12 mm of excess water, consistent with the mobilizable water from the vadose zone (20 mm). Moreover, the model is able to reproduce the post-seismic intensification of the diurnal streamflow cycles, supporting our suggestion of enhanced evapotranspiration after the earthquake. Our model estimates a post-seismic increase in daily

evapotranspiration of approximately 30-60% or an increase from 0.03 mm/day to 0.04-0.05 mm/day averaged across the whole catchment ($p < 0.01$, supplementary information and supplementary Table 6.1). Averaged over the entire catchment, these changes in evapotranspiration are too small to be biologically significant. Given the shallow root depth of the juvenile eucalyptus, however, we can hypothesize that under dry conditions, substantial evapotranspiration occurs only in the riparian zone. If we further restrict evapotranspiration to the lower riparian zone along the valley bottom and exclude the steeper tributaries, we can downsize the active zone to 15-50% of the entire riparian zone. As a result, evapotranspiration rates may reach values up to 2.4 mm/day which agrees well with the reported maximum rates of ~ 3 mm/day of comparable riparian vegetation [Baird and Maddock, 2005]. Thus, the increase in evapotranspiration is consistent with a spatial expansion of the ‘active zone’ after a rise of the groundwater level and capillary fringe while the evapotranspiration rates may remain the same. Note, however, that plants will also consume water from the vadose zone. Such water losses, however, are not reflected in the streamflow dynamics from which we calculated evapotranspiration.

Our results show that the hypothesized mechanisms are quantitatively sufficient, under plausible conditions, to account for the observed streamflow response and the inferred increase in evapotranspiration. Our analysis implies that seismo-hydrological processes can also occur in the vadose zone, a zone that is regarded as a critical zone for both understanding root-water uptake and runoff processes owing to the direct link to aquifers [Hattermann *et al.*, 2006]. Independent confirmation of our hypothesis could be made following future earthquakes with time series of soil moisture and piezometric depth profiles, and possibly stream water isotope data [Manga and Rowland, 2009]. Our study challenges the conventional view in which hydrological responses to earthquakes are restricted to the saturated zone.

6.1 Conceptual model of vadose zone water response to earthquakes



See previous page:

(a) Prior the earthquake: Low baseflow conditions (h_1 corresponds to the height of the cross-section of saturated zone) and plant-water availability is limited to deep rooting riparian vegetation. Thus, plant activity is relatively low. Thickness of black arrows indicates relative volume of subsurface flow and dots saturation level of each geological unit.

(b) During the earthquake: Ground shaking causes two effects. First, it dilatates the shallowest sediments and forms cracks. Water then migrates from saturated pores into the new cracks (red arrows) lowering the hydraulic head until the dilitant cracks are filled. As a result, streamflow is temporarily disrupted. Further, dilitant cracking enhance vertical hydraulic conductivity and thus improves connectivity between vadose zone water and the groundwater flow zone. Second, ground shaking mobilizes vadose zone water when $\Psi_{matrix} \leq \Psi_{seismic} + \Psi_{gravitational}$ (grey arrows). Upon established connectivity between vadose zone and groundwater zone, the released water recharges the underlying aquifer. Drainage is provided by preferential flow paths, e.g. root channels or soil cracks, clearing of clogged macro-pores by transient stresses from seismic waves and dilitant cracks. Horizontal permeability remains unchanged.

(c) After the earthquake: As the released vadose zone water recharges the groundwater, the groundwater table rises (h_2) and extends the ‘active zone’ of high root-water-uptake along the valley bottoms. There, the available water resources promote plant activity along the riparian buffer strips as reflected in intensified diurnal streamflow oscillation. Further, the higher groundwater table increases streamflow discharge.

Acknowledgments

The authors would like to thank Andrés Iroumé for providing the hydrometric data. C.H.M. benefited from an invitation by the University of California, Berkeley.

Author contributions

C.H.M. and J.W.K. analyzed the data. C.H.M. performed the numerical modeling. All authors contributed to the ideas presented in the manuscripts.

Competing financial interests

The authors declare no competing financial interests.

6.2 Supplementary Information

6.2.1. Methods

6.2.1.1. Observation of streamflow, rainfall and soil moisture.

Streamflow discharge was monitored by a flume equipped with a custom-built water stage recorder with a resolution of 2 mm. The sampling interval was 10 minutes. Rainfall was recorded by a Hobo tipping bucket close to the streamflow gauging station and at a meteorological station about 600 m north of the catchment. The rain gauge registers data with an accuracy of 0.2 mm. Soil moisture was manually estimated using a mobile TDR-Trime-Probe (IMKO) along transects of access tubes in 10 cm depth increments up to a maximum depth of 270 cm below surface. Access tubes were installed only in various adjacent catchments. There, the number of access tubes ranged between 6 and 15. The last soil moisture measurements before the earthquake were carried out on February 19th 2010.

6.2.1.2. Rescaling of evapotranspiration rates and normalization of discharge.

Evapotranspiration rates were rescaled using potential evapotranspiration ET_{pot} estimated by Penman-Monteith and a scale factor s :

$$ET_{rescaled}(mm/h) = ET_{pot} * s \quad \text{with} \quad s = \frac{[average(P) - average(Q)]}{average[ET_{pot}]} \quad (\text{eq. 6.1, 6.2})$$

Amplitudes of daily cycling of streamflow discharge were normalized to daily average discharge according to:

$$Amplitude = \frac{[\max(Q) - \min(Q)]}{average[Q]} \quad (\text{eq. 6.3})$$

6.2.1.3. Modelling.

6.2.1.3.1. Modelling of Groundwater flow.

Groundwater flow was simulated by a one-dimensional groundwater flow model,

$$S_s \frac{\partial h}{\partial t} = K \frac{\partial^2 h}{\partial x^2} + A - E_t \quad \text{with} \quad Q = -\frac{\partial h}{\partial x} * K * D_t \quad (\text{eq. 6.5, 6.6})$$

where Q represents discharge, S_s is specific storage (could also be specific yield in the linearized groundwater flow equation for an unconfined aquifer), h is hydraulic head and K is horizontal hydraulic conductivity, A is the co-seismic water recharge from vadose zone, E_t is the evapotranspiration flux from groundwater and D_t is the cross-sectional area of the aquifer. We assume both S_s and K are constant in space and time during the study period. The aquifer extends from $x=0$ at the catchment divide to $x=L$ at the stream. Boundary conditions are

$$h(L,t) = 0 \quad \text{and} \quad \frac{\partial h(0,t)}{\partial x} = 0$$

while the initial condition is defined as

$$h(x,0) = h_0(x) \quad \text{with} \quad 0 \leq x \leq L$$

Equation 5 is solved numerically with an implicit finite difference method. Although geometrically simplified, 1-D models are commonly used to interpret hydrological responses to earthquakes [Manga, 2001; Wang and Manga, 2010a; Wang *et al.*, 2004b].

6.2.1.3.2. Modelling of co-seismic water mobilization from the vadose zone.

Co-seismic recharge $A(t)$, the excess water released per unit volume averaged across the catchment area, is modelled following Wang *et al.*[2004b] by using a steep co-seismic arctangent saltus function

$$A = \left[\frac{\pi}{2} + \arctan c(t - t_0) \right] \quad (\text{eq. 6.7})$$

where the parameter c is fitted to the steepness of the increase of streamflow discharge and t_0 is the time of the earthquake.

In contrast to previous studies, we infer that the excess water mobilized by the earthquake comes at least partially from the vadose zone. Saturated flow is governed by Darcy's law [Hillel, 2003] and initiated when the negative pressure head/suction of matric potential Ψ_{matric} (adhesive intermolecular forces between water and soil solids and cohesive

forces between the water molecules [Hillel, 2003]) is exceeded by the seismic accelerations. Hence, an additional positive force is needed to release the capillary soil water from the pores. Seismic energy density e is defined as the maximum seismic energy available in a unit volume to do work on rock or sediment [Wang and Manga, 2010b] and may be estimated by

$$\log_{10} e \left(J/m^3 \right) = -3.03 \log_{10} r + 1.45M - 4.24 \quad (\text{eq. 6.8})$$

with earthquake Magnitude M and the epicentral distance r in kilometres. Seismic energy density in equation (8) is expressed in J/m^3 and can be treated as a pressure head (Pa) counteracting the matric potential.

Given this key assumption and the parameter values of $M=8.8$ and $r=115-130\text{km}$, e yields 10^2-10^3 Pa acting as a positive pressure head ($\Psi_{seismic}$) and the static threshold of saturation θ dynamically evolves during shaking according to

$$\theta_{(\Psi_{seismic} + \Psi_{matric})} = \left[1 + [\alpha * (\Psi_{seismic} + \Psi_{matric})]^n \right]^{-1 + \frac{1}{n}} \quad (\text{eq. 6.9})$$

where α and n represent the Van Genuchten empirical texture-specific parameters [Van Genuchten, 1980].

As a result, flow conditions dynamically switch from an unsaturated to saturated state once the seismic energy density exceeds the matric potential ($\Psi_{seismic} \geq \Psi_{matric}$). In fact, this estimate is a lower bound since flow already initiates under unsaturated flow conditions by gravity and, thus, vertical drainage from the vadose zone is already expected when $\Psi_{matric} \leq \Psi_{seismic} + \Psi_{gravitational}$. Given the possibility to drain, the mobilized soil moisture recharges the aquifer during the shaking. Although the relation between the seismic energy density, earthquake magnitude and epicentral distance was derived for Southern California [Wang, 2007], we use it here as a first approximation in the absence of a similar relation for Chile. The absence of a hydrological response to the Araucaria aftershock is consistent because its seismic energy density is much smaller – too small to release water from the vadose zone.

6.2.3.3. Inverse modelling of evapotranspiration.

We estimated evapotranspiration by three different methods: (1) simple spline interpolation linking maximum daily discharge, (2) considering maximum recharge rates during night [White, 1932] and (3) by ‘doing hydrology backwards’ as proposed by Kirchner [2009].

Daily evapotranspiration was estimated as the difference between a spline interpolation linking daily maximum discharge rates – as expected without evapotranspiration losses during night – and the observed discharge rates including the evapotranspiration signal. In addition

daily evapotranspiration rates were independently estimated by the method of *White* [1932] considering maximum recharge rates during night:

$$E_t = S_y (24r \pm sd) \quad (\text{eq. 6.10})$$

where S_y refers to a specific yield and r to the slope of the tangential line drawn to the increasing streamflow discharge (mm/h) during predawn/dawn times when E_t is negligible. Uncertainty is given by \pm one standard deviation (sd). Assuming the streamflow increase is proportional to the rate of groundwater recharge to the riparian zone, we then extend the tangential line over a 24h period and take the difference to the streamflow discharge rates to estimate the total water recharge to the riparian buffer zone [*Gribovszki et al.*, 2010]. The estimated recharge rate must be modified by the difference in the observed streamflow discharge rates over the 24h-period because streamflow discharge only rarely reaches the rates of the previous day.

Finally, we calculated evapotranspiration rates $E_t(t)$ following *Kirchner's* approach of “doing hydrology backwards”, a modelling procedure based on observable fluxes assuming a catchment-specific relationship between discharge and storage rather than on point-scale measured soil-hydrologic properties [*Kirchner*, 2009]. Here, evapotranspiration rates are a function of time and can be approximated using the conservation-of-mass equation when storage S (units of depth), precipitation P and discharge Q (both in units of depth per time) are known,

$$E_t = P - Q - \frac{\partial S}{\partial t} \quad (\text{eq. 6.11})$$

Assuming that discharge depends on water storage across the catchment only, the direct and invertible relation between water storage and discharge can be written as

$$Q = f(S) \quad \leftrightarrow \quad S = f^{-1}(Q)$$

Hence, Q can be expressed by using a catchment-specific function of water storage, which relates changes in discharge Q to changes in catchment specific storage S

$$\frac{\partial Q}{\partial t} = \frac{\partial Q}{\partial S} * \frac{\partial S}{\partial t} = \frac{\partial Q}{\partial S} (P - E_t - Q) \quad (\text{eq. 6.12})$$

The term $\frac{\partial Q}{\partial S}$ is the derivative of the storage-discharge relationship $f(S)$ and expresses the sensitivity of discharge to changes in storage. Owing to the assumption that S is a function of Q , $\frac{\partial Q}{\partial S}$ can be considered as the discharge sensitivity function $g(Q)$

$$\frac{\partial Q}{\partial S} = f'(S) = f'(f^{-1}(Q)) = g(Q) \quad (\text{eq. 6.13})$$

The discharge sensitivity function can then be approximated from observed fluxes

$$g(Q) = \frac{\partial Q}{\partial S} = \frac{\partial Q / \partial t}{\partial S / \partial t} = \frac{\partial Q / \partial t}{P - E - Q} \quad (\text{eq. 6.14})$$

Once this catchment specific discharge sensitivity function $g(Q)$ is identified, changes in storage can be inferred and thus losses or gains from discharge Q , precipitation P or evapotranspiration E_t can be estimated from the discharge time series [Kirchner, 2009]. In practice, $g(Q)$ is estimated as an empirical function from plotting the recession rate $(-\partial Q / \partial t)$ as a function of discharge Q . We approximated this function using a power law function of Q

$$g(Q) = \frac{\partial Q}{\partial S} = \frac{\partial Q / \partial t}{-Q} = a * Q^{b-1} \quad (\text{eq. 6.15})$$

with slope b and intercept a in which a reflects scaling, physical and/or geomorphic properties of the catchment [Rupp and Selker, 2006].

As no rainfall was recorded around the time of the earthquake ($P \approx 0$), evapotranspiration rates E_t are inferred by

$$E_t|_{P=0} = -\frac{\partial Q / \partial t}{g(Q)} - Q \approx -\frac{(Q_{t+1} - Q_{t-1}) / 2 \partial t}{[g(Q_{t+1}) + g(Q_{t-1})] / 2} - (Q_{t+1} + Q_{t-1}) / 2 \quad (\text{eq. 6.16})$$

for the time steps t [Kirchner, 2009].

In order to minimize the impact of evapotranspiration and rainfall fluxes on $g(Q)$, only discharge recession data during night within a period of no recorded rainfall 6h prior and at least 2hr after were considered to determine $g(Q)$ [Kirchner, 2009]. Owing to the lag effects of evapotranspiration on night-time streamflow during the dry season, the selection criteria were further expanded to rainless periods during the rainy season with relatively low evapotranspiration rates. In order to estimate the impact of $g(Q)$ on evapotranspiration, a sensitivity analysis for a and b was conducted in the range of \pm one standard error. The $g(Q)$ function was also applied in a simplified way in order to increase sensitivity of E_t to $-\frac{\partial Q / \partial t}{g(Q)}$. Because Q is two orders of magnitude smaller than potential evapotranspiration

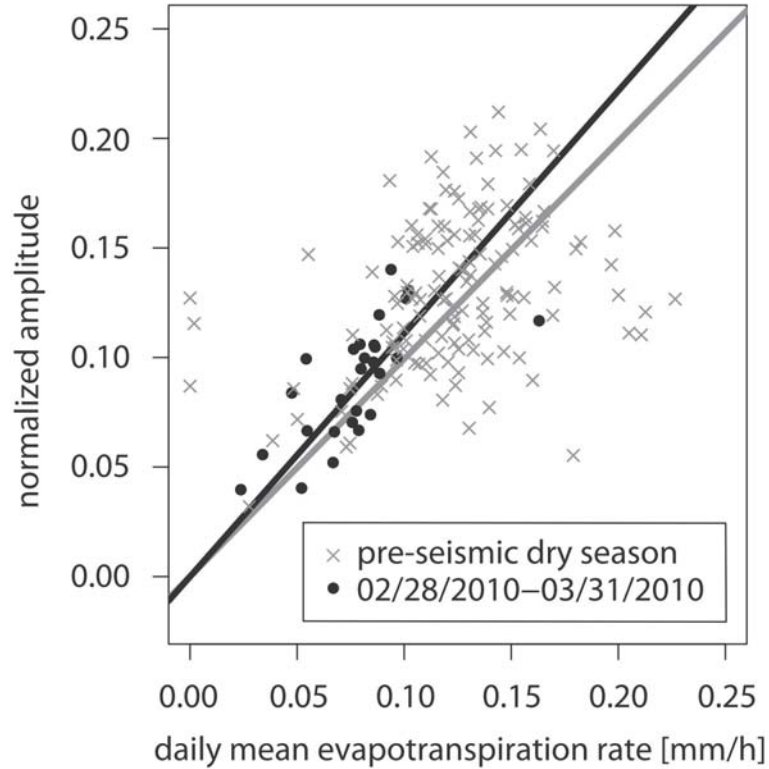
and there was no rainfall, we assume Q and P are negligible which thus simplifies E_t to

$$E_t|_{P=0, Q \ll E_t} = -\frac{\partial Q / \partial t}{g(Q)} \approx -\frac{(Q_{t+1} - Q_{t-1}) / 2}{[g(Q_{t+1}) + g(Q_{t-1})] / 2} \quad (\text{eq.6.17})$$

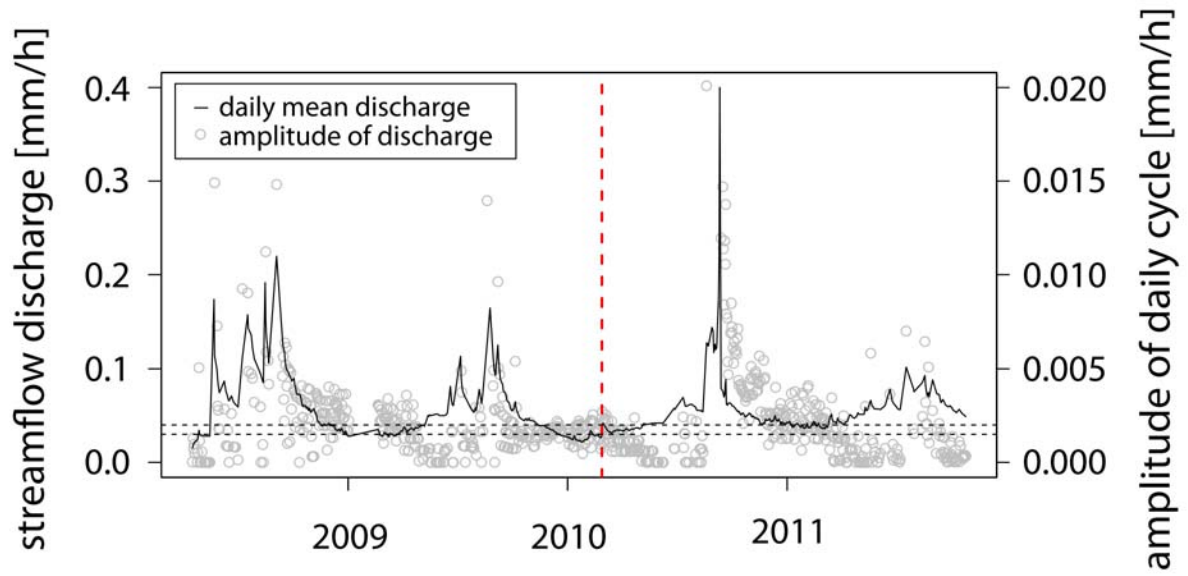
Possible earthquake effects on porosity were explored by comparing pre- and post-seismic discharge sensitivity functions $g(Q)$, since storage S is directly related to porosity [Freeze and Cherry, 1979].

Daily evapotranspiration values for the periods from February 20th – 26th and February 28th – March 11th were compared and statistically tested by Wilcoxon rank sum test at a significance level of $\alpha=5\%$. The relationship between changes in streamflow discharge amplitudes and changes in daily evapotranspiration prior and after the earthquake was assessed by applying analysis of covariance at the same significance level.

6.2.2. Supplementary Figures



Supplementary Figure 6.1. Rescaled evapotranspiration rate-diurnal streamflow amplitude relationships for pre- and immediate post-seismic periods during the baseflow conditions (rainfall=0) of the dry summer season months (Dec-March). Evapotranspiration rates ET were rescaled using the scaling factor. The black line shows the post-seismic regression ($y=1.11x\pm0.05$) and grey line shows the pre-seismic regression ($y=0.99x\pm0.03$) where x corresponds to daily mean evapotranspiration and y normalized amplitude. Both curves are forced through the origin. Uncertainty is given as standard deviation.



Supplementary Figure 6.2. Daily mean streamflow discharge (mm/h) and amplitudes of diurnal streamflow cycling (mm/h) for the period from April 17th 2008 to October 25th 2011. The red dashed line shows the time of the earthquake. The black dashed horizontal lines embrace the range of streamflow discharge as observed during the first days after the earthquake.

6.2.3. Supplementary Table

Supplementary Table 6.1. Estimated whole-catchment daily evapotranspiration (mm/day) by doing hydrology backwards, applying the approach by White and by spline interpolation.

Date	Hydrology backwards	White (1932)	Spline interpolation
20.02.2010			0.033
21.02.2010	0.076	0.034	0.036
22.02.2010	0.073	0.033	0.030
23.02.2010	0.071	0.033	0.028
24.02.2010	0.069	0.033	0.030
25.02.2010	0.069	0.034	0.017
26.02.2010	0.069	0.033	0.030
27.02.2010	-	-	
28.02.2010	0.108	-	0.047
01.03.2010	0.109	0.048	0.028
02.03.2010	0.107	0.046	0.033
03.03.2010	0.104	0.047	0.042
04.03.2010	0.101	0.048	0.045
05.03.2010	0.099	0.049	0.042
06.03.2010	0.094	0.050	0.047
07.03.2010	0.094		0.033
08.03.2010	0.092		0.031
09.03.2010	0.088		0.043
10.03.2010	0.086		0.040

Chapter VII

Summary and Conclusions

7.1. Summary and conclusions

I have studied hydrological and erosion processes associated with changing environmental conditions due to logging and an earthquake. Regarding the defined objectives (see Chapter 1.5) the main scientific outcomes can be summarized as follows.

7.1.1. Main results, implications and limitations

Chapter 2 addresses the fundamental needs to quantify the impact of exotic fast growing plantation forests on water balances in the study area.

Under the local hydro-climatic conditions, water consumption is controlled by the soil water supplies and thus more influenced by the hydro-climate than by species. Total evapotranspiration of eucalyptus plantation forests exceeded pine plantation forests despite the higher interception capacity of the latter. Nevertheless, the species differences are less distinctive than expected due to soil water supply limitation at the end of the dry season. At the same time all plantation forests show complete saturation after the rainy season regardless of the species. Hence the initial and final soil water contents are comparable and clear differences cannot show up. Under such conditions, the most prominent effect of tree species are higher evapotranspiration *rates* of eucalypts compared with pines. Hence, only under less water restricted conditions, would species differences intensify. Given the local climatic conditions, we therefore can conclude that water consumption is dictated by the hydro-climate instead of plantation forest species.

Prior to logging, the hydrological system is dominated by baseflow. Despite an eventually prominent role of event flow under saturated soil conditions, the hydrological system prior to timber harvest is clearly dominated by baseflow. Baseflow contributed about three quarters of the total flow. The baseflow is mainly fed from water stored in deep soil and saprolite layers and sustains streamflow even towards the end of the dry season. Deeper sources could not be detected. We therefore can regard the regional subsurface water resources as being unexpectedly large considering the small size and the topographical position of the catchments. However, they are not unlimited and assuming continuous afforestation, especially with eucalypts forests, they will progressively decline if no additional aquifers are accessible for the trees [Calder *et al.*, 1997]. The time series available are

relatively short and it is known that the discharge losses increase with plantation age for at least 20 years after planting [Farley *et al.*, 2005]. A (modeled) prediction of possible water shortage towards the end of the dry season remains therefore highly speculative. Assuming water shortage in the foreseeable future, the rural settlements of the study area will be particularly affected because they rely exclusively on local water supplies provided by the headwaters. Water shortage would also change the aquatic ecosystem of the streams; if there is a shift from perennial to intermittent flow regimes, as already observed following afforestation [e.g., Scott and Lesch, 1997] – even fundamentally so [Arscott *et al.*, 2010].

Chapter 3 provides novel insights into the near-surface hydrological and hydro-geomorphic response of timber harvest areas of different age. To this end, we conducted rainfall simulation experiments and linked the small-scale results to observations made at the catchment outlets.

Harvest areas are sources and sinks for runoff and erosion and may switch between both. Only when rainfall intensity exceeds surface storage capacity does connectivity of infiltration excess overland flow become established, which in turn promotes surface erosion. We identified a threshold rainfall intensity above which such connectivity is established on timber harvest areas. Under the local rainfall conditions, however, this threshold (~20 mm/h) is only exceeded in ~10% of all rainfall events (based on 30 min data). Assuming that not every rainfall event triggers overland flow, infiltration excess overland flow is the controlling overland flow mechanism in <10% of all occurring overland flow. Hence, harvest areas may indeed perform intermittently as sources for infiltration excess overland by connecting runoff paths to the drainage network. Nevertheless, for the bulk of the rainfall (>90%), overland flow (by this mechanism) remains unconnected. In this case, timber harvest areas promote ponding, groundwater recharge and sediment redistribution rather than erosion [Croke *et al.*, 1999b] (Fig. 7.1). Consequently, the bulk of the post-logging sediment flux cannot be explained by infiltration excess overland flow, exclusively. Instead, other mechanisms are required.

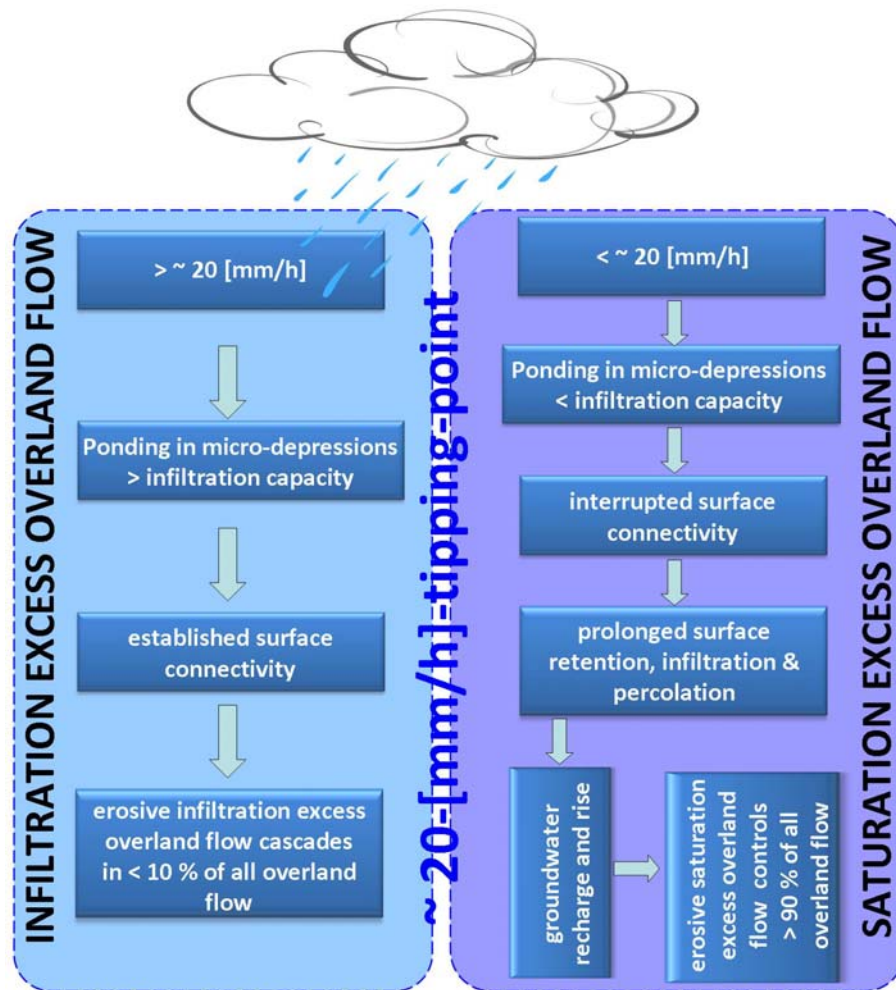


Figure 7.1: Simplified illustration of infiltration excess and saturation excess overland flow mechanisms on harvest areas. The percentage depicts relative importance/occurrence of each overland flow mechanism.

After logging, streamflow first decreases before it increases. Assuming dominant infiltration excess overland flow, streamflow discharge is not expected to diminish immediately after loggings but to increase. This disagrees with the observations made at the catchment outlet. Instead, here prolonged ponding due to missing overland flow connectivity recharges groundwater after timber harvest has disturbed the water repellent forest floor. The enhanced percolation then temporarily restricts the water available for streamflow generation. While groundwater storage is being refilled, streamflow decreases. After groundwater storage is refilled, streamflow then increases, intensified by cessation of evapotranspiration due to vegetation removal. In other words: Logging caused first a decrease in streamflow which is followed by an increase.

The sediment flux dynamics, their environmental controls and yields, and geomorphic work efficiency are analyzed in chapter 4 as a function of logging season. To this end, Quantile Regression Forests (QRF) showed up to be a robust tool to predict sediment fluxes at high temporal resolution and high accuracy under both high- and low-flow, as well as under changing environmental conditions of high impact logging.

The impact of logging on sediment transport depends on the logging season. Sediment flux intensified only after rainy season logging in which the overall increase was at the lower end of changes, compared with similar studies [e.g., Gomi *et al.*, 2005]. Dry season logging decreased sediment flux. This finding clearly supports a restriction of clear-cutting to dry seasons. Logging coincided with an increased contribution of moderate events compared with unlogged conditions. Thus immediate logging effects involve the reduction in sediment transport during peak flows while shifting hydro-geomorphic work towards less flashy, more moderate but more frequent events. This shift is more pronounced for dry-season logging. Hence, it is the seasonal timing of logging that controls the degree of shift in the frequency-magnitude relationship of sediment transport. Changes in frequency-magnitude relationships of sediment fluxes are important for flood and geomorphic hazard mitigation [e.g., Korup, 2012] and forest management practices [Istanbulluoglu *et al.*, 2004]. In other words: It is the season that clearly prescribes the impact of logging on sediment transport.

Logging may not change the runoff generation mechanism fundamentally. Predicting sediment flux is strongly controlled by antecedent low-intensity but long-lasting rainfall in both logged catchments (i.e., logged during dry or rainy seasons). Hence, both responses are consistent with saturation excess overland flow as the decisive overland flow mechanism triggering sediment fluxes – regardless of the season. However, rainy-season logging responded to shorter time periods compared to dry-season logging. This difference is consistent with higher sediment supply and relatively fast establishment of overland flow connectivity when logging is performed during rainy seasons when the soil is saturated. In this case, less water input is needed to initiate erosive overland flow. Coming back to pre-logging conditions (see chapter #2), the QRF based results thus indicate that it is the saturation excess overland flow that still controls overland flow mechanisms after logging. This finding is also in line with the outcomes of physics-based modeling.

To this day, the quantitative assessment of timber harvest impacts on water and soil resources are often still aimed at longer time periods [e.g., Walsh *et al.*, 2011]. Neglecting

“short-term” responses, however, may lead to premature conclusions. Our example clearly shows that short-term responses are important and that they may be quantified using QRF. QRF was capable of representing plausible sediment dynamics even on very high temporal resolution. In the worst case, the forestry profession may design inadequate “best management recommendations” if such short-term sediment dynamics remain unconsidered.

While the previous chapters analyzed the effect of man-made disturbances on water and sediment fluxes, chapters 5 and 6 explored streamflow responses to the Maule earthquake. The responses comprise three features: (1) Significant increase in streamflow discharge preceded by (2) an initial drop and (3) accompanied by amplified diurnal streamflow oscillations. The diurnal cycling implies interaction of earthquakes and the critical zone hydrologic processes. Hence, one can argue that both responses of the saturated zone and/or the vadose zone are plausible because both process systems may yield the same effects.

Hypothesis #1: Assuming saturated conditions, (undrained) subsurface consolidation caused the observed hydrological phenomena following the Maule earthquake. Thresholds of magnitude-distance relationships and seismic energy density, unchanged water temperature, the shallow source and a missing response to the Araucania aftershock, are consistent with subsurface consolidation of the saturated saprolite. Sandy and saturated material is prone to liquefaction – such as the saprolite during the time of the earthquake.

Assuming consolidation of the saturated zone, water from the saturated saprolite is mobilized. The mobilized water is then expected to wet the overlying vadose zone with the following three process responses:

1. The mobilized water is captured by the matric potential of the unsaturated soil. Because the saturation state is not reached, streamflow discharge is therefore temporarily disrupted, consistent with the observations.
2. After saturation, the hydraulic head rises which in turn increases streamflow and,
3. Expands the capillary fringe.

The latter provides additional water for plants’ root-water-uptake. Recorded amplified diurnal oscillations support higher post-seismic root-water-uptake. In contrast, alternative hypotheses show decisive/serious deficits.

- The topographical position and the homogeneous geology of the headwater catchments conflict with enhanced rock-specific vertical permeability which may release water from elevated areas feeding the streams at the foothills.

- The non-uniform geographical orientation of the catchments disagrees with uniform tilting of the landscape due to regional tectonic uplift or subsidence. In this case, one expects streamflow increase *or* decrease according to the catchment's orientation.
- Unchanged recession constants do not support enhanced lateral near-surface permeability. Moreover, even assuming that permeability increases across the whole catchments by an amount proportional to its pre-seismic values and we restrict the problem to subsurface flow conditions, discharge would increase proportionally to the permeability change, but subsurface water levels would fall.
- Unchanged water temperatures do not indicate involvement of deeper fluids.

Hence, assuming a response of the saturated zone, one can conclude that (undrained) consolidation is most probable. However, independent evidence, e.g. geomorphic features produced by liquefaction, is unavailable to verify this hypothesis.

Hypothesis #2: Response of vadose zone water to seismic shaking provides an alternative to explain streamflow increase and evapotranspiration increase following the Maule earthquake. We developed a model that proposes that when seismic energy density exceeds the threshold of soil water retention, unsaturated zone water (soil water) can be released into aquifers. The seismic energy density is also high enough to improve vertical connectivity by near-surface dilatancy.

Keeping the permeability unchanged (see chapter #5), we could successfully simulate diurnal streamflow oscillations and quantify evapotranspiration rates following the Maule earthquake. Based upon plausible key assumptions, i.e., (1) root-water uptake restricted to the deep rooting vegetated riparian zone and (2) all seismic energy is transformed into kinetic energy, the model showed that sufficient pore water can be released to explain the root-water uptake increase of 60% after the earthquake. Indeed, the assumption of kinetic energy only is strong.

Though the biological effect is small in this case, i.e. positive feedback effects are restricted to the first days after the earthquake, our findings suggest that under less water restricted conditions, earthquakes may indeed promote plant activity. On the other hand, assuming wetter soil conditions, water deficit stress is lower. Water deficit stress is required to trigger a significant intensification of vegetation activity when additional water is provided. Thus, the earthquake effects on root-water-uptake are limited by (1) water stress and (2) the amount of releasable pore water. Under these conditions, the window where such effects may

be important is small. Nevertheless, global tree-ring archives along active fault zones may be biased by biological footprints of earthquakes.

Hence, here we show the first evidence that hydrological responses can also occur in the vadose zone, hypothesis #2. As in the case for hypothesis #1, we cannot provide independent evidence. For example, isotopic water data, i.e. $\delta^{18}\text{O}$ -Cl-ratios could be used to distinguish between soil water and groundwater [Manga and Rowland, 2009].

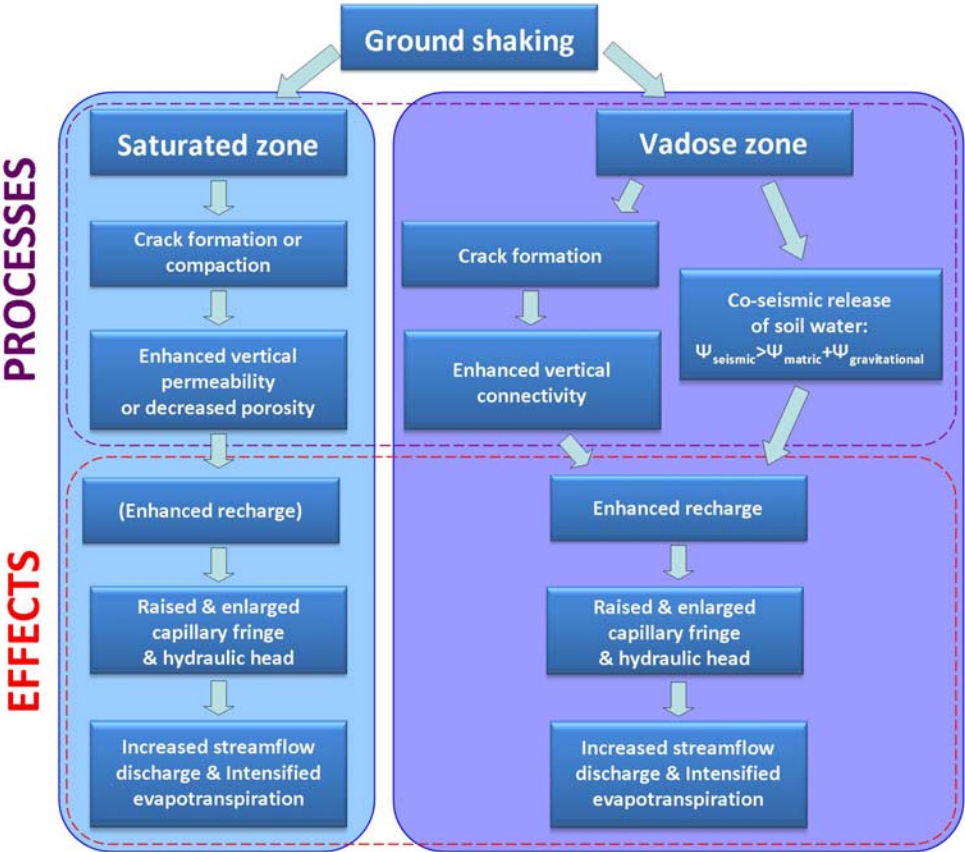


Figure 7.2: Opposing seismo-hydrological process mechanisms in saturated (hypothesis #1) and vadose zone (hypothesis #2) resulting into the same hydrological effects.

7.1.2. Synthesis

The current forest management practice is not sustainable but continuously deteriorates water and soil resources. Assuming ongoing afforestation in the current way, the regional groundwater resources are expected to be continuously depleted by the fast growing plantation forests. Clear cutting, which is conducted after the productivity of the plantation forests has declined, may help mitigate groundwater depletion, though only on short time scales. On longer time scales, starting from ~3-5 years after planting, the net effects of afforestation with pine and eucalypt on water resources are negative (e.g., [Scott and Lesch, 1997]). Considering the rotation cycles which are expected to be shortened due to increasing afforestation with *Eucalyptus globulus* replacing *Pinus radiata*, the negative net effects of plantation forestry on water resources is expected to intensify [Farley et al., 2005].

The commonly practised clear cutting should be restricted to dry summer conditions in order to minimize surface erosion as much as possible. Assessments of the implications of disturbance require the ability to benchmark the effects of disturbance against undisturbed system states [Wagener et al., 2010]. In a strict sense, such preconditions were not met: During the study period, timber roads were prepared in the presumably undisturbed control catchment and thus elevating the local sediment supply. Hence, the benchmarked erosion impacts of rainy and dry seasonal clear cutting should be considered as minimum estimates only.

Today's rotation cycles of <26 years are far too short to allow complete recovery of the initial soil's hydraulic properties. Since the control catchment has been previously logged, however, no strictly undisturbed soil hydraulic properties are available to benchmark against. Thus, the impact of and the resilience to high-impact logging on soil hydraulic properties cannot be exactly quantified.

Logging did not change the saturation-excess overland flow as the dominant runoff generation mechanism. Infiltration excess overland flow additionally contributes to surface erosion after logging – though to a minor extent. Thus, this study shows that saturation excess and infiltration excess overland flow do not conflict with each other but may occur simultaneously in timber harvest areas. Consequently, combining saturation excess and infiltration excess overland flow mechanisms along thresholds (Fig. 7.1) is potentially a good option to try to overcome some of the limitations of predictive erosion models such as WEPP

(infiltration excess) and TOPOG (saturation excess) that are widely used in managed forests [Croke and Nethery, 2006]. Available models that implement both mechanisms, e.g. Shetran [Ewen *et al.*, 2000] or InHM [VanderKwaak and Loague, 2001], are much more complex which limits their applicability for a broader scope [Bathurst, 2010]. In any case, suitable predictive models are needed for setting guidelines and standards of forest management in the next steps.

Both possible seismo-hydrological mechanisms are not verifiable with the data available. Both hypotheses are possible upon plausible assumptions and show the same effects. Hence, at this stage, an unambiguous differentiation between both mechanisms is impossible because none of the arguments supporting consolidation of the saturated zone response excludes a potential response of the vadose zone. More tricky, dilatancy and consolidation cannot occur at the same time because they differ in the sign of the pressure change. Hence, further research is needed (see below) to reveal the mechanisms in a more comprehensive and less ambiguous way. To this end, based on the presented work, I clearly suggest including vadose zone responses into earthquake hydrology to get a more sound understanding of earthquake-water interaction (Fig. 7.2). Ultimately, this challenges the conventional views of earthquake hydrology because it shows that restricting “earthquake hydrology” to groundwater exclusively may lead to a too narrow or even misleading picture of the system.

Finally, the streamflow responses to the Maule earthquake provide unique insights into coupled processes between tectonics, hydrology and soil physics. Nevertheless, their overall effects on water balance are small when compared with the hydrological effects of plantation forests or even single rainfall events (Fig. 7.3). Considering the estimated volume of excess water (i.e., the total volume of water released in excess of that expected in the absence of the earthquake) of ~10 mm, this volume is less than 1% of the water consumed by the plantation forests. Assuming wetter preconditions, i.e. saturated soil conditions and a hydrologically responsive saturated zone during the winter rainy season, this figure may be larger. However, effects of seismic shaking may eventually be more important. Considering that the recurrence intervals of Chilean high magnitude earthquakes are of the order of 80-120 years [Cisternas *et al.*, 2005a; Comte *et al.*, 1986], long-term effects on regional hydrogeological properties, i.e. repeating permeability changes and recovery as observed for the Wechuan earthquake [Xue *et al.*, 2013a], cannot be excluded.

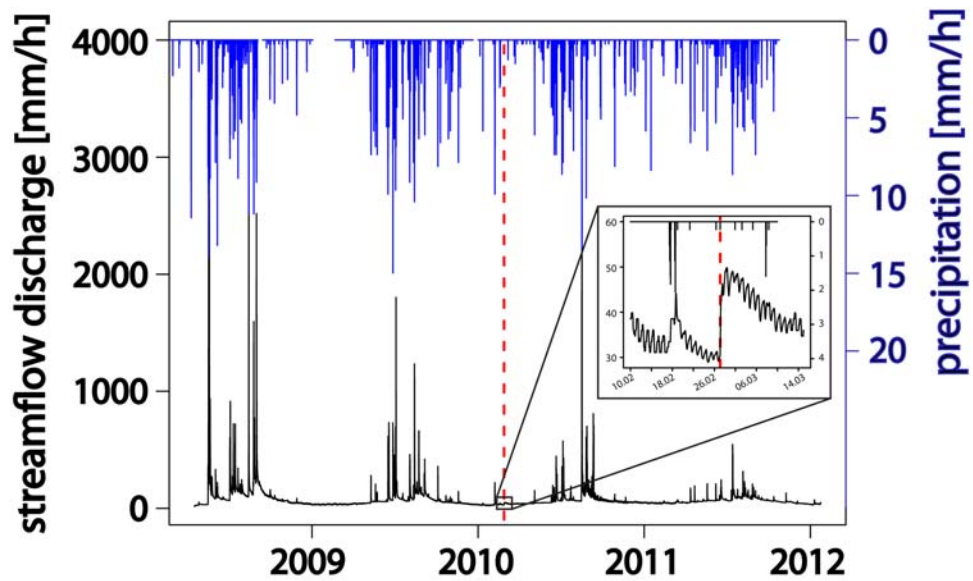


Figure 7.3: Hydrograph of Pich n grande covering the complete study period. The Maule earthquake on February 27th, 2010, is indicated by the red dashed line. The small inset show greater detail during the time of the earthquake.

7.1.3. Future work

While this thesis provided novel answers to some important questions related to forestry management and earthquake hydrology, it also raised some new questions. Based on my work, I therefore suggest the following further research:

7.1.3.1. Groundwater

A robust estimate of the groundwater volume and its dynamics is crucial. In this study, however, groundwater recharge was not quantified at a higher temporal resolution than the hydrological year. Therefore, future research about the hydrological effects of plantation forestry in the Nacimiento should include the investigation of groundwater recharge, storage, residence times and annual dynamics. This task could be tackled with drilling groundwater wells and using environmental isotopes. To this end additional information on subsurface structure would greatly contribute to a better understanding of the groundwater dynamics. Potential methods are geophysical techniques, such as GPR (ground penetrating radar) or electro-magnetic methods. This could provide a first order estimate of the total volume of

subsurface water resources, how strong they vary over the seasons and across the catchment. It may also help to answer how fast the water is transported. Further, evapotranspiration rates could be estimated at higher temporal resolution than the hydrological year. To better understand groundwater-evapotranspiration interaction, physics-based modelling could be further applied which might also provide quantitative estimates of groundwater recharge.

7.1.3.2. Hydrological and hydro-geomorphic processes

Mapping of the spatial variation of the saturated areas (in terms of hydrological response units, *HRUs*) which generate the bulk of runoff and sediment would complement the analysis of groundwater-surface interaction. When starting this study, we did not expect the runoff and erosion dynamics to be controlled so strongly by saturation excess overland flow.

Preferential flow paths that bypass low-conductive compacted soils are important for runoff generation in the studied catchments. In order to identify preferential flow paths and their importance, environmental tracers may provide valuable insights. This step would provide input for suitable predictive models, e.g. InHM [*VanderKwaak and Loague, 2001*] with a dual permeability approach.

Further, small-scale rainfall experiments during different seasons and thus under different hydro-climatic conditions could answer the question of whether runoff and erosion source-sink behaviour of timber harvest areas changes over the year. Such additional experiments should provide a more comprehensive understanding of sink-source behavior variations in space and time, even more so when combined with independent approaches such as environmental isotopes, e.g. ^{137}Cs or ^{210}Pb , as recently performed in the Nacimiento sites by *Schuller et al. [2013]*.

In this study, only erosion processes associated with overland flow are quantified. Plantations of *P. radiata* are prone to mass wasting because of their low root-strength compared with other species [*Watson et al., 1999*]. When logged, they rapidly decay in root-strength [*Sidle, 1991*]. Shallow landslides are also promoted by slow root-strength recovery rates and cumulative effects of preceding rotations [*Sidle et al., 2006*]. Given that root decay and regrowth have opposite trends over time, we expect maximum mass wasting rates 2-3 years after logging [*Watson et al., 1999*]. Hence, continuing the sediment flux monitoring could answer the question about the importance of less frequent but higher magnitude landsliding vs. “baseline” overland flow driven sediment fluxes in logged (disturbed) and

forested (undisturbed) areas. It would also provide the option to quantify recovery rates of sediment fluxes following clear-cutting.

7.1.3.3. Ecohydrology

More information about the hydro-ecological and micro-climatological impacts of plantation forestry in Chile would greatly improve our knowledge, leading to a more comprehensive ecologically oriented impact assessment of the current timber harvest practice. On the one hand, we expect that afforestation may increase summer water temperatures significantly because the lesser volume makes the stream water more responsive to energy available from global radiation and air temperature. On the other hand, the loss of shading after logging should increase water temperature because of the increased insolation reaching the water bodies. Further, increased nutrient flux is commonly associated with logging [Swank *et al.*, 2001]. We thus expect increasing nutrient export from the headwaters into the BíoBío River after logging. To this end, analyzing water temperature changes and nutrient fluxes associated with timber harvest and afforestation in the headwaters and the receiving BíoBío River would also be valuable. By extending this investigation to the receiving BíoBío River drainage, off site effects could be also assessed.

7.1.3.4. Earthquake hydrology

Earthquake hydrology remains in its infancy though significant progress has been achieved in the last decade. This is mainly due to the spatially and temporally limited responses to earthquakes. The study presented here showed evidence that both the vadose and saturated zone *may* respond to earthquake. To elucidate the underlying processes, a coupled approach of modelling efforts and experimental testing is promising.

An important step is to identify the source of the excess water. To this end, the developed model can be easily extended to test potential source areas close to the creek (riparian zone?) or at a distance from the creek by implementing spatially “distributed” responsive areas. The model can also be used to test possible effects of near-surface dilatancy by implementing a storage that dynamically changes over time, i.e. increasing the storage immediately after the earthquake for a short period of time.

However, the model may not answer all remaining questions because fundamental physical knowledge about how material responds to seismic stress is still limited. Hence, the proposed processes need to be tested in an experimental way. A fundamental step should

comprise an experimental setup to investigate in a quantitative way how material of different saturation state either tends to expand (dilatate) or compact when exposed to cyclic shaking of various amplitudes and frequencies. Following the same approach, the possible release of pore water may be verified by exposing unconsolidated material of various states of soil water contents to artificial shaking. To this end instrumented plots with soil moisture and piezometric loggers may be first irrigated and later exposed to artificially shaking, e.g. triggered explosions. In any case, future catchment experiments conducted in tectonically active regions should be equipped with piezometric and soil moisture loggers to verify possible vadose zone response.

Finally, inter-catchment comparisons may help address remaining questions about geological, topographical, tectonic, and scale controls that may mitigate or amplify hydrological responses to earthquakes. To this end, available data from geologically and topographically contrasting catchments of the Andes may be used to simulate streamflow responses by applying the model described. This approach may also be used to identify scaling controls on streamflow responses, i.e. is the initial drop only observable in smaller catchments while they are blurred in larger basins? And in that case, why?

Comparing hydrological and hydro-geomorphic responses to different earthquakes, such as the Maule Earthquake (thrust faulting, [Moreno *et al.*, 2010]) Chi-Chi earthquake (thrust faulting, [Wu *et al.*, 2008]), New Zealand (strike-slip faulting, [Gledhill *et al.*, 2011]) and the Loma Prieta earthquake, California, (strike-slip and thrust combination, [Kanamori and Satake, 1990]) may help to elucidate possible focal mechanism controls.

Last but not least, a more comprehensive impact assessment should be part of further research. Though the findings presented in this study suggest only small earthquake effects on the regional water balance, this is not necessarily the case for sediment budgets. We don't know. For example, *Hovius et al.* [in prep.] highlights the importance of seismic events on sediment budgets on global scale whereas this study did not show any enhancement of sediment fluxes following the earthquake. This does not necessarily mean, however, that intensified sediment fluxes due to the earthquake will not occur. Considering the root decay of the plantation forests, enhanced sediment fluxes are indeed expected for the near future. The task will then be to distinct between the earthquake and logging related signals. Ultimately, such analysis could also answer questions on whether landscape and thus ecological habitats along tectonically active margins are "biased" by earthquakes on longer time scales, i.e. 10^2 - 10^3 years. At least the intensified vegetation activity following the Maule earthquakes permit the conclusion that earthquakes may have biological effects under certain circumstances. To

this end, I also suggest a re-examination of biological Paleoclimate proxies such as tree ring records. It would not be the first bias to be found in the records due to infrequent natural disturbances: Recent studies showed systematic disturbed paleoclimatic tree ring archives due to volcanic eruptions [*D'Arrigo et al.*, 2013; *Mann et al.*, 2013].

7.1.4. Final remarks

Although, I present this work and the results as my work, I have to acknowledge the contributions of my co-authors. Without their contribution, this work would not have been possible.

Chapter VIII

Bibliography

- Alila, Y., R. Hudson, P.K. Kuras, M. Schnorbus, and K. Rasouli (2010), Reply to comment by Jack Lewis et al. on "Forests and floods: A new paradigm sheds light on age-old controversies", *Water Resour. Res.*, 46 (5), W05802.
- Alila, Y., P.K. Kuras, M. Schnorbus, and R. Hudson (2009), Forests and floods: A new paradigm sheds light on age-old controversies, *Water Resour. Res.*, 45 (8), W08416.
- Anderson, R.S., and S.P. Anderson (2010), *Geomorphology: The Mechanics and Chemistry of Landscapes*, Cambridge University Press.
- Andreassian, V., M. Perrin, and C. Michel (2004), Impact of imperfect potential evapotranspiration knowledge on the efficiency and parameters of watershed models, *J. Hydrol.*, 286, 19-35.
- Ansejo Santana, D. A. (2011), Transporte de sedimentos en la cuenca experimental Pichón, Región del Biobío, Chile, M.S. thesis, Fac. Sci. Forestales, Uni. Austral de Chile, Valdivia, Chile.
- Armesto, J., D. Manuschevich, C. Mora, R. Smith-Ramirez, A. Rozzi, A.M. Abarzua, and P. Marquet (2010), From the Holocene to the Anthropocene: a historical framework for land cover change in southwestern South America in the past 15.000 years, *Land Use Policy*, 27 (148-160).
- Arscott, D.B., S. Larned, M.R. Scarsbrook, and P. Lambert (2010), Aquatic invertebrate community structure along an intermittence gradient: Selwyn River, New Zealand, *J. North Am. Benthol. Soc.*, 29 (2), 530-545.
- Asselman, N.E.M.(2010), Fitting and interpretation of sediment rating curves, *J. Hydrol.*, 234, 228-248, doi: 10.1016/S0022-1694(00)00253-5.
- Attiwill, P.M. (1994), The disturbance of forest ecosystems - the ecological basis for conservative management, *For. Eco. Manag.*, 63 (2-3), 247-300.
- Baird, K.J., and T. Maddock (2005), Simulating riparian evapotranspiration: A new methodology and application for groundwater models, *J. Hydrol.*, 312 (1-4), 176-190.
- Bardossy, A. and F. Schmidt (2002): GIS approach to scale issues of perimeter-based shape indices for drainage basins, *Hydro. Sci. J.*, 47 (6), 931-941.
- Bathurst, J. (2013), Chilean hydrology, *Circulation - The newsletter of the British hydrological society*, 118, 2-5.
- Bathurst, J.C., S.J. Birkinshaw, F. Cisneros, J. Fallas, A. Iroumé, R. Iturraspe, M. Gavino Novillo, A. Urciuolo, A. Alvarado, C. Coello, A. Huber, M. Miranda, M. Ramirez, and R. Sarandon (2011a), Forest impact on floods due to extreme rainfall and

- snowmelt in four Latin American environments 2: Model analysis, *J. Hydrol.*, 400 (3-4), 292-304.
- Bathurst, J.C., A. Iroumé, F. Cisneros, J. Fallas, R. Iturraspe, M.G. Novillo, A. Urciuolo, B. de Bievre, V.G. Borges, C. Coello, P. Cisneros, J. Gayoso, M. Miranda, and M. Ramirez, (2011b) Forest impact on floods due to extreme rainfall and snowmelt in four Latin American environments 1: Field data analysis, *J. Hydrol.*, 400 (3-4), 281-291.
- Bathurst, J.C. (2010), Predicting Impacts of Land Use and Climate Change on Erosion and Sediment Yield in River Basins Using SHETRAN, in *Handbook of Erosion Modelling*, pp. 263-288, John Wiley & Sons, Ltd.
- Bathurst, J.C., J. Amezaga, F. Cisneros, M.G. Novillo, A. Iroumé, M.A. Lenzi, J.M. Aguirre, M. Miranda, and A. Urciuolo (2010), Forests and floods in Latin America: Science, management, policy and the EPIC FORCE project, *Water Int.*, 35 (2), 114-131.
- Benavides-Solorio, J. and L. H. MacDonald (2001), Post-fire runoff and erosion from simulated rainfall on small plots, Colorado Front Range, *Hydrol. Processes*, 15, 2931-2952, doi:10.1002/hyp.383.
- Beresnev, I.A., and P.A. Johnson (1994), Elastic-wave stimulation of oil production - A review of methods and results, *Geophysics*, 59 (6), 1000-1017.
- Beschta, R.L., M.R. Pyles, A.E. Skaugset, and C.G. Surfleet (2000), Peakflow responses to forest practices in the western cascades of Oregon, USA, *J. Hydrol.*, 233 (1-4), 102-120.
- Beschta, R.L. (1978), Long-Term Patterns of Sediment Production Following Road Construction and Logging in the Oregon Coast Range, *Water Resour. Res.*, 14 (6), 1011-1016.
- Beven, K. and P. Germann (1982), Macropores and water-flow in soils, *Water Resour. Res.*, 18, 1311-1325, doi:10.1029/WR018i005p01311.
- Birkinshaw, S.J., J.C. Bathurst, A. Iroumé, and H. Palacios (2011), The effect of forest cover on peak flow and sediment discharge-an integrated field and modelling study in central-southern Chile, *Hydrol. Processes*, 25 (8), 1284-1297.
- Blume, T., Zehe, E., Reusser, D. E., Iroumé, A. and A. Bronstert (2008), Investigation of runoff generation in a pristine, poorly gauged catchment in the Chilean Andes I: A multi-method experimental study, *Hydrol. Processes*, 22, 3661-3675, doi:10.1002/hyp.6971.

- Blume, T., E. Zehe, and A. Bronstert (2007), Rainfall-runoff response, event-based runoff coefficients and hydrograph separation, *Hydro. Sci. J.*, 52 (5), 843-862.
- Bookhagen, B., H.P. Echtler, D. Melnick, M.R. Strecker, and J.Q.G. Spencer (2006), Using uplifted Holocene beach berms for paleoseismic analysis on the Santa Maria Island, south-central Chile, *Geophys. Res. Lett.*, 33 (15).
- Bonan, G.B. (2008), Forests and Climate Change: Forcings, Feedbacks, and the Climate Benefits of Forests, 10.1126/science.1155121 *Science* 320 (5882), 1444-1449.
- Boothroyd, I., J. Quinn, E. Langer, K. Costley, and G. Steward (2004), Riparian buffers mitigate effects of pine plantation logging on New Zealand streams. 1. Riparian vegetation structure, stream geomorphology and periphyton, *For. Eco. Manag.*, 194, 199-213.
- Bosch, J.M., and J.D. Hewlett (1982), A review of catchment experiments to determine the effect of vegetation changes on water yield and evapotranspiration, *J. Hydrol.*, 55 (1-4), 3-23.
- Bowyer-Bower, T. A. S. and T. P. Burt (1989), Rainfall simulators for investigating soil response to rainfall, *Soil Technol.*, 2, 1-16.
- Breiman, L. (2001), Random forests, *Machine Learning*, 45, 5-32, doi:10.1023/A:1010933404324.
- Brenner, J. (2011), Modellierung des Sedimenttransports in einem forstwirtschaftlich genutzten, gerodeten Mikro Einzugsgebiet im südlichen Zentralchile, B.Sc. thesis, Inst. Earth. Environ. Sci., Uni. of Potsdam, Potsdam, Germany.
- Briggs, R.O. (1991), Effects of Loma Prieta earthquake on surface waters in Waddell Valley, *Water Resour. Bull.*, 27 (6), 991-999.
- Brodsky, E.E., E. Roeloffs, D. Woodcock, I. Gall, and M. Manga (2003), A mechanism for sustained groundwater pressure changes induced by distant earthquakes, *J. Geophys. Res.- Solid Earth*, 108 (B8), 2390, doi:10.1029/2002JB002321.
- Bronstert, A. and E. J. Plate (1997), Modelling of runoff generation and soil moisture dynamics for hillslopes and micro-catchments, *J. Hydrol.*, 198, 177-195, doi:10.1016/S0022-1694(96)03306-9.
- Bronstert, A., D. Kneis, and H. Bogena (2009), Interactions and feedbacks in hydrological change: Relevance and possibilities of modelling, *Hydrol. Wasserbewirt.*, 53 (5), 289-304.

- Brooks, S. M., Richards, K. S. and R. Nussbaum (1994), Simulator experiments of the varied consequences of rain forest logging for runoff and erosion., *Geogr. Ann. A., Phys. Geogr.*, 76, 143-152, doi: 10.2307/521033
- Brown, A.E., L. Zhang, T.A. McMahon, A.W. Western, and R.A. Vertessy (2005), A review of paired catchment studies for determining changes in water yield resulting from alterations in vegetation, *J. Hydrol.*, 310 (1-4), 28-61.
- Brown, G.W., and J.T. Krygier (1971), Clear-Cut Logging and Sediment Production in Oregon Coast Range, *Water Resour. Res.*, 7 (5).
- Burt, T. P., Donohoe, M. A. and A. R. Vann (1983), The effect of forestry drainage operations on upland sediment yields - the results of a storm-based study, *Earth Surf. Processes Landforms*, 8, 339-346, doi:10.1002/esp.3290080406.
- Calder, I. (1992), The hydrological impact of land-use change, in *Priorities for Water Resources Allocation and Management*, Natural Resources and Engineer Advisers Conference, Southampton.
- Calder, I.R., P.T.W. Rosier, K.T. Prasanna, and S. Parameswarappa (1997), Eucalyptus water use greater than rainfall input-a possible explanation from southern India, *Hydrol. Earth Sys. Sci. Sciences*, 1 (2), 249-255.
- Cammeraat, L.H. (2002), A review of two strongly contrasting geomorphological systems within the context of scale, *Earth Surf. Processes Landforms*, 27 (11), 1201-1222.
- Cammeraat, L. H. (1993), *MEDALUS Field Manual*, University of Bristol, Bristol.
- Cannon, S.H., R.M. Kirkham, and M. Parise (2001), Wildfire-related debris-flow initiation processes, Storm King Mountain, Colorado, *Geomorphology*, 39 (3-4), 171-188.
- Cao, Y., Z.Y. Ouyang, H. Zheng, Z.G. Huang, X.K. Wang, and H. Miao (2008), Effects of forest plantations on rainfall redistribution and erosion in the red soil region of southern China, *Land Degrad. Develop.*, 19 (3), 321-330.
- Carlyle-Moses, D.E. (2004), Throughfall, stemflow, and canopy interception loss fluxes in a semi-arid Sierra Madre Oriental matorral community, *J. Arid. Env.*, 58 (181-202).
- Carr, A., and K. Loague (2011), Physics-based simulations of the impacts forest management practices have on hydrological response, in *The Coast Redwoods in a changing California*, edited by R.B. Standiford, T.J. Weller, D.D. Piirto, and J.D. Stuart, pp. 41-51, USDA, Forest Service, Santa Cruz.
- Carrigan, C.R., G.C.P. King, G.E. Barr, and N.E. Bixler (1991), Potential for water-table excursions induced by seismic events at Yucca Mountain, Nevada, *Geology*, 19 (12), 1157-1160.

- Carroll, C., L. Merton, and P. Burger (2000), Impact of vegetative cover and slope on runoff, erosion, and water quality for field plots on a range of soil and spoil materials on central Queensland coal mines, *Aus. J. Soil Res.*, 38 (2), 313-327.
- Cerdà, A. (1997), Seasonal changes of the infiltration rates in a Mediterranean scrubland on limestone. *J. Hydrol.* 198, 209-225, doi: 10.1016/S0022-1694(96)03295-7.
- Cerdà, A. (1998), Effect of climate on surface flow along a climatological gradient in Israel: A field rainfall simulation approach. *J. Arid Environ.* 38, 145-159, doi: 10.1006/jare.1997.0342.
- Cerdà, A. and S. H. Doerr, S. H. (2005), Influence of vegetation recovery on soil hydrology and erodibility following fire: an 11-year investigation. *Int. J. of Wildland Fire* 14, 423-437, doi: 10.1071/WF05044.
- Chang, M. (2006), *Forest Hydrology. An Introduction to Water and Forests*, 474 pp., CRC Press Taylor & Francis.
- Chappell, N.A., I. Douglas, J.M. Hanapi, and W. Tych (2004), Sources of suspended sediment within a tropical catchment recovering from selective logging, *Hydrol. Processes*, 18 (4), 685-701.
- Charmoille, A., O. Fabbri, J. Mudry, Y. Guglielmi, and C. Bertrand (2005), Post-seismic permeability change in a shallow fractured aquifer following a M-L 5.1 earthquake (Fourbanne karst aquifer, Jura outermost thrust unit, eastern France), *Geophys. Res. Lett.*, 32 (18), L18406, doi:10.1029/2005GL023859.
- Chen, J.S., and C.Y. Wang (2009), Rising springs along the Silk Road, *Geology*, 37 (3), 243-246.
- Cisternas, M., B.F. Atwater, F. Torrejon, Y. Sawai, G. Machuca, M. Lagos, A. Eipert, C. Youlton, I. Salgado, T. Kamataki, M. Shishikura, C.P. Rajendran, J.K. Malik, Y. Rizal, and M. Husni (2005), Predecessors of the giant 1960 Chile earthquake, *Nature*, 437 (7057), 404-407.
- Clarke, M. A. and R. P. D. Walsh (2006), Long-term erosion and surface roughness change of rain-forest terrain following selective logging, Danum Valley, Sabah, Malaysia, *Catena*, 68, 109-123, doi:10.1016/j.catena.2006.04.002.
- Comte, D., A. Eisenberg, E. Lorca, M. Pardo, L. Ponce, R. Saragoni, S.K. Singh, and G. Suarez (1986), The 1985 Central Chile Earthquake - A repeat of previous great earthquakes in the region, *Science*, 233 (4762), 449-453.
- CONAMA, *Metodologías para la caracterización de la calidad ambiental*, 242 pp., Santiago de Chile, 1996.

- Coppus, R. (2002), Landscape sensitivity to erosion in three semi-arid central Andean Geo-Ecosystems, Doctoral thesis, Inst. Biodiversity Ecosys. Dyn., Uni. of Amsterdam, Amsterdam, Netherlands.
- Coppus, R. and A. C. Imeson (2002), Extreme events controlling sediment transport in a semi-arid sub-andean valley, *Earth Surf. Processes Landforms*, 27, 1365-1375, doi: 10.1002/esp.435
- Cornish, P.M. (1993), The effects of logging and forest regeneration on water yields in a moist eucalypt forest in New-South-Wales, Australia, *J. Hydrol.*, 150 (2-4), 301-322.
- Crawley, M.J. (2005), *Statistics - An introduction using R*, 327 pp., Wiley, Chichester.
- Crockford, R.H., and D.P. Richardson (1990), Partitioning of Rainfall in a Eucalypt Forest and Pine Plantation in Southeastern Australia .4. The Relationship of Interception and Canopy Storage Capacity, the Interception of These Forests, and the Effect on Interception of Thinning the Pine Plantation, *Hydrol. Processes*, 4 (2), 169-188.
- Crockford, R.H., and D.P. Richardson (2000), Partitioning of rainfall into throughfall, stemflow and interception: effect of forest type, ground cover and climate, *Hydrol. Processes*, 14 (16-17), 2903-2920.
- Croke, J.C., and P.B. Hairsine (2006), Sediment delivery in managed forests: a review, *Env. Rev.*, 14 (1), 59-87.
- Croke, J., and M. Nethery (2006), Modelling runoff and soil erosion in logged forests: Scope and application of some existing models, *Catena*, 67 (1), 35-49.
- Croke, J., Hairsine, P. and P. Fogarty (2001), Soil recovery from track construction and harvesting changes in surface infiltration, erosion and delivery rates with time, *For. Ecol. Manage.*, 143, 3-12, doi:10.1016/S0378-1127(00)00500-4.
- Croke, J., Hairsine, P. and P. Fogarty (1999a), Runoff generation and re-distribution in logged eucalyptus forests, south-eastern Australia, *J. Hydrol.*, 216, 56-77, doi:10.1016/S0022-1694(98)00288-1.
- Croke, J., Hairsine, P. and P. Fogarty (1999b), Sediment transport, redistribution and storage on logged forest hillslopes in south-eastern Australia, *Hydrol. Processes*, 13, 2705-2720, doi:10.1002/(SICI)1099-1085(19991215)13:17<2705::AID-HYP843>3.0.CO;2-Y.
- Croke, J., Mockler, S., Hairsine, P. and P. Fogarty (2006), Relative contributions of runoff and sediment from sources within a road prism and implications for total sediment delivery, *Earth Surf. Processes Landforms*, 31, 457-468, doi:10.1002/esp.1279.

- Dadson, S.J., N. Hovius, H. Chen, W.B. Dade, M.-L. Hsieh, S.D. Willett, J.-C. Hu, M.-J. Horng, M.-C. Chen, C.P. Stark, D. Lague, and J.-C. Lin (2003), Links between erosion, runoff variability and seismicity in the Taiwan orogen, *Nature*, 426 (6967), 648-651.
- D'Arrigo, R., R. Wilson, and K.J. Anchukaitis (2013), Volcanic cooling signal in tree ring temperature records for the past millennium, *J. Geophys. Res.- Atmospheres*, n/a.
- Davidson, E.A., A.C. de Araujo, P. Artaxo, J.K. Balch, I.F. Brown, M.M. C. Bustamante, M.T. Coe, R.S. DeFries, M. Keller, M. Longo, J.W. Munger, W. Schroeder, B.S. Soares-Filho, C.M. Souza, and S.C. Wofsy (2012), The Amazon basin in transition, *Science*, 481 (7381), 321-328.
- Deguchi, A., S. Hattori, and H.T. Park (2006), The influence of seasonal changes in canopy structure on interception loss: Application of the revised Gash model, *J. Hydrol.*, 318 (1-4), 80-102.
- Deichmann, N., and D. Giardini (2009), Earthquakes Induced by the Stimulation of an Enhanced Geothermal System below Basel (Switzerland), *Seismol. Res. Let.*, 80 (5), 784-798.
- de Gruijter, J. J., Brus, D. J., Bierkens, M. F. P. and M. Knotters (2006), Sampling for natural resource monitoring, 323 pp, Springer, Berlin, Heidelberg, New York.
- Dingman, S., L. (2002), *Physical Hydrology*, 600 pp., Prentice Hall, Upper Saddle River, N.J.
- Doerr, S. H., Shakesby, R. A. and R. P. D. Walsh (2000), Soil water repellency: Its causes, characteristics and hydro-geomorphological significance, *Earth-Sci. Rev.*, 51, 33-65, doi:10.1016/S0012-8252(00)00011-8.
- Douglas, I., T. Spencer, T. Greer, K. Bidin, W. Sinun, and W.W. Meng (1992), The Impact of Selective Commercial Logging on Stream Hydrology, Chemistry and Sediment Loads in the Ulu Segama Rain-Forest, Sabah, Malaysia, *Phil. Trans. Royal Soc. London – Biol. Sci.*, 335 (1275), 397-406.
- Dung, B.X., T. Gomi, S. Miyata, R.C. Sidle, K. Kosugi, and Y. Onda (2012), Runoff responses to forest thinning at plot and catchment scales in a headwater catchment draining Japanese cypress forest, *J. Hydrol.*, 444, 51-62.
- Dunne, T., Zhang, W. H. and B. F. Aubry (1991), Effects of Rainfall, Vegetation, and Microtopography on Infiltration and Runoff, *Water Resour. Res.*, 27, 2271-2285, doi:10.1029/91WR01585.
- Dunne, T., and Black, R.D. (1970), An Experimental investigation of runoff production in permeable soils, *Water Resour. Res.*, 6, 478-490, doi: 10.1029/WR006i002p00478.

- Dyck, S. and G. Peschke (1995), *Grundlagen der Hydrologie*, 532 pp., Verlag für Bauwesen, Berlin.
- Dye, P. (2013), A review of changing perspectives on Eucalyptus water-use in South Africa, *For. Eco. Manag.*, 301, 51-57.
- Ebel, B.A., K. Loague, D.R. Montgomery, and W.E. Dietrich (2008), Physics-based continuous simulation of long-term near-surface hydrologic response for the Coos Bay experimental catchment, *Water Resour. Res.*, 44 (7), W07417, doi:10.1029/2007WR006442.
- Elkhoury, J.E., E.E. Brodsky, and D.C. Agnew (2006), Seismic waves increase permeability, *Nature*, 441 (7097), 1135-1138, doi:10.1038/nature04798.
- Ewen, J., G. Parkin, and P.E. O'Connell (2000), Shetran: Distributed River Basin Flow and Transport Modeling System, *J. Hydrol. Eng.*, 5 (3), 250-258.
- FAO (2006), *Global Forest Assessment 2005*, in FAO Forestry Paper, pp. 320, Food and Agriculture Organization of the United Nations., Rome.
- FAO (2010), *Global Forest Resources Assessment 2010*, in FAO Forestry Paper, pp. 340, Food and Agriculture Organization of the United Nations., Rome.
- Fahey, B. (1994), The effect of plantation forestry on water yield in New Zealand, *New Zealand Forestry*, 39 (3), 18-23.
- Farley, K.A., E.G. Jobbagy, and R.B. Jackson (2005), Effects of afforestation on water yield: a global synthesis with implications for policy, *Global Change Biology*, 11 (10), 1565-1576.
- Faul, F. (2011), Einfluss von forstwirtschaftlichen Aktivitäten auf den Sedimenttransport in zwei Kleinzugsgebieten bei Nacimiento, Südchile, B.Sc. thesis, Inst. Earth Environ. Sci., Uni. of Potsdam, Potsdam, Germany.
- Fleischbein, K., W. Wilcke, R. Goller, J. Boy, C. Valarezo, W. Zech, and K. Knoblich (2005), Rainfall interception in a lower montane forest in Ecuador: effects of canopy properties, *Hydrol. Processes*, 19 (7), 1355-1371.
- Foley, J.A., R. DeFries, G.P. Asner, C. Barford, G. Bonan, S.R. Carpenter, F.S. Chapin, M.T. Coe, G.C. Daily, H.K. Gibbs, J.H. Helkowski, T. Holloway, E.A. Howard, C.J. Kucharik, C. Monfreda, J.A. Patz, I.C. Prentice, N. Ramankutty, and P.K. Snyder (2005), Global consequences of land use, *Science*, 309 (5734), 570-574.
- Francke, T., López-Tarazón, J. A. and B. Schroder (2008), Estimation of suspended sediment concentration and yield using linear models, random forests and quantile regression forests, *Hydrol. Processes*, 22, 4892-4904, doi:10.1002/hyp.7110.

- Francke, T., J.A. Lopez-Tarazon, D. Vericat, A. Bronstert, and Batalla, R.J. (2008b) Flood-based analysis of high-magnitude sediment transport using a non-parametric method, *Earth Surf. Processes Landforms*, 33, 2064-2077, doi: 10.1002/esp.1654.
- Freeze, R.A., and J.A. Cherry (1979), *Groundwater*, 604 pp., Prentice-Hall, Englewood Cliffs, N. J.
- Fuenzalida, H. (1971), *Climatología de Chile*, in *Corporación de Fomento de la Producción*, edited by G.E.d. Chile, pp. 99-152, Santiago de Chile.
- Gaybullaev, B., S.C. Chen, and Y.M. Kuo (2012), Large-scale desiccation of the Aral Sea due to over-exploitation after 1960, *J. Mount. Sci.*, 9 (4), 538-546.
- Gayoso, J., and A. Iroumé (1991), Compaction and soil disturbances from logging in southern Chile, *Ann. Sci. For.*, 48, 63-71, doi:10.1051/forest:19910105.
- Gerrits, A.M.J., H.H.G. Savenije, L. Hoffmann, and L. Pfister (2007), New technique to measure forest floor interception - an application in a beech forest in Luxembourg, *Hydrol. Earth Sys. Sci. Sciences*, 11 (2), 695-701.
- Gläser, C. (2009), *Analyse und Modellierung des Wasserhaushalts eines forstwirtschaftlich genutzten Einzugsgebietes in S dchile*, Diploma thesis, Technical University of Braunschweig, Braunschweig.
- Gledhill, K., J. Ristau, M. Reyners, B. Fry, and C. Holden (2011), The Darfield (Canterbury, New Zealand) M-w 7.1 Earthquake of September 2010: A Preliminary Seismological Report, *Seismol. Res. Let.*, 82 (3), 378-386.
- Gomi, T., R.D. Moore, and M.A. Hassan (2005), Suspended sediment dynamics in small forest streams of the Pacific Northwest, *J. Am. Wat. Res. Assoc.*, 41 (4), 877-898.
- Gomi, T., R.C. Sidle, and D.N. Swanston (2004), Hydrogeomorphic linkages of sediment transport in headwater streams, Maybeso Experimental Forest, southeast Alaska, *Hydrol. Processes*, 18 (4), 667-683.
- Gran, K.B., and D.R. Montgomery (2005), Spatial and temporal patterns in fluvial recovery following volcanic eruptions: Channel response to basin-wide sediment loading at Mount Pinatubo, Philippines, *Geol. Soc. Am. Bull.*, 117 (1-2), 195-211.
- Grant, G.E., and A.L. Wolff (1991), Long-term patterns of sediment transport after timber harvest, Western Cascade Mountains, Oregon, USA, in *Sediment and Stream Water Quality in a Changing Environment : Trends and Explanation*, pp. 31-40.
- Green, K.C., and Y. Alila (2012), A paradigm shift in understanding and quantifying the effects of forest harvesting on floods in snow environments, *Water Resour. Res.*, 48 (10), W10503.

- Green, R. N., Trowbridge, R. L. and K. Klinka (1993), Towards a taxonomic classification of humus forms, *For. Serv.. Monogr*, 29, 1-48.
- Gribovszki, Z., J. Szilágyi, and P. Kalicz (2010), Diurnal fluctuations in shallow groundwater levels and streamflow rates and their interpretation - A review, *J. Hydrol.*, 385 (1-4), 371-383, doi:10.1016/j.jhydrol.2010.02.001.
- Guntner, A., and A. Bronstert (2004), Representation of landscape variability and lateral redistribution processes for large-scale hydrological modelling in semi-arid areas, *J. Hydrol.*, 297 (1-4), 136-161.
- Hassan, M.A., M. Church, T.E. Lisle, F. Brardinoni, L. Benda, and G.E. Grant (2005), Sediment transport and channel morphology of small forested streams, *J. Am. Wat. Res. Assoc.*, 41 (853-876).
- Hassler, S. K., Zimmermann, B., van Breugel, M., Hall, J. S. and H. Elsenbeer (2011), Recovery of saturated hydraulic conductivity under secondary succession on former pasture in the humid tropics, *For. Ecol. Manage.*, 261, 1634-1642, doi:10.1016/j.foreco.2010.06.031.
- Hattermann, F.F., V. Krysanova, A. Habeck, and A. Bronstert (2006), Integrating wetlands and riparian zones in river basin modelling, *Ecol. Modell.*, 199 (4), 379-392.
- Henry, N. (1998), Overview of the Caspar Creek Watershed Study, in *Conference on coastal watersheds: the Casper Creek story.*, edited by R.R. Ziemer, pp. 1-9, U.S. Department of Agriculture, Forest Service, Pacific Southwest Research Station, Ukiah.
- Herrick, J. E., Whitford, W. G., de Soyza, A. G., Van Zee, J. W., Havstad, K. M., Seybold, C. A. and M. Walton (2001), Field soil aggregate stability kit for soil quality and rangeland health evaluations, *Catena*, 44, 27-35, doi:10.1016/S0341-8162(00)00173-9.
- Hillel, D. (2003), *Introduction to Environmental Soil Physics*, Academic Press, Burlington, MA, USA.
- Hofstede, R. G. M., Groenendijk, J. P., Coppus, R., Fehse, J. C. and J. Sevink (2002), Impact of pine plantations on soils and vegetation in the Ecuadorian High Andes, *Mt. Res. Dev.*, 22, 159-167, doi:10.1659/0276-4741(2002)022[0159:IOPPOS]2.0.CO;2.
- Holder, C.D. (2004), Rainfall interception and fog precipitation in a tropical montane cloud forest of Guatemala, *For. Eco. Manag.*, 190 (2-3), 373-384.
- Hovius, N., P. Meunier, C.-W. Lin, H. Chen, Y.-G. Chen, S. Dadson, M.-J. Horng, Lines, M.(2011), Prolonged seismically induced erosion and the mass balance of a large earthquake, *Earth Planet. Sci. Lett.*, 304, 347-355, doi: 10.1016/j.epsl.2011.02.005.

- Huang, J., Lacey, S. T. and P. J. Ryan (1996), Impact of forest harvesting on the hydraulic properties of surface soil, *Soil Sci.*, 161, 79-86, doi:10.1097/00010694-199602000-00001.
- Hubbart, J., T. Link, J. Gravelle, and W. Elliot (2007), Timber harvest impacts on water yield in the Continental/Maritime Hydroclimatic Region of the United States, *For. Sci.*, 53 (2), 169-180.
- Huber, A., and G. Garcia (1999), Importancia de los factores meteorológicos en la transpiración potencial de *Pinus radiata*, *Pyton*, 65, 143-152.
- Huber, A., and A. Iroumé (2001), Variability of annual rainfall partitioning for different sites and forest covers in Chile, *J. Hydrol.*, 248 (1-4), 78-92.
- Huber, A., and C. Oyarzun (1984), Factores reguladores de la intercepción en un bosque adulto de *Pinus radiata* D. Don, *Bosque*, 6 (2), 74-82.
- Huber, A., and C.E. Oyarzun (1983), Precipitación neta e intercepción en un bosque adulto de *Pinus radiata* (D. Don), *Bosque*, 5 (1), 13-21.
- Huber, A., and R. Trecaman (2004), Eficiencia del uso del agua en plantaciones de *Pinus radiata* en Chile, *Bosque*, 25 (3), 33-43.
- Huber, A., and R. Trecaman (2002), Efecto de la variabilidad interanual de las precipitaciones sobre el desarrollo de las plantaciones de *Pinus radiata* (D. Don) en la zona de los arenales, VIII Región, Chile, *Bosque*, 23 (2), 43-49.
- Huber, A., A. Iroumé, and J. Bathurst (2008), Effect of *Pinus radiata* plantations on water balance in Chile, *Hydrol. Processes*, 22 (1), 142-148.
- Huber, A., P. Barriga, and R. Trecaman (1998), Efecto de la densidad de plantaciones de *Eucalyptus nitens* sobre el balance hídrico en la zona de Collipulli, IX Región, Chile, *Bosque*, 19 (1), 61-69.
- Huber, A., C. Oyarzun, and A. Ellies (1985), Balance hidrico en tres plantaciones de *Pinus radiata* y una pradera, *Bosque*, 6 (5), 74-82.
- Huber, A., Iroumé, A., Mohr, C., and C. Frene (2010), Effect of *Pinus radiata* and *Eucalyptus globulus* plantations on water resource in the Coastal Range of Biobio region, Chile, *Bosque*, 31, 219-230, doi:10.4067/S0717-92002010000300006.
- Imeson, A. C., Verstraten, J. M., Vanmulligen, E. J. and J. Sevink (1992), The Effects of fire and water repellency on infiltration and runoff under Mediterranean type forest, *Catena*, 19, 345-361, doi:10.1016/0341-8162(92)90008-Y.
- INFOR (2008), Anuario Forestal 2008, in Boletín Estadístico, edited by C.d.I. Forestal, pp. 169, Santiago de Chile.

- INIA (1989), Mapa agroclimático de Chile, Santiago de Chile.
- Iroumé, A. (2005), Hydrological and sediment transport processes in forest plantations in Southern Chile, PhD thesis, Georg-August-University, Göttingen.
- Iroumé, A. (1992) Precipitación, escorrentía y producción de sedimentos en suspensión en una cuenca cercana a Valdivia, Chile, *Bosque*, 13, 15-23.
- Iroumé, A. (1990), Assessment of runoff and suspended sediment yield in a partially forested catchment in southern Chile, *Water Resour. Res.*, 26 (11), 2637-2642.
- Iroumé, A., and A. Huber (2002), Comparison of interception losses in a broadleaved native forest and a *Pseudotsuga menziesii* (Douglas fir) plantation in the Andes Mountains of southern Chile, *Hydrol. Processes*, 16 (12), 2347-2361.
- Iroumé, A., and A. Huber (2000), Intercepción de las lluvias por cubiertas de bosques y efecto en los caudales de crecida en una cuenca experimental en Malalcahuello, IX Región, Chile, *Bosque*, 21 (1), 45-56.
- Iroumé, A., and H. Palacios, Afforestation and changes in forest composition affect runoff in large river basins with pluvial regime and Mediterranean climate, Chile, *J. Hydrol.*, in rev.
- Iroumé, A., H. Palacios, J. Bathurst, and A. Huber (2010), Runoff and peakflows after clearcutting and the establishment of a new plantation in an experimental catchment, southern Chile, *Bosque*, 31 (2), 117-128.
- Iroumé, A., Mayen, O. and A. Huber (2006), Runoff and peak flow responses to timber harvest and forest age in southern Chile, *Hydrol. Processes*, 20, 37-50, doi:10.1002/hyp.5897.
- Iroumé, A., Huber, A. and K. Schulz (2005), Summer flows in experimental catchments with different forest covers, Chile, *J. Hydrol.*, 300, 300-313, doi:10.1016/j.jhydrol.2004.06.014.
- Istanbulluoglu, E., D.G. Tarboton, R.T. Pack, and C.H. Luce (2004), Modeling of the interactions between forest vegetation, disturbances, and sediment yields, *J. Geophys. Res.-Earth Surface*, 109 (F1).
- Jahn, R., Blume, H.-P., Asio, V.B., Spaargaren, O. and P. Schad (2006), *FAO Guidelines for Soil Description*, 97 pp, Food and Agriculture Organization of the United Nations (FAO), Rome.
- Jhorar, R.K., J.C. van Dam, W.G.M. Bastiaanssen, and R.A. Feddes (2004), Calibration of effective soil hydraulic parameters of heterogeneous soil profiles, *J. Hydrol.*, 285 (1-4), 233-247.

- Jones, J.A. (2000), Hydrologic processes and peak discharge response to forest removal, regrowth, and roads in 10 small experimental basins, western Cascades, Oregon, *Water Resour. Res.*, 36 (9), 2621-2642.
- Jones, J. A. and G. E. Grant (1996), Peak flow response to clear cutting and roads in small and large basins, western Cascades, Oregon, *Water Resour. Res.*, 32, 959-974, doi: 0.1029/95WR03493
- Jones, J.A., G.L. Achterman, L.A. Augustine, I.F. Creed, P.F. Ffolliott, L. MacDonald, and B.C. Wemple (2009), Hydrologic effects of a changing forested landscape-challenges for the hydrological sciences, *Hydrol. Processes*, 23 (18), 2699-2704.
- Kanamori, H., and K. Satake (1990), Broad-Band Study of the 1989 Loma-Prieta Earthquake, *Geophys. Res. Lett.*, 17 (8), 1179-1182.
- Karwan, D., J. Gravelle, and J. Hubbart (2007), Effects of timber harvest on suspended sediment loads in Mica Creek, Idaho, *For. Sci.*, 53 (2), 181-188.
- Kendall, C., and J.J. McDonnell (1998), *Isotope Tracers in Catchment Hydrology*, 839 pp., Elsevier, Amsterdam.
- Keppler, E.T. (1998), The summer flow and water yield response to timber harvest, pp. 35-43, USDA.
- Kirchner, J.W. (2009), Catchments as simple dynamical systems: Catchment characterization, rainfall-runoff modeling, and doing hydrology backward, *Water Resour. Res.*, 45, W02429.
- Kirchner, J.W. (2006), Getting the right answers for the right reasons: Linking measurements, analyses, and models to advance the science of hydrology, *Water Resour. Res.*, 42 (3).
- Klaassen, W., F. Bosveld, and E. de Water (1998), Water storage and evaporation as constituents of rainfall interception, *J. Hydrol.*, 212 (1-4), 36-50.
- Korup, O. (2012), Earth's portfolio of extreme sediment transport events, *Earth-Sci. Rev.*, 112 (3-4), 115-125.
- Kuras, P.K., Y. Alila, and M. Weiler (2012), Forest harvesting effects on the magnitude and frequency of peak flows can increase with return period, *Water Resour. Res.*, 48, W01544.
- Lane, P. N. J. and G. J. Sheridan (2002), Impact of an unsealed forest road stream crossing: Water quality and sediment sources, *Hydrol. Processes*, 16, 2599-2612, doi:10.1002/hyp.1050.

- Lane, P.N.J., J.C. Croke, and P. Dignan (2004), Runoff generation from logged and burnt convergent hillslopes: rainfall simulation and modelling, *Hydrol. Processes*, 18 (5), 879-892.
- Lane, P.N.J., A.E. Best, K. Hickel, and L. Zhang (2005), The response of flow duration curves to afforestation, *J. Hydrol.*, 310 (1-4), 253-265.
- Lara, A., C. Little, R. Urrutia, J. McPhee, C. Alvarez-Garreton, C.E. Oyarz n, D. Soto, P. Donoso, L. Nahuelhual, M. Pino, and I. Arismendi (2009), Assessment of ecosystem services as an opportunity for the conservation and management of native forests in Chile, *For. Eco. Manag.*, 258 (4), 415-424.
- Law, A. and M. Wiener (2002), Classification and Regression by randomForest, *R News*, 2, 18-22.
- Lee, M., T.K. Liu, K.F. Ma, and Y.M. Chang (2004), Reply to comment by N. Koizumi et al. on "Coseismic hydrological changes associated with dislocation of the September 21, 1999 Chichi earthquake, Taiwan", *Geophys. Res. Lett.*, 31 (13), L13604, doi:10.1029/2004GL020128.
- Levia, D.F., and E.E. Frost, A review and evaluation of stemflow literature in the hydrologic and biogeochemical cycles of forested and agricultural ecosystems, *J. Hydrol.*, 274 (1-4), 1-29, 2003.
- Levia, D.F., and E.E. Frost (2006), Variability of throughfall volume and solute inputs in wooded ecosystems, *Progr. Phys. Geogr.*, 30 (5), 605-632.
- Lewis, J., L.M. Reid, and R.B. Thomas (2010), Comment on "Forest and floods: A new paradigm sheds light on age-old controversies" by Younes Alila et al, *Water Resour. Res.*, 46.
- Link, T.E., M. Unsworth, and D. Marks (2004), The dynamics of rainfall interception by a seasonal temperate rainforest, *Agri. For. Meteo.*, 124 (3-4), 171-191.
- Little, C., A. Lara, J. McPhee, and R. Urrutia (2009), Revealing the impact of forest exotic plantations on water yield in large scale watersheds in South-Central Chile, *J. Hydrol.*, 374 (1-2), 162-170.
- Lorito, S., F. Romano, S. Atzori, X. Tong, A. Avallone, J. McCloskey, M. Cocco, E. Boschi, and A. Piatanesi (2011), Limited overlap between the seismic gap and coseismic slip of the great 2010 Chile earthquake, *Nature Geoscience*, 4 (3), 173-177.
- Madariaga, R., M. Metois, C. Vigny, and J. Campos (2010), Central Chile finally breaks, *Science*, 328 (5975), 181-182, doi:10.1126/science.1189197.

- Major, J.J., and L.E. Mark (2006), Peak flow responses to landscape disturbances caused by the cataclysmic 1980 eruption of Mount St. Helens, Washington, *Geol. Soc. Am. Bull.*, 118 (7-8), 938-958.
- Malmer, A. and H. Grip (1990), Soil disturbance and loss of infiltrability caused by mechanized and manual extraction of tropical rain-forest in Sabah, Malaysia, *For. Ecol. Manage.*, 38, 1-12, doi:10.1016/0378-1127(90)90081-L.
- Manga, M. (2001), Origin of postseismic streamflow changes inferred from baseflow recession and magnitude-distance relations, *Geophys. Res. Lett.*, 28 (10), 2133-2136, doi:10.1029/2000GL012481.
- Manga, M., and J.C. Rowland (2009), Response of Alum Rock springs to the October 30, 2007 Alum Rock earthquake and implications for the origin of increased discharge after earthquakes, *Geofluids*, 9 (3), 237-250, doi:10.1111/j.1468-8123.2009.00250.
- Manga, M., and C.-Y. Wang (2007), Earthquake Hydrology, in *Treatise on Geophysics*, edited by G. Schubert, pp. 293-320, Elsevier, Amsterdam.
- Manga, M., E.E. Brodsky, and M. Boone (2003), Response of streamflow to multiple earthquakes, *Geophys. Res. Lett.*, 30 (5), 1214, doi:10.1029/2002GL016618.
- Manga, M., I. Beresnev, E.E. Brodsky, J.E. Elkhoury, D. Elsworth, S.E. Ingebritsen, D.C. Mays, and C.Y. Wang (2012), Changes in permeability caused by transient stresses: Field observations, experiments, and mechanisms, *Rev. Geophys.*, 50.
- Mann, M.E., S. Rutherford, A. Schurer, S.F.B. Tett, and J.D. Fuentes (2013), Discrepancies between the modeled and proxy-reconstructed response to volcanic forcing over the past millennium: Implications and possible mechanisms, *J. Geophys. Res.-Atmospheres*, 118 (14), 7617-7627.
- May, C. (2007), Sediment and wood routing in steep headwater streams: an overview of geomorphic processes and their topographic signatures, *For. Sci.*, 53 (2), 119-130.
- Mayor, A.G., S. Bautista, and J. Bellot (2009), Factors and interactions controlling infiltration, runoff, and soil loss at the microscale in a patchy Mediterranean semiarid landscape, *Earth Surf. Processes Landforms*, 34 (12), 1702-1711.
- Megahan, W.F., J.G. King, and K. Seyesbagheri (1995), Hydrologic and erosional responses of a granitic watershed to helicopter logging and broadcast burning, *For. Sci.*, 41 (4), 777-795.
- Meinshausen, N.(2006), Quantile regression forests, *J. Machine Learning Res.*, 7, 983-999.
- Melnick, D., B. Bookhagen, M.R. Strecker, and H.P. Echtler (2009), Segmentation of megathrust rupture zones from fore-arc deformation patterns over hundreds to millions

- of years, Arauco peninsula, Chile, *J. Geophys. Res.-Solid Earth*, 114, doi:10.1029/2008JB005788.
- Michaelides, K., Lister, D., Wainwright, J. and A. J. Parsons (2009), Vegetation controls on small-scale runoff and erosion dynamics in a degrading dryland environment, *Hydrol. Processes*, 23, 1617-1630, doi:10.1002/hyp.7293.
- Micklin, P.P. (1988), Desiccation of the Aral Sea - a Water Management Disaster in the Soviet-Union, *Science*, 241 (4870), 1170-1175.
- Miyata, S., Kosugi, K., Gomi, T. and T. Mizuyama (2009), Effects of forest floor coverage on overland flow and soil erosion on hillslopes in Japanese cypress plantation forests, *Water Resour. Res.*, 45, doi:10.1029/2008WR007270.
- Mogi, K., H. Mochizuki, and Y. Kurokawa (1989), Temperature-changes in an artesian spring at Usami in the Izu Peninsula (Japan) and their relation to earthquakes, *Tectonophys.*, 159 (1-2), 95-108, doi:10.1016/0040-1951(89)90172-8.
- Mohr, C.H., R. Coppus, A. Huber, A. Iroumé, and Bronstert, A.(2013), Runoff Generation and soil erosion processes after clear cutting, *J. Geophys. Res.- Earth Surf.*, 118, 2013, doi:10.1002/jgrf.20047, 2013.
- Mohr, C.H., D.R. Montgomery, A. Huber, A. Bronstert, and Iroumé, A.(2012), Streamflow response in small upland catchments in the Chilean coastal range to the M-W 8.8 Maule earthquake on 27 February 2010, *J. Geophys. Res.- Earth Surf.*, 117, doi:10.111029/2011JF002138.
- Montgomery, D.R., and W.E. Dietrich (2002), Runoff generation in a steep, soil-mantled landscape, *Water Resour. Res.*, 38 (9), doi:10.1029/2001WR000822.
- Montgomery, D.R., and M. Manga (2003), Streamflow and water well responses to earthquakes, *Science*, 300 (5628), 2047-2049, doi:10.1126/science.1082980.
- Montgomery, D.R., H.M. Greenberg, and D.T. Smith (2003), Streamflow response to the Nisqually earthquake, *Earth Planet. Sci. Lett.*, 209 (1-2), 19-28, doi:10.1016/S0012-821X(03)00074-8.
- Montgomery, D.R., K.M. Schmidt, H.M. Greenberg, and W.E. Dietrich (2000), Forest clearing and regional landsliding, *Geology*, 28 (4), 311-314, doi:10.1130/0091-7613(2000)28<311:FCARL>2.0.CO;2.
- Montgomery, D. R., Dietrich, W. E., Torres, R., Anderson, S. P., Heffner, J. T. and K. Loague (1997), Hydrologic response of a steep, unchanneled valley to natural and applied rainfall, *Water Resour. Res.*, 33, 91-109, doi:10.1029/96WR02985.

- Moreno, M., M. Rosenau, and O. Oncken (2010), 2010 Maule earthquake slip correlates with pre-seismic locking of Andean subduction zone, *Nature*, 467 (7312), 198-U84, doi:10.1038/nature09349.
- Moreno, M., D. Melnick, M. Rosenau, J. Baez, J. Klotz, O. Oncken, A. Tassara, J. Chen, K. Bataille, M. Bevis, A. Socquet, J. Bolte, C. Vigny, B. Brooks, I. Ryder, V. Grund, B. Smalley, D. Carrizo, M. Bartsch, and H. Hase (2012), Toward understanding tectonic control on the Mw 8.8 2010 Maule Chile earthquake, *Earth Planet. Sci. Lett.*, 321-322 (0), 152-165.
- Moore, R.D., and S.M. Wondzell (2005), Physical hydrology and the effects of forest harvesting in the Pacific Northwest: A review, *J. Am. Wat. Res. Assoc.*, 41 (4), 763-784.
- Motha, J. A., Wallbrink, P. J., Hairsine P. B. and R. B. Grayson (2003), Determining the sources of suspended sediment in a forested catchment in southeastern Australia, *Water Resour. Res.*, 39, doi:10.1029/2001WR000794
- Mueller, E.N., A. Guntner, T. Francke, and G. Mamede (2010), Modelling sediment export, retention and reservoir sedimentation in drylands with the WASA-SED model, *Geosci. Model Develop.*, 3 (1), 275-291.
- Muirwood, R., and G.C.P. King (1993), Hydrological signatures of earthquake strain, *J. Geophys. Res.-Solid Earth*, 98 (B12), 22035-22068.
- Nakamura, Y., and H. Wakita (1984), Precise temperature measurement of groundwater for earthquake-prediction study, *Pure Appl. Geophys.* 164-174.
- Nearing, M.A.(1998) Why soil erosion models over-predict small soil losses and under-predict large soil losses, *Catena*, 32, 15-22, doi: 10.1016/S0341-8162(97)00052-0.
- Niklitschek, M.E. (2007), Trade liberalization and land use changes: Explaining the expansion of afforested land in Chile, *For. Sci.*, 53 (3), 385-394.
- O'Loughlin, C.L., L.K. Rowe, and A.J. Pearce (1978), Sediment yields from small forested catchments North Westland - Nelson, New Zealand, *J. Hydrol. New Zeal.*, 17 (1), 1-15.
- Onda, Y., Y. Komatsu, M. Tsujimura, and J. Fujihara (2001), The role of subsurface runoff through bedrock on storm flow generation, *Hydrol. Processes*, 15 (10), 1693-1706.
- Oyarzun, C. (1993), Evaluación del modelo U.S.L.E. para predecir pérdidas de suelo en áreas forestadas de la cuenca del río Biobío, *Bosque*, 14 (1), 45-54.
- Oyarzun, C., and L. Peña (1995), Soil erosion and overland flow in forested areas with pine plantations at coastal mountain range, central Chile, *Hydrol. Processes*, 9 (111-118).

- Oyarzun, C., A. Huber, and s. Vasquez (1985), Balance hídrico en tres plantaciones de *Pinus radiata*. I: Redistribución de las precipitaciones, *Bosque*, 6 (1), 3-13.
- Oyarzun, C.E., R. Godoy, and A. Sepulveda (1998), Water and nutrient fluxes in a cool temperate rainforest at the Cordillera de la Costa in southern Chile, *Hydrol. Processes*, 12 (7), 1067-1077.
- Papadopoulos, G.A., and G. Lefkopoulos (1993), Magnitude-distance relations for liquefaction in soil from earthquakes, *Bull. Seismo. Soc. Am.*, 83 (3), 925-938.
- Patterson, M. W. and N. Hoalst-Pullen (2011), Dynamic equifinality: The case of south-central Chile's evolving forest landscape, *Appl. Geogr.*, 31, 641-649, doi:10.1016/j.apgeog.2010.12.004.
- Parker, R.N., A.L. Densmore, N.J. Rosser, M. de Michele, Y. Li, R. Huang, S. Whadcoat, and D.N. Petley (2011), Mass wasting triggered by the 2008 Wenchuan earthquake is greater than orogenic growth, *Nature Geoscience*, 4 (7), 449-452.
- Parsons, A. J., Brazier, R. E., Wainwright, J. and D. M. Powell (2006), Scale relationships in hillslope runoff and erosion, *Earth Surf. Processes Landforms*, 31, 1384-1393, doi:10.1002/esp.1345.
- Pepin, E., S. Carretier, J.L. Guyot, and F. Escobar (2010), Specific suspended sediment yields of the Andean rivers of Chile and their relationship to climate, slope and vegetation, *Hydro. Sci. J.*, 55 (7), 1190-1205.
- Pizarro, R., S. Araya, C. Jordan, C. Farias, J.P. Flores, and P.B. Bro (2006), The effects of changes in vegetative cover on river flows in the Purapel river basin of central Chile, *J. Hydrol.*, 327 (1-2), 249-257.
- Pizarro, T., and H. Cuitino (1999), Evaluación cuantitativa de la erosión hídrica superficial en suelos desnudos de la Pre-Cordillera Andina y Valle Central de la VII Región, *Jornadas del CONAPHI*, 6.
- Putuhena, W.M. (2000), and I. Cordery, Some hydrological effects of changing forest cover from eucalypts to *Pinus radiata*, *Agri. For. Meteo.*, 100 (1), 59-72.
- R** Development Core Team, (2009), A language and environment for statistical computing, R Foundation for Statistical computing, Vienna, Austria, <http://www.R-project.org>.
- Rawls, W. J., R. A. Lajpat, D. L. Brakensiek and Al. Shirmohammadi (1993), Infiltration and soil water movement, in *Handbook of Hydrology*, edited by D. R. Maidment, pp. 5.1-5.51, McGraw-Hill, New York.
- Rehg, K., A. Packman, and J. Ren (2005), Effects of suspended sediment characteristics and bed sediment transport on streambed clogging., *Hydrol. Processes*, 19 (413-427).

- Reutebach, S., R. McGaughey, H.-E. Anderson and W. Carson (2003), Accuracy of a high-resolution lidar terrain model under a conifer forest canopy, *Can. J. Remote Sens.*, 29, 527- 535.
- Robinson, M., A. Cognard-Plancqb, C. Cosandey, J. David, P. Durand, H. F hrer, R. Hall, M. Hendriques, V. Marc, R. McCarthy, M. McDonnell, C. Martin, T. Nisbet, P. O’Dea, M. Rodgers, and A. Zollner (2003), Studies of the impact of forests on peakfows and basefows: a European perspective, *For. Eco. Manag.*, 186, 85-97.
- Roering, J.J., and M. Gerber (2005), Fire and the evolution of steep, soil-mantled landscapes, *Geology*, 33 (5), 349-352.
- Roeloffs, E. (1996), Poroelastic techniques in the study of earthquake-related hydrologic phenomena, *Adv. Geophys.*, Vol 37, 37, 135-195.
- Roeloffs, E., M. Sneed, D.L. Galloway, M.L. Sorey, C.D. Farrar, J.F. Howle, and J. Hughes (2003), Water-level changes induced by local and distant earthquakes at Long Valley caldera, California, *J. Volcanol. Geotherm. Res.*, 127 (3-4), 269-303, doi:10.1016/S0377-0273(03)00173-2.
- Roeloffs, E.A. (1998), Persistent water level changes in a well near Parkfield, California, due to local and distant earthquakes, *J. Geophys. Res.-Solid Earth*, 103 (B1), 869-889, doi:10.1029/97JB02335.
- Rojstaczer, S., and S. Wolf (1992), Permeability changes associated with large earthquakes - an example from Loma Prieta, California, *Geology*, 20 (3), 211-214, doi:10.1130/0091-7613(1992)020<0211:PCAWLE>2.3.CO;2.
- Rojstaczer, S., S. Wolf, and R. Michel (1995), Permeability enhancement in the shallow crust as a cause of earthquake-induced hydrological changes, *Nature*, 373 (6511), 237-239, doi:10.1038/373237aO.
- Rupp, D.E., and J.S. Selker (2006), On the use of the Boussinesq equation for interpreting recession hydrographs from sloping aquifers, *Water Resour. Res.*, 42 (12).
- Ruprecht, J.K., N.J. Schofield, D.S. Crombie, R.A. Vertessy, and G.L. Stoneman (1991), Early Hydrological Response to Intense Forest Thinning in Southwestern Australia, *J. Hydrol.*, 127 (1-4), 261-277.
- Sato, T., H. Wakita, K. Notsu, and G. Igarashi (1992), Anomalous hot-spring water changes - possible precursors of the 1989 volcanic-eruption off the east-coast of the Izu eninsula, *Geochem. J.*, 26 (2), 73-83.
- Scheffer, F. and P. Schachtschabel (2010), *Lehrbuch der Bodenkunde*, 584 pp., Spektrum Akademischer Verlag, Berlin.

- Schlatter, J., R. Grez, and V. Gerding (2003), *Manual para el reconocimiento de suelos*, 114 pp., Universidad Austral de Chile, Valdivia.
- Schoeneberger, P. J., Wysocki, D. A., Benham, E. C. and W. D. Broderson (2002), *Field book for describing and sampling soils*, 227 pp, Natural Resources Conservation Service, National Soil Survey Center, USDA, Lincoln, NE.
- Scholz, C. H. (2010), *The mechanics of Earthquakes and Faulting*, 471 pp., Cambridge University Press, Cambridge.
- Schuller, P., D.E. Walling, A. Iroumé, C. Quilodrán, A. Castillo, and A. Navas (2013), Using ^{137}Cs and ^{210}Pb and other sediment source fingerprints to document suspended sediment sources in small forested catchments in south-central Chile, *J. Environ. Radioactivity*, 124 (0), 147-159.
- Schuller, P., A. Iroume, D.E. Walling, H.B. Mancilla, A. Castillo, and R.E. Trumper (2006), Use of beryllium-7 to document soil redistribution following forest harvest operations, *J. Environ.l Qual.*, 35 (5), 1756-1763.
- Scott, D.F., and W. Lesch (1997), Streamflow responses to afforestation with *Eucalyptus grandis* and *Pinus patula* and to felling in the Mokobulaan experimental catchments, South Africa, *J. Hydrol.*, 199 (3-4), 360-377.
- Scott, D.F., and F.W. Prinsloo (2008), Longer-term effects of pine and eucalypt plantations on streamflow, *Water Resour. Res.*, 44.
- Seeger, M., (2007), Uncertainty of factors determining runoff and erosion processes as quantified by rainfall simulations. *Catena* 71, 56-67 (2007), doi: 10.1016/j.catena.2006.10.005.
- Seifert, W. (2011), *Statistische Auswertung von Beregnungsversuchen zur Bestimmung der Infiltrationsrate in S chile*, B.Sc. thesis, Inst. Earth. Environ. Sci., Uni. of Potsdam, Potsdam, Germany.
- Sheridan, G.J., P.J. Noske, P.N.J. Lane, and C.B. Sherwin (2008), Using rainfall simulation and site measurements to predict annual interrill erodibility and phosphorus generation rates from unsealed forest roads: Validation against in-situ erosion measurements, *CATENA*, 73 (1), 49-62.
- Sibson, R.H., and J.V. Rowland (2003), Stress, fluid pressure and structural permeability in seismogenic crust, North Island, New Zealand, *Geophy. J. Int.*, 154 (2), 584-594.
- Sidle, R.C.(1991) A conceptual-model of changes in root cohesion in response to vegetation management, *J. Environ. Qual.*, 20 (1), 43-52.

- Sidele, R.C., and Y. Onda (2004), Hydrogeomorphology: Overview of an emerging science, *Hydrol. Processes*, 18 (4), 597-602.
- Sidele, R.C., S. Sasaki, M. Otsuki, S. Noguchi, and A.R. Nik (2004), Sediment pathways in a tropical forest: effects of logging roads and skid trails, *Hydrol. Processes*, 18 (4), 703-720.
- Sidele, R.C., A.D. Ziegler, J.N. Negishi, A.R. Nik, R. Siew, and Turkelboom, F.(2006), Erosion processes in steep terrain - Truths, myths, and uncertainties related to forest management in Southeast Asia, *For. Ecol. Manage.*, 224, 199-225, doi: 10.1016/j.foreco.2005.12.019.
- Sparkes, R., F. Tilmann, N. Hovius, and J. Hillier (2010), Subducted seafloor relief stops rupture in South American great earthquakes: Implications for rupture behaviour in the 2010 Chile earthquake, *Earth Planet. Sci. Lett.*, 298 (1-2), 89-94, doi:10.1016/j.epsl.2010.07.029.
- Stednick, J.D. (1996), Monitoring the effects of timber harvest on annual water yield, *J. Hydrol.*, 176 (1-4), 79-95.
- Steubing, L., and A. Fangmeier (2001), *Pflanzenökologisches Praktikum*, 205 pp., Eugen Ulmer, Stuttgart.
- Strobl, C., Boulesteix, A. L., Kneib, T., Augustin, T. and A. Zeileis, (2008), Conditional variable importance for random forests, *Bmc Bioinf.*, 9, doi:10.1186/1471-2105-9-307.
- Sutton, W.R.J. (1999), The need for planted forests and the example of radiata pine, *New Forests*, 17 (1-3), 95-109.
- Swank, W.T., J.M. Vose, and K.J. Elliott (2001), Long-term hydrologic and water quality responses following commercial clearcutting of mixed hardwoods on a southern Appalachian catchment, *For. Eco. Manag.*, 143 (1-3), 163-178.
- Tertulliani, A., and L. Cucci (2009), Clues to the identification of a seismogenic source from environmental effects: the case of the 1905 Calabria (Southern Italy) earthquake, *Nat. Hazards Earth Syst. Sci.*, 9 (6), 1787-1803, doi:10.5194/nhess-9-1787-2009.
- Thomas, R.B., and W.F. Megahan (1998), Peak flow responses to clear-cutting and roads in small and large basins, western Cascades, Oregon: A second opinion, *Water Resour. Res.*, 34 (12), 3393-3403.
- Thompson, S., C.J. Harman, P. Reed, A. Montanari, R. Schumer, G. Bloeschl, A. Viglione, B. McGynn, T. Wagener, Y.F. Reinfelder, L. Marshall, E. Istanbulluoglu, P.A. Troch, J. Shaman, N. D., L. Band, H.H.G. Savenije, C. A., and J. Wilson (2011), Predictions

- under Change (PUC): Water, Earth and Biota in the Anthropocene, edited by M. Sivapalan, pp. 64.
- Tokunaga, T. (1999), Modelling of earthquake-induced hydrological changes and possible permeability enhancement due to the 17 January 1995 Kobe Earthquake, Japan, *J. Hydrol.*, 223 (3-4), 221-229, doi:10.1016/S0022-1694(99)00124-9.
- Tong, X.P., D. Sandwell, K. Luttrell, B. Brooks, M. Bevis, M. Shimada, J. Foster, R. Smalley, H. Parra, J.C.B. Soto, M. Blanco, E. Kendrick, J. Genrich, and D.J. Caccamise (2010), The 2010 Maule, Chile earthquake: Downdip rupture limit revealed by space geodesy, *Geophys. Res. Lett.*, 37.
- Toro, J., and S. Gessel (1999), Radiata pine plantations in Chile, *New Forests*, 18 (1), 33-44.
- Turnbull, L., J. Wainwright, and R.E. Brazier (2010), Changes in hydrology and erosion over a transition from grassland to shrubland, *Hydrol. Processes*, 24 (4), 393-414.
- Uyttendaele, G.Y.P., and A. Iroumé (2002), The solute budget of a forest catchment and solute fluxes within a *Pinus radiata* and a secondary native forest site, southern Chile, *Hydrol. Processes*, 16 (13), 2521-2536.
- VanderKwaak, J.E., and K. Loague (2001), Hydrologic-response simulations for the R-5 catchment with a comprehensive physics-based model, *Water Resour. Res.*, 37 (4), 999-1013.
- Van Genuchten, M.T. (1980), A Closed-Form Equation for Predicting the Hydraulic Conductivity of Unsaturated Soils, *Soil Sci. Soc. Am. J.*, 44 (5), 892-898.
- van Dijk, A., and R.J. Keenan (2007), Planted forests and water in perspective, *For. Eco. Manag.*, 251 (1-2), 1-9.
- van Dijk, A., and L.A. Bruijnzeel (2001), Modelling rainfall interception by vegetation of variable density using an adapted analytical model. Part 1. Model description, *J. Hydrol.*, 247 (230-238).
- Vega, J.A., C. Fernandez, and T. Fonturbel (2005), Throughfall, runoff and soil erosion after prescribed burning in gorse shrubland in Galicia (NW Spain), *Land Degrad. Develop.*, 16 (37-51).
- Vigny, C., A. Socquet, S. Peyrat, J.-C. Ruegg, M. Métois, R. Madariaga, S. Morvan, M. Lancieri, R. Lacassin, J. Campos, D. Carrizo, M. Bejar-Pizarro, S. Barrientos, R. Armijo, C. Aranda, M.-C. Valderas-Bermejo, I. Ortega, F. Bondoux, S. Baize, H. Lyon-Caen, A. Pavez, J.-P. Vilotte, M. Bevis, B. Brooks, R. Smalley, H. Parra, J.-C. Baez, M. Lanco, S. Cimbaro and E. Kendrick (2011), The 2010 Mw 8.8 Maule

- Megathrust Earthquake of Central Chile, monitored by GPS, *Science*, 332 (6032), 1417-1421, doi: 10.1126/science.1204132.
- Vorpahl, P., Elsenbeer, H., Märker, M. and B. Schröder (2012), How can statistical models help to determine driving factors of landslides?, *Ecol. Modell.*, 239, 27-39, doi: 10.1016/j.ecolmodel.2011.12.007.
- Wagener, T., M. Sivapalan, P.A. Troch, B.L. McGlynn, C.J. Harman, H.V. Gupta, P. Kumar, P.S.C. Rao, N.B. Basu, and J.S. Wilson (2010), The future of hydrology: An evolving science for a changing world, *Water Resour. Res.*, 46 (5), W05301, 2010.
- Wainwright, J., Parsons, A. J. and A. D. Abrahams (2000), Plot-scale studies of vegetation, overland flow and erosion interactions: Case studies from Arizona and New Mexico, *Hydrol. Processes*, 14, 2921-2943, doi:10.1002/1099-1085(200011/12)14:16/17<2921::AID-HYP127>3.0.CO;2-7.
- Wallbrink P. J. and J. Croke (2002): A combined rainfall simulator and tracer approach to assess the role of best management practices in minimizing sediment redistribution and loss in forests after harvesting, *For. Ecol. Manage.*, 170, 217-232, doi: 10.1016/S0378-1127(01)00765-4
- Walsh, R.P.D., K. Bidin, W.H. Blake, N.A. Chappell, M.A. Clarke, I. Douglas, R. Ghazali, A.M. Sayer, J. Suhaimi, W. Tych, and K.V. Annammala (2011), Long-term responses of rainforest erosional systems at different spatial scales to selective logging and climatic change, *Phil. Trans. Royal Soc. London –Biol. Sci.*, 366 (1582), 3340-3353, 2011.
- Wang, C. Y. (2007), Liquefaction beyond the near-field, *Seismol. Res. Lett.*, 78 (5), 512-517, doi:10.1785/gssrl.78.5.512.
- Wang, C.Y., and Y.P. Chia (2008), Mechanism of water level changes during earthquakes: Near field versus intermediate field, *Geophys. Res. Lett.*, 35 (12), L12402, doi:10.1029/2008GL034227.
- Wang, C.Y., and M. Manga (2010a), *Earthquakes and Water*, 225 pp., Springer, Berlin.
- Wang, C.Y., and M. Manga (2010b), Hydrologic responses to earthquakes and a general metric, *Geofluids*, 10 (1-2), 206-216, doi:10.1111/j.1468-8123.2009.00270.x.
- Wang, C.Y., C.H. Wang, and M. Manga (2004a), Coseismic release of water from mountains: Evidence from the 1999 (MW=7.5) Chi-Chi, Taiwan, earthquake, *Geology*, 32 (9), 769-772, doi:10.1130/G20753.1.

- Wang, C.Y., L.H. Cheng, C.V. Chin, and S.B. Yu (2001), Coseismic hydrologic response of an alluvial fan to the 1999 Chi-Chi earthquake, Taiwan, *Geology*, 29 (9), 831-834, doi:10.1130/0091-7613(2001)029<0831:CHROAA>2.0.CO;2.
- Wang, C.Y., M. Manga, D. Dreger, and A. Wong (2004b), Streamflow increase due to rupturing of hydrothermal reservoirs: Evidence from the 2003 San Simeon, California, Earthquake, *Geophys. Res. Lett.*, 31 (10), L10502, doi:10.1029/2004GL020124.
- Wang, C.Y., M. Manga, C.H. Wang and C.H. Chen (2012), Transient change in groundwater temperatures after earthquakes, *Geology*, 40 (2), 119-122, doi:10.1130/G32565.1.
- Watson, A., C. Phillips, and Marden, M.(1999) Root strength, growth, and rates of decay: Root reinforcement changes of two tree species and their contribution to slope stability, *Plant Soil*, 217, 39-47, doi: 10.1023/A:1004682509514.
- Webb, A.A., D. Dragovich, and R. Jamshidi (2012), Temporary increases in suspended sediment yields following selective eucalypt forest harvesting, *For. Eco. Manag.*, 283 (0), 96-105.
- Wemple, B.C., F.J. Swanson, and J.A. Jones (2001), Forest roads and geomorphic process interactions, Cascade Range, Oregon, *Earth Surf. Processes Landforms*, 26 (2), 191-204.
- Weiler, M. and F. Naef (2003), An experimental tracer study of the role of macropores in infiltration in grassland soils, *Hydrol. Processes*, 17, 477-493, doi:10.1002/hyp.1136.
- White, W.N. (1932), Method of estimating groundwater supplies based on discharge by plants and evaporation from soil - results of investigation in Escalante Valley, Utah, *Water Supply Paper*, 659 A, 1-105.
- Williams, G. P. (1989), Sediment concentration versus water discharge during single hydrologic events in rivers, *J. Hydrol.*, 111, 89-106, doi:10.1016/0022-1694(89)90254-0.
- Wilson, J.P., and J.C. Gallant (2000), *Terrain Analysis -Principles and Applications*, 479 pp., Wiley-Blackwell Publishing, Inc., New York.
- Wolman, M. G. and J. P. Miller (1960), Magnitude and frequency of forces in geomorphic processes. *J. Geol.* 68, 54-74.
- Wondzell, S.M., and J.G. King (2003), Postfire erosional processes in the Pacific Northwest and Rocky Mountain regions, *For. Eco. Manag.*, 178 (1-2), 75-87.
- Wosten, J.H.M., A. Lilly, A. Nemes, and C. Le Bas (1999), Development and use of a database of hydraulic properties of European soils, *Geoderma*, 90 (3-4), 169-185.

- Wu, L. and L. Pan (1997), A generalized solution to infiltration of single-ring infiltrometers by scaling, *Soil Sci. Soc. Am. J.*, 61, 1318-1322.
- Wu, Y.M., L. Zhao, C.H. Chang, and Y.J. Hsu (2008), Focal-mechanism determination in Taiwan by genetic algorithm, *Bull. Seismol. Soc. America*, 98 (2), 651-661.
- Xue, L., H.-B. Li, E.E. Brodsky, Z.-Q. Xu, Y. Kano, H. Wang, J.J. Mori, J.-L. Si, J.-L. Pei, W. Zhang, G. Yang, Z.-M. Sun, and Y. Huang (2013), Continuous permeability measurements record healing inside the Wenchuan Earthquake fault zone, *Science*, 340 (6140), 1555-1559.
- Zelt, R.B., and E.E. Wohl (2004), Channel and woody debris characteristics in adjacent burned and unburned watersheds a decade after wildfire, Park County, Wyoming, *Geomorphology*, 57 (3-4), 217-233.
- Zhou, G.Y., J.D. Morris, J.H. Yan, Z.Y. Yu, and S.L. Peng (2002), Hydrological impacts of reforestation with eucalypts and indigenous species: a case study in southern China, *For. Eco. Manag.*, 167, 209-222.
- Ziegler, A.D., J.N. Negishi, R.C. Sidle, S. Noguchi, and A.R. Nik (2006), Impacts of logging disturbance on hillslope saturated hydraulic conductivity in a tropical forest in PeninsularMalaysia, *Catena*, 67 (2), 89-104, doi:10.1016/j.catena.2006.02.008.
- Zimmermann, A., T. Francke, and H. Elsenbeer (2012), Forests and erosion: Insights from a study of suspended-sediment dynamics in an overland flow-prone rainforest catchment, *J. Hydrol.*, 428 (0), 170-181.

Acknowledgments

Writing this PhD thesis was not only the work of myself, there were many other people involved, supporting me in the one or other way. I thank all of them and want to namely acknowledge

- First, Anton Huber, for sharing his tremendous experience in Chilean forest hydrology. Your work inspired me many times.
- Axel Bronstert who gave me the opportunity and freedom to work on fascinating scientific questions, for discussions, and especially for the big work to review my thesis and supporting me in publishing my papers.
- Michael Manga and Chi-Wang for a very warm hosting and always having an open ear for discussions also after my unforgettable stay at Berkeley. Thank you also for reviewing parts of my thesis and our manuscript many times. I had the pleasure to meet Manoocher Shirzaei and Ben Mirus during my stay in Berkeley. Thank you for discussions and a warm receiving.
- Oliver Korup for sharing my passion for southern Chile, a great road trip through Argentina and for opportunity to start working as one of his Postdocs despite not having finished my PhD yet.
- Andrés Iroumé for supporting me in Chile, for discussions and co-authoring papers.
- Andreas Bauer for his excellent support during field under harsh conditions and for preparing many (!) of the figures, in particular the schematic hillslope profiles.
- Dave Montgomery for discussions and co-authoring my first first-author paper.
- Ruben Coppus for writing our paper, for sharing his extensive experience of field works and for having a great time together in Berlin.
- Many of the Chilean guys I met and who always helped me. Namely I'd like to acknowledge the help of Rodrigo – *El Soldado* – Bravo, Hardín Palacios, Hector Ulloa, Cristian Frêne, Cristian Alvarez, Manuel Cartagena, Odette Morales and Juan Pablo Navarro. In particular, I want to say many thanks to Sylvia Schönherr and Sylvia Soto for providing a second home in Chile during my long stays.
- Potsdam undergraduate students for helping during field works with always having a smile. Namely, I'd like to thank Winnie Seifert, Franziska Faul, Simon Plate, Johannes Brenner and Christian Gläser (University of Braunschweig).

- Jim Kirchner and Ryan Teuling for helping me with Matlab coding and explaining me how the hydrology backwards approach works. Further, I want to thank Jim for many discussions and reviewing our paper.
- My family for supporting me in many ways.
- Last but definitely not least: Thank you Nicole for patience and humor. Thank you Moritz showing me what really matters.

Curriculum Vitae

This page contains personal data. Therefore, this page has been intentionally left empty in the online publication.

Efecto de plantaciones de *Pinus radiata* y *Eucalyptus globulus* sobre el recurso agua en la Cordillera de la Costa de la región del Biobío, Chile

Effect of *Pinus radiata* and *Eucalyptus globulus* plantations on water resource in the Coastal Range of Biobío region, Chile

Anton Huber^{a*}, Andrés Iroumé^b, Christian Mohr^c, Cristian Frêne^a

*Autor de correspondencia: ^aUniversidad Austral de Chile, Facultad de Ciencias, Valdivia, Chile, tel.: 56-63-221359, ahuber@uach.cl

^bUniversidad Austral de Chile, Facultad de Ciencias Forestales y Recursos Naturales, Valdivia, Chile.

^cUniversity of Potsdam, Institute for Geoecology, Hydrology and Climatology, Potsdam, Germany.

SUMMARY

Rainfall redistribution, temporal oscillation of streamflow, variation of soil water content, evapotranspiration and sediment transport of two *Pinus radiata* and two *Eucalyptus globulus* catchments were determined. The catchments are located in the Coastal Range of southern central Chile. Due to their age, these plantations are to be harvested soon. The *P. radiata* plantations registered an interception loss of 17 and 16 %, values surpassing significantly the eucalyptus values of 10 and 11 %. The streamflows of the same catchments were 705 resp. 707 mm and 439 resp. 500 mm for the monitored period of 14 months. Despite the higher amount of rainfall reaching the soil in the eucalyptus-catchments, these catchments registered low streamflow compared to the pine-catchments. During the dry summer, all soils showed a severe reduction of their soil water content, exceeding the permanent wilt point in the soil's upper 30 cm. The *E. globulus*-catchments registered an evapotranspiration equal to 1,582 and 1,469 mm while it reached values of 1,357 and 1,298 in the *P. radiata*-catchments. These values correspond, for the *E. globulus*-catchments, to 74 and 68 % of total precipitation and 63 and 60 % for the *P. radiata*-catchments. These differences may be higher if water availability during summer drought does not limit the total evapotranspiration. The sediment export reached values of 237 and 615 kg/ha for the *P. radiata*-catchments and 152 and 125 kg/ha for the *E. globulus*-catchments during the monitored period.

Key words: streamflow, water balance, sediment transport, catchments, *Pinus radiata*, *Eucalyptus globulus*.

RESUMEN

Se estudió el efecto de plantaciones forestales sobre el recurso hídrico en cuencas de la vertiente este de la Cordillera de la Costa de la región del Biobío, en el centro sur de Chile. La redistribución de las precipitaciones, la oscilación temporal de los caudales, la fluctuación del contenido de agua edáfica, la evapotranspiración y el transporte de sedimentos fueron determinados para dos cuencas forestadas con *Pinus radiata* y dos con *Eucalyptus globulus*. De los 2.149 mm de precipitación registrada, las plantaciones de *P. radiata* interceptaron el 16 y 17 %, y las de *E. globulus* un 10 y 11 %, respectivamente. El caudal de los efluentes para las dos cuencas con *P. radiata* fue equivalente al 33 %, monto que superó a las con *E. globulus* que alcanzaron el 20 y 23 % de la precipitación. Durante el verano, los suelos presentaron una fuerte disminución de su contenido de agua, sobrepasando en los primeros 30 cm el punto de marchitez permanente. Las cuencas con *E. globulus* tuvieron una evapotranspiración equivalente al 76 y 70 %, y las de *P. radiata* al 65 y 64 %, respectivamente, de la precipitación. Estas diferencias pudieron ser superiores si la disponibilidad de agua, durante el estío, no hubiese sido una limitante para satisfacer los requerimientos máximos de agua de cada una de las especies. La exportación total de sedimentos para el período fue de 237 y 615 kg/ha en las cuencas con *P. radiata* y 152 y 125 kg/ha con *E. globulus*. Los resultados obtenidos siguen una tendencia semejante a los de investigaciones en estudios con condiciones edafoclimáticas y plantaciones similares.

Palabras clave: balance hídrico, transporte sedimentos cuencas, *Pinus radiata*, *Eucalyptus globulus*.

INTRODUCCIÓN

Hay opiniones diversas con respecto al real impacto que ocasionan las cubiertas forestales en el régimen hidrológico y en la magnitud de la erosión (Robinson *et al.* 2003, Andreassian *et al.* 2004, Boothroyd *et al.* 2004, Brown *et al.* 2005, Gomi *et al.* 2005, Farley *et al.* 2005, Hassan *et al.* 2005, Iroumé *et al.* 2006, Hubbart

et al. 2007, Huber *et al.* 2008, Scott y Prinsloo 2008). En general, estos autores concuerdan que, luego de unos años del establecimiento de una plantación, los caudales comienzan a disminuir debido a un aumento de la tasa evapotranspirativa. Luego de la cosecha final, los caudales recuperan los niveles que tenían al inicio y se incrementan las tasas de transporte de sedimento.

Los bosques en general y las plantaciones forestales en particular involucran una mayor cantidad de agua en la evapotranspiración y registran una superior pérdida de agua por intercepción del dosel en comparación a otros tipos de cubierta vegetal. La magnitud de estos alcances pasa por las características de las plantaciones (especie, edad y manejo), particularidades de las precipitaciones (cantidad e intensidad) y de las condiciones meteorológicas (Crockford y Richardson 2000, Van Dijk y Bruijnzeel 2001, Iroumé y Huber 2002, Carlyle-Moses 2004, Vega *et al.* 2005, Huber *et al.* 2008).

El transporte de sólidos suspendidos tiene un rol fundamental en el ciclo biogeoquímico de las cuencas forestadas (Karwan *et al.* 2007). Ellos degradan el hábitat acuático y rompen las conexiones en la relación suelo-agua, aumentan el transporte de contaminantes adsorbidos a las partículas e incrementan los costos de tratamiento asociados al uso público del agua (Rehg *et al.* 2005, Gomi *et al.* 2005). Las perturbaciones ocasionadas por el manejo de las plantaciones están relacionadas con un incremento en la producción de sedimentos suspendidos (Megahan *et al.* 1995, Karwan *et al.* 2007, Hubbart *et al.* 2007, May 2007), lo que implica importantes desafíos para la relación entre el manejo del bosque y la calidad de agua (Karwan *et al.* 2007).

Las unidades geomorfológicas más degradadas en la zona centro-sur de Chile están ubicadas en la vertiente oriental de la Cordillera de la Costa, en el llamado secano interior, especialmente las correspondientes a la región del Biobío. En tiempos pasados, esta zona estuvo cubierta por bosque nativo (Armesto *et al.* 2010) que fue intensamente explotado, dejando en muchos casos el suelo expuesto a la erosión. Actualmente, la mayor parte de esta superficie posee una cubierta herbácea, arbustiva, plantaciones forestales o se está usando en una actividad agrícola-ganadera precaria. La degradación de los suelos es más evidente en laderas con mayor pendiente y en suelos muy alterados debido a intervenciones silviculturales precedentes. El creciente deterioro de estos suelos restringe su uso a la actividad forestal, preferentemente a la forestación con especies exóticas de rápido crecimiento, que registra un notorio incremento en las últimas décadas. En la región del Biobío la superficie plantada con *Pinus radiata* D. Don (pino) y *Eucalyptus spp.* supera las 610.000 y 240.000 ha, respectivamente (INFOR 2008).

Si bien en Chile se ha realizado varios estudios sobre el consumo de agua de ambas especies (Huber *et al.* 1985, 1998, 2008, Oyarzún *et al.* 1985, Huber y García 1999, Huber e Iroumé 2001, Huber y Trecaman 2002, 2004, Iroumé *et al.* 2006), son escasos los antecedentes que indican la magnitud de los procesos erosivos que se registran en estas superficies forestadas (Oyarzún 1993, Oyarzún y Peña 1995, Pizarro y Cuitiño 1999).

Este trabajo pretende aportar al conocimiento sobre el impacto que tienen las plantaciones forestales sobre el recurso agua en la zona centro-sur de Chile. Las hipótesis de esta investigación son que: a) las distintas características

que tiene el dosel de las plantaciones forestales afectan las pérdidas de agua por intercepción y, por consiguiente, la cantidad total de agua que alcanza el suelo en cada cuenca; b) que los desiguales montos de agua involucrados en la evapotranspiración repercuten sobre el caudal de los efluentes y c) que las disimilitudes entre los valores de los diferentes componentes del balance hídrico y las particularidades de las cuencas definen la cantidad de sedimentos transportados. Para probar estas hipótesis, se plantean como objetivos específicos el confrontar la dinámica hídrica y el transporte de sedimentos por los efluentes de microcuencas forestadas con *Pinus radiata* y *Eucalyptus globulus* Labill (eucalipto), ubicadas en la vertiente este de la Cordillera de la Costa, en la región del Biobío, sur de Chile.

MÉTODOS

Características del área de estudio. Para el estudio se seleccionaron cuatro microcuencas hidrográficas ubicadas a 3 km al oeste de la ciudad de Nacimiento, región de Biobío, Chile (latitud 37° 28' S, longitud 72° 42' O), que pertenecen a la empresa Forestal Mininco S. A. (figura 1).

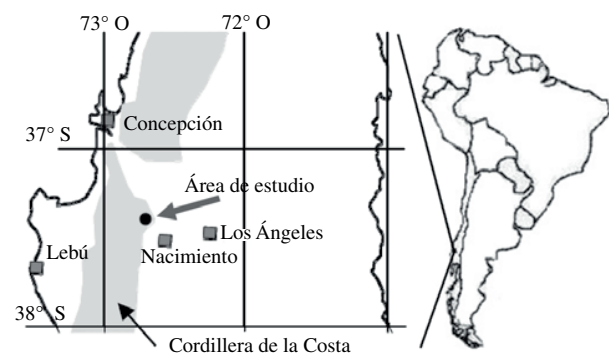


Figura 1. Localización de las cuencas forestales en Nacimiento, Chile.

Location of the forested catchments in Nacimiento, Chile.

Las cuencas están ubicadas en la vertiente este de la Cordillera de la Costa, distantes a menos de 1,5 km entre sí. Dos de estas cuencas están forestadas con *Pinus radiata* y las otras, con *Eucalyptus globulus*, todas en víspera de alcanzar la edad de rotación (cuadro 1). Los cauces de las cuencas se localizan en barrancos que se han labrado por la acción erosiva del agua a través del tiempo. La pendiente media supera el 20 %, la que le otorga una importante torrencialidad durante la época más lluviosa del año.

La zona posee un clima de tipo templado infratermal estenotérmico con un régimen mediterráneo perhúmedo (Fuenzalida 1971). La precipitación promedio anual de la zona es de 1.150 mm (INIA 1989) y se concentra de abril a septiembre. Posee una estación seca corta en verano (menos de cuatro meses) durante los cuales no llueve más del 5 % del total anual.

Cuadro 1. Características de las cuencas hidrográficas con *Pinus radiata* (pino) y *Eucalyptus globulus* (eucalipto).
Hydro-geomorphologic characteristics of the *Pinus radiata* and *Eucalyptus globulus* catchments.

Característica	Cuenca			
	Pino 1	Pino 2	Eucalipto 1	Eucalipto 2
Área de la cuenca (ha)	12,55	13,98	16,72	21,1
Longitud cauce principal (km)	0,47	0,41	0,45	0,62
Pendiente media (%)	25,2	30,3	27,7	36,5
Pendiente media del cauce (%)	22	24	26	27
Perímetro (km)	1,7	1,57	2,0	2,1
Índice de Gravelius	1,35	1,18	1,37	1,25
Altitud media (m)	327	331	369	320
Coefficiente orográfico (m ² /ha)	85,01	78,44	81,48	48,51
Densidad de drenaje (km/km ²)	4,67	4,40	5,91	6,67
Canal de alimentación (km/km ²)	0,21	0,23	0,17	0,15
Alejamiento medio (km)	1,34	1,09	1,11	1,35
Coefficiente de torrencialidad	37,16	31,48	35,33	31,63

Los eventos de lluvia de esta zona tienen diferente duración, pudiendo prolongarse hasta por varios días. Sus intensidades rara vez sobrepasan el equivalente a los 20 mm/h. Las precipitaciones de la zona son preferentemente del tipo ciclónico o frontal. Registran considerables diferencias interanuales en su cuantía y su distribución local está influida por la topografía de la cordillera. Durante los eventos de lluvia, y debido a la ubicación altitudinal de las cuencas, las plantaciones se encuentran, generalmente, inmersas en neblina o nubes.

La temperatura promedio anual del aire es de 13 °C y oscila entre los 7 °C julio y 19 °C enero. Durante el estío, en días con alta radiación solar, se pueden registrar temperaturas máximas que sobrepasan los 35 °C. Debido al rápido ascenso del estado térmico del aire, la humedad relativa puede descender a valores inferiores al 20 %¹. Estas condiciones meteorológicas propician una alta evaporación potencial.

La zona tiene suelos derivados de rocas metamórficas cuya textura está influida por su evolución y erosión. Son suelos franco-arenosos a arcillo-limosos en la superficie y en profundidad son franco a arcillosos, con drenaje interno moderado (Schlatter *et al.* 2003). En los sitios de estudio, el suelo tiene profundidades variables que fluctúan entre 0,5 y 3 m.

La velocidad de infiltración² de estos suelos, en estado saturado, oscila entre 3 y 10 mm/h. La dispersión de estos valores se debe principalmente a la heterogénea estructura de los suelos, que contienen una considerable cantidad de piedras y de rocas fragmentadas de diferentes tamaños.

¹ Registros realizados durante el estudio con termohigrógrafos.

² Determinados con infiltrómetros de doble anillo (Steubing y Fangmeier 2001).

A ello se agrega la compleja distribución espacial de las raíces de la vegetación herbácea, arbustiva y de las plantaciones forestales anteriores y actuales, además de las perturbaciones a las que estuvieron expuestos durante las actividades forestales precedentes. Estas características no son un obstáculo importante a la humectación en profundidad del suelo, considerando la intensidad de las lluvias en la zona de estudio.

Las características de las dos plantaciones de pino (Pino 1 y Pino 2) se presentan en el cuadro 2. Ellas fueron establecidas en 1987, la densidad inicial de las plantaciones fue de 1.250 árboles/ha y corresponden a una segunda rotación. En la fecha del estudio tenían 23 años de edad y, por consiguiente, estaban prontas a ser cosechadas. Presentaban dos raleos y una poda hasta los 6 m de altura.

Cuadro 2. Características de las plantaciones de *Pinus radiata* (pino) y *Eucalyptus globulus* (eucalipto).

Characteristics of the *Pinus radiata* and *Eucalyptus globulus* plantations.

Característica	Cuenca			
	Pino 1	Pino 2	Eucalipto 1	Eucalipto 2
Edad (años)	23	23	9	9
Altura media (m)	28,2	28,2	20,4	20,3
Densidad (árboles/ha)	320	315	1.174	1.326
DAP medio (cm)	36,0	35,4	15,9	15,2
Cobertura copa (%)	65	65	50	55
Altura poda (m)	5,9	5,7	Sin poda	Sin poda
Área basal (m ² /ha)	32,9	31,7	24,3	25,2
Zona <i>buffer</i> (ha)	1,5	0,9	0,8	1,0

El suelo de estas plantaciones estaba cubierto por un mantillo dominado por una capa de acículas que, en promedio, no sobrepasaba 2 a 3 cm de espesor, pero en sus microdepresiones con posibilidades de acumulaciones alcanzó hasta 8 cm de espesor. La cubierta herbácea era rala (< 25 %) y estaba conformada principalmente por gramíneas que, habitualmente, perecen durante el estío por estrés hídrico. La cubierta arbustiva era dispersa, conformada mayoritariamente por maqui (*Aristotelia chilensis* Mol.), zarzamora (*Rubus radicans* Cav.), además de algunas especies arbóreas todavía de baja altura como litre (*Lithraea caustica* Mol.), boldo (*Peumus boldus* Mol.), peumo (*Cryptocarya alba* Mol.), arrayán (*Luma apiculata* DC. Burret.), avellano (*Gevuina avellana* Mol.) y ocasionalmente roble (*Nothofagus obliqua* (Mirb.) Oerst.).

El efluente de la cuenca de Pino 1 poseía en toda su extensión una zona de protección con un ancho de 13 m ± 4 m. En la cuenca Pino 2, la zona de protección tenía un ancho de 11 m ± 3 m. El estrato arbustivo y arbóreo de estas zonas presentaba una cobertura que fluctuaba entre 50 y 70 %, conformada por quila (*Chusquea quila* Mol.), zarzamora, maqui, lingue (*Persea lingue* Nees.), arrayán, avellano, boldo y roble. La cobertura vegetal herbácea era baja (< 25 %) y, en conjunto, todos los estratos generaban una cobertura > 75 %.

Las particularidades de las dos plantaciones de eucalipto se presentan en el cuadro 2. Eucalipto 1 era una plantación de segunda rotación establecida en 1999. Eucalipto 2 tenía la misma edad pero de monte bajo, es decir, de regeneración por tocón, y cada tocón presentaba entre dos y tres fustes. El suelo de ambas cuencas presentaba un mantillo homogéneo que no sobrepasa 2 cm de espesor. La cubierta arbustiva era rala, conformada principalmente por retamillo (*Teline monspessulana* (L.) Koch) y algunos individuos de mosqueta (*Rubus ulmifolius* Schott f.). La vegetación herbácea era escasa y estaba conformada por algunas gramíneas que perecen durante el verano.

El efluente de la cuenca Eucalipto 1 presentaba en toda su extensión una zona de protección ripariana de una sección total de 41 m ± 6 m. En la parte baja de la microcuenca, cercana al vertedero, se observó una pequeña superficie anegada. El estrato arbustivo y arbóreo de esta zona presentó una cobertura cercana al 75 %, conformado por zarzamora, quila, maqui y retamillo, con presencia ocasional de algunos individuos arbóreos de tamaño menor de lingue, arrayán, peumo, roble y algunos árboles de pino. También se observaron algunos canelos (*Drimys winteri* Forster) y nalcas (*Gunnera tinctoria* (Mol.) Mierbel.) en la zona anegada. La cobertura herbácea era baja (< 25 %), conformada principalmente por enredaderas quilineja (*Luzuriaga radicans* Ruiz et Pavón.) y voqui (*Boquila trifoliolata* (DC) Decne), además de helechos (*Lophosoria quadripinnata* (Gmel.) Chr). El piso estaba cubierto por un mantillo fraccionado de hojas de eucalipto, con espesor promedio de 2 cm. En conjunto, todos los estratos generaban una cobertura > 75 %.

El efluente de la cuenca Eucalipto 2 también presentaba una protección ripariana con un ancho de 52 m ± 8 m en toda su extensión. El estrato arbustivo y arbóreo de esta franja mostraba una cobertura cercana al 60 %, conformada por zarzamora, quila, maqui y murta (*Ugni molinae* Turcz.), con presencia ocasional de boldo, lingue, peumo, roble, piñol (*Lomatia dentata* (Ruiz et Pavón) Br.), naranjillo (*Citronella mucronata* (Ruiz et Pavón) y chupón (*Greigia sphacelata* (Ruiz et Pavón) Regel). La cobertura herbácea era baja (< 25 %) y el piso estaba cubierto por un mantillo de hojas de eucalipto con espesor promedio de 3 cm. En conjunto, los diferentes estratos generaban una cobertura cercana al 65 %.

Aportes de agua. La cantidad de precipitación que llegó a las cuencas se determinó con dos pluviógrafos (Hobo®), ubicados a campo abierto, cerca de ellas. La cantidad total de agua que alcanzó el piso (precipitación neta) se fraccionó en precipitación directa y escurrimiento fustal [1].

$$P_n = P_d + P_f \quad [1]$$

Donde P_n = precipitación neta (mm), P_d = precipitación directa (mm) y P_f = escurrimiento fustal (mm).

Debido a la especial distribución temporal de las precipitaciones, el período de mediciones se tuvo que extender hasta septiembre 2009. Ello fue necesario para que los suelos, al final de este lapso de tiempo, alcanzaran un contenido de agua similar al que tuvieron al inicio. Esta condición es requisito indispensable para calcular la cantidad de agua involucrada en la evapotranspiración con la ecuación [4] que se presenta más adelante.

Las pérdidas de agua por intercepción se consideraron equivalentes al diferencial entre la precipitación total registrada a campo abierto y la precipitación neta [2].

$$I_c = P_p - P_n \quad [2]$$

Donde I_c = pérdidas de agua por intercepción (mm) y P_p = precipitación (mm).

Para lograr esta partición se delimitó, en cada cuenca, una parcela de 15 × 40 m. Las precipitaciones que alcanzaron el suelo (precipitación directa) se determinaron con una canaleta metálica en forma de V, de 15 cm de ancho y 30 m de largo, instalada a 30 cm sobre el suelo. La fracción de las precipitaciones que llegó al suelo, utilizando como senda de fluido el fuste de los árboles (escurrimiento fustal), fue recogida por collarines de goma sellados alrededor del tronco de 15 árboles según la metodología propuesta por Huber y Oyarzún (1984). El agua recogida, en cada caso, fue conducida a su respectivo registrador.

Para establecer si existieron diferencias significativas entre las pérdidas de agua por intercepción de las diferentes

cuenclas, se confrontaron los valores de estas mermas calculados para cada uno de los eventos de lluvia con la prueba Mann-Whitney.

Escorrentía. En los efluentes, a la salida de cada una de las cuencas, se construyó un vertedero de concreto armado tipo Thompson de paredes delgadas. Esta construcción tiene 3 m de largo, 1,5 m ancho y 1,5 m de alto con una escotadura de 60°, cuyo vértice estaba ubicado a 50 cm sobre su piso. Debido a la conformación pedregosa de la base de los cauces, las construcciones fueron insertadas a 50 cm de profundidad en el lecho del efluente para prevenir filtraciones subterráneas. Debido a esta necesidad, a lo ancho de toda la entrada de los vertederos se construyó un muro de 50 cm de alto. Esta obra transformó a los vertederos en receptáculos con una superficie de 4,5 m². Estas estructuras de cemento se aprovecharon como trampas para retener los sedimentos de arrastre y, simultáneamente, como colectores de los sedimentos en suspensión que se decantaron. En la pared frontal de los vertederos, a 20 cm de cada pared lateral y a la altura de la base de su piso, se empotraron dos compuertas de hierro de 30 cm de ancho y 20 de alto. Estas cerraduras se abrieron durante la limpieza de los vertederos, para facilitar la evacuación del agua y del material depositado en el fondo después de terminar los controles periódicos. Para determinar el caudal de los efluentes se instaló una estación fluviométrica en cada vertedero. Estos equipos funcionan con el principio del flotador. Fueron construidos en la Universidad Austral de Chile y tienen una precisión de 2 mm. Cada vertedero fue calibrado en terreno a través de aforos periódicos para cubrir un amplio rango de caudales y lograr con ello la correspondiente curva de aforo (ecuación polinomial de grado tres, $R^2 = 0,999$, $P < 0,01$). La frecuencia de registro se fijó en tres minutos.

Con esta información se determinó la variación temporal del caudal de cada efluente. Se realizaron comparaciones estadísticas con los valores horarios de los montos de escorrentía entre las cuencas mediante una prueba no paramétrica de comparaciones de pares U de Mann-Whitney. Todos los análisis estadísticos fueron desarrollados utilizando el programa R para Windows. En todos los análisis estadísticos las diferencias entre tratamientos se consideraron significativas cuando $P \leq 0,05$.

También se determinaron los coeficientes de escorrentía de cada cuenca por simple relación entre la escorrentía total del período de estudio y la precipitación para el mismo lapso de tiempo.

Para cada evento de lluvia que se manifestó en el hidrograma se determinó la fracción de la componente de escorrentía superficial que participó en el caudal total. Para esta partición se utilizó el método de la pendiente constante. A su vez, para cada cuenca, se determinó la variación periódica de la participación de la escorrentía superficial en el caudal total de los efluentes.

Transporte de sedimentos. Para determinar la cantidad de sedimentos en suspensión que pasó por cada vertedero se construyó una estructura rectangular flotante (50 × 30 cm) con tubos de PVC de 5 cm de diámetro. A esta armazón, en su zona central, se fijó una bomba eléctrica de 12 V, cuya bocatoma permaneció sumergida a 5 cm de profundidad. Esta localización se pudo mantener constante porque la estructura PVC estaba articulada a dos brazos móviles de 1,5 m de largo, fijados en la parte alta, al final de cada una de las paredes laterales del vertedero.

Para obtener muestras homogéneas, integradas y representativas de agua de los efluentes, la bomba movilizaba un volumen que siempre estaba en relación directa al caudal del efluente en el momento de la extracción. El agua de cuatro muestras diarias y para un período aproximado de siete días se almacenó en un recipiente. A esta agua se le determinó la concentración de sedimentos, utilizando un sistema de filtración con bomba de vacío. Se usaron filtros de fibra de vidrio (Advantec GF75 47 mm) que fueron secados a 60 °C por 48 horas. Este valor se multiplicó por el caudal del correspondiente período para establecer la carga de sedimentos en suspensión que fue evacuada por el efluente.

Periódicamente se cuantificaron los sedimentos acumulados en el fondo de los vertederos. Para ello se diseñó y construyó un artefacto que consiste en un disco de hierro de 8 cm de diámetro y 1 mm de espesor que, en su cara superior, tiene adosada una lámina delgada de goma. En el centro de la cara superior del disco de hierro tiene soldada una varilla de hierro de 5 mm de diámetro y 1,5 m de largo, cuyo extremo termina en un hilo 4,8 mm (3/16"). Seis de estas estructuras se distribuyeron en forma sistemática y equidistante en cada vertedero mediante sujeciones que las separaban a 40 cm de cada una de las paredes laterales.

Para establecer la cantidad de sedimentos que se depositaron sobre cada disco se sobrepuso a la varilla de hierro un tubo de acero de 4 cm de diámetro, que, en uno de sus extremos, tiene un borde cortante que hace contacto con la goma del disco de hierro. En la otra punta está soldado un mango que permite girar y presionar con fuerza el tubo contra la goma para lograr un buen cierre. Para mantener su equidistancia a la varilla y, por consiguiente, asegurar una ubicación concéntrica sobre el disco, el tubo tiene en su interior una guía flotante. Logrado este posicionamiento y contacto, el tubo de 4 cm de diámetro se presionaba en forma hermética contra el disco con una pieza que se atornillaba al hilo de la varilla de hierro. Posteriormente, se sacaba completamente el artefacto del vertedero y se transvasaba su contenido a un recipiente. Las muestras fueron secadas a 60 °C. El peso del material sólido anhidro se consideró como la cantidad de sedimentos que estuvieron depositados sobre la superficie del disco, delimitada por el tubo de 4 cm de diámetro menos el área ocupado por la varilla de hierro. Con esta metodología se determinó la cantidad de sedimentos que hubo por unidad de superficie

en cada uno de los discos. El valor promedio obtenido de los seis discos se extrapoló al área del piso del vertedero para calcular la cantidad total de sedimentos depositados en él. Debido a que en este caso sólo se contó con información semanal, se utilizó en el análisis estadístico mediante prueba no paramétrica de comparaciones de pares de Kruskal-Wallis entre las cuencas.

Agua edáfica y evapotranspiración. Aproximadamente cada 30 días se determinó la variación temporal y espacial del contenido de agua del suelo hasta los 2,5 m de profundidad. Para ello se hicieron mediciones con un equipo DTR (TRIME-FM3, sonda T3, Field Measurement Device Version P3 marca IMKO). Estos registros se hicieron en 10 puntos repartidos homogéneamente en superficie en cada una de las cuencas, con una secuencia en profundidad de 10 cm.

Para determinar la cantidad de agua involucrada en la evapotranspiración de las cuencas se utilizó la ecuación [3].

$$EvTr = Pp - Q - \Delta R - \Delta F \quad [3]$$

Donde $EvTr$ = evapotranspiración, Pp = precipitaciones, Q = escorrentía, ΔR = cambio en el almacenamiento de agua en el suelo y ΔF = cambio en almacenamiento de aguas subterránea (freática).

Como no se pudo determinar la variación periódica del contenido de agua subterránea, tampoco fue posible inferir la variación temporal de la evapotranspiración. En consecuencia, la cantidad de agua involucrada en la evapotranspiración sólo se pudo establecer para el período completo, al suponer que el contenido de agua subterránea al inicio del período de estudio fue similar a la del final ($\Delta F = 0$). En consecuencia, la ecuación original [3] se redujo a la ecuación [4].

$$EvTr = Pp - Q - \Delta R \quad [4]$$

RESULTADOS

Aportes de agua. La precipitación total del período (15 junio 2008-30 septiembre 2009) fue de 2.149 mm (cuadro 3). La mayor parte de las lluvias se registraron entre los meses de mayo y septiembre, mientras que los meses correspondientes al estío fueron excepcionalmente deficitarios en precipitaciones (cuadro 3).

En las cuencas con pino la confrontación de los valores de intercepción correspondientes a cada uno de los eventos de lluvia no registró diferencias estadísticas ($P = 0,846$), similar situación sucedió entre las cuencas con eucaliptos ($P = 0,370$) (cuadro 3). La plantación de Pino 1 tuvo una mayor intercepción que Eucalipto 1 y 2 ($P < 0,05$ y $P < 0,01$), semejante resultado se registró entre Pino 2 y las dos cuencas con eucalipto ($P < 0,01$ y $P < 0,001$).

Escorrentía. El coeficiente de escorrentía para las dos cuencas con pino fue del 33 % y para las de Eucalipto 1 y 2 del 20 y 23 %, respectivamente (cuadro 3). Las cantidades diarias de agua que pasaron por los vertederos de las cuencas forestadas con pino durante todo el período no tuvieron diferencias significativas ($P = 0,680$). Diferente fue la situación entre Eucalipto 1 y 2 ($P < 0,05$). También hubo diferencias significativas entre Pino 1 y Eucalipto 1 ($P < 0,01$) y entre Pino 2 y Eucalipto 1 ($P < 0,01$). La escorrentía total en la cuenca de Pino 1 mostró tendencia a ser mayor que Eucalipto 2, pero las diferencias no fueron significativas ($P = 0,588$). Resultado similar se obtuvo entre las cuencas de Pino 2 y Eucalipto 2 ($P < 0,356$).

La participación de la componente subsuperficial en el caudal total para las cuencas con Pino 1 y 2 fue del 73 y 74 %, respectivamente, y para las cuencas Eucalipto 1 y 2 del 70 y 75 %, respectivamente. No hubo diferencias significativas entre los valores periódicos de las cuencas con pino ($P = 0,230$) ni entre las de eucalipto ($P = 0,298$). Similares resultados se obtuvieron entre las cuencas Pino 1 y Eucalipto 1 y 2 ($P = 0,267$; $P = 0,305$) y entre Pino 2 y Eucalipto 1 y 2 ($P = 0,258$; $P = 0,317$).

Agua edáfica y evapotranspiración. La variación espacial y temporal del contenido de agua edáfica para las cuatro cuencas en los primeros 2,5 m de profundidad se presenta en la figura 2 y la variación periódica del contenido total de agua del perfil en el cuadro 3.

La cantidad de agua involucrada en la evapotranspiración total para el período completo de Pino 1 y 2 fue equivalente a 1.405 y 1.388 mm, respectivamente (cuadro 3), que corresponden al 65 y 64 % de la precipitación total, respectivamente. Para Eucalipto 1 y 2 estos valores fueron del 76 y 70 %, lo que equivale a 1.630 y 1.511 mm, respectivamente (cuadro 3). Cuando se hicieron estas relaciones entre la cantidad de agua extraída exclusivamente del suelo (evapotranspiración neta) y la cantidad de agua que efectivamente alcanzó el suelo (precipitación neta), los valores disminuyeron para Pino 1 y 2 a un 58 y 56 %, y para Eucalipto 1 y 2 al 73 y 66 %, respectivamente.

Transporte de sedimentos. La variación temporal de la cantidad total de sedimentos (fondo y en suspensión) para cada una de las cuencas está resumida en el cuadro 3. Los valores periódicos entre las cuencas con pino no presentaron diferencias estadísticas ($P = 0,311$). Tampoco las hubo entre las cuencas plantadas con eucalipto ($P = 0,305$). Resultados semejantes se obtuvieron entre las cuencas Pino 1 y Eucalipto 1 y 2 ($P = 0,291$, $P = 0,301$) y Pino 2 y Eucalipto 1 y 2 ($P = 0,316$ y $P = 0,301$).

DISCUSIÓN

Precipitaciones. Las precipitaciones para el período de 14 meses son similares a la suma de las precipitaciones promedio mensuales correspondientes al mismo lapso de

Cuadro 3. Valores periódicos y totales de la precipitación (Pp), intercepción (Ic), caudal (Q), escorrentía superficial (Es), caudal base (Cb), evapotranspiración (EvTr), contenido de agua edáfica (0-2,5 m) (R) y transporte total de sedimentos (St) para las cuencas con *Pinus radiata* (pino, P) y *Eucalyptus globulus* (eucalipto, E).

Values of total precipitation (Pp), interception loss (Ic), streamflow (Q), event flow (Es), base flow (Cb), evapotranspiration (EvTr), soil water content 0-2,5 m) (R) and total sediment export (St) for *Pinus radiata* (P) and *Eucalyptus globulus* (E) catchments for the monitored periods.

Mes	Año 2008						Año 2009									
	6	7	8	9	11	12	1	2	3	4	5	6	7	8	9	
Día	15	10	13	30	8	20	7	13	18	16	20	18	14	15	30	
Período	1 2 3 4 5						6 7 8 9 10 11 12 13 14 Σ									
P1	Pp (mm)	209	231	412	38	32	1	6	4	16	156	237	308	266	234	2.149
	Ic (mm)	38	39	43	12	19	3	4	2	7	37	37	43	38	35	357
	Q (mm)	58	115	174	26	11	2	2	2	2	6	19	92	63	133	705
	Es (mm)	17	18	66	1	0	0	0	0	2	7	35	20	22		188
	Cb (mm)	41	97	109	25	10	2	2	2	2	4	12	56	43	111	517
	EvTr (mm)	-	-	-	-	-	-	-	-	-	-	-	-	-	-	1.405
	R (mm)	923	941	950	855	770	506	483	467	450	555	711	775	959	962	-
	St (kg/ha)	32	41	15	4	3	1	0	0	0	1	41	36	52	11	237
P2	Ic (mm)	41	33	40	11	16	3	4	3	5	32	39	38	35	37	337
	Q (mm)	62	113	170	30	15	3	2	2	3	7	11	91	68	129	707
	Es (mm)	24	20	59	1	1	0	0	0	2	6	33	19	21		185
	Cb (mm)	38	93	112	30	14	3	2	2	2	5	5	58	49	108	522
	EvTr (mm)	-	-	-	-	-	-	-	-	-	-	-	-	-	-	1.388
	R (mm)	912	935	942	838	724	458	435	411	406	498	727	782	957	966	-
	St (kg/ha)	96	102	34	6	7	2	1	1	3	8	86	127	127	14	615
E1	Ic (mm)	21	35	32	15	16	2	2	3	1	6	22	12	28	20	215
	Q (mm)	44	95	127	23	11	3	2	1	2	4	15	45	26	40	439
	Es (mm)	17	16	40	1	0	0	0	0	2	8	23	10	12		130
	Cb (mm)	26	79	87	23	11	3	2	1	1	2	7	22	16	29	309
	EvTr (mm)	-	-	-	-	-	-	-	-	-	-	-	-	-	-	1.630
	R (mm)	905	928	940	760	712	467	426	409	389	525	693	745	980	985	-
	St (kg/ha)	68	22	11	6	2	0	1	2	1	3	17	10	7	2	152
E2	Ic (mm)	31	36	30	18	9	1	2	4	2	13	20	20	31	18	235
	Q (mm)	56	99	151	28	14	3	3	2	2	6	16	42	28	50	500
	Es (mm)	17	12	43	0	1	0	0	0	2	8	21	10	11		124
	Cb (mm)	39	86	108	28	14	3	3	2	2	4	8	21	18	39	376
	EvTr (mm)	-	-	-	-	-	-	-	-	-	-	-	-	-	-	1.511
	R (mm)	924	941	951	816	747	522	502	494	484	579	778	823	1.055	1.062	-
	St (kg/ha)	51	15	9	6	2	0	1	1	3	4	14	8	7	2	125

Fecha inicio del estudio: 15 junio 2008. -: sin datos.

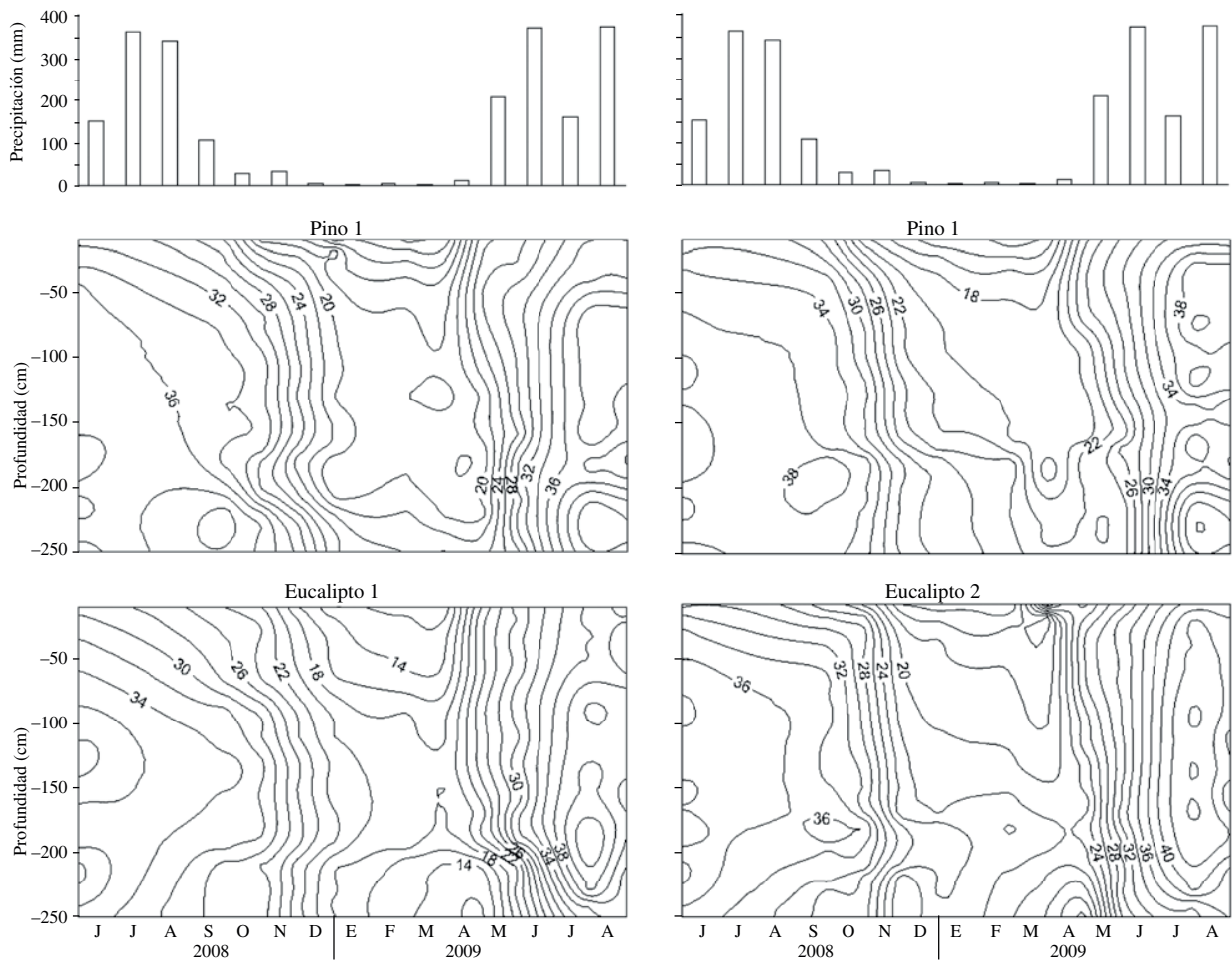


Figura 2. Variación temporal y espacial del contenido de agua edáfica (% volumétrico) para las cuencas con *Pinus radiata* (pino) y *Eucalyptus globulus* (eucalipto).

Spatio-temporal variation of soil water content (% Vol) of catchments forested with *Pinus radiata* and *Eucalyptus globulus*.

tiempo para la zona (INIA 1989). En general, mantienen su distribución temporal, resaltando el déficit pluviométrico durante el verano.

Durante los períodos correspondientes al estío, prácticamente la totalidad de las precipitaciones son interceptadas por la cubierta arbórea. Las diferencias entre las características de las plantaciones de pino y eucalipto son las principales responsables de la desigual pérdida de agua por interceptación. Estas disimilitudes se deben principalmente a que las coníferas tienen una mayor capacidad de retención de agua que las latifoliadas (Crockford y Richardson 2000, Huber y Iroumé 2001, Link *et al.* 2004, Fleischbein *et al.* 2005). También influye la menor edad que tienen las plantaciones de eucalipto, que por consiguiente poseen un dosel menos desarrollado. Estas condiciones generan una inferior cobertura del dosel, a pesar de que estas plantaciones tienen una mayor densidad. Por consiguiente, la precipitación neta en las cuencas con eucalipto es significativamente superior a las con pino.

Las pérdidas de agua por interceptación determinadas en el estudio son inferiores a las registradas por Huber y Oyarzún (1984), Huber *et al.* (1998, 2008), Klaassen *et al.* (1998), Iroumé y Huber (2000, 2002), Huber y Iroumé (2001), Fleischbein *et al.* (2005), Deguchi *et al.* (2006), Cao *et al.* (2008) en otras localidades de Chile. Ello se debe principalmente a la ubicación altitudinal de las cuencas, que permiten que las plantaciones se encuentren frecuentemente inmersas en neblina o nubes durante los eventos de lluvia. Bajo estas condiciones meteorológicas, los árboles interceptan una parte de la nubosidad para entregarla como un adicional a la precipitación directa. Esta situación subvalora levemente el real valor de las pérdidas de agua por interceptación de estas plantaciones en la zona. Durante algunos eventos de lluvia de poca monta y muy baja intensidad, el aporte adicional de agua por interceptación de la neblina permite que al suelo llegue una cantidad de lluvia que supera la precipitación a campo abierto. De todas maneras, el aporte de agua por estas fuentes en

comparación a los aportes anuales por precipitación es muy bajo para esta localidad. Estas tendencias coinciden con las obtenidas por otros autores (Klaassen *et al.* 1998, Holder 2004, Knoblich 2005).

Agua edáfica. La variación espacial y temporal del agua en el suelo es similar en las cuatro cuencas. A partir del período 4, cuando disminuyen las precipitaciones y las condiciones meteorológicas incrementan la intensidad de la evapotranspiración, se registra una disminución en las reservas de agua edáfica. Esta situación se manifiesta en todo el perfil considerado, pero con mayor intensidad en los primeros 1,5 m de profundidad. En los períodos 8 y 9, el contenido de agua del suelo en los primeros 20 cm desciende a valores inferiores a los del punto de marchitez permanente (14 % volumétrico). Este estado se manifiesta especialmente en la componente herbácea de la cubierta vegetal que se extingue por falta de agua.

Al comienzo del estudio, que coincide con la época más lluviosa del año, el contenido de agua del suelo en los primeros 2,5 m de profundidad es similar para todas las cuencas. Este valor está cercano a la capacidad máxima de retención de agua. Durante el tiempo con menores precipitaciones y mayores consumos de agua por evapotranspiración, las reservas de agua disminuyen para alcanzar un mínimo a principio de otoño. En consecuencia, la cantidad de agua disponible para el desarrollo de los árboles desciende considerablemente. A partir del período 10, que coincide con el inicio de la nueva temporada de invierno y una disminución de la intensidad de la evapotranspiración, comienza una paulatina recarga de agua, que alcanza en todas las cuencas su máximo en septiembre.

La diferencia máxima entre los contenidos extremos de agua del perfil de los suelos, durante todo el período, en las cuencas con pino (512 y 560 mm) y eucalipto (596 y 578 mm) es reducida. Ello se debe principalmente a que al inicio del estudio el perfil de los suelos de las distintas cuencas está prácticamente saturado y que al final del estío poseen un mínimo que también es similar entre ellos. Esta última situación se logra porque la mayor parte del agua edáfica, especialmente en los primeros 1,5 m, ha sido consumida durante el estío por las plantaciones. En consecuencia, esta condición es una restricción para que las plantaciones puedan alcanzar su mayor potencial de crecimiento durante el verano (Carroll *et al.* 2000, Zhou *et al.* 2002, Andreassian *et al.* 2004). A su vez, es una circunstancia que reduce las diferencias que pueden existir entre los consumos extremos de agua de las dos especies, especialmente durante el período deficitario en precipitaciones (Putuhena y Cordery 2000).

Escorrentía. La variación temporal del caudal de los cuatro efluentes de las cuencas está regulada principalmente por el régimen anual de las precipitaciones, la variación del contenido de agua del suelo y la evapotranspiración (Blume *et al.* 2007, Mayor *et al.* 2009).

El agotamiento extremo de la reserva de agua edáfica durante el estío explica por qué el aumento de las precipitaciones de marzo a junio no incrementa en forma similar el caudal de los efluentes. Esta agua se requiere para saturar el perfil del suelo y, con ello, crear las condiciones para generar una escorrentía superficial capaz de incrementar en forma significativa el caudal de los efluentes.

El caudal total de los efluentes de las dos cuencas de pino para todo el período es el mismo, lo que incide en forma idéntica en sus correspondientes coeficientes de escorrentía. Esta situación puede ser consecuencia de la similitud que hay entre ambas cuencas y en las características de las plantaciones forestales.

La cuenca de Eucalipto 1 registra un menor coeficiente de escorrentía en comparación a Eucalipto 2. Esta diferencia podría ser consecuencia de la menor pendiente media de las laderas que tiene la cuenca Eucalipto 1 (Carroll *et al.* 2000, Blume *et al.* 2007). Los coeficientes de escorrentía tienen una fuerte variación temporal por estar influidos por las condiciones climáticas, especialmente por el régimen de las precipitaciones, el grado de saturación de los suelos y la evapotranspiración (Blume *et al.* 2007).

Los efluentes de las cuencas con pino registran para todo el período un mayor caudal que las con eucalipto, a pesar de que al suelo les llega una menor cantidad de agua por tener una superior pérdida por intercepción.

El agua de origen subsuperficial es el principal componente del caudal total en todos los efluentes de las cuencas. Su participación varía según la distribución temporal de las precipitaciones. Durante el invierno, especialmente cuando los suelos están saturados, la escorrentía superficial aumenta su participación relativa en el caudal total en desmedro de la escorrentía subsuperficial. Situación contraria sucede durante el estío, donde la falta de precipitaciones importantes permite que la escorrentía subsuperficial tenga una participación exclusiva (Onda *et al.* 2001, Blume *et al.* 2007).

Evapotranspiración. Los montos de evapotranspiración para ambas especies concuerdan con los resultados de otros estudios realizados en Chile que usaron metodologías distintas (Huber y Oyarzún 1985, Oyarzún *et al.* 1985, Huber *et al.* 1998, 2008, Huber y Trecaman 2002, 2004).

La evapotranspiración incluidas las pérdidas de agua por intercepción para todo el período son inferiores en las cuencas con pino que en las con eucalipto. En consecuencia, en el presente estudio las plantaciones de eucalipto registran una mayor evapotranspiración. Este resultado se puede deber a las características propias de cada especie y por disponer de una superior cantidad de agua edáfica como consecuencia de las inferiores pérdidas por intercepción.

Durante la época más deficitaria en precipitaciones, la evapotranspiración se sustenta, exclusivamente, de la reserva de agua edáfica. En consecuencia, al final del estío las plantaciones han consumido la mayor parte del

agua. Esta situación inhibe la evapotranspiración durante el verano, lo que reduce la diferencia potencial de consumo máximo de agua entre las dos especies. En consecuencia, el efecto de la distinta edad, densidad y manejo de las plantaciones no se va a manifestar con todo su rigor en la evapotranspiración. Por consiguiente, la máxima diferencia entre los requerimientos potenciales de agua entre pino y eucalipto se va a presentar recién cuando tengan acceso a toda el agua requerida durante el año y, especialmente, durante el estío.

En consecuencia, la evapotranspiración de las diferentes plantaciones está más bien regulada por la disponibilidad de agua en el suelo durante el período deficitario en precipitaciones que por la capacidad potencial de consumo de cada una de ellas.

Transporte de sedimentos. La cantidad total de sedimentos transportados por los efluentes de las cuencas con pino es mayor que en las con eucalipto. Esta diferencia se puede explicar por el mayor ancho que tienen las zonas de protección de los efluentes de las cuencas con eucalipto. Las características propias de las zonas de protección influyen en la capacidad de retención de sedimentos (Boothroyd *et al.* 2004, Gomi *et al.* 2005, Hassan *et al.* 2005).

Sorprende la mayor cantidad de sedimentos evacuados en la cuenca Pino 2. Este resultado puede ser consecuencia del paso obligado que tiene el efluente por una pequeña zona de inundación que podría aportar un adicional de sedimentos.

La variación temporal de la exportación de sedimentos está influida principalmente por el régimen de las precipitaciones y, por consiguiente, por la intensidad de la escorrentía superficial (Beschta *et al.* 2000, Gomi *et al.* 2005, Karwan *et al.* 2007). El mayor transporte de sedimentos se concentra en los períodos más lluviosos y cuando los suelos están saturados. Esta condición edáfica es importante en la generación del caudal superficial, que incluso puede superar a la de la intensidad de las precipitaciones (Cammeraat 2002, Seeger *et al.* 2004, Mayor *et al.* 2009, Turnbull *et al.* 2010).

Las desiguales características topográficas de las cuencas, las particularidades de cada una de las coberturas del suelo, la distinta intensidad con que están perturbados los suelos debido a intervenciones silviculturales precedentes, las características de las franjas de protección en los cauces y los disímiles montos de la escorrentía superficial de las cuencas, con iguales o distintas cubiertas forestales, son las responsables de la dispar intensidad del transporte de sedimentos (Scott y Lesch 1997, Moore y Wondzell 2005, Gomi *et al.* 2005, Karwan *et al.* 2007).

Según la CONAMA (1996), los montos de sedimentos evacuados por los efluentes por unidad de superficie en el presente estudio son considerados como ligeros. Sus totales son superiores a los informados por Oyarzún y Peña (1995), que utilizaron el método de parcelas de erosión para su cuantificación. También superan los valores recopilados por

Gomi *et al.* (2005) para distintas plantaciones de coníferas ubicadas en el Pacífico noroeste de EE.UU., que oscilan entre uno y 100 kg/ha. Estas plantaciones están ubicadas en suelos de origen metamórfico que tienen una pluviometría anual que fluctúa entre los 700 y 2.500 mm.

CONCLUSIONES

Debido a las diferentes características del dosel, las pérdidas de agua por intercepción son mayores en las cuencas cubiertas con pino que en las de eucalipto. La cantidad de agua involucrada en la evapotranspiración en las cuencas de pino es inferior a las de eucalipto. Esto influye en forma inversa en el monto de los caudales de los efluentes de las correspondientes cuencas. La carga de sedimento es superior en las cuencas de pino que en las de eucalipto, situación que podría ser explicada por las distintas características de las zonas de protección de orilla de cauces.

AGRADECIMIENTOS

El estudio fue financiado con aportes del Fondo Nacional de Investigaciones Científicas y Tecnológicas (FONDECYT) a través del Proyecto N° 1070218 y el importante apoyo de la empresa Forestal Mininco S. A. También se agradece a los colaboradores en el proyecto Srs. Rodrigo Bravo y Carlos Torres.

REFERENCIAS

- Andreassian V, C Perrin, C Michel. 2004. Impact of imperfect potential evapotranspiration knowledge on the efficiency and parameters of watershed models. *Journal of Hydrology* 286:19-35.
- Armesto J, D Manushevich, C Mora, R Smith-Ramírez, A Rozzi, A Abarzúa, P Marquet. 2010. From the Holocene to the Anthropocene: a historical framework for land cover change in southwestern South America in the past 15.000 years. *Land Use Policy* 27: 148-160.
- Beschta R, M Pyles, A Skaugset, C Surfleet. 2000. Peakflow responses to forest practices in the western cascades of Oregon, USA. *Journal of Hydrology* 233: 102-120.
- Blume T, E Zehe, A Bronstert. 2007. Rainfall runoff response, runoff coefficients and baseflow separation. *Hydrological Sciences Journal* 52: 843-862.
- Boothroyd I, J Quinn, E Langer, K Costley y G Steward. 2004. Riparian buffers mitigate effects of pine plantation logging on New Zealand streams. 1. Riparian vegetation structure, stream geomorphology and periphyton. *Forest Ecology and Management* 194: 199-213.
- Brown A, L Zhang, T McMahon, A Western, R Vertessy. 2005. A review of paired catchment studies for determining changes in water yield resulting from alterations in vegetation. *Journal of Hydrology* 310: 28-61.

- Bruijnzeel LA. 2001. Hydrology of tropical montane cloud forests: a reassessment. *Land Use and Water Resources Research* 1: 1-18.
- Cammeraat L. 2002. A review of two strongly contrasting geomorphological systems within the context of scale. *Earth Surface Processes and Landforms* 27: 1201-1222.
- Carlyle-Moses DE. 2004. Throughfall, stemflow, and canopy interception loss fluxes in a semi-arid Sierra Madre Oriental matorral community. *Journal of Arid Environments* 58: 181-202.
- Cao Y, Z Ouyang, H Zheng, Z Huang, X Wang, H Miao. 2008. Effects of forest plantations on rainfall redistribution and erosion in the red soil region of southern China. *Land Degradation and Development* 19: 321-330.
- Carroll C, L Merton, P Burger. 2000. Impact of vegetative cover and slope on runoff, erosion, and water quality for field plots on a range of soil and spoil materials on central Queensland coal mines. *Australian Journal of Soil Research* 38: 313-327.
- CONAMA (Comisión Nacional del Medio Ambiente, CL). 1996. Metodologías para la caracterización de la calidad ambiental. Santiago, Chile. 242 p.
- Crockford R, D Richardson. 2000. Partitioning of rainfall into throughfall, stemflow and interception: effect of forest type, ground cover and climate. *Hydrological Processes* 14: 2903-2920.
- Deguchi A, S Hattori, H Park. 2006. The influence of seasonal changes in canopy structure on interception loss: Application of the revised Gash Model. *Journal of Hydrology* 318: 80-102.
- Farley K, E Jobbágy, R Jackson. 2005. Effects of afforestation on water yield: a global synthesis with implications for policy. *Global Change Biology* 11: 1565-1576.
- Fleischbein K, W Wilcke, J Boy, C Valarezo, W Zech, K Knoblich. 2005. Rainfall interception in a lower montane forest in Ecuador: effects of canopy properties. *Hydrological Processes* 19: 1355-1371.
- Fuenzalida H. 1971. Climatología de Chile. In Corporación de Fomento de la Producción ed. Geografía Económica de Chile. Santiago, Chile. p. 99-152.
- Gomi T, R Moore, M Hassan. 2005. Suspended sediment dynamics in small forest streams of the Pacific Northwest. *Journal of the American Water Resources Association* (August): 877-898.
- Hassan M, M Church, T Lisle, F Brardinoni, L Benda, G Grant. 2005. Sediment transport and channel morphology of small forested streams. *Journal of the American Water Resources Association* 41: 853-876.
- Holder C. 2004. Rainfall interception and fog precipitation in a tropical montane cloud forest in Guatemala. *Forest Ecology and Management* 190: 373-384.
- Hubbard J, T Link, J Gravelle, W Elliot. 2007. Timber harvest impacts on water yield in the Continental/Maritime Hydroclimatic Region of the United States. *Forest Science* 53(2): 169-180.
- Huber A, P Barriga, R Trecaman. 1998. Efecto de la densidad de plantaciones de *Eucalyptus nitens* sobre el balance hídrico en la zona de Collipulli, IX Región, Chile. *Bosque* 19(1): 61-69.
- Huber A, R Trecaman. 2004. Eficiencia del uso del agua en plantaciones de *Pinus radiata* en Chile. *Bosque* 25(3): 33-43.
- Huber A, G García. 1999. Importancia de los factores meteorológicos en la transpiración potencial de *Pinus radiata*. *Pyton* 65: 143-152.
- Huber A, A Iroumé. 2001. Variability of annual rainfall partitioning for different sites and forest covers in Chile. *Journal of Hydrology* 248: 78-92.
- Huber A, C Oyarzún. 1984. Factores reguladores de la interceptación en un bosque adulto de *Pinus radiata* D. Don. *Bosque* 6(2): 74-82.
- Huber A, R Trecaman. 2002. Efecto de la variabilidad interanual de las precipitaciones sobre el desarrollo de las plantaciones de *Pinus radiata* (D. Don) en la zona de los arenales, VIII Región, Chile. *Bosque* 23(2): 43-49.
- Huber A, A Iroumé, J Bathurst. 2008. Effect of *Pinus radiata* plantations on water balance in Chile. *Hydrological Processes* 22: 142-148.
- Huber A, C Oyarzún, A Ellies. 1985. Balance hídrico en tres plantaciones de *Pinus radiata* y una pradera. *Bosque* 6(2): 74-82
- INFOR (Instituto Forestal, CL). 2008. Anuario Forestal 2008. Boletín Estadístico 121. Centro de Información Forestal, sede Metropolitana, Santiago, Chile. 169 p.
- INIA (Instituto de Investigaciones Agropecuarias, CL). 1989. Mapa agroclimático de Chile. Santiago, Chile. INIA. 221 p.
- Iroumé A, O Mayen, A Huber. 2006. Runoff and peak flow responses to timber harvest and forest age in southern Chile. *Hydrological Processes* 20: 37-50.
- Iroumé A, A Huber. 2000. Interceptación de las lluvias por cubiertas de bosques y efecto en los caudales de crecida en una cuenca experimental en Malalcahuello, IX Región Chile. *Bosque* 21 (1): 45-56.
- Iroumé A, A Huber. 2002. Comparison of interception losses in a broadleaved native forest and a *Pseudotsuga menziesii* (Douglas fir) plantation in the Andes Mountains of southern Chile. *Hydrological Processes* 16: 2347-2361.
- Iroumé A, O Mayen, A Huber. 2006. Runoff and peakflow responses to timber harvest and forest age in southern Chile. *Hydrological Processes* 20: 37-50.
- Karwan D, J Gravelle, J Hubbard. 2007. Effects of timber harvest on suspended sediment loads in Mica Creek, Idaho. *Forest Science* 53(2): 181-188.
- Klaassen W, F Boseveld, E De Walter. 1998. Water storage and evaporation as constituents of rainfall interception. *Journal of Hydrology* (212-213): 36-50.
- Knoblich K. 2005. Rainfall interception in a lower montane forest in Ecuador: effects of canopy properties. *Hydrological Processes* 19: 1355-1371.
- Link T, M Unsworth, D Marks. 2004. The dynamics of rainfall interception by a seasonal temperate rainforest. *Agricultural and Forest Management* 124: 171-191.
- May C. 2007. Sediment and wood routing in steep headwater streams: an overview of geomorphic processes and their topographic signatures. *Forest Science* 53(2): 119-130.
- Mayor A, S Bautista, J Bellot. 2009. Factors and interactions controlling infiltration, runoff, and soil loss at the microscale in a patchy Mediterranean semiarid landscape. *Earth Surface Processes Landforms* 34: 1702-1711.
- Megahan W, J King, K Seyesbagheri. 1995. Hydrologic and erosional responses of a granitic watershed to helicopter logging and broadcast burning. *Forest Science* 41(4): 777-795.
- Moore R, S Wondzell. 2005. Physical hydrology and the effects of forest harvesting in the Pacific northwest: a review. *Journal of the American Water Resources Association* 41: 763-784.

- Onda Y, Y Komatsu, M Tsujimura, J Fujihara. 2001. The role of subsurface runoff through bedrock on storm flow generation. *Hydrological Processes* 15: 1693-1706.
- Oyarzún C. 1993. Evaluación del modelo U.S.L.E. para predecir pérdidas de suelo en áreas forestadas de la cuenca del río Biobío. *Bosque* 14(1): 45-54.
- Oyarzún C, L Peña. 1995. Soil erosion and overland flow in forested areas with pine plantations at coastal mountain range, central Chile. *Hydrological Processes* 9: 111-118.
- Oyarzún C, A Huber, S Vásquez. 1985. Balance hídrico en tres plantaciones de *Pinus radiata*. I: Redistribución de las precipitaciones. *Bosque* 6 (1): 3-13.
- Pizarro T, H Cuitiño. 1999. Evaluación cuantitativa de la erosión hídrica superficial en suelos desnudos de la Pre-Cordillera Andina y Valle Central de la VII Región. In VI Jornadas del CONAPHI. Chile.
- Putuhena W, I Cordery. 2000. Some hydrological effects of changing forest cover from eucalypts to *Pinus radiata*. *Agricultural and Forest Meteorology* 100: 59-72.
- Rehg K, A Packman, J Ren. 2005. Effects of suspended sediment characteristics and bed sediment transport on streambed clogging. *Hydrological Processes* 19: 413-427.
- Robinson M, A Cognard-Plancqb, C Cosandey, J David, P Durand, H Führer, R Hall, M Hendriques, V Marc, R McCarthy, M McDonnell, C Martin, T Nisbet, P O'Dea, M Rodgers, A Zollner. 2003. Studies of the impact of forests on peakflows and baseflows: a European perspective. *Forest Ecology and Management* 186: 85-97.
- Schlatter J, R Grez, V Gerding. 2003. Manual para el reconocimiento de suelos. 3ª Edición. Valdivia, Chile, Universidad Austral de Chile. 114 p.
- Scott D, F Prinsloo. 2008. Longer-term effects of pine and eucalypt plantations on streamflow. *Water Resource Research* 44: 1-8.
- Scott D, W Lesch. 1997. Streamflow responses to afforestation with *Eucalyptus grandis* and *Pinus patula* and to felling in the Mokobulaan experimental catchments, South Africa. *Journal of Hydrology* 199: 360-377.
- Seeger M, M Errea, S Beguería, J Arnáez, C Martí, J García-Ruiz. 2004. Catchment soil moisture and rainfall characteristics as determinant factors for discharge/suspended sediment hysteretic loops in small headwater catchments in the Spanish Pyrenees. *Journal of Hydrology* 288: 299-311.
- Steubing L, A Fangmeier. 2001. Pflanzan-ökologisches Praktikum. Stuttgart, Alemania. Eugen Ulmer. 205 p.
- Turnbull L, J Wainwright, R Brazier. 2010. Changes in hydrology and erosion over a transition from grassland to shrubland. *Hydrological Processes* 24: 393-414.
- Van Dijk A, L Bruijnzeel. 2001. Modelling rainfall interception by vegetation of variable density using an adapted analytical model. Part 1. Model description. *Journal of Hydrology* 247:230-238.
- Vega JA, C Fernández, T Fonturbel. 2005. Throughfall, runoff and soil erosion after prescribed burning in gorse shrubland in Galicia (NW Spain). *Land Degradation & Development* 16: 37-51.
- Zhou G, J Morris, J Yan, Y Zy, S Peng. 2002. Hydrological impacts of reforestation with eucalypts and indigenous species: a case study in southern China. *Forest Ecology and Management* 167: 209-222.

Recibido: 08.03.10

Aceptado: 09.08.10